Carbon-on-Gold Films and Spontaneous Adsorption of Aryldiazonium Salts for Surface Plasmon Resonance Sensing

by

Thuy Phuong Nguyen

A thesis submitted in partial fulfilment of the requirements for the degree of
Doctor of Philosophy

Department of Chemistry
University of Alberta

© Thuy Phuong Nguyen, 2021

Abstract

Over the past decades, surface plasmon resonance (SPR) technology has gained popularity as a powerful analytical technique for the study of biomolecular interactions and medical diagnostics. This is made possible thanks to the well-established gold-thiolate chemistry. However, the limited sensitivity and long-term stability of gold substrates and alkanethiol self-assembled monolayers motivate us to explore lamellar carbon-on-metal structures as SPR substrates and the spontaneous adsorption of aryldiazonium salts as surface functionalization strategies.

Our electron-beam evaporation process allows very thin, defect-free, well-adhered carbon films to be deposited on metal substrates, leading to minimal sensitivity loss for carbon-on-gold films and enhanced sensitivity for carbon-on-silver films in SPR measurements compared with previous reports. With further optimization of the deposition process and SPR instrumental setup, we believe that the sensitivity of carbon-on-silver films can be increased even more.

Spontaneous adsorption of aryldiazonium salts provides a fast and simple strategy to pattern surfaces selectively with stable monolayers of chemical linkers, which are viable for the covalent attachment of biomolecules on SPR substrates. This surface chemistry, together with carbon-on-gold films, were utilized to develop a proof-of-concept immunoassay, showing improved performance compared with the physical adsorption of biomolecules.

This thesis demonstrates that a combination of carbon-on-metal films and spontaneously grafted diazonium layers can be a potential alternative to Au-thiolate SAMs for SPR sensing, thereby improving the performance of SPR-based biosensors.

What is more, carbon-on-metal substrates also have potential as a versatile analytical platform that are compatible with not only SPR but also electrochemistry and SERS techniques, opening a pathway for new, exciting nanostructures and sensing schemes to be developed with analysis power never seen before.

Preface

This thesis is an original work by Thuy Nguyen under the supervision of Professor Mark T. McDermott. Parts of this research have been in collaboration with others and have been published. Below are details for each experimental chapter.

Chapter 2 is published as Nguyen, T.P.; McCreery, R.L.; McDermott M.T. Evaluation of the electroanalytical performance of carbon-on-gold films prepared by electron-beam evaporation. Analyst **2020**, 145, 5041-5052. I was responsible for most of the experimental design, data collection, data analysis, and writing of the manuscript/chapter. Critical inputs, suggestions, and recommendations were provided by Dr. McCreery and Dr. McDermott. XPS data were collected by the nanoFAB facility at the University of Alberta.

I was responsible for most of the experimental design, data collection, data analysis, and writing of Chapter 3. Critical inputs, suggestions, and recommendations were provided by Dr. McDermott. FT-IRRAS data were collected by the Analytical and Instrumentation Laboratory at the Department of Chemistry. XPS data were collected by the nanoFAB facility at the University of Alberta.

I was responsible for most of the experimental design, data collection, data analysis, and writing of Chapter 4. Critical inputs, suggestions, and recommendations were provided by Dr. McCreery and Dr. McDermott. FT-IRAAS data were collected by the Analytical and Instrumentation Laboratory at the Department of Chemistry. XPS data were collected by the nanoFAB facility at the University of Alberta. Part of electron-transfer rate data at gold electrodes were collected by Hanul Choi, an undergraduate researcher in our lab.

I was responsible for most of the experimental design, data collection, data analysis, and writing of Chapter 5. Critical inputs, suggestions, and recommendations were provided by Dr. McDermott. FT-IRRAS data were collected by the Analytical and Instrumentation Laboratory at the Department of Chemistry. XPS data were collected by the nanoFAB facility at the University of Alberta.

I was responsible for most of the experimental design, data collection, data analysis, and writing of Chapter 6. Critical inputs, suggestions, and recommendations

were provided by Dr. McDermott. Part of SERS data was collected with Dr. Casey Rusin.

Acknowledgements

Finishing my thesis has been an amazing milestone, which would not have been possible without the support of, encouragement from, and interactions with so many great individuals and groups that I have encountered during my time at the University of Alberta.

First and foremost, I am extremely grateful to my PhD supervisor, Dr. Mark McDermott. Thank you, Mark, for accepting me into your research group and continuously supporting me throughout my years in graduate school. Your patience and guidance have helped me become a better researcher and person. I am forever indebted to you, Mark.

I am extremely thankful for my supervisory committee members, Dr. Richard McCreery and Dr. Julie Gibbs, for their support, guidance, and suggestions during my PhD. It was really helpful discussing the status and direction of my research with them. Dr. McCreery and his group have been extremely accommodating in making their equipment and expertise available to me and training me to work in their lab. It was also my honor to have Dr. McCreery as a co-author in my first paper, in which I have learned a great deal from him to improve my research writing skills. Thank you!

In addition, I would like to thank my fellow group members, both past and present: Dr. Greg Kaufman, Dr. Shereen Elbayomy, Dr. Rongbing Du, Dr. Albert Cao, Dr. Sunil Rajput, Dr. Kenny Xu, Dr. Ahmed Mahmoud, Dr. Casey Rusin, Dr. Abdelhaq Benkaddour, Nicole Jankovic, Amy Mao, Taylor Lynk, and Akib Khandaker. You guys always have been available for advice, help, and friendship. I am especially thankful for your help during my early years of graduate school when I desperately needed help to get started with my research and adjust to life in Canada.

I also would like to thank all the staff in the Department of Chemistry for their assistance over the years: Wayne Moffat and Jennifer Jones for their help with FT-IRRAS measurements, the Machine Shop staff, Anita Weiler, Dr. Yoram Apelblat, Ryan Lewis, and Dr. Jillian Buriak and Dr. Mike Serpe for giving me access to and training on their instruments. Special thanks go to Dr. Anna Jordan for her dedication in helping me edit my thesis. I am indebted to you, Anna, for your support,

encouragement, and delicious cookies. Thanks to all the staff at the nanoFAB facility for XPS sample analysis and training on dicing saw and AFM instruments.

Last but not least, I am grateful for my family and friends' encouragement and mental support despite the vast geographical distances between us: my grandmother, Sam; my parents, Bao and Tam; my sister, Tram; my friends Hang, Ngoc, Ha, Duong, Tay, and Hue. I could not be where I am and who I am today without them. I am also thankful for the new friends I have made in Canada: Hiromi and her husband Chad, Thuc, and Cerrise. They have made my time here a lot more enjoyable and unforgettable.

Table of Contents

List of Tables

List of Figures

List of Abbreviations

ACN	Acetonitrile
AFM	Atomic force microscopy
Ag	Silver
AQMS	Sodium anthraquinone-2-sulfonate
ATR	Attenuated total reflectance
Au	Gold
BBD	4-bromobenzene diazonium tetrafluoroborate
BDD	Boron-doped diamond
Br	Bromo
BSA	Bovine serum albumin
CBD	4-carboxybenzene diazonium tetrafluoroborate
CCD	Charge-coupled device
CMBD	4-carboxymethylbenzene diazonium tetrafluoroborate
COOH	Carboxyl
CP	Carboxyphenyl
CV	Cyclic voltammetry
DI	Deionized water
DNA	Deoxyribonucleic acid
eC	Electron-beam evaporated carbon
eC/Ag	Carbon-on-silver
eC/Au	Carbon-on-gold
ECR	Electron cyclotron resonance
EDC	1-ethyl-3-(3-dimethylaminopropyl) carbodiimide hydrochloride
ET	Electron-transfer
EtOH	Ethyl alcohol
FcTMA	(Ferrocenylmethyl)trimethylammonium
Fib	Fibrinogen
FT-IRRAS	Fourier transform infrared reflection-absorption spectroscopy
GC	Glassy carbon

HOPG	Highly oriented pyrolytic graphite
IgG	Immunoglobulin
ITO	Indium tin oxide
MBN	4-mercaptobenzonitrile
NBD	4-nitrobenzene diazonium tetrafluoroborate
NH_2	Amino
NHS	N-hydroxysuccinimide
NO_2	Nitro
NP	Nitrophenyl
O/C	Oxygen-to-carbon ratio
OCP	Open circuit potential
OH	Hydroxyl
PBS	Phosphate buffer saline
PPF	Pyrolyzed photoresist film
PQ	9,10-phenanthrenequinone
rms	Root-mean-square
RSD	Relative standard deviation
S/N	Signal-to-noise ratio
SAM(s)	Self-assembled monolayer(s)
SCE	Saturated calomel electrode
SDS	Sodium dodecyl sulfate
SECM	Scanning electrochemical microscopy
SERS	Surface-enhanced Raman spectroscopy
Si	Silicon
$Si_{1-x}C_x$:H	Amorphous silicon-carbon alloy
SiO_x	Silicon dioxide-based glass
SnO_2:Sb	Antimony-doped tin
SPR	Surface plasmon resonance
SPRi	Surface plasmon resonance imaging
$TBABF_4$	Tetrabutylammonium tetrafluoroborate
TOF-SIMS	Time-of-flight secondary ion mass spectrometry

UPD	Underpotentially deposited
UV	Ultraviolet
XPS	X-ray photoelectron spectroscopy

List of Symbols

Å	Angstrom
ω	Angular frequency
i_{pa}	Anodic peak current
K_{ADS}	Binding constant
C^0	Capacitance
i_{pc}	Cathodic peak current
cm	Centimeter
Δ%R	Change in reflectivity
Q	Charge
R^2	Coefficient of determination
º	Degree
ºC	Degree Celsius
ε	Dielectric constant
K_D or K_d	Dissociation constant
A	Electrode area
eV	Electron volt
F	Faraday constant
k^0	Heterogeneous electron-transfer rate constant
b	Hill coefficient
h	Hour
K	Kelvin
kcal	Kilocalorie
kDA	Kilodalton
µA	Microampere
µF	Microfarad
µL	Microliter
µm	Micrometer
µM	Micromolar
mL	Milliliter

mM	Millimolar
mW	Milliwatt
min	Minute
mol	Mole
ng	Nanogram
nm	Nanometer
n or N	Number of samples
Ω	Ohm
ΔE_p	Peak-to-peak separation
pmol	Picomole
k	Propagation constant
n	Refractive index
ν	Scan rate
s	Second
m	Slope
c	Speed of light
Γ	Surface coverage
θ	Theta
R_u	Uncompensated cell resistance
V	Volt

Chapter 1. Introduction

1.1 Research Scope and Objectives

Since the first demonstration of surface plasmon resonance (SPR) principle and application in gas sensing in the early 1980s, SPR-based biosensors have become an important tool for detecting analytes of importance in medical diagnostics, environmental monitoring, food safety, and security. Current SPR technology primarily relies on the use of thin gold substrates and alkanethiol self-assembled monolayers, which have found limitations in terms of sensitivity and long-term stability. This thesis explores the viability of employing carbon-on-metal substrates and aryldiazonium chemistry in SPR biosensors to circumvent the above-mentioned limitations.

Experimental research objectives include the following: (1) fabricating and characterizing carbon-on-gold films; (2) demonstrating feasibility of modifying carbon-on-gold films by spontaneous grafting of aryldiazonium salts; (3) demonstrating viability of carbon-on-metal films for use as SPR substrates; and (4) demonstrate application of carbon-on-gold films and aryldiazonium chemistry in a SPR-based immunoassay.

This chapter introduces relevant topics that are critical to the understanding of SPR-based biosensor development, including (1) history, physics, and instrumentation, (2) alkanethiolate self-assembled monolayers, (3) lamellar structures as SPR substrates, and (4) aryldiazonium surface chemistry.

1.2 History, Physics, and Instrumentation

Surface plasmons, also known as surface plasmon polaritons or surface plasma waves, are resonant oscillations of conduction electrons at the metal-dielectric interface stimulated by incident light. Surface plasmons were observed first in 1902 by Wood,[1] who reported abnormal narrow dark bands in the spectrum of light diffracted from a metallic diffraction grating. These anomalies were theorized to be associated with the excitation of electromagnetic waves on the surface of the

diffraction grating in 1941 by Fano[2] and later explained in terms of surface plasmon resonance in 1968 by Ritchie et al.[3] In 1968, surface plasmons excited optically by attenuated total reflection configurations were proposed by Otto[4] and Kretschmann and Raether,[5] establishing convenient methods to observe surface plasmons and the basis for most SPR instrumentation today. The potential of SPR for sensing applications was realized first in 1983 for the detection of gas and biomolecular interactions.[6] Since the first commercial SPR instrument was developed in 1990 by Biacore (now GE Healthcare),[7] SPR sensing has been employed widely in the applications of biomedical diagnostics,[8–10] pharmaceutical development,[11] biotechnology,[12–15] security,[16,17] food safety,[18,19] and environmental monitoring.[20]

The simplest geometry in which a surface plasmon can exist is at the interface of two media with dielectric constants of opposite signs, such as a metal and a dielectric.[21] A surface plasmon is a transverse magnetic (or p-polarized) mode, whose magnetic field lies in the plane of the metal–dielectric interface and is perpendicular to the direction of propagation.[21] The intensity of the magnetic field maximizes at the interface and decays exponentially into both the metal and dielectric.[21] The propagation constant of a surface plasmon at a metal–dielectric interface can be expressed as:

$$k_{sp} = \frac{\omega}{c}\sqrt{\frac{\varepsilon_m \varepsilon_s}{\varepsilon_m + \varepsilon_s}} \quad (1)$$

where ω is the angular frequency, c is the speed of light, and ε_m and ε_s are the dielectric constants of the metal film and the surrounding media, respectively. Since ε_m is a complex entity ($\varepsilon_m = \varepsilon_{mr} + i\varepsilon_{mi}$), k_{sp} also is a complex entity, whose real part is associated with the effective refractive index of the surface plasmon and the imaginary part with the attenuation of the surface plasmon in the direction of propagation.[22]

Surface plasmons can be supported by a metal having a dielectric constant with a negative real and small imaginary parts.[23] In the visible and near infrared regions, gold and silver fulfil this condition.[21] Gold substrates are employed preferably because they are optically and chemically stable. Silver exhibits sharper

angular resonance than gold, leading to enhanced sensitivity, but its widespread use is limited by poor long-term stability due to the ease of surface oxidation.[24]

Surface plasmons can be excited optically if the component wave vector parallel to the interface of the incident light (k_x) matches the propagation constant of the surface plasmon (k_{sp});[22] k_x is given by:

$$k_x = \frac{\omega}{c} \tag{2}$$

where ω is the angular frequency and c is the speed of light. As k_{sp} is always larger than k_x, surface plasmons cannot be excited directly by light incident onto a metal surface.[21] In order to lower k_{sp} or increase k_x for resonance to occur, different optical configurations and plasmonic materials must be used.[25] The coupling between light and surface plasmons can be achieved by prism, grating, or waveguide coupling.[21]

The most common method to excite surface plasmons optically is by using a prism coupler in the Krestchmann[5] attenuated total reflection configuration (Figure 1-1). In this configuration, p-polarized light is reflected off the base of a high refractive index prism, and the reflectivity is measured. A thin layer of gold (~50 nm) is placed in contact with the base of the prism, followed by a bulk dielectric (e.g., water or buffer). When p-polarized light propagating in a medium of high refractive index n_p (prism) encounters a medium of lower refractive index n_s (water/buffer), it is totally reflected at an incident angle exceeding the critical angle ($\theta_{critical}$) given by Snell's law as:

$$\sin\theta_{critical} = \frac{n_s}{n_p} \tag{3}$$

This phenomenon is termed total internal reflection, and the reflectivity of light ideally is 100%. Even though light is reflected totally, the electric field of the light penetrates the medium of lower refractive index, resulting in an evanescent wave which decays exponentially from the interface. The evanescent wave can tunnel through the metal thin film to excite the surface plasmons at the other metal–dielectric interface. The surface plasmons absorb energy from the incident light and decrease the reflectivity from 100%, resulting in an observed dip in the light intensity. The angle at which there is a minimum in reflected intensity is called the surface plasmon resonance angle. The resonance condition can be expressed as:

$$k_x = \frac{\omega}{c} n_p \sin\theta = \mathrm{Re}\{k_{sp}\} \quad (4)$$

where θ is the incident angle and $\mathrm{Re}\{k_{sp}\}$ is the real part of k_{sp}.[21,22]

A change in the refractive index of the surrounding media within ~200 nm[26] of the sensing interface alters the propagation constant of the surface plasmon; and consequently, through the resonance condition it changes the resonance angle, resonance wavelength, and the intensity and phase of the reflected light. These changes can be monitored by angular, wavelength, intensity, and phase modulation.[21,22] Intensity modulation, also known as surface plasmon resonance imaging or SPRi, can be used for high throughput multiplexed sensing.[27]

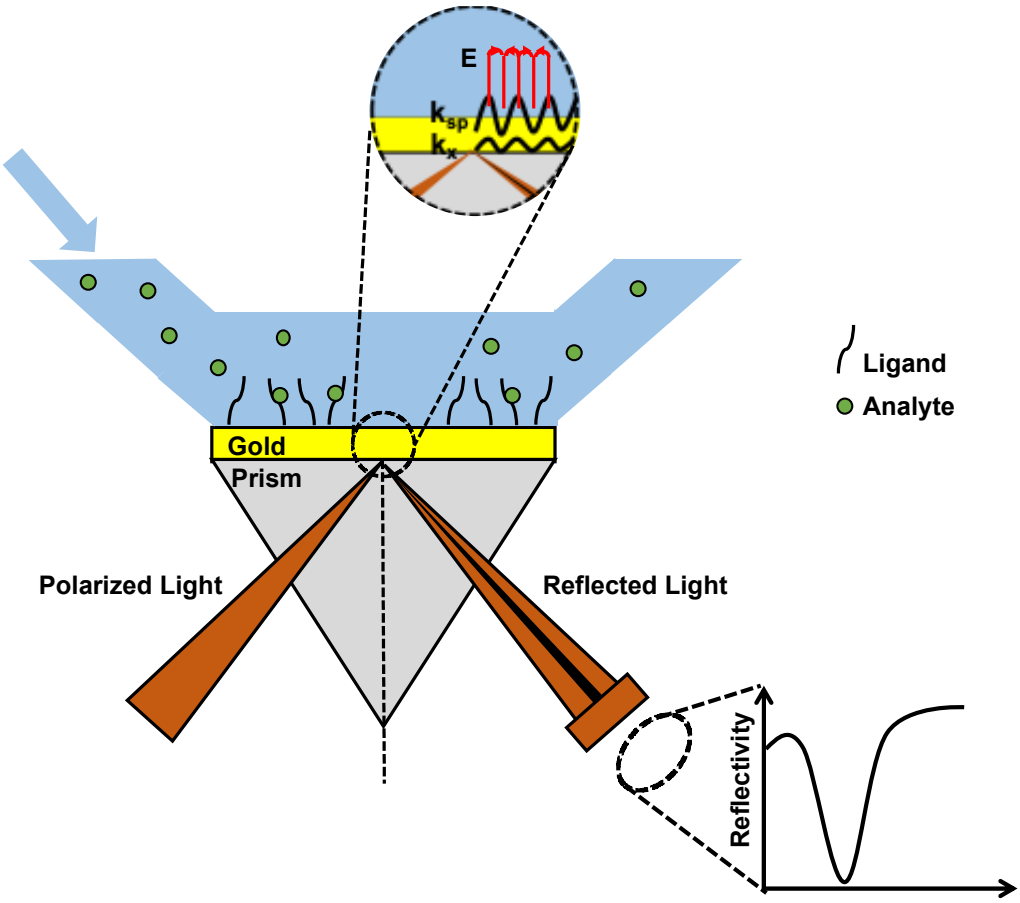

Figure 1-1. General principle of SPR in the Krestchmann configuration. See text for details. E: evanescent field; k_x: wave vector of incident light; k_{sp}: wave vector of surface plasmons.

SPR-based biosensors consist of a biorecognition element and an SPR transducer. The biorecognition element (ligand) selectively interacts with an analyte.

The SPR transducer translates the binding event into an output signal (angular, wavelength, intensity, or phase).[21,22] The principle of a surface plasmon resonance imaging biosensing system used in this work is demonstrated in Figure 1-2. Binding of the analyte to the ligand immobilized on the gold surface shifts the SPR curve to a higher angle, and the resulting increase in reflected intensity is measured with a charge-coupled device (CCD) detector at a fixed incident wavelength and angle within a linear part of the SPR curve.[27]

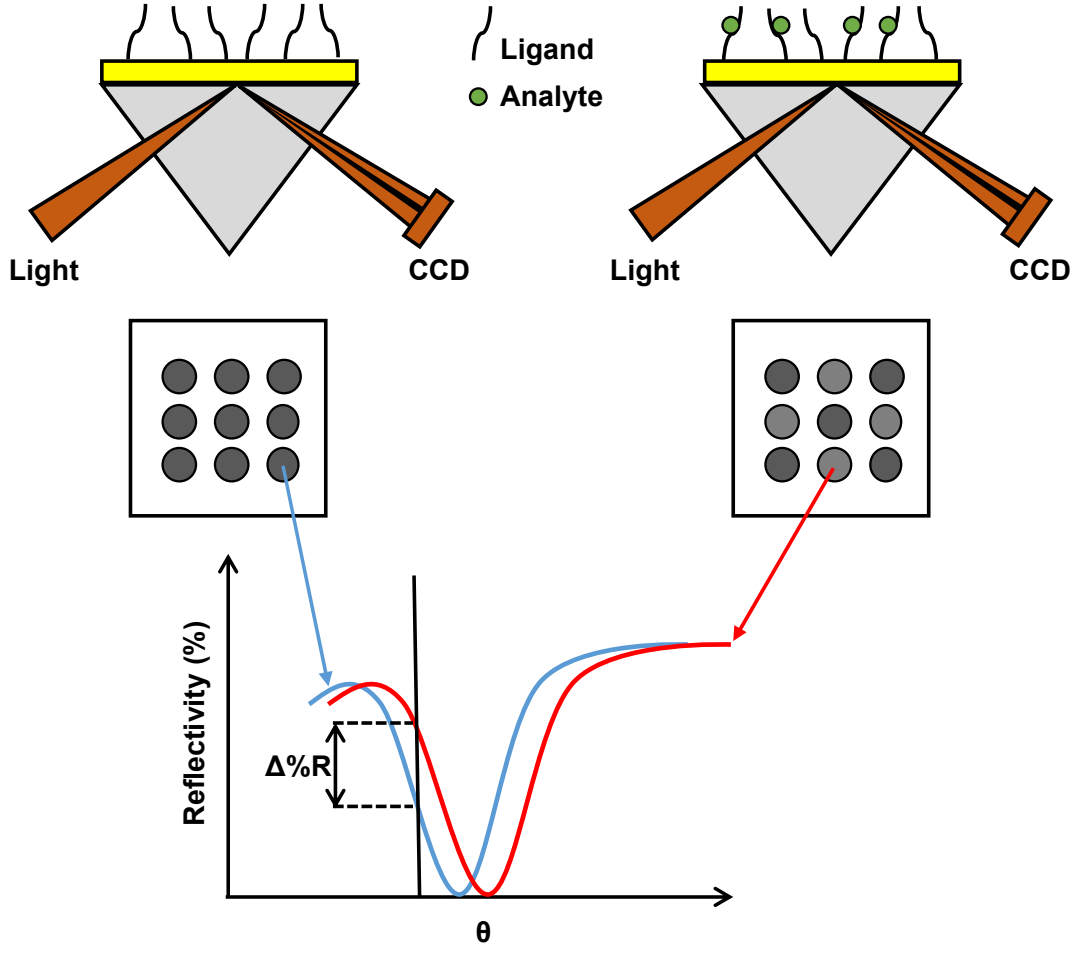

Figure 1-2. General principle of surface plasmon resonance imaging. The reflected light of the whole array is detected by a CCD detector. Binding of the analyte to the corresponding ligand results in a shift of the SPR curve to a higher angle and is detected simultaneously at every spot of the array as a change in the reflectivity (Δ%R) when measured at a fixed incident angle.

Depending on the detection format (i.e., direct, sandwich, competition, or inhibition), either the biorecognition element or the analyte is immobilized on the

gold surface, and the other is contained in a liquid sample. In the direct, sandwich, and competitive detection format, the biorecognition element is physisorbed or attached covalently onto the gold surface. Covalent attachment often is preferred, as it offers strong and stable linkages and easy regeneration of the sensor surface, which can remove the analyte but not the surface-attached ligand. Covalent immobilization usually includes coupling of amine, aldehyde, or thiol on previously formed self-assembled monolayers of functional groups.[22] As such, the choice of surface chemistry is critical to the performance of SPR-based biosensors and will be discussed in the next section.

1.3 Alkanethiolate Self-assembled Monolayers

The employed surface chemistry has to enable efficient immobilization while preserving the biological activity and minimizing non-specific binding to the surface. The most common strategy to functionalize gold surfaces is self-assembled monolayers (SAMs) of alkanethiols discovered in the 1980s by Nuzzo and Allara.[28] The thiol containing compounds spontaneously chemisorb onto the gold surface to form a gold–thiolate bond, which can be summarized by the following reaction:[29]

$$R–(CH_2)_n–SH + Au \rightarrow R–(CH_2)_n–S^-Au^+ + ½\ H_2$$

where R is the terminal functional group, such as –COOH, $–NH_2$, –OH, etc.

Although alkanethiols adsorb spontaneously also on silver,[30] copper,[31] palladium,[32] platinum,[33] nickel,[34] and iron,[35] gold is the most employed substrate, and SAMs on gold are by far the most extensively studied and well-characterized. The main reason is that there is no stable surface oxide layer on gold under ambient conditions, which simplifies cleaning and/or preparation procedures. Adsorption of alkanethiols on gold generally is performed in 10–1000 μM solutions in different solvents, depending on the nature of the thiol molecule.[29] To form a well-ordered SAM, adsorption times can vary from 2 to 12 h for long chain alkanethiols to at least 24 h for short chain alkanethiols or thiols with terminal groups different from $–CH_3$.[29]

Mixed monolayers can be produced by immersing the gold substrate in a solution containing a mixture of alkanethiols. The resulting SAMs consist of a

reasonably homogenous mixture of the components,[36] and the mole fraction of the surface component is related to its mole fraction in solution.[37] The formation of mixed SAMs layers can allow for control of the density of surface attached biorecognition element[38] and produce surface layers that can perform multiple functions, i.e. immobilizing biorecognition elements and minimizing non-specific binding.[39,40]

The adsorption of alkanethiols on the gold surface has been shown to proceed via two distinct steps (Figure 1-3).[41,42] The first step involves a surface-head group interaction and is diffusion limited; a disorganized, incomplete layer is formed within a few minutes of contact between the clean metal surface and the alkanethiol solution. The second step, also known as surface crystallization, involves the slow reorganization of the alkyl chains into an organized, densely packed, two-dimensional layer over several hours. The order of the monolayer is due to the van der Waals interactions between the alkyl chains. SAMs with alkyl chains of $n > 9$ yield more crystalline structure, whereas shorter chains form more disorganized, liquid-like layer because of the limited chain-chain interactions.[43]

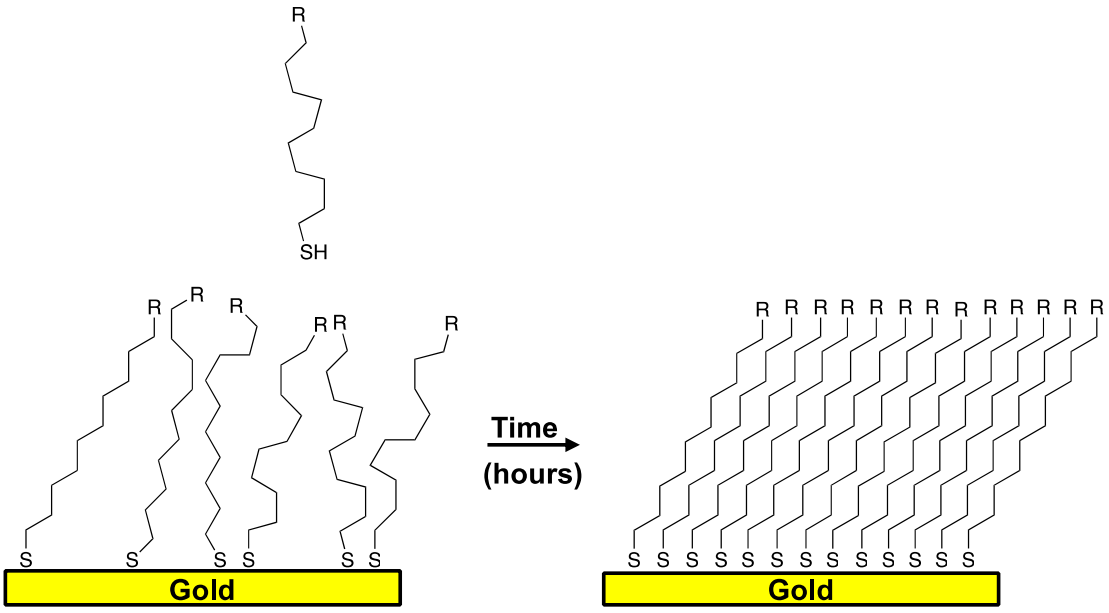

Figure 1-3. Scheme of the different steps during the self-assembly of alkanethiol on a gold surface: initial adsorption followed by the reorganization and crystallization of the SAM.

The monolayer formed is well characterized, and the alkyl chains have been shown to be in the all trans-conformation, tilted ~20–30° with respect to the surface normal.[44] Alkanethiol SAMs on gold usually are not defect-free. Less defective SAMs are formed on a smoother surface[45] and by molecules with longer alkyl chains[43] and/or terminal groups smaller than the footprint of the alkyl chain (~20 Å).[36] The integrity of SAMs also contributes to the thermal stability of SAMs. SAMs with few defects (i.e., high integrity) are more stable because alkanethiols organized into the two-dimensional structure are harder to remove than individual alkanethiols.[46,47]

Gold–thiol chemistry often faces stability issues.[48,49] The gold–thiol bond strength is 50 kcal/mol[29] and is described as a pseudo-covalent bond.[44] The sulfur atom is prone to oxidation to either sulfinates ($–SO_2$) or sulfonates ($–SO_3$).[44] The rate of oxidation depends on the alkyl chain length (shorter-chain length SAMs oxidize much faster than long-chain ones)[50,51] and the chemical nature of the terminal functional group.[47] The oxidized SAM is bound less strongly to the gold surface,[52] desorbing from the surface and thereby impairing the performance of the final device. SAMs are typically stable within a potential window between +1.0 and –1.0 V vs SCE (depending on alkyl chain length, terminal group, and the gold surface quality),[45,53,54] at temperatures below 100 ºC[55] and for a week or two in air.[44] The poor long-term stability of SAMs is particularly problematic in such applications as on-surface combinatorial chemistry (due to the harsh chemical conditions used) and photolithography (due to the oxidation of the gold–sulfur bond by ultraviolet radiation).[56]

The readily formed, thoroughly characterized gold–thiol chemistry gives rise to its popularity in the field of SPR-based biosensors. Additionally, the availability of alkanethiols with various terminal functional groups enables the convenient formation of ordered interfaces with a well-defined chemistry. Although alkanethiol SAM on gold is used extensively, the poor long-term stability of this surface chemistry is a serious limitation with practical implications. Therefore, alternative surface chemistry has to be explored for the fabrication of high-performance SPR sensing interfaces.

1.4 Lamellar Structure as SPR Substrates

Gold has been the substrate of choice for SPR sensing due to its stability in aqueous environments and ease of functionalization by alkanethiol SAMs. However, gold does not produce the highest SPR sensitivity. Indium tin oxide (ITO) can achieve high sensitivity in the infrared range,[57] while silver is the most appealing substrate in the conventional visible range.[58] Silver can be functionalized with alkanethiol SAMs similar to gold,[30] but its widespread use is limited by poor long-term stability. Silver is more prone to surface oxidation than gold, and the resulting oxidized surface complicates the ability to control the interfacial chemistry for biosensing applications. A strategy to circumvent this limitation is by depositing an overcoating on top of the surface plasmon active metal film (Figure 1-4); the overcoating thickness has to be on the order of a few nanometers to retain high sensitivity because the SPR signal decays exponentially within 200 nm from the interface.[26] The overlayer protects the underlying metal film and simultaneously opens the door for new surface chemistries other than alkanethiol SAMs to be used. The overlayers under investigation include oxide-based and carbon-based layers.

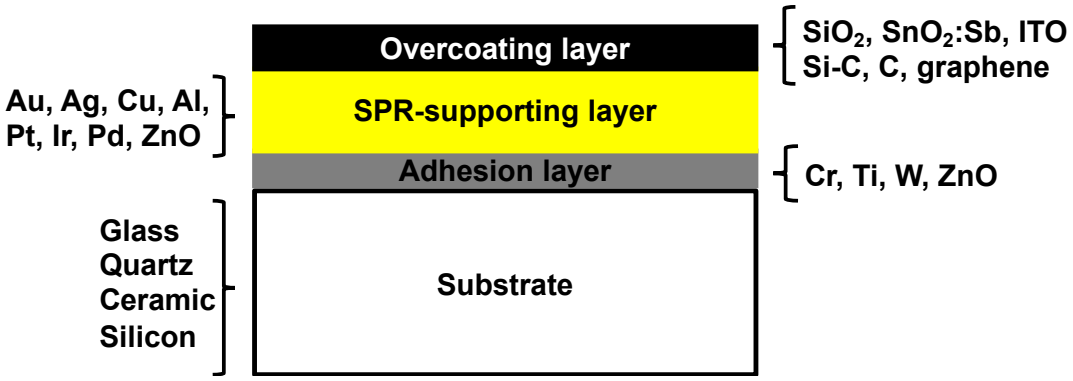

Figure 1-4. Different materials used in SPR substrate fabrication.

1.4.1 Oxide-based Overcoatings

Silicon dioxide-based materials, or glass, are routinely used in biosensing, particularly in the fabrication of DNA and proteins arrays as they are inexpensive and easily functionalized with the well-developed silane-coupling chemistry.[22,59] An early developed silica overlayer suffered from the poor stability of the gold/SiO_2 interface;

the thin silica layer peeled off the surface within a few minutes upon immersion into water and PBS buffer.[22] A more recently developed strategy for the formation of 3–100 nm silica films includes sol-gel deposition of 3-(mercaptopropyl)trimethoxysilane on gold, followed by hydrolysis of the terminal trimethoxysilyl groups to silanol groups necessary for the condensation reaction of spin-coated tetramethoxysilane.[60] A different approach employs layer-by-layer deposition of poly(allylamine hydrochloride) and sodium silicate, followed by calcination at high temperature to form stable silicate films of 2–15 nm.[61] A stable, smooth, and very hydrophilic gold/SiO_2 interface was obtained by spin coating of poly(hydroxymethylsiloxane) and post-treatment with plasma oxidation.[62,63] Stable silica films as thin as 7 nm can be deposited directly on gold using plasma-enhanced chemical vapor deposition of a silane and nitrous oxide gaseous mixture, negating the need for an additional titanium adhesion layer between the gold and the silica films.[64] The robust silane-coupling chemistry developed for glass bioassay has been exploited on these silicate films, which have been demonstrated in the fabrication of several DNA and protein assays.[61,65,66] However, silica coating finds limitation in electrochemical SPR because of the sluggish charge transfer manifested in its insulating nature.[64,67]

Antimony-doped tin (SnO_2:Sb) and indium tin oxide (ITO) have emerged as promising coatings for electrochemical SPR applications due to a low resistivity of 10^{-4}–10^{-2} Ω cm.[68–70] The biorecognition element can be coupled on ITO and SnO_2:Sb surfaces using the same silane-coupling chemistry as silica-based lamellar structures.[22] SnO_2:Sb has a high imaginary part of the dielectric constant ($\varepsilon = 1.91 + i0.249$) and thus a yellow color and additional light absorption, leading to a significant decrease in the photon-plasmon coupling efficiency and broadening of the SPR curve.[22] The ITO overlayer is optically transparent and does not deteriorate the SPR signal like SnO_2:Sb as only a shift to larger resonance angle is observed.[22]

Having an oxide-based overcoating can decrease the sensitivity of the SPR supporting metals with the surrounding refractive index change; 7 nm SiO_x, 8.5 nm ITO, and 5.5 nm SnO_2:Sb coatings on Au decrease the sensitivity of bare Au substrates by ~20%, 17%, and 35%, respectively.[22] The same thicknesses of ITO and

SnO_2:Sb coatings on Ag lowered the sensitivity of bare Ag by 9% and 44%, respectively.[22] Only ITO coating Ag can provide a 35% sensitivity enhancement rivalling bare Au substrates.[22] However, the main drawback of these oxide-like overcoatings is with the silane chemistry, as it is not entirely well controlled.[22] In addition, the Si–O–Si bonds are prone to hydrolysis when subject to harsh environments such as highly saline conditions.[22]

1.4.2 Carbon-based Overcoatings

Carbon-based surfaces can protect the underlying metals effectively while allowing for more well-developed and robust chemistry to be used, such as UV light-mediated functionalization with alkene-containing molecules[71] and electrografting strategies.[72] The bonds formed are often covalent, leading to enhanced stability of the final device. Lockett et al.[73,74] demonstrated SPRi-, carbon-based DNA arrays prepared by sputtering amorphous carbon on gold and silver substrates. Then, photofunctionalization with alkene-containing molecules was used for the in-situ synthesis of oligonucleotide arrays, which was impossible with traditional gold/thiol substrates due to the exposure of the surface to UV light and oxidizing chemical conditions. A minimum carbon film thickness of 7.5 nm was needed to support array synthesis adequately, as thinner films sometimes delaminated and rendered the substrates unusable. An amorphous carbon overlayer resulted in a decrease in photo-plasmon coupling efficiency and broadening of the SPR curve, and, consequently, sensitivity loss due to its complex dielectric function ($\varepsilon = 2.19 + i0.63$).[22] A 7.5 nm thick carbon film corresponded to 42% loss of sensitivity relative to a bare gold film. A carbon film of the same thickness deposited on silver is 12% more sensitive than the carbon-on-gold counterpart but is inadequate to rival bare gold substrates.[73,74]

Another approach involves depositing amorphous silicon-carbon alloys, or a-$Si_{1-x}C_x$:H, on gold and silver substrates by plasma-enhanced chemical vapor deposition.[75] The silicon and carbon contents can be fine-tuned to change the material properties, such as optical transparency. When deposited on gold, a 5 nm thick a-$Si_{0.63}C_{0.37}$:H retained the sensitivity of bare gold. When deposited on silver, the same silicon-carbon layer increased the sensitivity by 175% compared to bare gold. The

silicon-carbon alloy can be functionalized with alkene-containing molecules through the formation of stable Si–C covalent bonds. A biotin-streptavidin proof-of-concept experiment was conducted on the Ag/a-$Si_{0.63}C_{0.37}$:H substrates, and a detection limit of 6 ng/mL of streptavidin was reported. Although such interface represents an ideal candidate for sensitive SPR, the amorphous silicon-carbon alloy coating was not homogenous as some pinholes and intermixing with the metal have been observed.

More recently, graphene has been investigated as an alternative coating on silver and gold. Graphene can be grown by chemical vapor deposition, then transferred mechanically onto gold; however, unavoidable defects can arise from the transfer process.[76] Recently, graphene directly grown on gold has been demonstrated.[77] Each graphene monolayer has been shown to absorb 2.3% of the incident light due to its complex dielectric function.[78] Additional layers of graphene shift the resonance angles to higher angles, decrease photo-plasmon coupling efficiency, and broaden the SPR curve; the effects are more pronounced on gold than on silver.[78,79] Aside from the protection that it can provide, graphene also can enhance the sensitivity of SPR-based sensors by increasing adsorption of biomolecules through π-π stacking interactions compared with the gold surface.[78] The overall sensitivity of graphene-based SPR substrates, therefore, depends on the number of graphene sheets and the enhanced adsorption efficiency on graphene.

1.5 Aryldiazonium Surface Chemistry for SPR Sensing

The poor stability of SAMs on gold has prompted researchers to explore the reductive adsorption of aryl diazonium salts as an alternative.[80] Diazonium salts can be grafted electrochemically and form covalent bonds which are more stable than the Au–S bonds, leading to enhanced stability of the adlayer.[81] The electroreduction of diazonium salts was pioneered in 1992 by Pinson and coworkers,[82] and investigated further by several groups, including the McCreery,[83,84] Downard,[85–88] Bélanger,[89] and Gooding groups.[90] Aside from forming strong covalent bonds with the surface, aryl diazonium salts are easy to prepare, available with a wide range of reactive functional groups, and rapidly (electro)deposited.[91]

The electrografted aryl layers are formed by a one-electron electrochemical reduction of the diazonium ion and concomitant dinitrogen loss, resulting in an aryl radical that reacts with the substrate surface to form the initial film. The generated aryl radical can attack already grafted molecules on the surface, thereby forming multilayers.[92] The thickness of the layer typically ranges from a few layers up to ~100 nm.[93] A large number of substrates can be electrografted by aryl diazonium salts, including different forms of carbon, metals, oxides, semiconductors, and polymers.[92] Figure 1-5 illustrates the electrochemical modification of a substrate by diazonium compounds, resulting in a multilayered structure with possible azo bonds within the layer or at the substrate-aryl layer interface. Physisorbed dimers also are likely to be present.[91] Formation of the aryl layers is less ordered and not as homogenous as alkanethiol SAMs.[80] Monolayers can be formed with careful control over the charge passed during the electrochemical reduction process[84] by using aryl diazonium salts with steric hinderance at the 3,5-positions[94] or bulky protecting groups.[95]

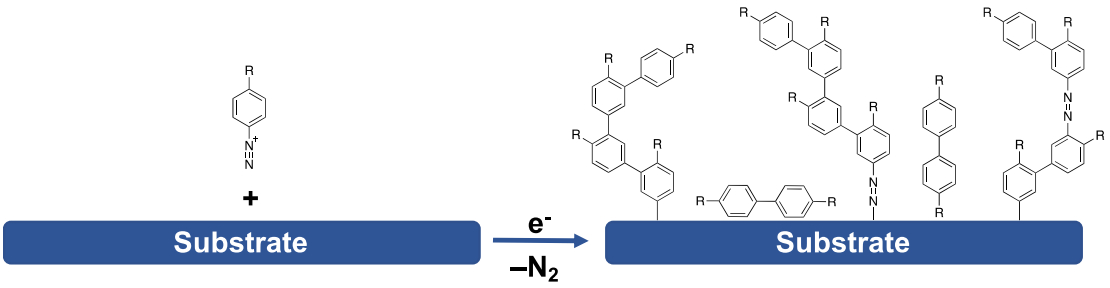

Figure 1-5. Modification of surfaces by (electro)chemical reduction of diazonium salts.

The lack of control in using aryl diazonium chemistry is compensated by the greater stability of the resulting structure. The C–C bond formed between the phenyl radical and the carbon surface is significantly stronger than Au–S bond (~4eV vs ~1.6 eV).[96] The strength of Au(111)–aryl bond theoretically is comparable with the Au(111)–S bond,[97] but experimental work by our group provided direct evidence for the enhanced stability of aryl diazonium-derived layers over SAMs.[81] Aryl layers have been shown to withstand annealing up to 700 K without being lost from the surface,[98] potential cycling between –2 V/SCE to 1.8 V/SCE depending on the para substituent,[99] sonication in various solvents,[72] and storage for several months in air.[72]

The formation of mixed layers of aryl diazonium salts via electrografting was reported first by Dequaire[100] and coworkers in 2003 and still is in its infancy, as little is known about the resulting structures. From a binary mixture of aryl diazonium salts, the ratio of the components on the surface is shown to be governed by the redox potential of each salt, i.e., the species with the more positive reduction potential dominates on the surface.[101] It is unclear as of now the distribution of the two components and the thicknesses of the layers. The level of sophistication of mixed layer thiolate SAMs has not been achieved with diazonium chemistry.[44,90]

The grafting of aryl diazonium salts also can occur spontaneously, i.e., by immersing the substrate in a solution of an aryldiazonium salt, and it has been reported on carbon,[102,103] metals,[102,103] and semiconductors.[104] Spontaneous grafting widens the range of substrates that can be modified by aryl diazonium salts to poor conductors, nanostructured materials, and nanoparticles in suspension.[105–109] Additionally, spontaneous grafting is simple and convenient to scale-up for industrial production.[110] It is believed that a substrate with enough reducing potential provides the electrons necessary for the spontaneous reduction of the aryl diazonium cation via a redox reaction.[111] On glassy carbon (GC), carbon black, and pyrolyzed photoresist films (PPF), spontaneously grafted aryl films have been shown to have similar characteristics to those grafted electrochemically, but they generally are thinner and form more slowly.[111] Several parameters have been found to affect the spontaneous attachment, including immersion time, diazonium salt concentration, and solvents, as well as the nature of the substrate and the diazonium compound. The mechanism of the spontaneous grafting reaction is not as well understood as the electrochemical route.[111]

Immobilization of biomolecules[112–114] and formation of low fouling surfaces[115,116] on Au SPR chips has been demonstrated with electrochemical reduction of diazonium salts. The electrochemical deposition allows for localized functionalization.[117] The gold surface can be modified first with the diazonium salt, followed by attachment of the biomolecule.[112,114] Alternatively, an aniline derivative is conjugated to the antibody, followed by diazotation of the aniline-antibody conjugation and subsequent electrodeposition on the surface.[113] The harsh conditions

employed for diazotation (20 mM HCl and 20 mM $NaNO_2$ at ice cold temperature) may not be compatible with all proteins;[80] this can be circumvented by conjugating the aryl diazonium salt to the protein directly.[118] The application of spontaneously grafted aryl layers to immobilize biomolecules on SPR substrates remains unexplored, even though it potentially facilitates functionalization of multispot SPRi chips with various aryl diazonium salts and thus immobilization of the biorecognition element by simple drop-casting.

1.6 Thesis Outline

This thesis demonstrates the viability of employing carbon-on-metal substrates and spontaneous grafting of aryldiazonium salts to improve the sensitivity and long-term stability of SPR-based biosensors. Combination of carbon-on-metal films and spontaneously adsorbed diazonium layers can be a potential alternative to thiolate SAMs on Au for SPR sensing.

Chapter 2 thoroughly characterizes the physicochemical properties of carbon-on-gold films prepared by electron-beam evaporation. Specifically, carbon microstructure, O/C ratio, wettability, and roughness were probed. In addition, the electroanalytical performance of carbon-on-gold electrodes was highlighted, focusing on potential window, capacitance, electron-transfer rates, adsorption, and stability. Such information is crucial in guiding and understanding the subsequent surface modification of these films, particularly by electrografting methods. The promising performance of carbon-on-gold electrodes should open the door to their applications in electrochemical and electrochemical SPR biosensors.

Chapter 3 explores surface modification of carbon-on-gold films by spontaneous grafting of aryldiazonium salts. The effects of deposition conditions, such as immersion time, solvent, aryldiazonium salt concentration, and para-substituent, on resulting adlayers were studied. A combination of spectroscopic and electrochemical techniques was employed to optimize grafting conditions as well as to understand the structure-reactivity relationships of carbon surfaces. Insights into the reaction mechanism and the nature of the surface–aryl layer bond also were

presented. Detail examination of spontaneous grafting of aryldiazonium sets the stage for its application in interfacial design for carbon-based SPR and electrochemical biosensors and beyond.

Chapter 4 demonstrates the feasibility of carbon-on-metal films as SPR substrates. The thickness of the carbon layer was varied, and the effects of carbon thicknesses on SPR sensitivity and pinhole density were investigated. A defect-free, well-adhered 2 nm thick eC film coating was deposited on goal and silver substrates. Notably, enhanced sensitivity was observed with carbon-on-silver substrates in comparison to the gold counterparts. Non-specific adsorption of proteins on carbon-on-gold films also was presented. A collection of techniques was employed to quantify and characterize adsorbed protein layers. The results obtained in this chapter pave the way for future studies on the development of carbon-based bioassays as well as novel non-fouling surface chemistry.

Chapter 5 reports an SPR-based immunoassay utilizing carbon-on-gold films as substrates and spontaneous grafting of aryldiazonium salts to immobilize biomolecules. The grafted aryl layers were characterized and used to immobilize biomolecules covalently, and their performance was compared with physical adsorption. Good SPR specific signal, regeneration potentialities, preserved biological activity of immobilized protein A, and favorable orientation of captured antibody were obtained. Selective patterning of the sensing surface also was demonstrated. The results show the viability of spontaneous grafting of aryl diazonium salts for facile immobilization of biomolecules on SPRi substrates. Based on the good demonstration results presented in this chapter and the inherent stability of the covalent aryl–surface bonds, spontaneous adsorption of diazonium salts can be a potential complement to the prevalent Au-SAM chemistry in the development of sensitive, stable SPR biosensors.

References

(1) Wood, R. W. XLII. *On a Remarkable Case of Uneven Distribution of Light in a Diffraction Grating Spectrum*. *Lond. Edinb. Dublin Philos. Mag. J. Sci.* **1902**, *4* (21), 396–402. https://doi.org/10.1080/14786440209462857.

(2) Fano, U. The Theory of Anomalous Diffraction Gratings and of Quasi-Stationary Waves on Metallic Surfaces (Sommerfeld's Waves). *J. Opt. Soc. Am.* **1941**, *31* (3), 213. https://doi.org/10.1364/JOSA.31.000213.

(3) Ritchie, R.; Arakawa, E.; Cowan, J.; Hamm, R. Surface-Plasmon Resonance Effect in Grating Diffraction. *Phys. Rev. Lett.* **1968**, *21* (22), 1530–1533. https://doi.org/10.1103/PhysRevLett.21.1530.

(4) Otto, A. Excitation of Nonradiative Surface Plasma Waves in Silver by the Method of Frustrated Total Reflection. *Z. Für Phys. Hadrons Nucl.* **1968**, *216* (4), 398–410. https://doi.org/10.1007/BF01391532.

(5) Kretschmann, E.; Raether, H. Radiative Decay of Non Radiative Surface Plasmons Excited by Light. *Z. Naturforschung Part -Astrophys. Phys. Phys. Chem.* **1968**, *23*, 2135–2136.

(6) Liedberg, B.; Nylander, C.; Lunström, I. Surface Plasmon Resonance for Gas Detection and Biosensing. *Sens. Actuators* **1983**, *4*, 299–304. https://doi.org/10.1016/0250-6874(83)85036-7.

(7) O'Shannessy, D. J.; Brigham-Burke, M.; Peck, K. Immobilization Chemistries Suitable for Use in the BlAcore Surface Plasmon Resonance Detector. *Anal. Biochem.* **1992**, *205*, 132–136.

(8) El-Sayed, I. H.; Huang, X.; El-Sayed, M. A. Surface Plasmon Resonance Scattering and Absorption of Anti-EGFR Antibody Conjugated Gold Nanoparticles in Cancer Diagnostics: Applications in Oral Cancer. *Nano Lett.* **2005**, *5* (5), 829–834. https://doi.org/10.1021/nl050074e.

(9) Frasconi, M.; Tortolini, C.; Botrè, F.; Mazzei, F. Multifunctional Au Nanoparticle Dendrimer-Based Surface Plasmon Resonance Biosensor and Its Application for Improved Insulin Detection. *Anal. Chem.* **2010**, *82* (17), 7335–7342. https://doi.org/10.1021/ac101319k.

(10) Bhatia, P.; Gupta, B. D. Fabrication and Characterization of a Surface Plasmon Resonance Based Fiber Optic Urea Sensor for Biomedical Applications. *Sens. Actuators B Chem.* **2012**, *161* (1), 434–438. https://doi.org/10.1016/j.snb.2011.10.056.

(11) Boozer, C.; Kim, G.; Cong, S.; Guan, H.; Londergan, T. Looking towards Label-Free Biomolecular Interaction Analysis in a High-Throughput Format: A Review of New Surface Plasmon Resonance Technologies. *Curr. Opin. Biotechnol.* **2006**, *17* (4), 400–405. https://doi.org/10.1016/j.copbio.2006.06.012.

(12) Jeong, J.-A.; Kim, H.-K. Low Resistance and Highly Transparent ITO–Ag–ITO Multilayer Electrode Using Surface Plasmon Resonance of Ag Layer for Bulk-Heterojunction Organic Solar Cells. *Sol. Energy Mater. Sol. Cells* **2009**, *93* (10), 1801–1809. https://doi.org/10.1016/j.solmat.2009.06.014.

(13) Kim, J.; Choi, H.; Nahm, C.; Park, B. Surface-Plasmon Resonance for Photoluminescence and Solar-Cell Applications. *Electron. Mater. Lett.* **2012**, *8* (4), 351–364. https://doi.org/10.1007/s13391-012-2117-8.

(14) Sadrolhosseini, A. R.; Moksin, M. M.; Yunus, W. M. M.; Talib, Z. A.; Abdi, M. M. Surface Plasmon Resonance Detection of Copper Corrosion in Biodiesel Using Polypyrrole-Chitosan Layer Sensor. *Opt. Rev.* **2011**, *18* (4), 331–337. https://doi.org/10.1007/s10043-011-0064-5.

(15) Qiao, L.; Wang, D.; Zuo, L.; Ye, Y.; Qian, J.; Chen, H.; He, S. Localized Surface Plasmon Resonance Enhanced Organic Solar Cell with Gold Nanospheres. *Appl. Energy* **2011**, *88* (3), 848–852. https://doi.org/10.1016/j.apenergy.2010.09.021.

(16) Golub, E.; Pelossof, G.; Freeman, R.; Zhang, H.; Willner, I. Electrochemical, Photoelectrochemical, and Surface Plasmon Resonance Detection of Cocaine Using Supramolecular Aptamer Complexes and Metallic or Semiconductor Nanoparticles. *Anal. Chem.* **2009**, *81* (22), 9291–9298. https://doi.org/10.1021/ac901551q.

(17) Riskin, M.; Tel-Vered, R.; Lioubashevski, O.; Willner, I. Ultrasensitive Surface Plasmon Resonance Detection of Trinitrotoluene by a Bis-Aniline-Cross-Linked Au Nanoparticles Composite. *J. Am. Chem. Soc.* **2009**, *131* (21), 7368–7378. https://doi.org/10.1021/ja9001212.

(18) Lu, X.; Zheng, H.; Li, X.-Q.; Yuan, X.-X.; Li, H.; Deng, L.-G.; Zhang, H.; Wang, W.-Z.; Yang, G.-S.; Meng, M.; Xi, R.-M.; Aboul-Enein, H. Y. Detection of Ractopamine Residues in Pork by Surface Plasmon Resonance-Based Biosensor Inhibition Immunoassay. *Food Chem.* **2012**, *130* (4), 1061–1065. https://doi.org/10.1016/j.foodchem.2011.07.133.

(19) Li, Y.; Liu, X.; Lin, Z. Recent Developments and Applications of Surface Plasmon Resonance Biosensors for the Detection of Mycotoxins in Foodstuffs. *Food Chem.* **2012**, *132* (3), 1549–1554. https://doi.org/10.1016/j.foodchem.2011.10.109.

(20) Kreno, L. E.; Hupp, J. T.; Van Duyne, R. P. Metal−Organic Framework Thin Film for Enhanced Localized Surface Plasmon Resonance Gas Sensing. *Anal. Chem.* **2010**, *82* (19), 8042–8046. https://doi.org/10.1021/ac102127p.

(21) Homola, J. Surface Plasmon Resonance Sensors for Detection of Chemical and Biological Species. *Chem. Rev.* **2008**, *108* (2), 462–493. https://doi.org/10.1021/cr068107d.

(22) Wijaya, E.; Lenaerts, C.; Maricot, S.; Hastanin, J.; Habraken, S.; Vilcot, J.-P.; Boukherroub, R.; Szunerits, S. Surface Plasmon Resonance-Based Biosensors: From the Development of Different SPR Structures to Novel Surface Functionalization Strategies. *Curr. Opin. Solid State Mater. Sci.* **2011**, *15* (5), 208–224. https://doi.org/10.1016/j.cossms.2011.05.001.

(23) Zayats, A. V.; Smolyaninov, I. I.; Maradudin, A. A. Nano-Optics of Surface Plasmon Polaritons. *Phys. Rep.* **2005**, *408* (3–4), 131–314. https://doi.org/10.1016/j.physrep.2004.11.001.

(24) Homola, J.; Yee, S. S.; Gauglitz, G. Surface Plasmon Resonance Sensors: Review. *Sens. Actuators B Chem.* **1999**, *54* (1–2), 3–15. https://doi.org/10.1016/S0925-4005(98)00321-9.

(25) Homola, J. *Surface Plasmon Resonance Based Sensors*; Springer: Berlin, Germany, 2006.

(26) Frutos, A. G.; Corn, R. M. SPR of Ultrathin Organic Films. *Anal. Chem.* **1998**, *70* (13), 449A-455A. https://doi.org/10.1021/ac981909r.

(27) Ritzefeld, M.; Sewald, N. Real-Time Analysis of Specific Protein-DNA Interactions with Surface Plasmon Resonance. *J. Amino Acids* **2012**, *2012*, 1–19. https://doi.org/10.1155/2012/816032.

(28) Nuzzo, R. G.; Allara, D. L. Adsorption of Bifunctional Organic Disulfides on Gold Surfaces. *J. Am. Chem. Soc.* **1983**, *105* (13), 4481–4483. https://doi.org/10.1021/ja00351a063.

(29) Vericat, C.; Vela, M. E.; Benitez, G.; Carro, P.; Salvarezza, R. C. Self-Assembled Monolayers of Thiols and Dithiols on Gold: New Challenges for a Well-Known System. *Chem. Soc. Rev.* **2010**, *39* (5), 1805. https://doi.org/10.1039/b907301a.

(30) Harris, A. L.; Rothberg, L.; Dubois, L. H.; Levinos, N. J.; Dhar, L. Molecular Vibrational Energy Relaxation at a Metal Surface: Methyl Thiolate on Ag(111). *Phys. Rev. Lett.* **1990**, *64* (17), 2086–2089. https://doi.org/10.1103/PhysRevLett.64.2086.

(31) Azzaroni, O.; Vela, M. E.; Fonticelli, M.; Benítez, G.; Carro, P.; Blum, B.; Salvarezza, R. C. Electrodesorption Potentials of Self-Assembled Alkanethiolate Monolayers on Copper Electrodes. An Experimental and Theoretical Study. *J. Phys. Chem. B* **2003**, *107* (48), 13446–13454. https://doi.org/10.1021/jp036319y.

(32) Love, J. C.; Wolfe, D. B.; Haasch, R.; Chabinyc, M. L.; Paul, K. E.; Whitesides, G. M.; Nuzzo, R. G. Formation and Structure of Self-Assembled Monolayers of Alkanethiolates on Palladium. 13.

(33) Williams, J. A.; Gorman, C. B. Alkanethiol Reductive Desorption from Self-Assembled Monolayers on Gold, Platinum, and Palladium Substrates. *J. Phys. Chem. C* **2007**, *111* (34), 12804–12810. https://doi.org/10.1021/jp072869a.

(34) Mekhalif, Z.; Riga, J.; Pireaux, J.-J.; Delhalle, J. Self-Assembled Monolayers of *n* -Dodecanethiol on Electrochemically Modified Polycrystalline Nickel Surfaces. *Langmuir* **1997**, *13* (8), 2285–2290. https://doi.org/10.1021/la960528a.

(35) Pirlot, C.; Delhalle, J.; Pireaux, J. J.; Mekhalif, Z. Surface Modification of Polycrystalline Iron Surfaces by N-Dodecanethiol: An XPS Investigation. *Surf. Coat. Technol.* **2001**, *138* (2–3), 166–172. https://doi.org/10.1016/S0257-8972(00)01130-0.

(36) Bain, C. D.; Troughton, E. B.; Tao, Y. T.; Evall, J.; Whitesides, G. M.; Nuzzo, R. G. Formation of Monolayer Films by the Spontaneous Assembly of Organic Thiols from Solution onto Gold. *J. Am. Chem. Soc.* **1989**, *111* (1), 321–335. https://doi.org/10.1021/ja00183a049.

(37) Bertilsson, L.; Liedberg, B. Infrared Study of Thiol Monolayer Assemblies on Gold: Preparation, Characterization, and Functionalization of Mixed Monolayers. *Langmuir* **1993**, *9* (1), 141–149. https://doi.org/10.1021/la00025a032.

(38) Gooding, J. J.; Mearns, F.; Yang, W.; Liu, J. Self-Assembled Monolayers into the 21st Century: Recent Advances and Applications. *Electroanalysis* **2003**, *15* (2), 81–96. https://doi.org/10.1002/elan.200390017.

(39) Jung, L. S.; Nelson, K. E.; Stayton, P. S.; Campbell, C. T. Binding and Dissociation Kinetics of Wild-Type and Mutant Streptavidins on Mixed Biotin-Containing Alkylthiolate Monolayers. *Langmuir* **2000**, *16* (24), 9421–9432. https://doi.org/10.1021/la000144r.

(40) Nelson, K. E.; Gamble, L.; Jung, L. S.; Boeckl, M. S.; Naeemi, E.; Golledge, S. L.; Sasaki, T.; Castner, D. G.; Campbell, C. T.; Stayton, P. S. Surface Characterization of Mixed Self-Assembled Monolayers Designed for Streptavidin Immobilization. *Langmuir* **2001**, *17* (9), 2807–2816. https://doi.org/10.1021/la001111e.

(41) Ulman, A. Formation and Structure of Self-Assembled Monolayers. *Chem. Rev.* **1996**, *96* (4), 1533–1554. https://doi.org/10.1021/cr9502357.

(42) Dubois, L. H.; Nuzzo, R. G. Synthesis, Structure, and Properties of Model Organic Surfaces. *Annu. Rev. Phys. Chem.* **1992**, *43* (1), 437–463. https://doi.org/10.1146/annurev.pc.43.100192.002253.

(43) Porter, M. D.; Bright, T. B.; Allara, D. L.; Chidsey, C. E. D. Spontaneously Organized Molecular Assemblies. 4. Structural Characterization of n-Alkyl Thiol Monolayers on Gold by Optical Ellipsometry, Infrared Spectroscopy, and Electrochemistry. *J. Am. Chem. Soc.* **1987**, *109* (12), 3559–3568. https://doi.org/10.1021/ja00246a011.

(44) Gooding, J. J.; Ciampi, S. The Molecular Level Modification of Surfaces: From Self-Assembled Monolayers to Complex Molecular Assemblies. *Chem. Soc. Rev.* **2011**, *40* (5), 2704. https://doi.org/10.1039/c0cs00139b.

(45) Losic, D.; Gooding, J. J.; Shapter, J. G.; Hibbert, D. B.; Short, K. The Influence of the Underlying Gold Substrate on Glucose Oxidase Electrodes Fabricated Using Self-Assembled Monolayers. *Electroanalysis* **2001**, *13* (17), 1385–1393. https://doi.org/10.1002/1521-4109(200111)13:17<1385::AID-ELAN1385>3.0.CO;2-L.

(46) Losic, D.; Shapter, J. G.; Gooding, J. J. Influence of Surface Topography on Alkanethiol SAMs Assembled from Solution and by Microcontact Printing. *Langmuir* **2001**, *17* (11), 3307–3316. https://doi.org/10.1021/la001462t.

(47) Wong, S.-S.; Porter, M. D. Origin of the Multiple Voltammetric Desorption Waves of Long-Chain Alkanethiolate Monolayers Chemisorbed on Annealed Gold Electrodes. *J. Electroanal. Chem.* **2000**, *485* (2), 135–143. https://doi.org/10.1016/S0022-0728(00)00106-6.

(48) Yang, G.; Amro, N. A.; Starkewolfe, Z. B.; Liu, G. Molecular-Level Approach To Inhibit Degradations of Alkanethiol Self-Assembled Monolayers in Aqueous Media. *Langmuir* **2004**, *20* (10), 3995–4003. https://doi.org/10.1021/la0499160.

(49) Cortés, E.; Rubert, A. A.; Benitez, G.; Carro, P.; Vela, M. E.; Salvarezza, R. C. Enhanced Stability of Thiolate Self-Assembled Monolayers (SAMs) on Nanostructured Gold Substrates. *Langmuir* **2009**, *25* (10), 5661–5666. https://doi.org/10.1021/la804251a.

(50) Hutt, D. A.; Leggett, G. J. Influence of Adsorbate Ordering on Rates of UV Photooxidation of Self-Assembled Monolayers. *J. Phys. Chem.* **1996**, *100* (16), 6657–6662. https://doi.org/10.1021/jp952734h.

(51) Cooper, E.; Leggett, G. J. Static Secondary Ion Mass Spectrometry Studies of Self-Assembled Monolayers: Influence of Adsorbate Chain Length and Terminal Functional Group on Rates of Photooxidation of Alkanethiols on Gold. *Langmuir* **1998**, *14* (17), 4795–4801. https://doi.org/10.1021/la9802567.

(52) English, R. D.; Van Stipdonk, M. J.; Sabapathy, R. C.; Crooks, R. M.; Schweikert, E. A. Characterization of Photooxidized Self-Assembled Monolayers and Bilayers by Spontaneous Desorption Mass Spectrometry. *Anal. Chem.* **2000**, *72* (24), 5973–5980. https://doi.org/10.1021/ac0008892.

(53) Everett, W. Russell.; Welch, T. L.; Reed, Laura.; Fritsch-Faules, Ingrid. Potential-Dependent Stability of Self-Assembled Organothiols on Gold Electrodes in Methylene Chloride. *Anal. Chem.* **1995**, *67* (2), 292–298. https://doi.org/10.1021/ac00098a010.

(54) Finklea, H. O.; Avery, S.; Lynch, M.; Furtsch, T. Blocking Oriented Monolayers of Alkyl Mercaptans on Gold Electrodes. *Langmuir* **1987**, *3* (3), 409–413. https://doi.org/10.1021/la00075a024.

(55) Garg, N.; Carrasquillo-Molina, E.; Lee, T. R. Self-Assembled Monolayers Composed of Aromatic Thiols on Gold: Structural Characterization and Thermal Stability in Solution. *Langmuir* **2002**, *18* (7), 2717–2726. https://doi.org/10.1021/la0115278.

(56) Ulman, A. *An Introduction to Ultrathin Organic Films: From Langmuir-Blodgett to Self-Assembly*; Academic Press: Boston, MA, 1991.

(57) Franzen, S. Surface Plasmon Polaritons and Screened Plasma Absorption in Indium Tin Oxide Compared to Silver and Gold. *J. Phys. Chem. C* **2008**, *112* (15), 6027–6032. https://doi.org/10.1021/jp7097813.

(58) Liu, H.; Wang, B.; Leong, E. S. P.; Yang, P.; Zong, Y.; Si, G.; Teng, J.; Maier, S. A. Enhanced Surface Plasmon Resonance on a Smooth Silver Film with a Seed Growth Layer. *ACS Nano* **2010**, *4* (6), 3139–3146. https://doi.org/10.1021/nn100466p.

(59) Couture, M.; Zhao, S. S.; Masson, J.-F. Modern Surface Plasmon Resonance for Bioanalytics and Biophysics. *Phys. Chem. Chem. Phys.* **2013**, *15* (27), 11190. https://doi.org/10.1039/c3cp50281c.

(60) Kambhampati, D. K.; Jakob, T. A. M.; Robertson, J. W.; Cai, M.; Pemberton, J. E.; Knoll, W. Novel Silicon Dioxide Sol−Gel Films for Potential Sensor Applications: A Surface Plasmon Resonance Study. *Langmuir* **2001**, *17* (4), 1169–1175. https://doi.org/10.1021/la001250w.

(61) Phillips, K. S.; Han, J.-H.; Martinez, M.; Wang, Z.; Carter, D.; Cheng, Q. Nanoscale Glassification of Gold Substrates for Surface Plasmon Resonance Analysis of Protein Toxins with Supported Lipid Membranes. *Anal. Chem.* **2006**, *78* (2), 596–603. https://doi.org/10.1021/ac051644y.

(62) Satriano, C.; Marletta, G.; Kasemo, B. Oxygen Plasma-Induced Conversion of Polysiloxane into Hydrophilic and Smooth SiO_x Surfaces: Hydrophilic and Smooth SiO_x Surfaces by O_2 Plasma of Polysiloxane. *Surf. Interface Anal.* **2008**, *40* (3–4), 649–656. https://doi.org/10.1002/sia.2764.

(63) Satriano, C.; Edvardsson, M.; Ohlsson, G.; Wang, G.; Svedhem, S.; Kasemo, B. Plasma Oxidized Polyhydroxymethylsiloxane—A New Smooth Surface for Supported Lipid Bilayer Formation. *Langmuir* **2010**, *26* (8), 5715–5725. https://doi.org/10.1021/la903826d.

(64) Szunerits, S.; Boukherroub, R. Electrochemical Investigation of Gold/Silica Thin Film Interfaces for Electrochemical Surface Plasmon Resonance Studies.

Electrochem. Commun. **2006**, *8* (3), 439–444. https://doi.org/10.1016/j.elecom.2006.01.006.

(65) Phillips, K. S.; Wilkop, T.; Wu, J.-J.; Al-Kaysi, R. O.; Cheng, Q. Surface Plasmon Resonance Imaging Analysis of Protein-Receptor Binding in Supported Membrane Arrays on Gold Substrates with Calcinated Silicate Films. *J. Am. Chem. Soc.* **2006**, *128* (30), 9590–9591. https://doi.org/10.1021/ja0628102.

(66) Gifford, L. K.; Sendroiu, I. E.; Corn, R. M.; Lupták, A. Attomole Detection of Mesophilic DNA Polymerase Products by Nanoparticle-Enhanced Surface Plasmon Resonance Imaging on Glassified Gold Surfaces. *J. Am. Chem. Soc.* **2010**, *132* (27), 9265–9267. https://doi.org/10.1021/ja103043p.

(67) Manesse, M.; Stambouli, V.; Boukherroub, R.; Szunerits, S. Electrochemical Impedance Spectroscopy and Surface Plasmon Resonance Studies of DNA Hybridization on Gold/SiOx Interfaces. *The Analyst* **2008**, *133* (8), 1097. https://doi.org/10.1039/b804825h.

(68) Manesse, M.; Sanjines, R.; Stambouli, V.; Boukherroub, R.; Szunerits, S. Preparation and Characterization of Antimony-Doped SnO2 Thin Films on Gold and Silver Substrates for Electrochemical and Surface Plasmon Resonance Studies. *Electrochem. Commun.* **2008**, *10* (7), 1041–1043. https://doi.org/10.1016/j.elecom.2008.04.036.

(69) Szunerits, S.; Castel, X.; Boukherroub, R. Surface Plasmon Resonance Investigation of Silver and Gold Films Coated with Thin Indium Tin Oxide Layers: Influence on Stability and Sensitivity. *J. Phys. Chem. C* **2008**, *112* (40), 15813–15817. https://doi.org/10.1021/jp8049137.

(70) Szunerits, S.; Castel, X.; Boukherroub, R. Preparation of Electrochemical and Surface Plasmon Resonance Active Interfaces: Deposition of Indium Tin Oxide on Silver Thin Films. *J. Phys. Chem. C* **2008**, *112* (29), 10883–10888. https://doi.org/10.1021/jp8025682.

(71) Sun, B.; Colavita, P. E.; Kim, H.; Lockett, M.; Marcus, M. S.; Smith, L. M.; Hamers, R. J. Covalent Photochemical Functionalization of Amorphous Carbon Thin Films for Integrated Real-Time Biosensing. *Langmuir* **2006**, *22* (23), 9598–9605. https://doi.org/10.1021/la061749b.

(72) Bélanger, D.; Pinson, J. Electrografting: A Powerful Method for Surface Modification. *Chem. Soc. Rev.* **2011**, *40* (7), 3995. https://doi.org/10.1039/c0cs00149j.

(73) Lockett, M. R.; Weibel, S. C.; Phillips, M. F.; Shortreed, M. R.; Sun, B.; Corn, R. M.; Hamers, R. J.; Cerrina, F.; Smith, L. M. Carbon-on-Metal Films for Surface Plasmon Resonance Detection of DNA Arrays. *J. Am. Chem. Soc.* **2008**, *130* (27), 8611–8613. https://doi.org/10.1021/ja802454c.

(74) Lockett, M. R.; Smith, L. M. Fabrication and Characterization of DNA Arrays Prepared on Carbon-on-Metal Substrates. *Anal. Chem.* **2009**, *81* (15), 6429–6437. https://doi.org/10.1021/ac900807q.

(75) Touahir, L.; Niedziółka-Jönsson, J.; Galopin, E.; Boukherroub, R.; Gouget-Laemmel, A. C.; Solomon, I.; Petukhov, M.; Chazalviel, J.-N.; Ozanam, F.; Szunerits, S. Surface Plasmon Resonance on Gold and Silver Films Coated

with Thin Layers of Amorphous Silicon−Carbon Alloys. *Langmuir* **2010**, *26* (8), 6058–6065. https://doi.org/10.1021/la903896m.

(76) Szunerits, S.; Maalouli, N.; Wijaya, E.; Vilcot, J.-P.; Boukherroub, R. Recent Advances in the Development of Graphene-Based Surface Plasmon Resonance (SPR) Interfaces. *Anal. Bioanal. Chem.* **2013**, *405* (5), 1435–1443. https://doi.org/10.1007/s00216-012-6624-0.

(77) Oznuluer, T.; Pince, E.; Polat, E. O.; Balci, O.; Salihoglu, O.; Kocabas, C. Synthesis of Graphene on Gold. *Appl. Phys. Lett.* **2011**, *98* (18), 183101. https://doi.org/10.1063/1.3584006.

(78) Wu, L.; Chu, H. S.; Koh, W. S.; Li, E. P. Highly Sensitive Graphene Biosensors Based on Surface Plasmon Resonance. *Opt. Express* **2010**, *18* (14), 14395. https://doi.org/10.1364/OE.18.014395.

(79) Choi, S. H.; Kim, Y. L.; Byun, K. M. Graphene-on-Silver Substrates for Sensitive Surface Plasmon Resonance Imaging Biosensors. *Opt. Express* **2011**, *19* (2), 458. https://doi.org/10.1364/OE.19.000458.

(80) Gooding, J. J. Advances in Interfacial Design for Electrochemical Biosensors and Sensors: Aryl Diazonium Salts for Modifying Carbon and Metal Electrodes. *Electroanalysis* **2008**, *20* (6), 573–582. https://doi.org/10.1002/elan.200704124.

(81) Shewchuk, D. M.; McDermott, M. T. Comparison of Diazonium Salt Derived and Thiol Derived Nitrobenzene Layers on Gold. *Langmuir* **2009**, *25* (8), 4556–4563. https://doi.org/10.1021/la8040083.

(82) Delamar, M.; Hitmi, R.; Pinson, J.; Saveant, J. M. Covalent Modification of Carbon Surfaces by Grafting of Functionalized Aryl Radicals Produced from Electrochemical Reduction of Diazonium Salts. *J. Am. Chem. Soc.* **1992**, *114* (14), 5883–5884. https://doi.org/10.1021/ja00040a074.

(83) Liu, Y.-C.; McCreery, R. L. Reactions of Organic Monolayers on Carbon Surfaces Observed with Unenhanced Raman Spectroscopy. *J. Am. Chem. Soc.* **1995**, *117* (45), 11254–11259. https://doi.org/10.1021/ja00150a024.

(84) Anariba, F.; DuVall, S. H.; McCreery, R. L. Mono- and Multilayer Formation by Diazonium Reduction on Carbon Surfaces Monitored with Atomic Force Microscopy "Scratching." *Anal. Chem.* **2003**, *75* (15), 3837–3844. https://doi.org/10.1021/ac034026v.

(85) Downard, A. J. Potential-Dependence of Self-Limited Films Formed by Reduction of Aryldiazonium Salts at Glassy Carbon Electrodes. *Langmuir* **2000**, *16* (24), 9680–9682. https://doi.org/10.1021/la000866i.

(86) Brooksby, P. A.; Downard, A. J. Electrochemical and Atomic Force Microscopy Study of Carbon Surface Modification via Diazonium Reduction in Aqueous and Acetonitrile Solutions. *Langmuir* **2004**, *20* (12), 5038–5045. https://doi.org/10.1021/la049616i.

(87) Downard, A. J.; Prince, M. J. Barrier Properties of Organic Monolayers on Glassy Carbon Electrodes. *Langmuir* **2001**, *17* (18), 5581–5586. https://doi.org/10.1021/la010499q.

(88) Downard, A. J. Electrochemically Assisted Covalent Modification of Carbon Electrodes. *Electroanalysis* **2000**, *12* (14), 1085–1096.

https://doi.org/10.1002/1521-4109(200010)12:14<1085::AID-ELAN1085>3.0.CO;2-A.

(89) Louault, C.; D'Amours, M.; Bélanger, D. The Electrochemical Grafting of a Mixture of Substituted Phenyl Groups at a Glassy Carbon Electrode Surface. *ChemPhysChem* **2008**, *9* (8), 1164–1170. https://doi.org/10.1002/cphc.200800016.

(90) Jiang, C.; Moraes Silva, S.; Fan, S.; Wu, Y.; Alam, M. T.; Liu, G.; Justin Gooding, J. Aryldiazonium Salt Derived Mixed Organic Layers: From Surface Chemistry to Their Applications. *J. Electroanal. Chem.* **2017**, *785*, 265–278. https://doi.org/10.1016/j.jelechem.2016.11.043.

(91) Mahouche-Chergui, S.; Gam-Derouich, S.; Mangeney, C.; Chehimi, M. M. Aryl Diazonium Salts: A New Class of Coupling Agents for Bonding Polymers, Biomacromolecules and Nanoparticles to Surfaces. *Chem. Soc. Rev.* **2011**, *40* (7), 4143. https://doi.org/10.1039/c0cs00179a.

(92) Pinson, J.; Podvorica, F. Attachment of Organic Layers to Conductive or Semiconductive Surfaces by Reduction of Diazonium Salts. *Chem. Soc. Rev.* **2005**, *34* (5), 429. https://doi.org/10.1039/b406228k.

(93) Ceccato, M.; Bousquet, A.; Hinge, M.; Pedersen, S. U.; Daasbjerg, K. Using a Mediating Effect in the Electroreduction of Aryldiazonium Salts To Prepare Conducting Organic Films of High Thickness. *Chem. Mater.* **2011**, *23* (6), 1551–1557. https://doi.org/10.1021/cm1033244.

(94) Combellas, C.; Kanoufi, F.; Pinson, J.; Podvorica, F. I. Sterically Hindered Diazonium Salts for the Grafting of a Monolayer on Metals. *J. Am. Chem. Soc.* **2008**, *130* (27), 8576–8577. https://doi.org/10.1021/ja8018912.

(95) Chrétien, J.-M.; Ghanem, M. A.; Bartlett, P. N.; Kilburn, J. D. Covalent Tethering of Organic Functionality to the Surface of Glassy Carbon Electrodes by Using Electrochemical and Solid-Phase Synthesis Methodologies. *Chem. - Eur. J.* **2008**, *14* (8), 2548–2556. https://doi.org/10.1002/chem.200701559.

(96) McCreery, R. L. Advanced Carbon Electrode Materials for Molecular Electrochemistry. *Chem. Rev.* **2008**, *108* (7), 2646–2687. https://doi.org/10.1021/cr068076m.

(97) de la Llave, E.; Ricci, A.; Calvo, E. J.; Scherlis, D. A. Binding between Carbon and the Au(111) Surface and What Makes It Different from the S−Au(111) Bond. *J. Phys. Chem. C* **2008**, *112* (45), 17611–17617. https://doi.org/10.1021/jp8036395.

(98) Allongue, P.; Delamar, M.; Desbat, B.; Fagebaume, O.; Hitmi, R.; Pinson, J.; Savéant, J.-M. Covalent Modification of Carbon Surfaces by Aryl Radicals Generated from the Electrochemical Reduction of Diazonium Salts. *J. Am. Chem. Soc.* **1997**, *119* (1), 201–207. https://doi.org/10.1021/ja963354s.

(99) D'Amours, M.; Bélanger, D. Stability of Substituted Phenyl Groups Electrochemically Grafted at Carbon Electrode Surface. *J. Phys. Chem. B* **2003**, *107* (20), 4811–4817. https://doi.org/10.1021/jp027223r.

(100) Ruffien, A.; Dequaire, M.; Brossier, P. Covalent Immobilization of Oligonucleotides on P-Aminophenyl-Modified Carbon Screen-Printed Electrodes for Viral DNA Sensing. *Chem. Commun.* **2003**, No. 7, 912–913. https://doi.org/10.1039/b300439b.

(101) Jiang, C.; Alam, M. T.; Parker, S. G.; Darwish, N.; Gooding, J. J. Strategies To Achieve Control over the Surface Ratio of Two Different Components on Modified Electrodes Using Aryldiazonium Salts. *Langmuir* **2016**, *32* (10), 2509–2517. https://doi.org/10.1021/acs.langmuir.5b04550.

(102) Adenier, A.; Cabet-Deliry, E.; Chaussé, A.; Griveau, S.; Mercier, F.; Pinson, J.; Vautrin-Ul, C. Grafting of Nitrophenyl Groups on Carbon and Metallic Surfaces without Electrochemical Induction. *Chem. Mater.* **2005**, *17* (3), 491–501. https://doi.org/10.1021/cm0490625.

(103) Adenier, A.; Barré, N.; Cabet-Deliry, E.; Chaussé, A.; Griveau, S.; Mercier, F.; Pinson, J.; Vautrin-Ul, C. Study of the Spontaneous Formation of Organic Layers on Carbon and Metal Surfaces from Diazonium Salts. *Surf Sci* **2006**, *600* (21), 4801–4812. https://doi.org/10.1016/j.susc.2006.07.061.

(104) de Villeneuve, C. H.; Pinson, J.; Bernard, M. C.; Allongue, P. Electrochemical Formation of Close-Packed Phenyl Layers on Si(111). *J. Phys. Chem. B* **1997**, *101* (14), 2415–2420. https://doi.org/10.1021/jp962581d.

(105) Ghosh, D.; Chen, S. Solid-State Electronic Conductivity of Ruthenium Nanoparticles Passivated by Metal–Carbon Covalent Bonds. *Chem. Phys. Lett.* **2008**, *465* (1–3), 115–119. https://doi.org/10.1016/j.cplett.2008.09.066.

(106) Ghosh, D.; Pradhan, S.; Chen, W.; Chen, S. Titanium Nanoparticles Stabilized by Ti−C Covalent Bonds. *Chem. Mater.* **2008**, *20* (4), 1248–1250. https://doi.org/10.1021/cm703423k.

(107) Griffete, N.; Herbst, F.; Pinson, J.; Ammar, S.; Mangeney, C. Preparation of Water-Soluble Magnetic Nanocrystals Using Aryl Diazonium Salt Chemistry. *J. Am. Chem. Soc.* **2011**, *133* (6), 1646–1649. https://doi.org/10.1021/ja108928b.

(108) Laurentius, L.; Stoyanov, S. R.; Gusarov, S.; Kovalenko, A.; Du, R.; Lopinski, G. P.; McDermott, M. T. Diazonium-Derived Aryl Films on Gold Nanoparticles: Evidence for a Carbon–Gold Covalent Bond. *ACS Nano* **2011**, *5* (5), 4219–4227. https://doi.org/10.1021/nn201110r.

(109) Mirkhalaf, F.; Paprotny, J.; Schiffrin, D. J. Synthesis of Metal Nanoparticles Stabilized by Metal−Carbon Bonds. *J. Am. Chem. Soc.* **2006**, *128* (23), 7400–7401. https://doi.org/10.1021/ja058687g.

(110) Assresahegn, B. D.; Brousse, T.; Bélanger, D. Advances on the Use of Diazonium Chemistry for Functionalization of Materials Used in Energy Storage Systems. *Carbon* **2015**, *92*, 362–381. https://doi.org/10.1016/j.carbon.2015.05.030.

(111) Barrière, F.; Downard, A. J. Covalent Modification of Graphitic Carbon Substrates by Non-Electrochemical Methods. *J. Solid State Electrochem.* **2008**, *12* (10), 1231–1244. https://doi.org/10.1007/s10008-008-0526-2.

(112) Mandon, C. A.; Blum, L. J.; Marquette, C. A. Aryl Diazonium for Biomolecules Immobilization onto SPRi Chips. *ChemPhysChem* **2009**, *10* (18), 3273–3277. https://doi.org/10.1002/cphc.200900599.

(113) Corgier, B. P.; Bellon, S.; Anger-Leroy, M.; Blum, L. J.; Marquette, C. A. Protein−Diazonium Adduct Direct Electrografting onto SPRi-Biochip. *Langmuir* **2009**, *25* (16), 9619–9623. https://doi.org/10.1021/la900762s.

(114) Fioresi, F.; Rouleau, A.; Maximova, K.; Vieillard, J.; Boireau, W.; Caille, C. E.; Soulignac, C.; Zeggari, R.; Clamens, T.; Lesouhaitier, O.; Mofaddel, N.; Derf, F. L. Electrografting of Diazonium Salt for SPR Application. *Mater. Today Proc.* **2019**, *6*, 340–344. https://doi.org/10.1016/j.matpr.2018.10.428.

(115) Menegazzo, N.; Zou, Q.; Booksh, K. S. Characterization of Electrografted 4-Aminophenylalanine Layers for Low Non-Specific Binding of Proteins. *New J. Chem.* **2012**, *36* (4), 963. https://doi.org/10.1039/c2nj20930f.

(116) Gam-Derouich, S.; Gosecka, M.; Lepinay, S.; Turmine, M.; Carbonnier, B.; Basinska, T.; Slomkowski, S.; Millot, M.-C.; Othmane, A.; Ben Hassen-Chehimi, D.; Chehimi, M. M. Highly Hydrophilic Surfaces from Polyglycidol Grafts with Dual Antifouling and Specific Protein Recognition Properties. *Langmuir* **2011**, *27* (15), 9285–9294. https://doi.org/10.1021/la200290k.

(117) Harper, J. C.; Polsky, R.; Wheeler, D. R.; Dirk, S. M.; Brozik, S. M. Selective Immobilization of DNA and Antibody Probes on Electrode Arrays: Simultaneous Electrochemical Detection of DNA and Protein on a Single Platform. *Langmuir* **2007**, *23* (16), 8285–8287. https://doi.org/10.1021/la701775g.

(118) Polsky, R.; Harper, J. C.; Dirk, S. M.; Arango, D. C.; Wheeler, D. R.; Brozik, S. M. Diazonium-Functionalized Horseradish Peroxidase Immobilized via Addressable Electrodeposition: Direct Electron Transfer and Electrochemical Detection. *Langmuir* **2007**, *23* (2), 364–366. https://doi.org/10.1021/la062916a.

Chapter 2. Characterization of Carbon-on-Gold Films: Physicochemical Properties and Electrochemical Performance[a]

2.1 Introduction

Carbon materials have been used for more than a century in various electrochemical applications, such as electroanalysis, energy storage, and electrosynthesis, with often cited advantages, including a wide potential window, superior mechanical stability, and low cost.[1,2] Recently, disposable electrodes have received greater attention because of the rising need for on-spot, in situ monitoring, and point-of-care testing in biomedical, pharmaceutical, industrial, and environmental fields, where no pretreatment or cleaning between measurements is preferred.[3] Of particular interest are screen-printed carbon electrodes, which can be produced easily and massively using thick film technology.[3,4] However, these films often yield slow electron-transfer rates and widely varied analytical performance. This is due to the addition of polymeric binders and other additives to the carbon inks that tend to pacify the carbon particles in various ink formulations.[5,6]

Thin carbon film electrodes with high purity and fast electron kinetics have been developed to overcome the above-mentioned problems. These films are prepared by various fabrication processes, such as pyrolysis of organic films,[7,8] chemical vapor deposition of organic gases,[2,9,10] sputtering,[11–15] and electron-beam evaporation.[16–19] The bulk and surface chemistry of the films, which dictate their electrochemical performance, depend greatly on the fabrication procedure. For example, pyrolyzed photoresist film (PPF) is a disordered, sp^2 hybridized carbon material with a very flat surface [~0.5 nm root-mean-square (rms) roughness] and low surface oxide level compared to polished glassy carbon (GC).[8] Boron-doped diamond (BDD) thin films can be made by chemical vapor deposition from a mixture of methane and a source of boron, often B_2H_6 in hydrogen plasma.[2] BDD consists of sp^3-hybridized carbon atoms and has a rough, polycrystalline morphology, with grain

[a] The contents of this chapter have been copied and/or adapted from the following publication Nguyen, T. P.; McCreery, R. L.; McDermott, M. T. Evaluation of the Electroanalytical Performance of Carbon-on-Gold Films Prepared by Electron-Beam Evaporation. *The Analyst*, **2020**, *145*(14), 5041–5052.

boundaries at the surface and a small fraction of a nondiamond carbon impurity.[2] PPF and BDD electrodes exhibit electron-transfer rates for outer-sphere redox systems similar to polished GC, but they are less reactive to inner-sphere redox systems and have significantly lower capacitance and adsorption.[2,8,20]

Carbon films prepared by various sputtering methods, such as electron cyclotron resonance (ECR) and unbalanced magnetron sputtering, have been studied extensively by Niwa and co-workers. These carbon films, usually ~40 nm thick, can be deposited at room temperature with un ultraflat surface and tuneable sp^3/sp^2 ratios by varying deposition conditions; rms roughness ranging from 0.07–0.68 nm and sp^3 contents ranging from 13–53% were reported.[21,22] They generally exhibit a wide potential window, low background current, electron-transfer rates for $Ru(NH_3)_6^{3+/2+}$ and $Fe(CN)_6^{3-/4-}$ similar to polished GC, high stability, and lower adsorption.[22] Their high S/N, resulting from the low background current and suppression of electrode fouling by electroactive species without pretreatment, proved advantageous in detecting analytically important molecules, such as bisphenol A, alkylphenols, serotonin, and oligonucleotides.[12,22–24]

Electron-beam evaporation also has been used to produce thin, amorphous carbon films, with interesting properties and a wide range of applications.[16–19,25] Compared to sputtered films, evaporated films generally have significantly higher purity and, consequently, higher conductivity due to a lower inclusion of residual gaseous impurities.[26] Electron beam deposited carbon (eC) was investigated initially for use as transparent carbon electrodes.[17,18] Our group previously reported eC films deposited on highly doped silicon substrates. Very thin eC films (7 nm thick) exhibit a near atomic flat surface (rms roughness ~0.1 nm) and electron-transfer rates of several benchmark redox systems comparable to polished GC and PPF.[16] The recent use of eC to fabricate highly stable carbon-based molecular electronic devices has been reviewed by Sachan et al.[27] The inherently low conductivity of eC and resulting ohmic potential losses can be overcome by depositing eC on a thin layer of metal like Au.[25] A 10 nm eC layer on a 30 nm thick gold layer decreases the sheet resistance from 10^4–10^5 Ω/□ for eC alone to 1.05 Ω/□ for the eC/Au film.[25] Taking advantage of the extreme flatness and high conductivity of the eC/Au bilayer, Morteza Najarian et

al. studied electron-transfer kinetics on a multilayer $KCl_{1000}/eC_{10}/TiC_3/Au_{30}/Cr_3/Si/SiO_{x300}$ film electrode (subscripts indicate thicknesses in nm) by scanning electrochemical microscopy (SECM).[19] The KCl layer was deposited in-vacuo without exposure of the eC/Au film to air, then removed by dissolution in the aqueous electrolyte under study. Heterogeneous electron-transfer rates exceeding 14 cm/s and 6.9 cm/s were obtained for (ferrocenylmethyl)trimethylammonium ($FcTMA^+$) and $Ru(NH_3)_6^{3+}$ redox systems, which were and continue to be among the highest rate constants reported for carbon electrodes due partly to the multilayer film structure and to the SECM measurement method.[28–35]

In this chapter, we report the physical, chemical, and electrochemical characterization of 10 nm eC deposited directly onto an Au film (which will be referred to as eC/Au hereinafter). The direct contact between the eC and Au,[36,37] and the gold thickness of 42 nm are chosen with an eye towards future surface plasmon resonance (SPR) applications. Carbon-on-gold films have shown promise as SPR substrates.[37,38] A thin carbon overlayer can provide protection for the easily oxidized but more surface plasmon-active metals than gold such as silver to be used as SPR substrates.[36,37] Additionally, self-assembled monolayers (SAMs) of thiols have been the dominant surface chemistry on gold, but the gold-sulfur bond is susceptible to oxidation and photodecomposition.[39] The well-developed carbon-based chemistry, notably electrochemical grafting, is a powerful and robust alternative to SAMs.[40,41] The differences in substrate layer composition and film thicknesses relative to that examined by Morteza Najarian et al.[19] motivated us to explore our eC/Au films thoroughly. This chapter aims to characterize the electroanalytical performance of eC/Au electrodes with more commonly used electrochemical methods and to compare this performance to polished GC. Approaches that are common to characterize carbon electrodes were applied here to examine the electrochemical properties of eC/Au; surface properties, electron-transfer kinetics, adsorption, and stability were investigated. Benchmark redox systems, which previously have been classified according to the sensitivity of their electron transfer kinetics to the surface chemistry of a carbon electrode,[1] were used here to enable comparison between different carbon

electrodes. An understanding of the physicochemical and electrochemical properties of eC/Au should promote its use as a disposable electroanalytical material and electrochemical SPR substrate as well as broaden the surface chemistry for SPR substrates via electrochemical modifications.

2.2 Experimental

2.2.1 Chemicals and Materials

Concentrated sulfuric acid (95%–98%, Caledon); potassium chloride (ACS reagent, 99.0-100.5%, Aldrich); potassium ferricyanide (certified reagent, Caledon); dopamine hydrochloride (Aldrich); hexaammineruthenium(III) chloride (98%, Aldrich); ferrocene (98%, Aldrich); perchloric acid (70%, ACS reagent, Fisher); tetrabutylammonium tetrafluoroborate ($TBABF_4$) (99%, Aldrich); 2-propanol (certified ACS, Fisher); acetonitrile (for HPLC, gradient grade, ≥99.9%, Aldrich); acetone (ACS reagent, ≥99.5%, Aldrich); 9,10-phenanthrenequinone (PQ) (95%, Aldrich); sodium anthraquinone-2-sulfonate (AQMS) (HPLC, ≥ 98%, Aldrich); activated carbon (Caledon); and lead(II) oxide (certified, Fisher). All were used as received, except PQ was recrystallized from ethyl alcohol. Solutions were prepared fresh daily and purged with nitrogen gas for 10 min before use. Aqueous solutions were prepared with deionized water (DI) purified and deionized through a Barnstead E-Pure system (18.2 MΩ·cm, ThermoFisher).

2.2.2 Film Preparation

P-type, (100) oriented silicon wafers were diced into 1.3 × 1.85 cm^2 chips to serve as substrates. The substrates were cleaned by sonication in acetone, isopropyl alcohol, and DI water for 15 min each, dried with nitrogen gas, and loaded into the evaporation vacuum chamber (Kurt Lesker PVD 75). The chamber was pumped to a typical pressure of below 5×10^{-6} Torr and remained between 10^{-6} and 10^{-5} Torr during deposition. Layers shown in Figure 2-1A were deposited without breaking vacuum, with thicknesses and evaporation rates as follows: Cr adhesion layer (2 nm,

0.03 nm/s, Au (42 nm, 0.03 nm/s), and eC (10 nm, 0.01 nm/s). The target for eC deposition was spectroscopically pure graphite rods (SPI Supplies, PA). Evaporation rates and thicknesses were controlled with a quartz crystal microbalance.

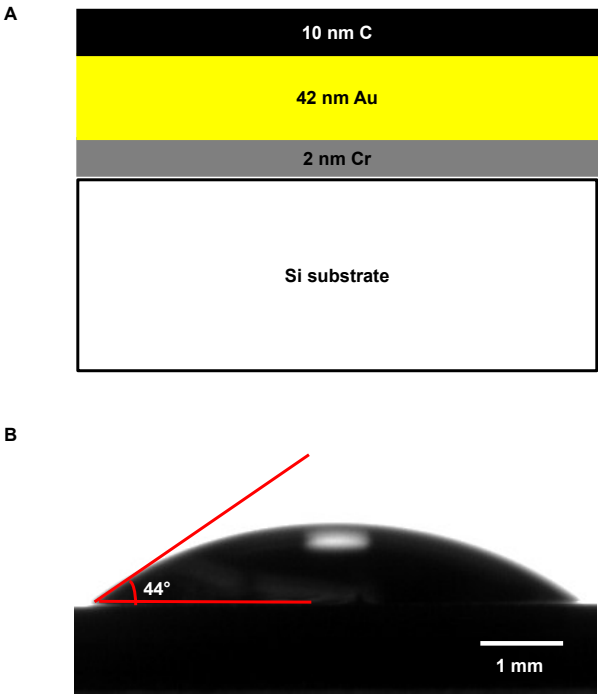

Figure 2-1. (A) Illustration of an eC/Au film with indicated thicknesses of deposited layers on Si substrate. (B) Representative static contact angle image of a 4 μL drop of DI water resting on a freshly prepared eC/Au film (~10 min of ambient air exposure).

2.2.3 Surface Characterization

Raman spectroscopy. Raman spectra were collected by a Renishaw InVia Raman microscope using an Ar excitation laser (514.5 nm) with 30 mW power through a 50× objective. The instrument was calibrated with a Si standard prior to use.

X-ray photoelectron spectroscopy (XPS). XPS spectra were collected at room temperature using a Kratos Axis (Ultra) spectrometer with monochromatized Al K_α (1486.71 eV) at nanoFAB. The spectrometer was calibrated by Au $4f_{7/2}$ binding energy (84.0 eV), with reference to the Fermi level. The analysis chamber pressure is lower than 5×10^{-10} Torr. CasaXPS software was used for atomic ratio calculations and component analysis. Note: Adventitious carbon was likely present and thus complicated the interpretation of C 1s spectra.

Water contact angle. Water contact angles were measured with a 4 μL droplet using a Ráme-Hart goniometer (model 590) equipped with DROPimage advanced software. The reported values were averages of two measurements on different areas of each sample (N = 3).

Atomic force microscopy (AFM). Surface roughness was characterized by AFM using a Veeco/Digital Instruments Multi-Mode NanoScope IV and commercial Si_3N_4 cantilevers (Nanosensors) in tapping mode. The scan rate was 2 Hz. Several images of sizes 500 nm × 500 nm, 1 μm × 1 μm, 2 μm × 2 μm, and 4 μm × 4 μm were taken on different areas of each sample (N = 6). The root-mean-square (rms) roughness values were determined and averaged from these images using Gwyddion software.

2.2.4 Electrochemical Characterization

All electrochemical measurements were conducted with a three-electrode cell and a bipotentiostat (model AFCBP1, Pine Instruments) on at least three samples. Home-made Ag/AgCl/KCl (3.5 M) and Ag/Ag^+ (0.2 M Ag^+ in acetonitrile containing 0.1 M $TBABF_4$) reference electrodes were used for aqueous solutions and acetonitrile solutions, respectively. A Pt mesh was used as a counter electrode, and eC/Au and GC were used as working electrodes. GC (Tokai GC 20) plates (2.5 cm × 6 cm) were polished manually in 1, 0.3, and 0.05 μm alumina slurries with a Microcloth polishing cloth (Buehler), followed by sonication in DI water for 15 min prior to use. The geometrical working electrode area was defined by a viton O-ring. Chronoamperometry in 1 mM $Fe(CN)_6^{3-}$ in 1 M KCl yielded an electrode area of 0.319 ± 0.005 cm^2 (N = 3).

Stripping of underpotentially deposited lead. Lead from 1 mM PbO in 1 M $HClO_4$ solution was deposited onto the working electrode by stepping the potential from open circuit to –0.4 V for 5 s. The underpotentially deposited lead subsequently was stripped oxidatively at a scan rate of 0.5 V/s.

Electrode kinetics. The redox systems under investigation were as follows: 1 mM $Fe(CN)_6^{3-}$ in 1 M KCl, 1 mM $Ru(NH_3)_6^{3+}$ in 1 M KCl, 1 mM dopamine in 0.1 M H_2SO_4, and 1 mM ferrocene in acetonitrile containing 0.1 M $TBABF_4$. Heterogenous

electron-transfer rate constants were calculated for a simple one-electron redox system using the method of Nicholson,[42] as detailed previously.[16]

Adsorption measurements. The electrodes were immersed in 10 μM AQMS in 1 M $HClO_4$ and 10 μM PQ in 1 M $HClO_4$ solutions for 10 min and rinsed well with DI water. Then, cyclic voltammograms were obtained in 1 M $HClO_4$ at a scan rate of 0.1 V/s. Surface coverage of quinones was quantified by measuring the area under the voltammetric reduction wave using the method described by Brown and Anson.[43]

2.3 Results and Discussion

The relationship between the physicochemical properties of carbon materials and their electroanalytical performance has been a long-term interest to researchers and is explored here for eC/Au films. Material and surface properties, such as carbon microstructure, sp^3/sp^2 carbon ratio, O/C ratio, roughness, and wettability, were probed for these films. Electrochemical properties of eC/Au have been assessed briefly by cyclic voltammetry[19] and are investigated further here, including potential window, capacitance, electron-transfer rates for four benchmark redox species, adsorption, and stability of electrochemical response. In a previous report, a TiC adhesion layer between eC and Au was needed to prevent delamination of the eC film during electrochemical experiments.[19] We did not observe delamination of the eC layer for our films, indicating good adhesion of the film to the substrate.

2.3.1 Surface Characterization

Carbon microstructure. Raman spectroscopy, which is used regularly to characterize carbon materials, was used here to investigate the microstructure of the eC/Au films. The Raman spectrum for a 10 nm thick eC layer on Au (Figure 2-2) contains a broad, featureless band between 1200 and 1600 cm^{-1}. This is similar to that observed for eC deposited onto Si[16] and the multilayer $KCl_{1000}/eC_{10}/TiC_3/Au_{30}/Cr_3/Si/SiO_{x300}$ film (subscripts indicate thicknesses in nm) previously reported.[19] The spectrum suggests that the eC/Au film is comprised of disordered amorphous carbon containing both sp^2- and sp^3- hybrids. This spectral feature also is observed for microcrystalline graphite.[44] Deconvolution of the Raman spectrum into the G (graphitic) and D

(disordered) bands observed for graphitic materials and subsequent analysis resulted in ~30% sp^3 hybridized carbon, or an sp^3/sp^2 ratio of ~0.43 (Figure 2-2).

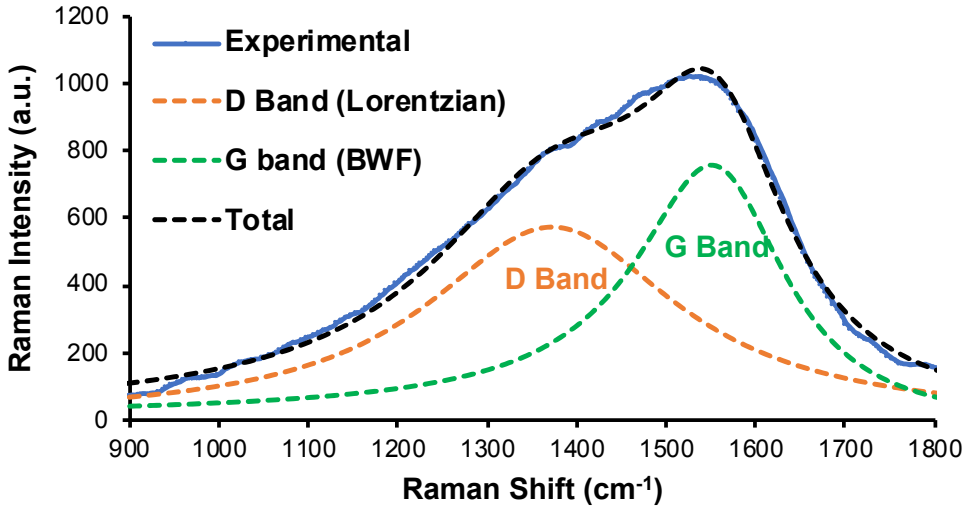

Figure 2-2. Raman spectrum of eC/Au (514.5 nm, 30 mW, 100 s, 50x). Breit-Wigner-Fano (BWF) and Lorentzian fittings for D and G bands, respectively, results in excellent deconvolution with low residuals, as suggested by Ferrari and Robertson.[45] The relative positions of D (1372 cm^{-1}) and G (1559 cm^{-1}) bands were used to estimate sp^3 content.[45]

O/C and sp^3/sp^2 ratios. Oxide groups on the surface of carbon materials are known to influence their electrochemical properties. The amount of surface oxides typically is quantitated with XPS, which was employed here to determine the O/C ratio. XPS was also used to quantify the sp^3/sp^2 ratio of eC/Au films by deconvoluting the C1s peak. Survey spectra (Figure 2-3) do not contain an Au peak, consistent with uniform coverage of the Au layer by eC and low pinhole density. Analysis of the XPS spectrum shows that eC/Au surfaces exhibit an O/C ratio of 5.8 ± 0.2% after brief exposure to air during sample transfer. This is less than the typical O/C of 8–15% of polished GC.[46] Analysis of the high resolution C1s peak results in an sp^3/sp^2 ratio of ~0.38 (Figure 2-4), which is in good agreement with Raman results and indicates that the majority of carbon atoms are sp^2 hybridized. Besold et al. proposed that electron beam evaporated carbon films on SiO_2 are comprised of graphitic clusters (sp^2-hybridized carbon) arranged within a diamond-like framework (sp^3-hybdridized carbon).[44] This description is consistent with our results.

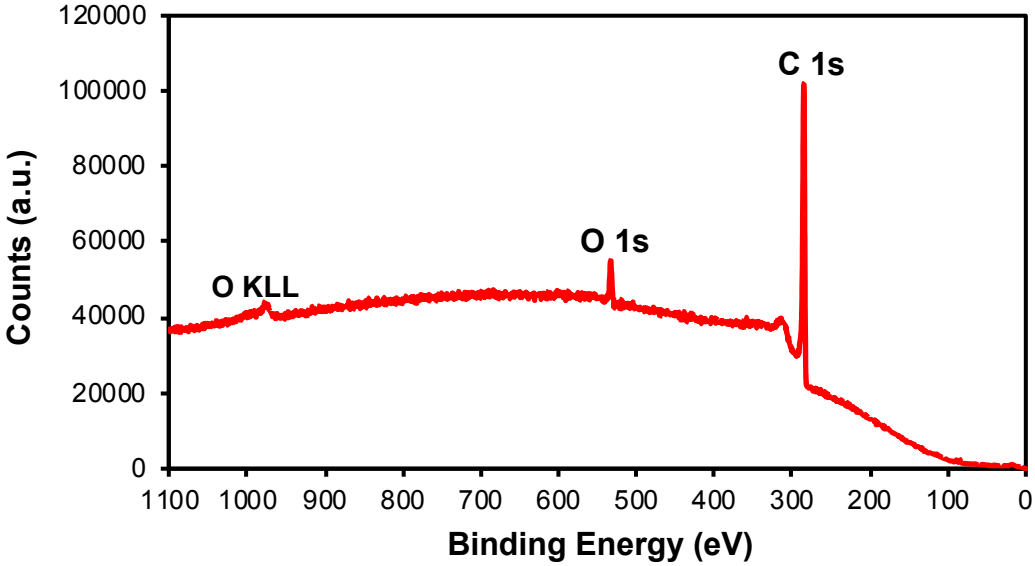

Figure 2-3. XPS survey spectrum of freshly prepared eC/Au.

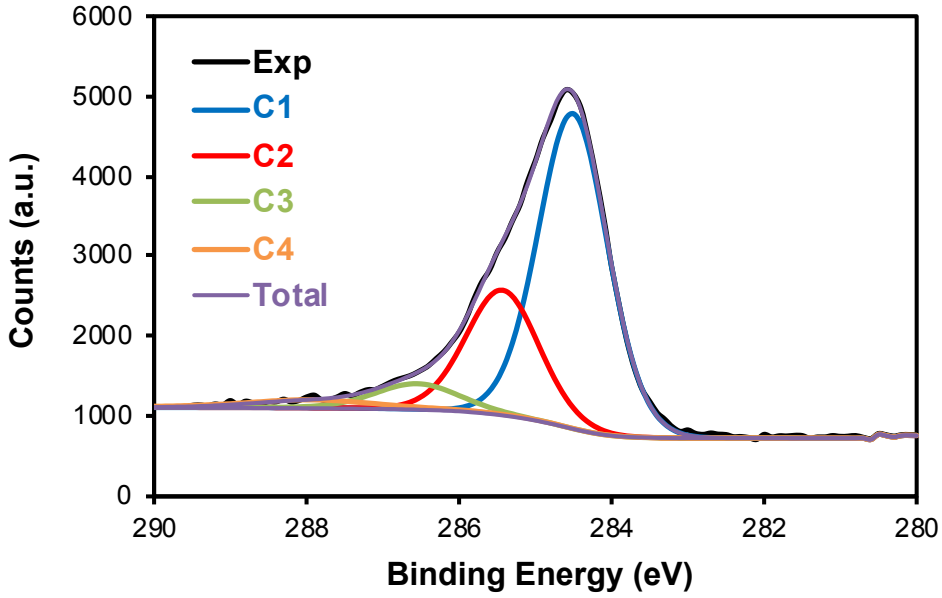

Figure 2-4. XPS C1s high resolution spectrum of freshly prepared eC/Au. The C1s peak can be decomposed into 4 components. The peaks at 284.3 eV (C1) and 285.3 eV (C2) are assigned to sp^2 and sp^3 hybrids, respectively.[47] The peaks at 286.5 eV (C3) and 288 eV (C4) are assigned to C–O and C=O bonds, respectively.

Wettability. The wettability of the films was studied by measuring the water contact angle on the surface. The water contact angle on eC/Au films is 44 ± 2° (Figure 2-1B), indicative of a hydrophilic surface. This value is similar to amorphous carbon films prepared by magnetron sputtering (44°)[48] and is lower than diamond-like

carbon films fabricated by plasma immersion ion implantation (68.4°),[49] filtered cathodic vacuum arc technique (77.6°),[50] laser arc process (60°),[51] and chemical vapor deposition (75°).[52] The contact angle of water on freshly polished GC is 37–45°.[53]

Roughness. Both the carbon film and the underlying Cr/Au film were examined to understand the roughness of the eC layer. Figure 2-5 shows AFM images (A) and line scan profiles (B) of Cr_2/Au_{42} and $Cr_2/Au_{42}/eC_{10}$ films deposited on a Si substrate (the subscripts indicate thicknesses in nm).

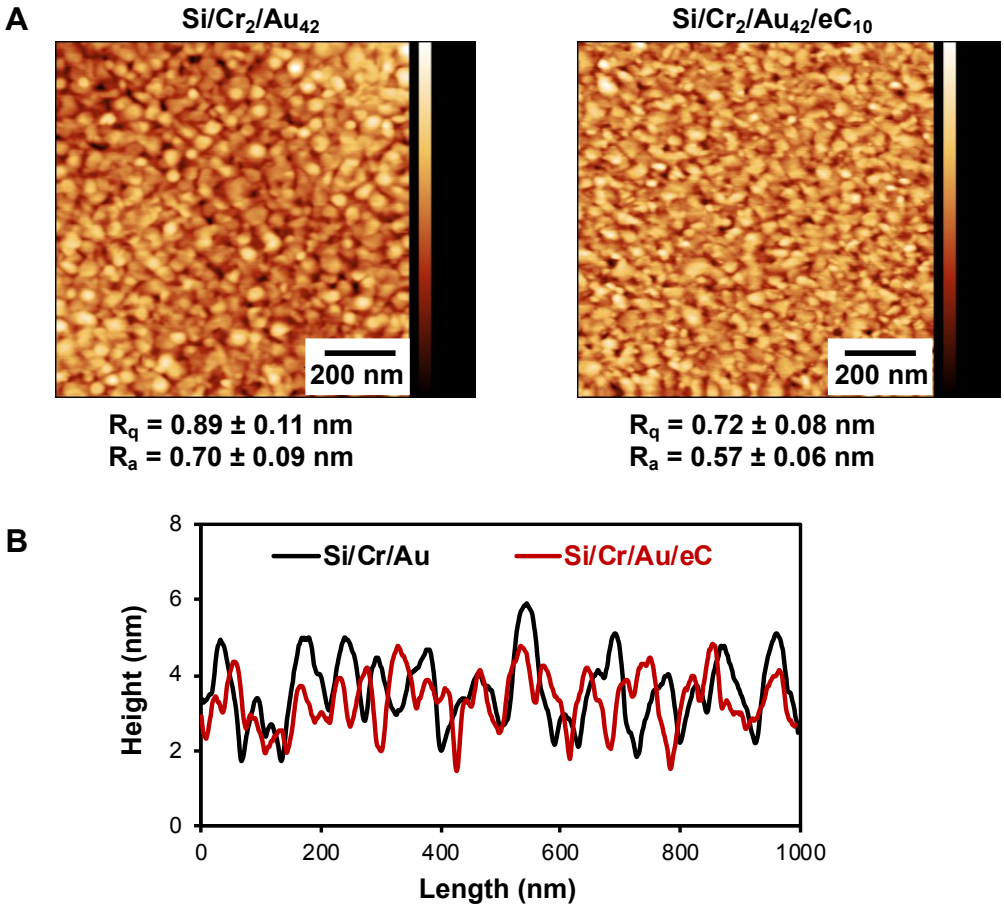

Figure 2-5. (A) AFM images of $Si/Cr_2/Au_{42}$ (Au) and $Si/Cr_2/Au_{42}/eC_{10}$ (eC/Au) films (subscripts indicate thicknesses in nm). (B) AFM line scan profiles of the surfaces shown in panel A.

Island features are observed on the gold film, with a rms roughness (R_q) of 0.89 nm. A 10 nm thick eC layer deposited on top of this relatively rough Au film exhibits a smoother surface, with a rms roughness of 0.72 nm. The decreased roughness during eC deposition may be due to the amorphous and non-diffusing

nature of eC, in addition to more rapid C–C bond formation in depressions in the Au surface. The eC/Au surface is rougher than PPF (rms roughness 0.5 nm),[8] eC/Si (rms roughness 0.07–0.11 nm),[16] and ECR-sputtered carbon/Si (average roughness 0.07 nm).[12] Compared to polished GC (rms roughness 4.1 nm),[54] however, eC/Au has a very smooth surface.

2.3.2 Electrochemical Characterization

The presence of pinholes, or incomplete coverage of the 10 nm eC film thus exposing the underlying Au, was explored here by stripping of underpotentially deposited (UPD) lead. A monolayer of lead adatoms can be deposited on Au surfaces at potentials slightly more positive than for bulk deposition of lead.[55–60] This lead monolayer subsequently can be stripped oxidatively from the gold surface. Figure 2-6 contains stripping voltammograms at Au and eC/Au surfaces. Here, an Au film ($Si/Cr_2/Au_{42}$) served as a control. A sharp oxidative stripping wave at –0.2 V can be observed for the control gold film, which is characteristic of lead stripping from the Au(111) crystal plane.[55] This wave is absent for the eC/Au film, implying that no lead was deposited and that pinholes are either absent or present in undetectably low density. A previous investigation of similar eC films used the electrochemical oxidation of the underlying metal (Cu and Ni) as a probe for pinholes and reported a similar finding.[19]

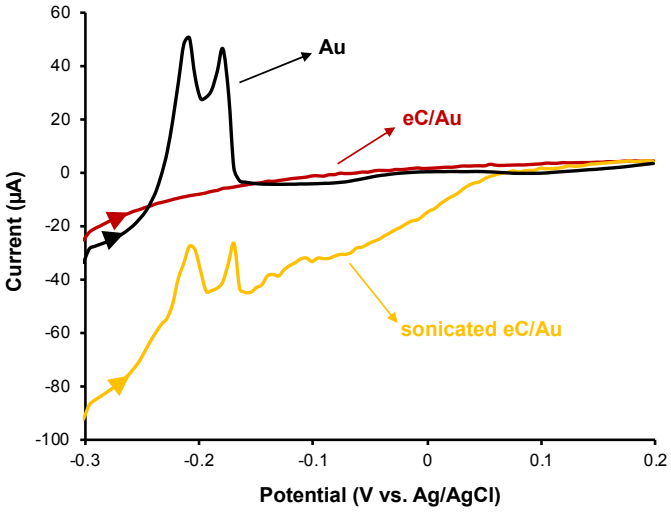

Figure 2-6. Linear sweep voltammograms for the stripping of lead UPD from Au, eC/Au, and sonicated eC/Au surfaces (ν = 0.5 V/s).

Adsorbed organic impurities are known to influence the electrochemical reactivity of carbon electrodes, and a treatment involving ultrasonication in a mixture of activated carbon and 2-propanol has been shown to reduce the amount of adsorbed impurities significantly.[1] The ability to mass produce eC/Au film electrodes and store them may prompt researchers to use this procedure in the future to clean the surface following storage. We thus monitored the stability of our eC films following ultrasonic treatment. eC/Au films were sonicated in 2-propanol/acetonitrile (50:50 v/v) with an equal volume of activated carbon for 10 min, followed by sonication in DI water for 10 min. Figure 2-6 also contains the UPD lead stripping result following this treatment. Exposure of the gold layer is confirmed by the sharp oxidative wave observed at –0.2 V, similar to that of the control gold film. Thus, the ultrasonic treatment clearly caused observable delamination of the carbon layer and exposure of the gold layer. This electrode cleaning procedure will not be applicable to eC/Au films. However, commercial production of hundreds of eC/Au electrodes on Si wafers, with protection by KCl or other dissolvable films without eC exposure to air, may provide an effective alternative to sonication.[61]

Potential window and electrode capacitance. Carbon electrodes, in general, enjoy the advantage of a wide potential window in most solvents. Voltammetric scans in 0.05 M H_2SO_4 reveal similar potential limits for polished GC (2.5 V) and eC/Au

(2 V) (Figure 2-7). Compared to BDD (potential window of 3.5 V)[2] and ECR-sputtered carbon films (potential window of 3.4–3.7 V),[22] the potential window of eC/Au is not as wide. However, it is still wider than most metal electrodes and thus applicable for a wide range of redox analytes. Also, the background current is less than 50 μA/cm^2, between –0.6 and 1.4 V at eC/Au, which is much lower than polished GC (typically 200 μA/cm^2). This suggests that the surface is composed of a low level of electroactive and ionizable surface carbon–oxygen functionalities, consistent with the XPS results described above.

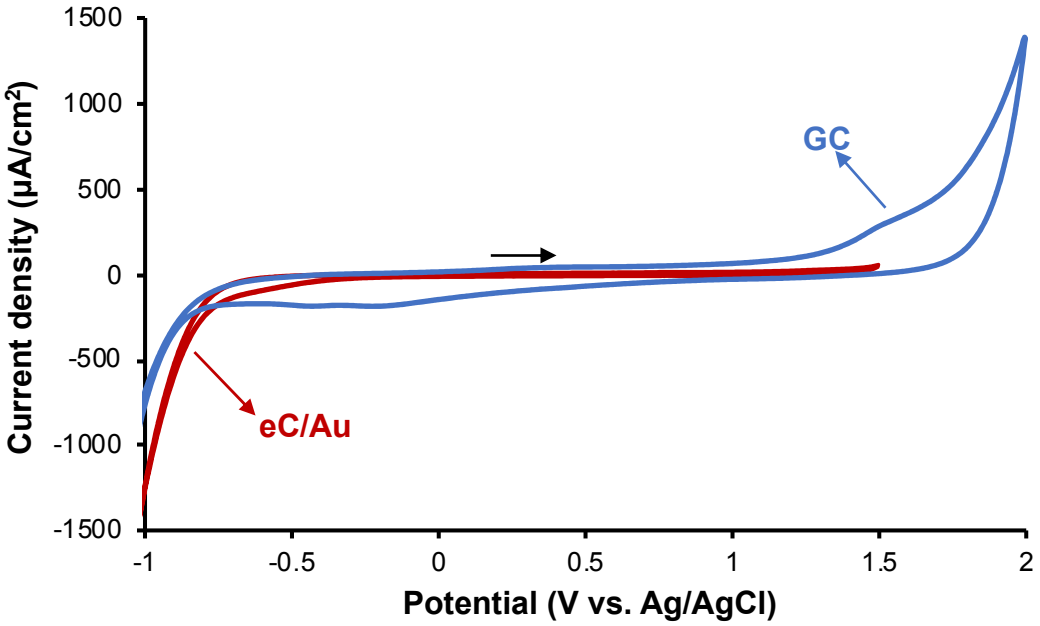

Figure 2-7. Background voltammograms of eC/Au and polished GC in H_2SO_4 0.05 M, ν = 0.1 V/s. The current is normalized to the electrode area to give current density. Black arrow indicates scan direction.

A more quantitative measure of background current is electrode capacitance. Capacitance values were obtained from cyclic voltammograms in 1 M KCl and 1 M $HClO_4$ over a range of scan rates (0.05–1 V/s) (Figures 2-8 and 2-9) and are reported in Table 2-1. Capacitance values for eC/Au in 1 M KCl and in 1 M $HClO_4$ are less than 50% of those for polished GC. The electrode capacitance of eC/Au in 1 M KCl is comparable with sputtered carbon films (11.1–11.6 μF/cm^2) and slightly higher than BDD and PPF (4–8 and 9.2 μF/cm^2, respectively).[2,8,23] The low capacitance of

eC/Au can be attributed to reduced electroactive or ionizable surface carbon–oxygen functionalities, a smoother surface, and space-charge effects, as is observed at the basal plane of HOPG.[62,63] We attribute the higher capacitance in 1 M $HClO_4$ compared to 1 M KCl observed on both eC/Au and polished GC to a mild electrochemical pretreatment effect. Electrochemical pretreatment has been reported to increase roughness and oxygen-containing groups for GC and sputtered carbon electrodes, which is assumed to contribute to the increased background current.[23] Clearly, eC/Au offers a reasonably wide potential window and low background current and capacitance, both of which are attractive for improved signal-to-background in electrochemical measurements.

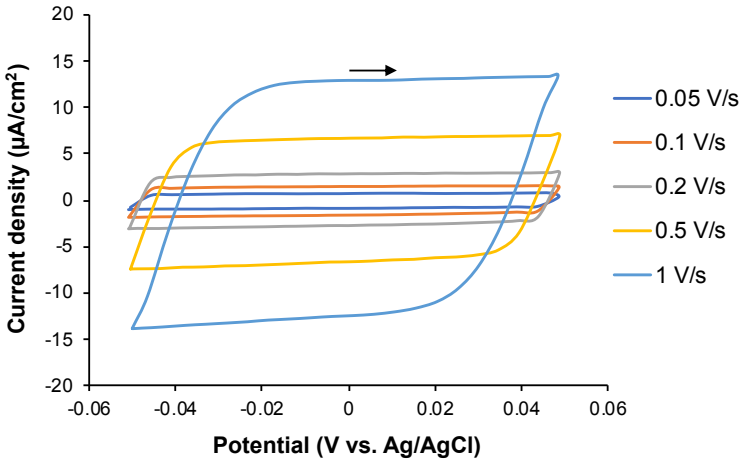

Figure 2-8. Scan rate dependent background current for eC/Au in 1 M KCl. Black arrow indicates scan direction.

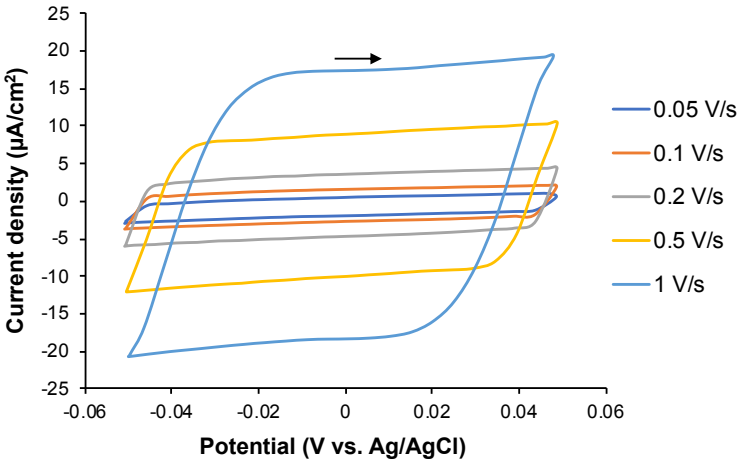

Figure 2-9. Scan rate dependent background current for eC/Au in 1 M HClO4. Back arrow indicates scan direction.

Table 2-1. Electrochemical Results for eC/Au and GC

	k^0 (cm/s)[a]			ΔE_p (mV) (ν = 0.1 V/s)	C^0 (μF/cm^2)		Γ (pmol/cm^2)	
Electrodes	$Fe(CN)_6^{3-/4-}$ (1 M KCl)	$Ru(NH_3)_6^{3+/2+}$ (1 M KCl)	ferrocene$^{+/0}$ (0.1 M $TBABF_4$)	dopamine (0.1 M H_2SO_4)	KCl (1 M)	$HClO_4$ (1 M)	AQMS (1 M $HClO_4$)	PQ (1 M $HClO_4$)
eC/Au	7.4×10^{-3} (4.5%)[b]	2.5×10^{-2} (13%)	3.9×10^{-3} (7.5%)	226 ± 7	12 ± 1	19 ± 2	ND	1.6 ± 0.1
GC	1.2×10^{-2} (9.2%)	1.4×10^{-2} (10%)	3.4×10^{-3} (9.1%)	138 ± 8	31 ± 2	45 ± 5	136 ± 50	105 ± 30

[a]All k^0 values were determined from ΔE_p values corrected for iR_u error and from 5 different scan rates per sample.
[b]Values in parentheses are the relative standard deviation of the mean for at least 3 different eC/Au electrodes.

Electrode kinetics. As noted above, very high electron-transfer (ET) rates have been measured at similar eC electrodes by SECM.[19] There is a large body of literature that employs cyclic voltammetry (CV) to measure the ET kinetics of carbon electrodes;[1] thus, for a more complete comparison, we used CV to measure the ET rate constants of several aqueous as well as non-aqueous based benchmark redox systems at eC/Au electrodes and compared them with polished GC electrodes. These redox systems were chosen based on their different sensitivity to the carbon surface structure. Figure 2-10 contains cyclic voltammograms of $Fe(CN)_6^{3-}$ (A), $Ru(NH_3)_6^{3+}$ (B), dopamine (C), and ferrocene (D) at eC/Au and polished GC. eC/Au electrodes show well-defined, symmetric voltammograms, which are qualitatively comparable to GC for all redox systems under study. In addition, the peak current is

linear with $\nu^{1/2}$ over a range of scan rates (0.05–1 V/s), and the cathodic to anodic peak currents ratio is nearly 1 for all scan rates, consistent with currents controlled by semi-infinite linear diffusion and quasi-reversible ET kinetics. Heterogeneous ET rate constants were calculated for simple one-electron redox systems using the Nicholson method and are summarized in Table 2-1. All reported k^0 values were corrected for sample resistance by the method detailed previously.[8,16] The uncompensated cell resistance R_u was determined to be 47.0 ± 0.5 Ω (Figure 2-11). The effects of electrode resistance on electron transfer kinetics at pyrolyzed photoresist films (PPF) were observed in a report by Ranganathan et al.[64] Specifically, ΔE_p of $Fe(CN)_6^{3-/4-}$ and $Ru(NH_3)_6^{3+/2+}$ increased with higher concentrations, implying a significant contribution from the iR drop in the PPF electrode due to its thinness. In a later report,[65] they noted that the resistance within the PPF increases the observed peak separation according to:

$$\Delta E_{p,corrected} = \Delta E_{p,observed} - 2 \mid i \mid R_u \quad (1)$$

where i is the peak current in amperes, R_u is the uncompensated cell resistance in ohms, $\Delta E_{p,observed}$ is the observed ΔE_p in the presence of the uncompensated cell resistance in volts, and $\Delta E_{p,corrected}$ is the corrected ΔE_p in volts. Rearranging Eq. (1), we obtain:

$$\Delta E_{p,observed} = 2 \mid i \mid R_u + \Delta E_{p,corrected} \quad (2)$$

In our previous work,[66] we reported that a plot of $\Delta E_{p,observed}$ vs i from voltammograms at a common scan rate would yield a linear relationship, in which the slope of the fit equals to $2R_u$. The concentrations of $Fe(CN)_6^{3-}$ can be varied to affect the different peak currents. Since $i_{pc}/i_{pa} \sim 1$ for $Fe(CN)_6^{3-}$ at eC/Au electrodes, either i_{pc} or i_{pa} can be used in the calculations.

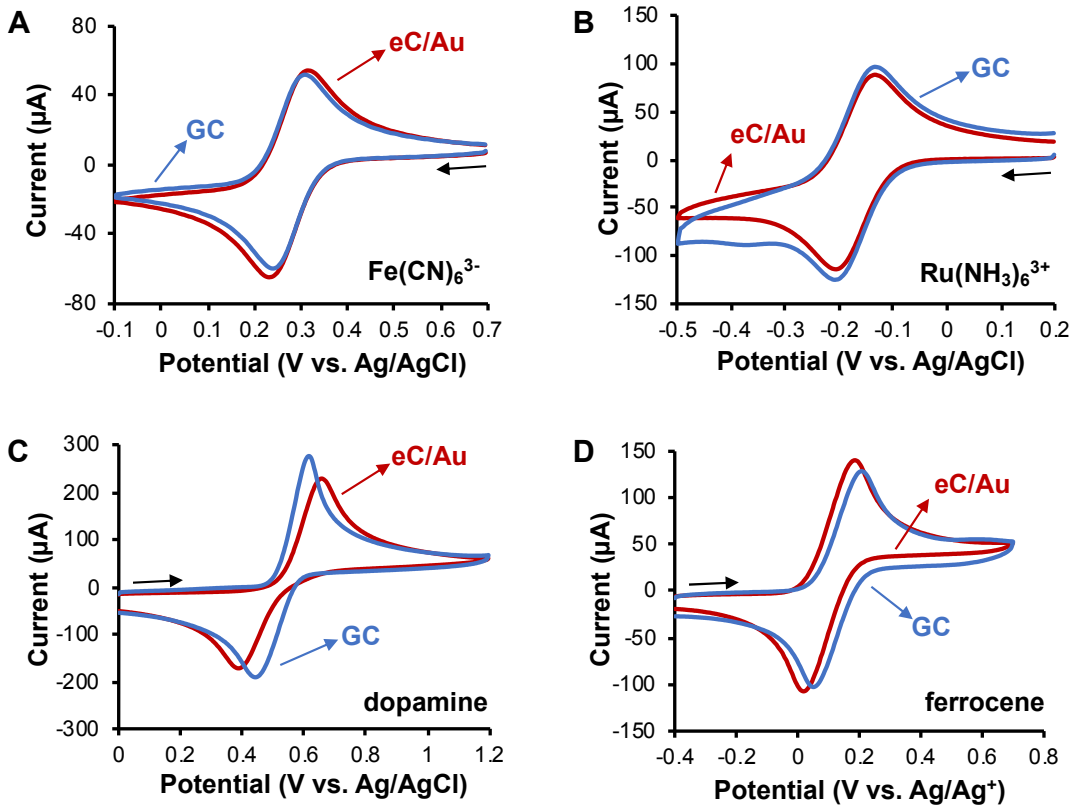

Figure 2-10. Cyclic voltammograms of 4 benchmark redox systems at eC/Au and polished GC. (A) 1 mM $Fe(CN)_6^{3-}$ (1 M KCl, ν = 0.05 V/s). (B) 1 mM $Ru(NH_3)_6^{3+}$ (1 M KCl, ν = 0.2 V/s). (C) 1 mM dopamine (0.1 M H_2SO_4, ν = 0.2 V/s). (D) 1 mM ferrocene (0.1 M tetrabutylammonium tetrafluoroborate in acetonitrile, ν = 0.1 V/s). Black arrows indicate scan direction.

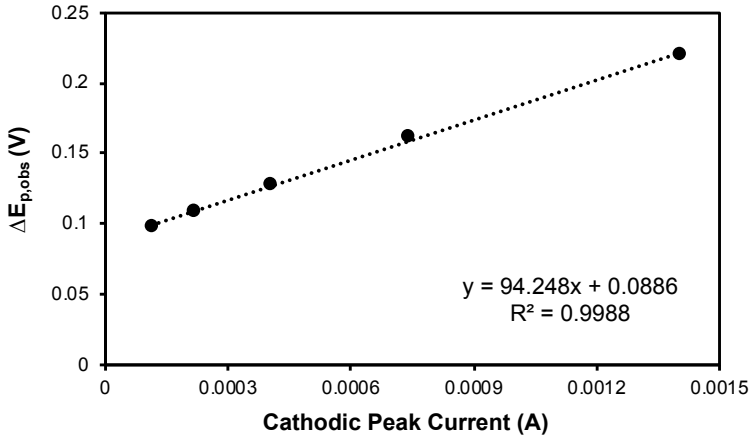

Figure 2-11. Representative plot of $\Delta E_{p,obs}$ vs cathodic peak current from cyclic voltammetry of $Fe(CN)_6^{3-}$ (1 M KCl, ν = 0.1 V/s) at an eC/Au film. The concentration of $Fe(CN)_6^{3-}$ was varied from 1 to 16 mM to affect the different peak currents. The slope of each least-squares, linear fit yields $2R_u$.

It is now known that $Fe(CN)_6^{3-/4-}$ is not a simple outer-sphere system, and its ET rate depends on the electrode surface condition. The rate is influenced by the fraction of edge plane as well as surface cleanliness, but it is relatively insensitive to surface oxides as long as anionic oxide groups are absent.[46] The ET rate also is influenced by adsorbed monolayers, the extent of which depends on the type and coverage of the adsorbate.[46] Here, eC/Au yields a somewhat lower rate constant for $Fe(CN)_6^{3-/4-}$ compared to polished GC, which can be ascribed to the reduced sp^2 content of eC/Au in comparison with GC.

$Ru(NH_3)_6^{3+/2+}$ and ferrocene$^{+/0}$ in acetonitrile are known to be insensitive to surface chemistry or adsorbed monolayers and, therefore, are considered to be simple outer-sphere redox systems.[1] For these systems, the ET rate depends on the electronic properties of the electrode and the self-exchange rate of the redox systems but not on the interaction with a surface site or functional group.[54] The cyclic voltammetric determined rate constants at eC/Au electrodes are slightly higher than those at a polished GC surface. These results suggest that the density of electronic states of eC/Au is sufficient to support rapid ET for outer-sphere redox systems. eC/Au exhibits a much larger peak separation for dopamine, reflecting a slower ET rate compared to polished GC (Table 2-1). However, this value is still among the smallest reported for thin carbon film electrodes (Table 2-2).

Table 2-2. Comparison of Electron-transfer Kinetics at Various Carbon Film Electrodes

Electrode	k^0 for $Ru(NH_3)_6^{3+/2+}$ ($\times 10^{-2}$ cm/s)	k^0 for $Fe(CN)_6^{3-/4-}$ ($\times 10^{-2}$ cm/s)	ΔE_p of dopamine (mV)
ECR-75[22]	reversible	1.22	472
ECR-20[22]	reversible	0.24	464
BDD (NRL*)[20]	1.2	1.7	480
BDD (USU*)[20]	1.7	1.9	509
Pyrolyzed 7-nm eC/Si[16]	4.6	1.4	119
7-nm eC/Si[16]	1.9	0.27	227
Pyrolyzed 200-nm eC/Si[16]	2.7	2.9	130
200-nm eC/Si[16]	4.3	0.57	243
PPF[8]	2	1.2	287
eC/Au (this work)	2.5	0.74	226

*NRL: Naval Research Laboratory; USU: Utah State University

A slow ET rate for dopamine also was observed on PPF,[8] sputtered carbon films,[22] and BDD.[20] Dopamine oxidation is known to require adsorption sites.[20] Thus, dopamine ET kinetics slow significantly when such interactions are unfavorable. The slow kinetics of dopamine at eC/Au can be attributed to several factors such as decreased ionizable surface carbon-oxygen functionalities, which facilitate proton transfer, low roughness, and a low density of edge plane adsorption sites. The sluggish kinetics resulting from weak electrocatalysis for dopamine is consistent with weak quinone adsorption discussed below.

Table 2-2 compares ET kinetics of $Ru(NH_3)_6^{3+/2+}$, $Fe(CN)_6^{3-/4-}$, and dopamine at different carbon film electrodes. Overall, eC/Au exhibits fast electron kinetics for these three redox systems and is comparable to ECR-sputtered carbon films, BDD, and PPF. Interestingly, eC behaviors most resemble non-pyrolyzed 200-nm eC/Si, implying similar surface and bulk properties. The voltammetric results in Table 2-2 indicate that eC/Au is electrochemically active and yields reproducible response without any pretreatment. The most favorable electrochemical results for GC, BDD, and PPF are often accompanied by a pretreatment procedure. There have been numerous pretreatment procedures reported for GC, including mechanical polishing, sonication in solvent suspended activated carbon, vacuum heat treatment, and laser activation.[1] The results for BDD in Table 2-2 correspond to electrodes that were

treated with acid and hydrogen plasma to remove nondiamond carbon impurities and produce a hydrogen terminated surface.[20] PPF[8] and eC/Si films from our previous work[16] also were sonicated in activated carbon/isopropanol, followed by deionized water prior to use. In summary, eC/Au electrodes can provide high electrochemical reactivity without the need for surface pretreatment procedures.

Adsorption. It is known that carbon electrodes are susceptible to passivation via the adsorption of organic molecules. Typically, quinone-type molecules are used as model systems to study adsorption to carbon since adsorbed quinones are electroactive and their coverage can be measured easily. The adsorption of two quinones from a low concentration (10 μM) on eC/Au was investigated using CV. Figure 2-12 contains cyclic voltammograms of 9,10-phenanthrenequinone (PQ) and anthraquinone-2-sulfonate (AQMS) at eC/Au and polished GC. Both of these species are known to adsorb strongly to carbon electrodes and undergo a reversible two-proton, two-electron redox reaction.[43,67] Figure 2-12A shows the voltammograms of PQ on both electrodes, and Figure 2-12B shows the voltammogram of PQ on eC/Au with a reduced current scale. Parts C and D are similar data for AQMS. For both quinones, pairs of symmetric peaks are observed at GC, which is characteristic of surface-confined redox species. In contrast, PQ yields very little current on eC/Au, and the adsorption current for AQMS is negligible. These observations indicate very weak adsorption for both quinones on eC/Au. Integration of the voltammetric redox waves was used to evaluate surface coverage, and the results are presented in Table 2-1. eC/Au shows negligible adsorption of PQ (~2 pmol/cm^2) compared to GC (~105 pmol/cm^2), and the adsorption of AQMS is below the voltammetric detection limit. The negligible adsorption indicates that eC/Au is potentially less subjective to electrode fouling, leading to improved stability and reproducibility in electrochemical measurements.

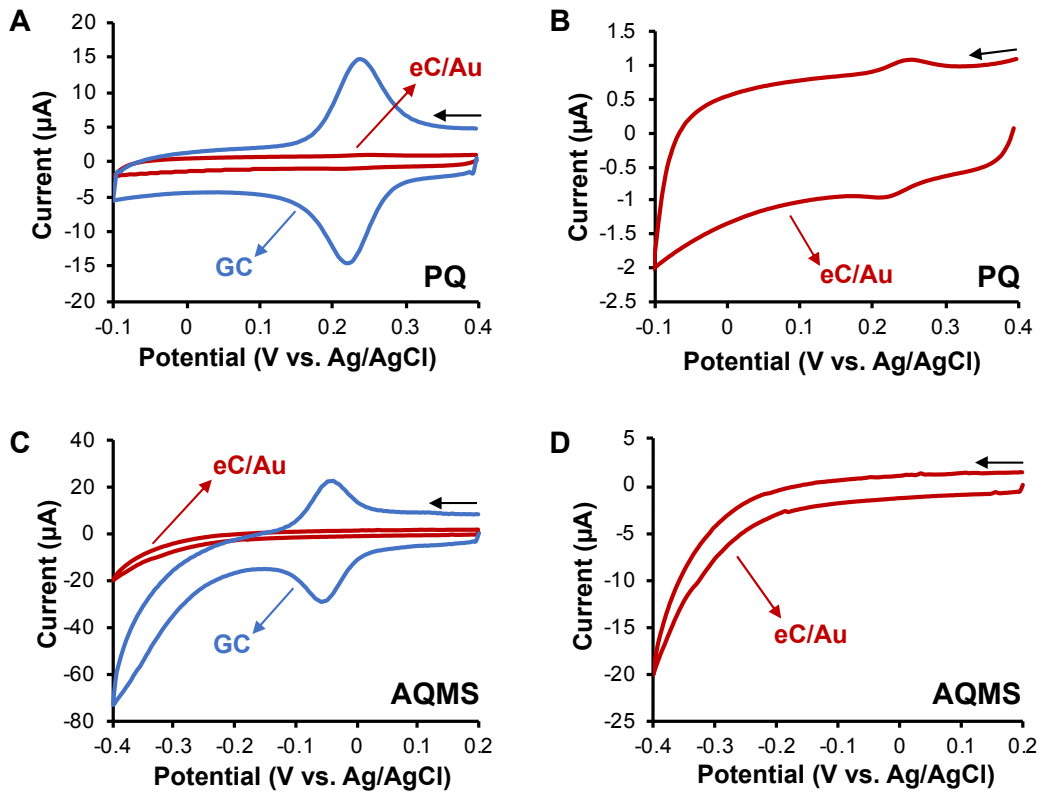

Figure 2-12. Cyclic voltammograms of PQ (A) and AQMS (C) at eC/Au and polished GC. Cyclic voltammograms of PQ (B) and AQMS (D) at eC/Au with a reduced current scale. The concentration of the quinones was 10 μM in 1 M $HClO_4$. The scan rate was 0.1 V/s. Black arrows indicate scan direction.

The low measurable adsorption of PQ and AQMS on eC/Au is due to either low coverage or adsorption in an electro-inactive configuration. We believe that the former factor is more relevant here. PQ and AQMS have been shown to physisorb strongly at monolayer coverage to disordered carbon surfaces, like pyrolytic graphite and GC.[43,68] However, low coverage of quinones has been measured at other carbon electrodes, such as the basal plane of highly oriented pyrolytic graphite (HOPG) (< 1 pmol/cm^2),[67] BDD (~3 pmol/cm^2),[69] PPF (~20 pmol/cm^2),[8] and non-pyrolyzed eC/Si (28–30 pmol/cm^2).[16] In addition, weak adsorption of alkylphenols and bisphenol A was observed at sputtered carbon films.[12,22] Adsorption of species like quinones can be promoted by two electrode properties, surface chemistry and electronic effects. For the basal plane of HOPG, the adsorption mechanism of quinones is thought to depend on an electrostatic attraction between the adsorbate and partial surface charges.[67] Xu et al. compared the adsorption of anthraquinone-2,6-

disulfonate at GC, hydrogenated GC, HOPG, and BDD and proposed that surface chemistry plays a more important role in the adsorption than do electronic effects.[69] Weak adsorption on PPF was explained partly by surface effects, such as a low roughness factor and O/C ratio.[8] Niwa and co-workers also attributed the weak interactions between the adsorbates and sputtered carbon films to the extreme flatness of the surface and the low concentration of oxygen-containing groups.[12,22] In our previous study, we observed an increase in quinone adsorption after pyrolyzing eC/Si films. The increased surface roughness and adsorption sites followed graphitization result in increased quinone adsorption.[16] In light of the above-mentioned studies, we attribute the insignificant adsorption of quinones at eC/Au, in part, to a reduced density of adsorption sites due to lower sp^2 content (~70% vs 100% of GC). In addition, the ultraflat surface and low carbon-oxygen functionalities of eC/Au likely contribute. The minimal adsorption of quinone molecules points to a beneficial property of eC/Au electrodes regarding electrode stability due to fouling.

2.3.3 Stability

The shelf-life stability of eC/Au electrodes was evaluated using several observations. The O/C ratio of eC/Au films increased from 5.6–6% to 8.0–8.4% after one week. Aging in air for 15 days increased water contact angle from 44 ± 2° to 71 ± 3° (Figure 2-13A), suggesting that the surface becomes more hydrophobic with air exposure. This phenomenon also was observed on polished GC,[53] HOPG,[70] and graphene,[71] and was ascribed to the adsorption of hydrocarbons or similar hydrophobic impurities present in ambient air. Unlike HOPG[70] and graphene[71] whose water contact angles quickly increased by ~40% within 15–20 min of air exposure, eC/Au films show a much slower increase in water contact angles with time (~16% increase after 1 day, Figure 2-13B). Stability of electrochemical performance was investigated by tracking voltammetric peak separations of $Ru(NH_3)_6^{3+/2+}$ and dopamine over time (Figure 2-13C and D). Similar trends were observed for both eC/Au and GC electrodes. For an outer-sphere redox system like $Ru(NH_3)_6^{3+/2+}$, the peak separation and thus electrochemical reactivity did not change significantly after 2 weeks (two-tailed t-test at 95%, N = 3). For the inner-sphere redox system

dopamine, the peak separation increased significantly after 2 weeks (two-tailed t-test at 95%, N = 3). We attribute the slower ET rate of dopamine to reduced adsorption sites resulting from the adsorption of airborne impurities. Adsorption of airborne contaminants have been reported previously to have minor effect on the ET rate of $Ru(NH_3)_6^{3+}$, but they decelerate the ET rates of $Fe(CN)_6^{4-}$ at aged HOPG[72] and dopamine at aged GC.[53] BDD shows weak adsorption of quinone and good electrochemical reactivity for $Fe(CN)_6^{3-/4-}$ and $Ru(NH_3)_6^{3+/2+}$ after exposure to ambient air for two weeks.[2] Although eC/Au exhibits negligible quinone adsorption, it is still prone to air oxidation and adsorption of airborne hydrocarbons, like most graphitic carbon electrodes, albeit slower than that reported for graphene and HOPG. Graphitic carbon materials are subject to surface oxidation and fouling because they tend to react with oxygen and water to form various oxides, such as phenols, lactones, carbonyls, ethers, and carboxylates.[73] eC/Au possesses significant sp^2 carbon (~70%), thus behaving similarly to GC in this respect. Nonpolar, hydrogen-terminated surfaces, like BDD and hydrogenated GC, are less subject to deactivation because of a lower affinity for polar impurities in ambient air and a stable chemical composition due to slow reaction with oxygen/water.[73,74] As noted above, a KCl protective layer has been shown to improve the shelf-life of eC/Au films for storage and shipment purposes and may enable commercial production of disposable eC/Au electrodes.[19]

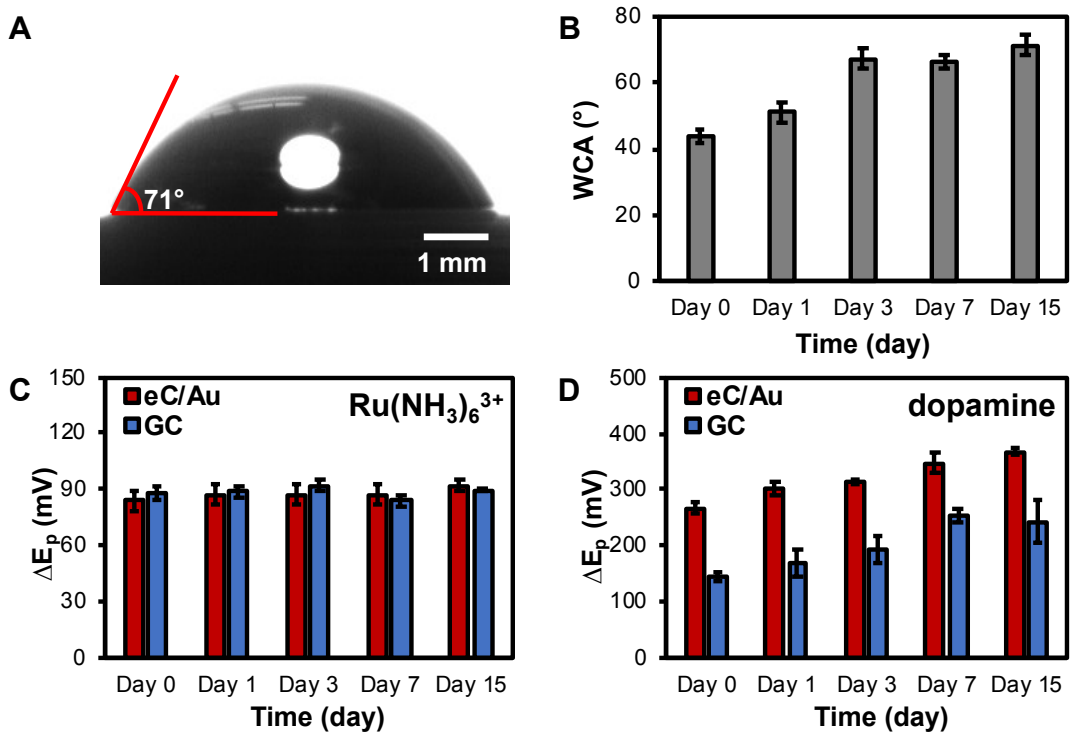

Figure 2-13. (A) Representative static contact angle image of a 4 µL drop of DI water resting on an eC/Au film after 15 days of ambient air exposure. (B) Bar graph of water contact angle (WCA) measured on eC/Au over time. (C) Bar graph of ΔE_p of 1 mM $Ru(NH_3)_6^{3+}$ (1 M KCl, ν = 0.5 V/s) measured on eC/Au and GC over time. (D) Bar graph of ΔE_p of 1 mM dopamine (0.1 M H_2SO_4, ν = 0.2 V/s) measured on eC/Au and GC over time. Error bars are ±1 standard deviation.

2.4 Conclusion

Electron-beam deposited carbon on a gold layer provides an ultraflat surface and a disordered amorphous structure consisting of ~30% sp^3 hybridized carbon. The electrochemical reactivity of eC/Au is generally similar to polished GC for outer-sphere redox systems but yields slower electron-transfer rates for systems that require surface interaction (dopamine). eC/Au differs from polished GC in that it has lower background current and abnormally weak adsorption of quinones, which are attractive for electroanalytical applications. eC/Au is still subject to surface oxidation and adsorption of airborne impurities similar to graphitic materials, which slowed the electron-transfer kinetics of dopamine over time but did not impact $Ru(NH_3)_6^{3+}$ significantly. The differences in electrochemical reactivity between eC/Au and polished GC might stem from surface properties (low roughness factor, low oxygen functionalities, and lower fraction of edge plane) and, possibly, bulk electronic

properties. eC/Au can be deposited on cheap, non-conducting substrates, like plastic, to mass-produce disposable electrodes with higher purity than carbon paste or screen-printed carbon electrodes. The electrochemical reactivity of eC/Au can make it useful as an electrochemical SPR substrate. Also, eC/Au should be more widely applicable as a SPR substrate compared to Au by providing access to a richer pool of attachment chemistries available via electrochemical modifications.

References

(1) McCreery, R. L. Advanced Carbon Electrode Materials for Molecular Electrochemistry. *Chem. Rev.* **2008**, *108* (7), 2646–2687. https://doi.org/10.1021/cr068076m.

(2) Xu, J.; Granger, M. C.; Chen, Q.; Strojek, J. W.; Lister, T. E.; Swain, G. M. Peer Reviewed: Boron-Doped Diamond Thin-Film Electrodes. *Anal. Chem.* **1997**, *69* (19), 591A-597A. https://doi.org/10.1021/ac971791z.

(3) Mohamed, H. M. Screen-Printed Disposable Electrodes: Pharmaceutical Applications and Recent Developments. *TrAC - Trends Anal. Chem.* **2016**, *82*, 1–11. https://doi.org/10.1016/j.trac.2016.02.010.

(4) Taleat, Z.; Khoshroo, A.; Mazloum-Ardakani, M. Screen-Printed Electrodes for Biosensing: A Review (2008-2013). *Microchim. Acta* **2014**, *181* (9–10), 865–891. https://doi.org/10.1007/s00604-014-1181-1.

(5) Wang, J.; Tian, B.; Nascimento, V. B.; Angnes, L. Performance of Screen-Printed Carbon Electrodes Fabricated from Different Carbon Inks. *Electrochimica Acta* **1998**, *43* (23), 3459–3465. https://doi.org/10.1016/S0013-4686(98)00092-9.

(6) Fanjul-Bolado, P.; Hernández-Santos, D.; Lamas-Ardisana, P. J.; Martín-Pernía, A.; Costa-García, A. Electrochemical Characterization of Screen-Printed and Conventional Carbon Paste Electrodes. *Electrochimica Acta* **2008**, *53* (10), 3635–3642. https://doi.org/10.1016/j.electacta.2007.12.044.

(7) Niwa, Osamu.; Tabei, Hisao. Voltammetric Measurements of Reversible and Quasi-Reversible Redox Species Using Carbon Film Based Interdigitated Array Microelectrodes. *Anal. Chem.* **1994**, *66* (2), 285–289. https://doi.org/10.1021/ac00074a016.

(8) Ranganathan, S.; McCreery, R. L. Electroanalytical Performance of Carbon Films with Near-Atomic Flatness. *Anal. Chem.* **2001**, *73* (5), 893–900. https://doi.org/10.1021/ac0007534.

(9) Eriksson, A.; Norekrans, A. S.; Carlsson, J. O. Surface Structural and Electrochemical Investigations of Pyrolytic Carbon Film Electrodes Prepared by Chemical Vapour Deposition Using Ethene as Carbon Source. *J. Electroanal. Chem.* **1992**, *324* (1–2), 291–305. https://doi.org/10.1016/0022-0728(92)80052-6.

(10) Mani, R. C.; Sunkara, M. K.; Baldwin, R. P.; Gullapalli, J.; Chaney, J. A.; Bhimarasetti, G.; Cowley, J. M.; Rao, A. M.; Rao, R. Nanocrystalline Graphite for Electrochemical Sensing. *J. Electrochem. Soc.* **2005**, *152* (4), E154. https://doi.org/10.1149/1.1870772.

(11) Schlesinger, R. Development of Thin Film Electrodes Based on Sputtered Amorphous Carbon. *J. Electrochem. Soc.* **1997**, *144* (1), 6. https://doi.org/10.1149/1.1837358.

(12) You, T.; Niwa, O.; Tomita, M.; Ichino, T.; Hirono, S. Electrochemical Oxidation of Alkylphenols on ECR-Sputtered Carbon Film Electrodes with Flat Sub-Nanometer Surfaces. *J. Electrochem. Soc.* **2002**, *149* (12), E479. https://doi.org/10.1149/1.1516222.

(13) Hirono, S.; Umemura, S.; Tomita, M.; Kaneko, R. Superhard Conductive Carbon Nanocrystallite Films. *Appl. Phys. Lett.* **2002**, *80* (3), 425–427. https://doi.org/10.1063/1.1435402.

(14) Zeng, A.; Liu, E.; Tan, S. N.; Zhang, S.; Gao, J. Cyclic Voltammetry Studies of Sputtered Nitrogen Doped Diamond-like Carbon Film Electrodes. *Electroanalysis* **2002**, *14* (15–16), 1110–1115. https://doi.org/10.1002/1521-4109(200208)14:15/16<1110::AID-ELAN1110>3.0.CO;2-E.

(15) Benlahsen, M.; Cachet, H.; Charvet, S.; Debiemme-Chouvy, C.; Deslouis, C.; Lagrini, A.; Vivier, V. Improvement and Characterization of the Electrochemical Reactivity of Amorphous Carbon Nitride Electrodes. *Electrochem. Commun.* **2005**, *7* (5), 496–499. https://doi.org/10.1016/j.elecom.2005.03.003.

(16) Blackstock, J. J.; Rostami, A. A.; Nowak, A. M.; McCreery, R. L.; Freeman, M. R.; McDermott, M. T. Ultraflat Carbon Film Electrodes Prepared by Electron Beam Evaporation. *Anal. Chem.* **2004**, *76* (9), 2544–2552. https://doi.org/10.1021/ac035003j.

(17) Mattson, J. S.; Smith, C. A. Optically Transparent Carbon Film Electrodes for Infrared Spectroelectrochemistry. *Anal. Chem.* **1975**, *47* (7), 1122–1125. https://doi.org/10.1021/ac60357a070.

(18) DeAngelis, T. P.; Hurst, R. W.; Yacynych, A. M.; Mark, H. B.; Heineman, W. R.; Mattson, J. S. Carbon and Mercury–Carbon Optically Transparent Electrodes. *Anal. Chem.* **1977**, *49* (9), 1395–1398. https://doi.org/10.1021/ac50017a026.

(19) Morteza Najarian, A.; Chen, R.; Balla, R. J.; Amemiya, S.; McCreery, R. L. Ultraflat, Pristine, and Robust Carbon Electrode for Fast Electron-Transfer Kinetics. *Anal. Chem.* **2017**, *89* (24), 13532–13540. https://doi.org/10.1021/acs.analchem.7b03903.

(20) Granger, M. C.; Witek, M.; Xu, J.; Wang, J.; Hupert, M.; Hanks, A.; Koppang, M. D.; Butler, J. E.; Lucazeau, G.; Mermoux, M.; Strojek, J. W.; Swain, G. M. Standard Electrochemical Behavior of High-Quality, Boron-Doped Polycrystalline Diamond Thin-Film Electrodes. *Anal. Chem.* **2000**, *72* (16), 3793–3804. https://doi.org/10.1021/ac0000675.

(21) Kamata, T.; Kato, D.; Ida, H.; Niwa, O. Structure and Electrochemical Characterization of Carbon Films Formed by Unbalanced Magnetron (UBM)

Sputtering Method. *Diam. Relat. Mater.* **2014**, *49*, 25–32. https://doi.org/10.1016/j.diamond.2014.07.007.

(22) Jia, J.; Kato, D.; Kurita, R.; Sato, Y.; Maruyama, K.; Suzuki, K.; Hirono, S.; Ando, T.; Niwa, O. Structure and Electrochemical Properties of Carbon Films Prepared by a Electron Cyclotron Resonance Sputtering Method. *Anal. Chem.* **2007**, *79* (1), 98–105. https://doi.org/10.1021/ac0610558.

(23) Sekioka, N.; Kato, D.; Ueda, A.; Kamata, T.; Kurita, R.; Umemura, S.; Hirono, S.; Niwa, O. Controllable Electrode Activities of Nano-Carbon Films While Maintaining Surface Flatness by Electrochemical Pretreatment. *Carbon* **2008**, *46* (14), 1918–1926. https://doi.org/10.1016/j.carbon.2008.08.006.

(24) Kato, D.; Sekioka, N.; Ueda, A.; Kurita, R.; Hirono, S.; Suzuki, K.; Niwa, O. A Nanocarbon Film Electrode as a Platform for Exploring DNA Methylation. *J. Am. Chem. Soc.* **2008**, *130* (12), 3716–3717. https://doi.org/10.1021/ja710536p.

(25) Morteza Najarian, A.; Szeto, B.; Tefashe, U. M.; McCreery, R. L. Robust All-Carbon Molecular Junctions on Flexible or Semi-Transparent Substrates Using "Process-Friendly" Fabrication. *ACS Nano* **2016**, *10* (9), 8918–8928. https://doi.org/10.1021/acsnano.6b04900.

(26) Anderson, J. L.; Winograd, N. Film Electrodes. In *Laboratory Techniques in Electroanalytical Chemistry*; Kissinger, P. T., Heineman, W. R., Eds.; Marcel Dekker: New York, 1996; pp 333–366.

(27) Sachan, P.; Mondal, P. C. Versatile Electrochemical Approaches towards the Fabrication of Molecular Electronic Devices. *The Analyst* **2020**, *145* (5), 1563–1582. https://doi.org/10.1039/C9AN01948K.

(28) Dumitrescu, I.; Dudin, P. V.; Edgeworth, J. P.; Macpherson, J. V.; Unwin, P. R. Electron Transfer Kinetics at Single-Walled Carbon Nanotube Electrodes Using Scanning Electrochemical Microscopy. *J. Phys. Chem. C* **2010**, *114* (6), 2633–2639. https://doi.org/10.1021/jp908830d.

(29) Patten, H. V.; Meadows, K. E.; Hutton, L. A.; Iacobini, J. G.; Battistel, D.; McKelvey, K.; Colburn, A. W.; Newton, M. E.; MacPherson, J. V.; Unwin, P. R. Electrochemical Mapping Reveals Direct Correlation between Heterogeneous Electron-Transfer Kinetics and Local Density of States in Diamond Electrodes. *Angew. Chem. - Int. Ed.* **2012**, *51* (28), 7002–7006. https://doi.org/10.1002/anie.201203057.

(30) Güell, A. G.; Ebejer, N.; Snowden, M. E.; McKelvey, K.; Macpherson, J. V.; Unwin, P. R. Quantitative Nanoscale Visualization of Heterogeneous Electron Transfer Rates in 2D Carbon Nanotube Networks. *Proc. Natl. Acad. Sci. U. S. A.* **2012**, *109* (29), 11487–11492. https://doi.org/10.1073/pnas.1203671109.

(31) Chen, R.; Nioradze, N.; Santhosh, P.; Li, Z.; Surwade, S. P.; Shenoy, G. J.; Parobek, D. G.; Kim, M. A.; Liu, H.; Amemiya, S. Ultrafast Electron Transfer Kinetics of Graphene Grown by Chemical Vapor Deposition. *Angew. Chem. - Int. Ed.* **2015**, *54* (50), 15134–15137. https://doi.org/10.1002/anie.201507005.

(32) Nioradze, N.; Chen, R.; Kurapati, N.; Khvataeva-Domanov, A.; Mabic, S.; Amemiya, S. Organic Contamination of Highly Oriented Pyrolytic Graphite as Studied by Scanning Electrochemical Microscopy. *Anal. Chem.* **2015**, *87* (9), 4836–4843. https://doi.org/10.1021/acs.analchem.5b00213.

(33) Chen, R.; Hu, K.; Yu, Y.; Mirkin, M. V.; Amemiya, S. Focused-Ion-Beam-Milled Carbon Nanoelectrodes for Scanning Electrochemical Microscopy. *J. Electrochem. Soc.* **2016**, *163* (4), H3032–H3037. https://doi.org/10.1149/2.0071604jes.

(34) Chen, R.; Balla, R. J.; Li, Z.; Liu, H.; Amemiya, S. Origin of Asymmetry of Paired Nanogap Voltammograms Based on Scanning Electrochemical Microscopy: Contamination Not Adsorption. *Anal. Chem.* **2016**, *88* (16), 8323–8331. https://doi.org/10.1021/acs.analchem.6b02273.

(35) Tan, S. Y.; Lazenby, R. A.; Bano, K.; Zhang, J.; Bond, A. M.; Macpherson, J. V.; Unwin, P. R. Comparison of Fast Electron Transfer Kinetics at Platinum, Gold, Glassy Carbon and Diamond Electrodes Using Fourier-Transformed AC Voltammetry and Scanning Electrochemical Microscopy. *Phys. Chem. Chem. Phys.* **2017**, *19* (13), 8726–8734. https://doi.org/10.1039/c7cp00968b.

(36) Lockert, M. R.; Weibel, S. C.; Phillips, M. F.; Shortreed, M. R.; Sun, B.; Corn, R. M.; Hamers, R. J.; Cerrina, F.; Smith, L. M. Carbon-on-Metal Films for Surface Plasmon Resonance Detection of DNA Arrays. *J. Am. Chem. Soc.* **2008**, *130* (27), 8611–8613. https://doi.org/10.1021/ja802454c.

(37) Lockett, M. R.; Smith, L. M. Fabrication and Characterization of DNA Arrays Prepared on Carbon-on-Metal Substrates. *Anal. Chem.* **2009**, *81* (15), 6429–6437. https://doi.org/10.1021/ac900807q.

(38) Lockett, M. R.; Weibel, S. C.; Phillips, M. F.; Shortreed, M. R.; Sun, B.; Corn, R. M.; Hamers, R. J.; Cerrina, F.; Smith, L. M. Carbon-on-Metal Films for Surface Plasmon Resonance Detection of DNA Arrays. *J. Am. Chem. Soc.* **2008**, *130* (27), 8611–8613. https://doi.org/10.1021/ja802454c.

(39) Ulman, A. *An Introduction to Ultrathin Organic Films: From Langmuir-Blodgett to Self-Assembly*; Academic Press: Boston, MA, 1991.

(40) Pinson, J.; Podvorica, F. Attachment of Organic Layers to Conductive or Semiconductive Surfaces by Reduction of Diazonium Salts. *Chem. Soc. Rev.* **2005**, *34* (5), 429. https://doi.org/10.1039/b406228k.

(41) Bélanger, D.; Pinson, J. Electrografting: A Powerful Method for Surface Modification. *Chem. Soc. Rev.* **2011**, *40* (7), 3995. https://doi.org/10.1039/c0cs00149j.

(42) Nicholson, R. S. Theory and Application of Cyclic Voltammetry for Measurement of Electrode Reaction Kinetics. *Anal. Chem.* **1965**, *37* (11), 1351–1355. https://doi.org/10.1021/ac60230a016.

(43) Brown, A. P.; Anson, F. C. Cyclic and Differential Pulse Voltammetric Behavior of Reactants Confined to the Electrode Surface. *Anal. Chem.* **1977**, *49* (11), 1589–1595. https://doi.org/10.1021/ac50019a033.

(44) Besold, J.; Thielsch, R.; Matz, N.; Frenzel, C.; Born, R.; Möbius, A. Surface and Bulk Properties of Electron Beam Evaporated Carbon Films. *Thin Solid Films* **1997**, *293* (1–2), 96–102. https://doi.org/10.1016/S0040-6090(96)09000-1.

(45) Ferrari, A. C.; Robertson, J. Interpretation of Raman Spectra of Disordered and Amorphous Carbon. *Phys. Rev. B* **2000**, *61* (20), 14095–14107. https://doi.org/10.1103/PhysRevB.61.14095.

(46) Chen, P.; McCreery, R. L. Control of Electron Transfer Kinetics at Glassy Carbon Electrodes by Specific Surface Modification. *Anal. Chem.* **1996**, *68* (22), 3958–3965. https://doi.org/10.1021/ac960492r.

(47) Díaz, J.; Paolicelli, G.; Ferrer, S.; Comin, F. Separation of the Sp 3 and Sp 2 Components in the C1 *s* Photoemission Spectra of Amorphous Carbon Films. *Phys. Rev. B* **1996**, *54* (11), 8064–8069. https://doi.org/10.1103/PhysRevB.54.8064.

(48) Zhou, Y.; Wang, B.; Song, X.; Li, E.; Li, G.; Zhao, S.; Yan, H. Control over the Wettability of Amorphous Carbon Films in a Large Range from Hydrophilicity to Super-Hydrophobicity. *Appl. Surf. Sci.* **2006**, *253* (5), 2690–2694. https://doi.org/10.1016/j.apsusc.2006.05.118.

(49) Kwok, S. C. H.; Wang, J.; Chu, P. K. Surface Energy, Wettability, and Blood Compatibility Phosphorus Doped Diamond-like Carbon Films. *Diam. Relat. Mater.* **2005**, *14* (1), 78–85. https://doi.org/10.1016/j.diamond.2004.07.019.

(50) Chen, J. S.; Lau, S. P.; Tay, B. K.; Chen, G. Y.; Sun, Z.; Tan, Y. Y.; Tan, G.; Chai, J. W. Surface Energy of Amorphous Carbon Films Containing Iron. *J. Appl. Phys.* **2001**, *89* (12), 7814–7819. https://doi.org/10.1063/1.1375808.

(51) Schulz, H.; Leonhardt, M.; Scheibe, H. J.; Schultrich, B. Ultra Hydrophobic Wetting Behaviour of Amorphous Carbon Films. *Surf. Coat. Technol.* **2005**, *200* (1-4 SPEC. ISS.), 1123–1126. https://doi.org/10.1016/j.surfcoat.2005.02.019.

(52) Mattia, D.; Bau, H. H.; Gogotsi, Y. Wetting of CVD Carbon Films by Polar and Nonpolar Liquids and Implications for Carbon Nanopipes. *Langmuir* **2006**, *22* (4), 1789–1794. https://doi.org/10.1021/la0518288.

(53) Kuo, T. C.; McCreery, R. L. Surface Chemistry and Electron-Transfer Kinetics of Hydrogen-Modified Glassy Carbon Electrodes. *Anal. Chem.* **1999**, *71* (8), 1553–1560. https://doi.org/10.1021/ac9807666.

(54) McCreery, R. L.; Cline, K. K.; McDermott, C. A.; McDermott, M. T. Control of Reactivity at Carbon Electrode Surfaces. *Colloids Surf. Physicochem. Eng. Asp.* **1994**, *93* (C), 211–219. https://doi.org/10.1016/0927-7757(94)02899-0.

(55) Finot, M. O.; Braybrook, G. D.; McDermott, M. T. Characterization of Electrochemically Deposited Gold Nanocrystals on Glassycarbon Electrodes. *J. Electroanal. Chem.* **1999**, *466* (2), 234–241. https://doi.org/10.1016/S0022-0728(99)00154-0.

(56) Adzic, R.; Yeager, E.; Cahan, B. D. Optical and Electrochemical Studies of Underpotential Deposition of Lead on Gold Evaporated and Single-Crystal Electrodes. *J. Electrochem. Soc.* **1974**, *121* (4), 474. https://doi.org/10.1149/1.2401841.

(57) Engelsmann, K. Underpotential Deposition of Lead on Polycrystalline and Single-Crystal Gold Surfaces Part II. Kinetics. *J. Electroanal. Chem.* **1980**, *114*, 11–24. https://doi.org/10.1016/0368-1874(80)80360-1.

(58) Engelsmann, K.; Lorenz, W. J.; Schmidt, E. Underpotential Deposition of Lead on Polycrystalline and Single-Crystal Gold Surfaces. Part I. Thermodynamics. *J. Electroanal. Chem.* **1980**, *114* (1), 1–10. https://doi.org/10.1016/S0022-0728(80)80431-1.

(59) Hamelin, A. Underpotential Deposition of Lead on Single Crystal Faces of Gold. Part I. The Influence of Crystallographic Orientation of the Substrate. *J. Electroanal. Chem.* **1984**, *165* (1–2), 167–180. https://doi.org/10.1016/S0022-0728(84)80095-9.

(60) Hamelin, A.; Lipkowski, J. Underpotential Deposition of Lead on Gold Single Crystal Faces. Part II. General Discussion. *J. Electroanal. Chem.* **1984**, *171* (1–2), 317–330. https://doi.org/10.1016/0022-0728(84)80123-0.

(61) Chen, R.; Najarian, A. M.; Kurapati, N.; Balla, R. J.; Oleinick, A.; Svir, I.; Amatore, C.; McCreery, R. L.; Amemiya, S. Self-Inhibitory Electron Transfer of the Co(III)/Co(II)-Complex Redox Couple at Pristine Carbon Electrode. *Anal. Chem.* **2018**, *90* (18), 11115–11123. https://doi.org/10.1021/acs.analchem.8b03023.

(62) Gerischer, H. An Interpretation of the Double Layer Capacity of Graphite Electrodes in Relation to the Density of States at the Fermi Level. *J. Phys. Chem.* **1985**, *89* (20), 4249–4251. https://doi.org/10.1021/j100266a020.

(63) Gerischer, H.; McIntyre, R.; Scherson, D.; Storck, W. Density of the Electronic States of Graphite: Derivation from Differential Capacitance Measurements. *J. Phys. Chem.* **1987**, *91* (7), 1930–1935. https://doi.org/10.1021/j100291a049.

(64) Ranganathan, S.; McCreery, R.; Majji, S. M.; Madou, M. Photoresist-Derived Carbon for Microelectromechanical Systems and Electrochemical Applications. *J. Electrochem. Soc.* **2000**, *147* (1), 277. https://doi.org/10.1149/1.1393188.

(65) Ranganathan, S.; McCreery, R. L. Electroanalytical Performance of Carbon Films with Near-Atomic Flatness. *Anal. Chem.* **2001**, *73* (5), 893–900. https://doi.org/10.1021/ac0007534.

(66) Blackstock, J. J.; Rostami, A. A.; Nowak, A. M.; McCreery, R. L.; Freeman, M. R.; McDermott, M. T. Ultraflat Carbon Film Electrodes Prepared by Electron Beam Evaporation. *Anal. Chem.* **2004**, *76* (9), 2544–2552. https://doi.org/10.1021/ac035003j.

(67) McDermott, M. T.; McCreery, R. L. Scanning Tunneling Microscopy of Ordered Graphite and Glassy Carbon Surfaces: Electronic Control of Quinone Adsorption. *Langmuir* **1994**, *10* (11), 4307–4314. https://doi.org/10.1021/la00023a062.

(68) Brown, A. P.; Koval, C.; Anson, F. C. Illustrative Electrochemical Behavior of Reactants Irreversibly Adsorbed on Graphite Electrode Surfaces. *J. Electroanal. Chem.* **1976**, *72*, 379–387.

(69) Xu, J.; Chen, Q.; Swain, G. M. Anthraquinonedisulfonate Electrochemistry: A Comparison of Glassy Carbon, Hydrogenated Glassy Carbon, Highly Oriented Pyrolytic Graphite, and Diamond Electrodes. *Anal. Chem.* **1998**, *70* (15), 3146–3154. https://doi.org/10.1021/ac9800661.

(70) Kozbial, A.; Li, Z.; Sun, J.; Gong, X.; Zhou, F.; Wang, Y.; Xu, H.; Liu, H.; Li, L. Understanding the Intrinsic Water Wettability of Graphite. *Carbon* **2014**, *74*, 218–225. https://doi.org/10.1016/j.carbon.2014.03.025.

(71) Li, Z.; Wang, Y.; Kozbial, A.; Shenoy, G.; Zhou, F.; McGinley, R.; Ireland, P.; Morganstein, B.; Kunkel, A.; Surwade, S. P.; Li, L.; Liu, H. Effect of

Airborne Contaminants on the Wettability of Supported Graphene and Graphite. *Nat. Mater.* **2013**, *12* (10), 925–931. https://doi.org/10.1038/nmat3709.

(72) Patel, A. N.; Collignon, M. G.; OConnell, M. A.; Hung, W. O. Y.; McKelvey, K.; MacPherson, J. V.; Unwin, P. R. A New View of Electrochemistry at Highly Oriented Pyrolytic Graphite. *J. Am. Chem. Soc.* **2012**, *134* (49), 20117–20130. https://doi.org/10.1021/ja308615h.

(73) Luong, J. H. T.; Male, K. B.; Glennon, J. D. Boron-Doped Diamond Electrode: Synthesis, Characterization, Functionalization and Analytical Applications. *Analyst* **2009**, *134* (10), 1965–1979. https://doi.org/10.1039/b910206j.

(74) Chen, Q.; Swain, G. M. Structural Characterization, Electrochemical Reactivity, and Response Stability of Hydrogenated Glassy Carbon Electrodes. *Langmuir* **1998**, *14* (24), 7017–7026. https://doi.org/10.1021/la980907z.

Chapter 3. Spontaneous Grafting of Aryldiazonium Salts on Carbon-on-Gold Substrates

3.1 Introduction

Carbon materials have found applications in environmental remediation, energy conversion/storage, optical coatings, bioimaging, and medical devices due to their versatility in electronic, optical, and chemical properties.[1] Amorphous carbon, prepared by either sputtering or electron-beam evaporation, has been employed as electrodes,[2–8] optically transparent electrodes,[9,10] surface plasmon resonance substrates,[11,12] and molecular electronic junctions.[13,14] Many of these applications depend on the control of the interfacial structures, properties, and reactivities of the surface, which can be enabled by grafting molecular layers to the surface. Therefore, strategies to functionalize of carbon surfaces have been the subject of intense investigations.

Aryldiazonium attachment, which can be induced electrochemically or occur spontaneously from solution, is a versatile approach to modify carbon surfaces. Electrochemical grafting of aryldiazonium salts offers stable covalent attachment of a wide variety of useful functional groups to a surface but often with difficulty to control the film structure; hence, it usually leads to formation of disordered multilayers.[15–19] The spontaneous grafting of aryldiazonium salts is less well-understood but potentially more advantageous since no electrical contact is required, thus, is applicable to a wide range of substrates, such as poor conductors, nanostructured materials, and nanoparticles in suspension.[20–24] This "device-less" approach is also simple and convenient to scale-up for industrial production.[25]

The spontaneous grafting of aryldiazonium salts to amorphous carbon substrates has not been studied extensively. Colavita and co-workers demonstrated that the rates and yields of the spontaneous attachment from aqueous solutions correlate with the graphitic content of the amorphous carbon substrates, as does the proportion of azo linkages in the resulting adlayers.[1,26–28] However, deposition conditions other than immersion time, i.e., solvent, aryldiazonium ion concentration,

and para-substituent other than nitro group, remain unexplored, as do the thicknesses and properties of the resulting organic films from the spontaneous attachment.

In this chapter, we aim to address these questions by studying the spontaneous attachment of several aryldiazonium salts at amorphous carbon substrates prepared by electron-beam evaporation. The carbon layer is 10 nm thick and was deposited on a 42 nm gold layer for future SPR applications. Carbon-on-gold substrates also have been used in molecular electronic junctions. Here, we would like to investigate whether the spontaneous grafting at amorphous carbon surfaces can be extended to other aryldiazonium salts in addition to 4-nitrobenzene diazonium tetrafluoroborate (NBD). Also, we would like to investigate whether the electron withdrawing abilities of the para-substituents influence the grafting. Therefore, 4-carboxybenzene diazonium tetrafluoroborate (CBD) and 4-bromobenzene diazonium tetrafluoroborate (BBD) were chosen. CBD gives grafted carboxyphenyl (CP) groups, which would be useful as tether layers for subsequent coupling reactions. The modified surfaces will be referred to by the symbol of the substrate and followed by the para-substituent of the diazonium salt used for the derivatization, for example, eC-NO_2. A combination of spectroscopic and electrochemical techniques was used to optimize the grafting conditions as well as to understand the structure and properties of the grafted layers and the structure-reactivity relationships of carbon surfaces.

3.2 Experimental

3.2.1 Chemicals and Materials

Concentrated sulfuric acid (95–98%, Caledon); potassium chloride (ACS reagent, 99.0–100.5%, Aldrich); potassium ferricyanide (certified reagent, Caledon); tetrabutylammonium tetrafluoroborate ($TBABF_4$) (99%, Aldrich); 2-propanol (certified ACS, Fisher); acetonitrile (ACN, for HPLC, gradient grade, ≥99.9%, Aldrich); acetone (ACS reagent, ≥99.5%, Aldrich) were used as received. 4-nitrobenzenediazonium tetrafluoroborate (NBD), 4-bromobenzenediazonium tetrafluoroborate (BBD), and 4-carboxybenzene diazonium tetrafluoroborate (CBD) were synthesized and recrystallized before use, as detailed elsewhere.[29] Solutions

were prepared fresh and purged with nitrogen gas for 10 min before use. Aqueous solutions were prepared with deionized water (DI), purified, and deionized through a Barnstead E-Pure system (18.2 MΩ cm, ThermoFisher).

3.2.2 Film Preparation

Chromium, gold, and carbon layers were deposited onto p-type, (100) oriented silicon wafers, which were diced into 1.3 × 1.85 cm^2 chips. The silicon chips were cleaned by sonication in acetone, isopropyl alcohol, and DI for 15 min each, dried with nitrogen gas, and then loaded into the evaporation vacuum chamber (Kurt Lesker PVD 75). The chamber was pumped to a typical pressure of less than 5 × 10^{-6} Torr. Layers shown in Figure 3-1 were deposited without breaking vacuum with thicknesses and evaporation rates as follows: Cr adhesion layer (2 nm, 0.02 nm/s), Au (42 nm, 0.03 nm/s), and eC (10 nm, 0.01 nm/s). The target for carbon deposition was spectroscopically pure graphite rods (SPI Supplies, PA). Evaporation rates were controlled with a quartz crystal microbalance.

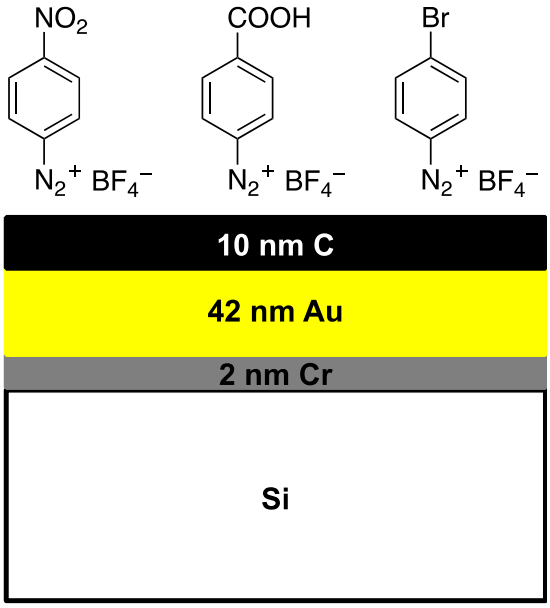

Figure 3-1. Illustration of an eC electrode with indicated thicknesses of deposited layers on a Si substrate and the aryldiazonium salts that were used in this work.

3.2.3 Surface Modification

Modified surfaces were prepared by immersing electron-beam evaporated carbon electrodes (eC) and glassy carbon electrodes (GC) in DI or ACN containing the aryldiazonium salts. The aryldiazonium salts used in this work are shown in Figure 3-1. The surface reactions were carried out in the dark to avoid photodecomposition of the diazonium salts.[30] Before modification, GC plates (Tokai GC 20, 2.5 cm × 6 cm) were polished manually in successively 1, 0.3, and 0.05 μm alumina slurries on Microcloth polishing cloth (Buehler), followed by sonication in DI for 15 min. The eC electrodes were used as deposited. After modification, the eC and GC electrodes were rinsed well with DI or ACN to remove physisorbed material and dried with nitrogen gas. Removing physisorbed material by sonicating the modified substrates in organic solvents was not used because it would delaminate the carbon layer.

3.2.4 Surface Characterization

Cyclic voltammetry (CV) and open circuit potentials (OCPs) were performed with a three-electrode cell and a bipotentiostat (model AFCBP1, Pine Instruments). Home-made Ag|AgCl|KCl (3.5 M) and $Ag|Ag^+$ (0.2 M in ACN containing 0.1 M $TBABF_4$) reference electrodes were used for aqueous and non-aqueous solutions, respectively. A Pt mesh was used as a counter electrode. Modified eC or GC served as working electrodes, the geometrical area of which were defined by a Viton O-ring. Chronoamperometry in 1 mM $Fe(CN)_6^{3-}$ in 1 M KCl yielded an electrode area of 0.319 ± 0.005 cm^2 (N = 3). CV experiments were conducted in nitrogen-purged 0.1 M H_2SO_4 at room temperature (22 ± 1 °C). The surface coverage of nitrophenyl groups was determined by integrating the peak area associated with the reduction of nitro groups obtained during the first scan using Origin software. OCPs were measured using the above-described three-electrode cell in ~10 mL of DI or ACN, all contained in a 20 mL beaker. The cell was stirred with a magnetic stirring bar during these measurements. The electrode was equilibrated in DI or ACN for about 5 min before a small volume of NBD (dissolved in the respective solvent) was added to the stirred cell to bring the final cell concentration of NBD to 1 mM.

Infrared reflection-absorption spectroscopy (IRRAS) spectra were collected

on a Nicolet 8700 Fourier transform infrared (FTIR) spectrometer (Thermo Fisher Scientific) equipped with a mercury cadmium telluride (MCT) detector, a specular reflectance accessory (80 Spec, Pike Technologies). 1024 spectra were collected at 80° incidence and 4 cm^{-1} resolution using a bare gold slide as background.

X-ray Photoelectron Spectroscopy (XPS) experiments were performed at room-temperature at nanoFAB using Kratos Axis (Ultra) spectrometer with monochromatized Al K_α (1486.71 eV). The spectrometer was calibrated by Au $4f_{7/2}$ binding energy (84.0 eV) with reference to the Fermi level. The analysis chamber pressure is better than 5×10^{-10} Torr. CASA XPS was used for atomic ratio calculations and component analysis. Note: Adventitious carbon was likely present and thus complicated the interpretation of C 1s spectra.

Water Contact Angle measurements were performed with a 4 μL droplet volume using a Ráme-Hart goniometer (model 590) equipped with DROPimage advanced software. The reported values are the averages of two measurements on each sample (N = 3).

Atomic Force Microscopy (AFM) images were collected with a Dimension Edge Atomic Force Microscope (Bruker) using commercial Si tips with a resonant frequency of 300 kHz and a force constant of 40 N/m (Tap300, Ted Pella, Inc.). The scan rate was 1–2 Hz, and the scanning density was 512 lines/frame. The thicknesses of the organic layers were determined by "AFM scratching", as previously described by Anariba et. al.[31] The applied force was determined empirically so that it is sufficient to remove the organic layers without damaging the surface. A set point voltage of 0.5 V was used for all experiments. AFM images were processed with NanoScope Analysis v1.40. The images, with the exclusion of the 'scratched' regions, were flattened with a first-order polynomial before analysis. Then, a line-scan profile was drawn across the scratched region to determine the thickness of the organic layer. At least 9 line-scan profiles were averaged to determine scratch depths reported in Table 3-2.

3.3 Results and Discussion

Electron-beam deposited carbon on a gold substrate (eC) has been characterized thoroughly in Chapter 2. Specifically, eC provides an ultraflat surface with a root-mean-square (rms) roughness of 0.72 ± 0.08 nm and is composed of disordered amorphous carbon with ~30% sp^3 content. The surface of eC is hydrophilic (water contact angle 44° ± 2°) and low in oxygenated functionalities (O/C ratio 5.8 ± 0.2%). The electrochemical performance of eC also was studied and compared with the conventional glassy carbon electrode. eC exhibits low background current and fast electron-transfer kinetics for benchmark redox systems, which makes it attractive as an electrode material for sensor applications and useful as a working electrode for cyclic voltammetry (CV) and open circuit potential (OCP) measurements in this chapter.

First, we tested whether aryldiazonium salts can be grafted on eC without electrochemical induction. Successful modification of eC with NBD was confirmed by FT-IRRAS and water contact angle measurements. Figure 3-2 contains an absorbance spectrum obtained from eC-NO_2 after eC was immersed in 1 mM NBD aqueous solution for 30 min. Based on spontaneous grafting of NBD at sputtered amorphous carbon substrate,[27] the two peaks at 1524 and 1354 cm^{-1} are assigned to the asymmetric and symmetric stretching modes of the nitro group. A band at around 2300 cm^{-1} due to the diazo stretch is absent in the spectrum, indicating that the nitrophenyl (NP) film was formed by a radical attachment mechanism.[32]

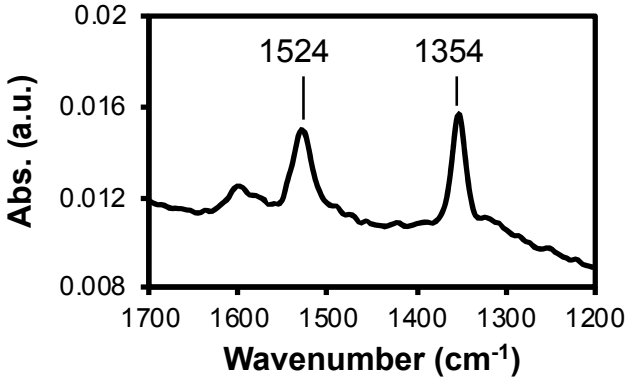

Figure 3-2. FT-IRRAS spectrum showing the stretching mode region of the nitro group recorded on eC modified by immersion in 1 mM NBD aqueous solution for 30 min.

Polished GC gives a water contact angle of 50° and increases to 58 ± 4° (N = 4) after grafting with NP film.[33] Water contact angle on eC-NO_2 (Figure 3-3A) increased from 44° ± 2° to 51° ± 3°, slightly more hydrophobic than bare eC and consistent with the presence of a surface-attached NP film. From this, we went on to investigate the effects of grafting conditions, i.e., deposition time, concentration of NBD, solvent, para-substituent, and substrate, on grafting yields, and the properties of the grafted organic layers.

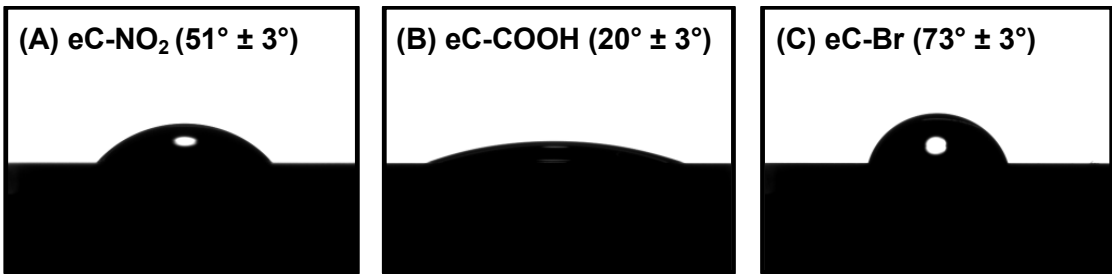

Figure 3-3. Contact angle measurements on eC modified by immersion in 1 mM NBD (A), CBD (B), and BBD (C) aqueous solutions for 30 min.

Deposition time. eC was immersed in 1 mM NBD aqueous solution for predetermined times, then removed from the deposition solution, rinsed with DI, dried with nitrogen gas, and characterized by CV in 0.1 M H_2SO_4. Surface-attached NP groups can be reduced electrochemically to phenylamine groups, and the charge associated with the electroreduction of surface-bound NP can be calculated to give the yield of the spontaneous grafting reactions. Figure 3-4A depicts a representative CV on eC-NO_2 after 30 min immersion. On the first scan, the broad irreversible wave at –0.6 V is attributed to the 6-electron reduction of NP to aminophenyl groups (eq 1), and the small anodic wave near 0.4 V is attributed to the reoxidation of hydroxyaminophenyl groups (eq 2) produced as intermediates of the reduction. On the second scan, the reduction wave disappeared completely, indicating that all surface-bound NP groups have been reduced. The reversible wave observed near 0.3 V is ascribed to the interconversion of hydroxyaminophenyl/nitrosophenyl groups (eq 3).[34,35]

$$\text{eC–Ph–NO}_2 + 6\text{H}^+ + 6\text{e}^- \rightarrow \text{eC–Ph–NH}_2 + 2\text{H}_2\text{O} \quad (1)$$

$$\text{eC–Ph–NO}_2 + 4\text{H}^+ + 4\text{e}^- \rightarrow \text{eC–Ph–NHOH} + \text{H}_2\text{O} \quad (2)$$

$$eC{-}Ph{-}NO + 2H^+ + 2e^- \leftrightarrow eC{-}Ph{-}NHOH \quad (3)$$

The absence of a reduction peak near 0 V suggested that no physisorbed aryldiazonium cations were present.[36] CV demonstrates that eC has been readily modified with NP groups by spontaneous grafting with NBD in aqueous medium and that the nitrobenzene diazonium cations did not simply physisorb to the surface, in agreement with FT-IRRAS (see above) and XPS results (see below).

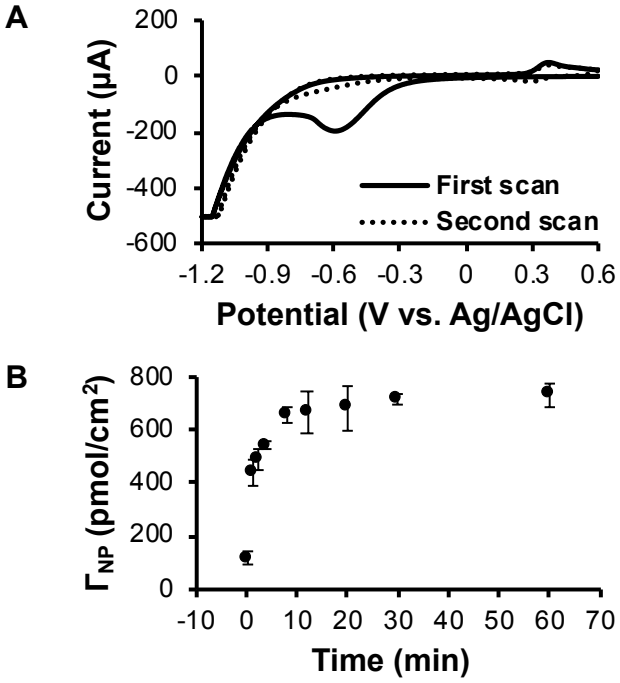

Figure 3-4. (A) Cyclic voltammogram obtained in 0.1 M H_2SO_4 at 0.2 V/s on eC modified by immersion in 1 mM NBD aqueous solution for 30 min. (B) Surface coverage of nitrophenyl (NP) groups, Γ_{NP}, on eC as a function of deposition time in 1 mM NBD aqueous solution.

Surface coverage of NP groups, Γ_{NP}, can be calculated from the total charge passed during NP reduction and hydroxyaminophenyl oxidation according to $\Gamma_{NP} = Q/nFA$, where Q is the charge integrated under the CV peak, $n = 6$ is the number of electrons involved per NP group, F is the Faraday constant, and A is the geometric electrode area determined from chronoamperometry.[27] Given that the NP reduction peak is much larger than the hydroxyaminophenyl oxidation peak, the latter was ignored in determining Γ_{NP}. The NP reduction peak was integrated and normalized to the electrode area to obtain Γ_{NP} in Figure 3-4B. Grafting occurred at eC for all immersion times, and a rapid increase in Γ_{NP} was observed during the first 10

min of the deposition, followed by a plateau at longer immersion times. Γ_{NP} reached a steady-state value of (7.3 ± 0.5) × 10^{-10} mol/cm^2 after 30 min, less than the ideal closest packing concentration of 12 × 10^{-10} mol/cm^2 for a monolayer determined theoretically.[37] In comparison with other carbon substrates, the steady-state Γ_{NP} at eC is comparable to the value of ~8 × 10^{-10} mol/cm^2 reported for NBD-grafted sputtered carbon electrodes deposited on stainless steel substrates[27] and is 59% of that found at GC under the same deposition conditions, as shown in Figure 3-5.

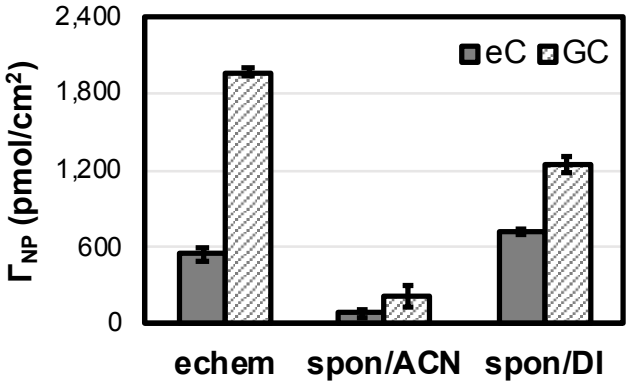

Figure 3-5. Surface coverage of nitrophenyl groups, Γ_{NP}, on modified eC (solid gray columns) and GC (striped gray columns) electrodes. "echem": electrochemical grafting by two sweeps CV at 0.2 V/s with 1 mM NBD and 0.1 M $TBABF_4$ in ACN. "sspon/ACN": spontaneous grafting by immersion in 1 mM NBD in ACN for 30 min. "spon/DI": spontaneous grafting by immersion in 1 mM NBD in DI for 30 min.

Concentration of NBD. To study the effect of NBD concentration on Γ_{NP}, eC was immersed in various concentrations of NBD while keeping the immersion time constant. After 30 min, eC was removed from the deposition solution, rinsed with DI, dried with nitrogen gas, and characterized by CV in 0.1 M H_2SO_4. Γ_{NP} was calculated, as described above, and plotted against NBD concentration in Figure 3-6. Higher concentrations of NBD resulted in higher Γ_{NP}, and Γ_{NP} reached a steady-state value at a concentration of 10^{-3} M or higher. The dependence of surface coverage of NP groups on NBD concentration also has been studied at other substrates. For example, Mesnage et al. reported that similar amounts of NP groups were obtained on gold when the diazonium salt concentration was higher than 10^{-5} M and that this amount was undetectable when the concentration was below 10^{-8} M, as determined by

IR-ATR.[38] Adenier et al. observed that doubling NBD concentrations quadrupled NP surface coverage on GC and doubled NP film thickness on iron.[39]

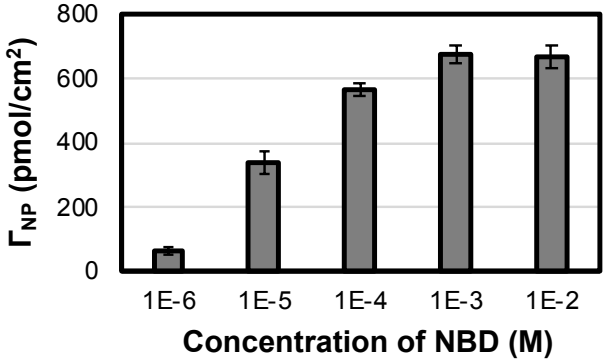

Figure 3-6. Surface coverage of nitrophenyl groups, Γ_{NP}, on eC immersed in various concentrations of NBD in aqueous solutions for 30 min.

Solvent. The spontaneous grafting process also was carried out in a non-aqueous medium with the use of ACN, the solvent usually used in the electrochemical grafting of aryldiazonium salts. eC was immersed in 1 mM NBD dissolved in either DI or ACN. After 30 min, eC was removed from the deposition solutions, rinsed with DI or ACN, dried with nitrogen gas, and characterized by CV in 0.1 M H_2SO_4 and XPS. Surface coverage of nitrophenyl groups on eC electrodes, Γ_{NP}, was determined from CV and presented in Figure 3-5. Electrochemical grafting of 1 mM NBD in ACN by two potential cycles from 0.1 V to –0.7 V at 0.2 V/s was included for comparison because this procedure was classified as producing near monolayer coverage.[32] Spontaneous grafting of NBD in an aqueous medium (spon/DI) produced NP surface coverage slightly higher than electrochemical modification (echem) and higher than spontaneous grafting in ACN (spon/ACN) by a factor of 8. The effect of solvent on spontaneous grafting of aryldiazonium salts varies at different substrates. Downard et al. reported that GC shows similar reactivity toward spontaneous grafting of NBD in ACN and aqueous acid, reaching a surface coverage of ~32 $\times$ 10^{-10} mol/cm^2 after 30 min in both media.[40] In our lab, we observed a lower surface coverage of NP at GC in ACN than in DI (Figure 3-5). These different observations could stem from the differences in sources of GC and polishing and deposition procedures that were used. Lower grafting yield in ACN than aqueous medium also

was reported for gold[38] and PPF,[40] but it is unclear why. On copper, however, Chamoulaud et al. reported that spontaneous grafting of in-situ generated NBD in aqueous acid is less efficient than in ACN and attributed this to the spontaneous formation of Cu(II) and a less favorable OCP value in aqueous media.[41]

We then conducted XPS analysis to characterize the NP films at NBD-modified eC. Survey spectra of modified eC exhibit the characteristic C 1s, O 1s, and N 1s at about 285, 530, and 400 eV, respectively (Figure 3-7A). Table 3-1 summarizes the atomic composition of unmodified eC and eC modified by spontaneous and electrochemical reduction of NBD. In line with CV results, spontaneous grafting of NBD in aqueous solutions yielded %N/C and %O/C higher than in ACN and comparable to electrochemical induction method.

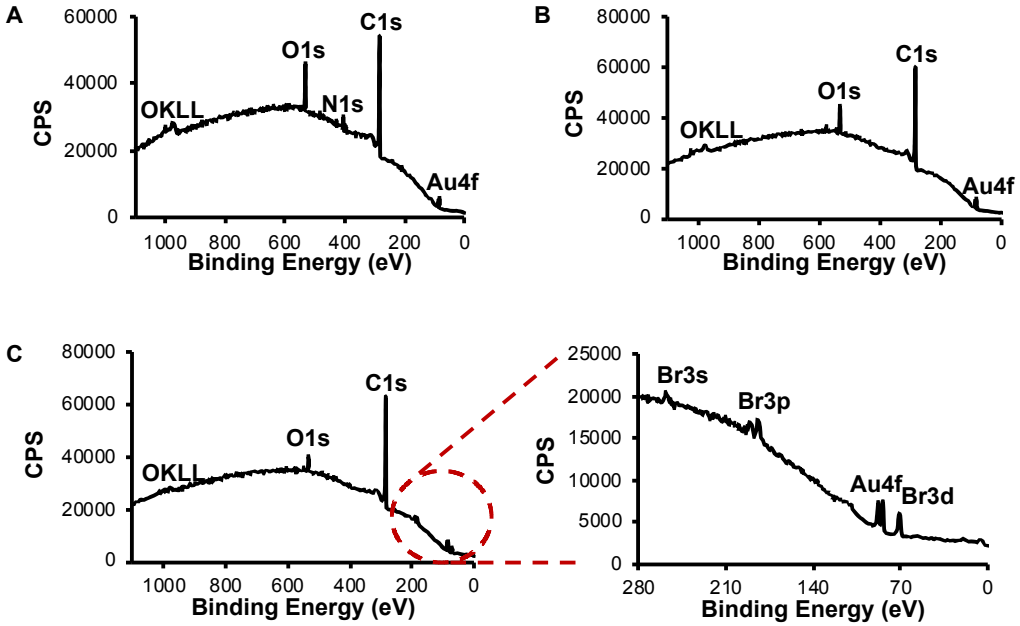

Figure 3-7. XPS survey spectra of eC modified by immersion in 1 mM NBD (A), 1 mM CBD (B), and 1 mM BBD (C) aqueous solutions for 30 min.

Table 3-1. Chemical Composition of Bare and Modified eC Electrodes Obtained from XPS

	%C 1s[a]	%O 1s[b]	%N 1s[c]	%O/C	%N/C	N400/N406
bare eC	94.4	5.5	ND	5.8 ± 0.2	ND	ND
spon/ACN	85.4	12.0	2.4	14.1	2.8	0.79
spon/DI	81.0 ± 0.6	12.7 ± 0.5	6.0 ± 0.1	15.6 ± 0.0	7.4 ± 0.2	0.54 ± 0.03
echem	81.4	12.8	5.7	15.7	7.0	0.55

[a]C 1s corresponds to the peak at 284.5 eV, [b]O 1s corresponds to the peak at 532.5 eV, [c]N 1s corresponds to the sum of the peaks attributed to nitro and azo groups.

Figure 3-8 contains N 1s regions of unmodified and NBD-modified eC electrodes. The N 1s spectra of modified electrodes display two peaks with maxima centred around 406 and 400 eV, with the former assigned to the nitro groups[35,39,41–43] and the latter to the azo moieties[1,43] or the reduction of the nitro groups inside the spectrometer by the X-ray beam.[39,42] The presence of azo linkages can result from the attack of non-reduced aryldiazonium ions on the surface (direct grafting) or on already grafted NP moieties (multilayer formation). The N 1s core-level spectra of modified electrodes shows no peaks at 403.8 and 405.1 eV, which are characteristic of diazonium cations,[35,44] indicating that nitrobenzene diazonium cations did not simply physisorb to the electrode surface. The N 1s region of the unmodified electrode shows no peak, indicating that the observed peaks arise from grafting of NP groups.

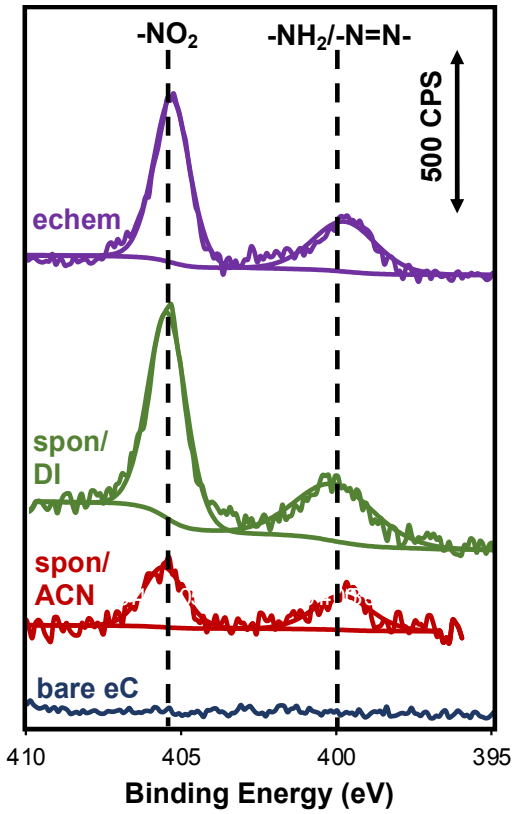

Figure 3-8. XPS N 1s core level spectra of bare (blue) and modified eC electrodes. "spon/ACN" (red): spontaneous grafting by immersion in 10 mM NBD in ACN for 150 min. "spon/DI" (green): spontaneous grafting by immersion in 1 mM NBD in DI for 30 min. "echem" (purple): electrochemical grafting by 2 sweeps CV at 0.2 V/s with 1 mM NBD and 0.1 M $TBABF_4$ in ACN.

From the integrated signal intensities of N 1s peaks, N 1s 400/N 1s 406 of spon/DI eC is similar to that of echem eC and lower than that of spon/ACN eC. Compared to other substrates, the proportion of azo linkages of spon/DI eC (~35%) is structurally similar to NBD spontaneously grafted and electrografted gold[43] (~35%) and electrografted GC[33] (34–42%). Given that the expected N 1s 400/N 1s 406 for NBD molecules adsorbing with a diazo group intact is 2:1 and attributing the peak located at 400 eV to the presence of azo bridges, it can be calculated that the percentages of total NP groups attached through azo linkages are 40% for spon/ACN and 27% for spon/DI and echem electrodes. Since low surface coverages of NP in ACN were obtained by both CV and XPS, it can be deduced that most of the azo bonds are located at the surface of eC. In summary, XPS results demonstrate that NP films formed by spontaneous reaction in DI appear similar to those electrografted but different from those spontaneously grafted in ACN in terms of yield and structure.

Herein, we have focused our attention on spontaneous grafting of aryldiazonium salts in aqueous media because the reaction appears substantially more facile and rapid.

It is worth noting that physisorbed materials likely present in the aryl films for both solvents and perhaps more so for DI because cleaning by sonication cannot be used for eC/Au substrates, as discussed in Chapter 2. In addition, as the pH of DI in our lab is ~5.5, diazonium salts dissolved in DI are likely transformed into the less stable diazohydroxides and diazoates.[45] These derivatives can also graft spontaneously on metals[46] and graphene sheets.[47] Even though diazonium salts are more stable in aqueous acid, spontaneous grafting of diazonium salts has been observed at neutral[46] or basic pH.[48]

Para-substituent on aryldiazonium salt. The spontaneous grafting on amorphous carbon reported to date concerns aryldiazonium salts bearing only nitro groups;[1,26–28] thus, it is our intention to expand this reaction to other less electron-withdrawing para-substituents such as carboxy and bromo groups. The reduction peak potentials of 0.1 mM NBD, CBD, and BBD vs SCE were reported to be 0.20, 0.10, and 0.02 V (at GC in 0.1 M $TBABF_4$/ACN), which correlates well with the electron-withdrawing properties of these substituents.[42] Additionally, carboxyphenyl (CP) films that resulted from grafting of CBD are useful as tether layers for subsequent coupling reagents. CP and bromophenyl (BP) films are not electroactive, but their presence can be detected by water contact angle measurements and XPS. eC was immersed in 1 mM aqueous solutions of the salts for 30 min, then removed from the deposition solution, rinsed with DI, dried with nitrogen gas, and characterized by water contact angle, XPS and AFM. The results are summarized in Table 3-2.

Table 3-2. Results from water contact angle (WCA), XPS, and AFM characterization of bare eC and eC modified with NBD (eC-NO_2), CBD (eC-COOH), and BBD (eC-Br)

	WCA/Wettability	XPS/Atomic composition	AFM/Film thickness
eC	44° ± 2°	O/C: 5.8% - 8%	NA
eC-NO_2	51° ± 3°	N/C: 7.4 ± 0.2%	1.9 ± 0.3 nm
eC-COOH	20° ± 3°	O/C: 11.9 ± 0.1%	1.2 ± 0.2 nm
eC-Br	73° ± 3°	Br/C: 1.77 ± 0.02%	0.6 ± 0.2 nm

Water contact angle. Successful modification is evident from a decrease in water contact angles for eC-COOH and an increase for eC-Br, rendering hydrophilic

surfaces for the former and hydrophobic surfaces for the latter (Figure 3-3B, C). Microcontact printing of CBD in acidic medium on PPF decreases water contact angles from 68 ± 2° to 31 ± 2°, consistent with the attachment of hydrophilic CP groups.[36]

AFM. The thicknesses of organic films were measured with AFM scratching, which is ideally to be conducted on low roughness surfaces like PPF.[36] The low surface roughness of eC facilitates AFM measurements of the organic film thicknesses. Briefly, the surface was scratched with an AFM tip to remove a small section of the grafted film; next, without changing the tip, the ploughed area was profiled to determine the film thickness. Figure 3-9 shows a topographic image following scratching at eC-NO_2 and the corresponding cross-sectional depth profile of the top image. The high topographical features on the side of the scratch are debris that has built up during the scratch. The procedure also was carried out for eC-COOH and eC-Br, and the average film thicknesses are reported in Table 3-2. Spontaneous grafting of aryldiazonium salts slightly smoothen the substrate surface (modified substrates have a roughness of ~0.5–0.6 nm) and resulted in the formation of homogenous layers. NBD yielded the highest thickness, and BBD the lowest, which appears to correlate with the trend in electron withdrawing effect of the para-substituents. Anariba et al. also found a correlation between the ease of reduction of the diazonium salt and the resulting film thickness electrochemically grafted to PPF substrates.[31] As a monolayer of NP groups oriented vertically to the surface has a calculated thickness of 0.79 nm,[40] we can estimate that NBD formed 2–3 layers, CBD 1–2 layers, and BBD close to a monolayer at eC, resembling those formed by microcontact printing of NBD and CBD inks at PPF.[40]

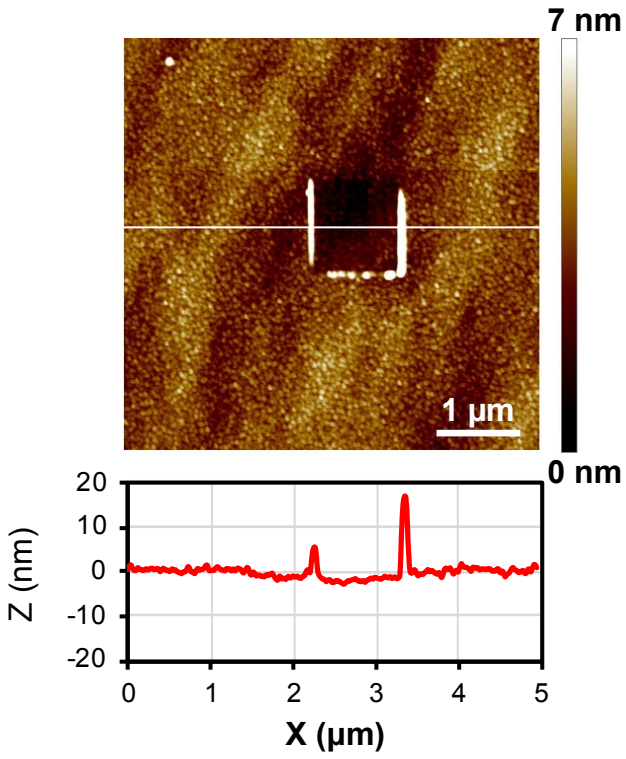

Figure 3-9. AFM topographic image followed scratching at eC modified by immersion in 1 mM NBD aqueous solution for 30 min and cross-sectional depth profile of the top image.

XPS. Successful modification of eC with CBD and BBD is evidenced from an increase in the O/C ratio (Figure 3-7B) and the presence of Br 3d peak at 71 eV (Figure 3-7C), respectively. Figure 3-10 shows the high-resolution spectrum of Br 3d peak which was fitted with Br 3d5/2 and Br 3d3/2 due to spin-orbit coupling; this peak is absent on unmodified eC. Table 3-2 contains the atomic ratios of unmodified and modified substrates. The O/C ratio of eC-COOH increased to 12%, ~8% of which can be attributed to the native oxides on unmodified eC surface and the rest to the carboxyl functional groups. XPS atomic ratios suggest that NBD results in the highest grafting yields and BBD the lowest, which again corresponds with the electron-withdrawing effect of the para substituents.

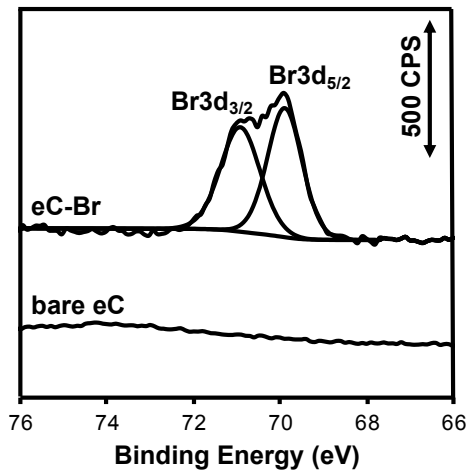

Figure 3-10. XPS Br 3d core level spectra of bare eC and eC modified by immersion in 1 mM BBD aqueous solution for 30 min.

eC-COOH and eC-Br also show peaks at 400 eV in the N 1s core level spectra, as shown in Figure 3-11. This peak corresponds to a reduced nitrogen atom identified as azo linkages, as discussed above. This suggests the existence of azo bonds in the structure of the organic layers formed by all three aryldiazonium salts, and the reduction of nitro groups by X-ray beam alone cannot explain the emergence of N 1s peak at 400 eV. Since very thin organic layers were formed as determined by AFM, these azo bonds likely are located at the film-substrate interface.

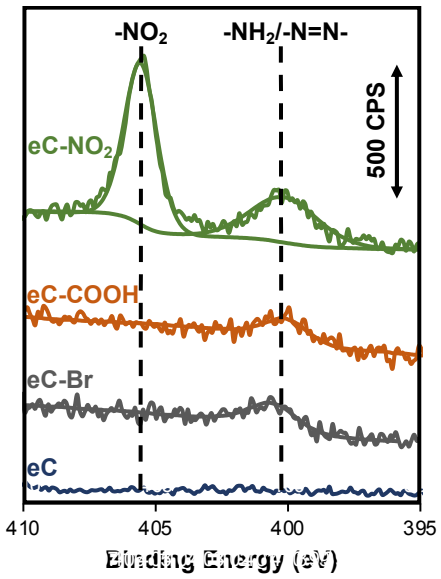

Figure 3-11. XPS N 1s core level spectra of bare (blue) and modified eC electrodes obtained by immersion in 1 mM NBD (green), CBD (orange), BBD (grey) aqueous solutions for 30 min.

Role of the substrate in film formation. We have shown that spontaneous grafting of aryldiazonium salts on amorphous carbon substrates prepared by electron-beam evaporation is feasible, grafting is more facile in aqueous medium than in ACN, and that grafting yield at eC is lower than GC under the same deposition conditions. As an attempt to explain the different grafting yields observed in different media and substrates, we monitored the OCPs of eC and GC electrodes in response to the addition of NBD. Monitoring OCP is assumed to give an indication of the reducing power of the substrate and has been used to study the behavior of gold,[35] copper,[41,49] and GC.[50,51]

Figure 3-12 demonstrates that eC and GC are qualitatively similar: in both media, adding NBD resulted in an immediate and significant jump in the OCPs, while adding just the solvents caused no sudden change in OCPs. There was no clear association between the magnitude of potential jump and grafting yield for both eC and GC electrodes. The surge in OCPs is followed by a slow decrease in DI and a slow increase in ACN. Reproducible behavior was obtained when different electrodes were used, but the initial potentials of eC could vary by as much as ~0.15 V. Among-sample variation in OCP was also observed at GC[50,51] and gold[35] and was thought to stem from variations in surface structure, cleanliness, residual solution O_2 concentration, as well as the electrolytic solution used.

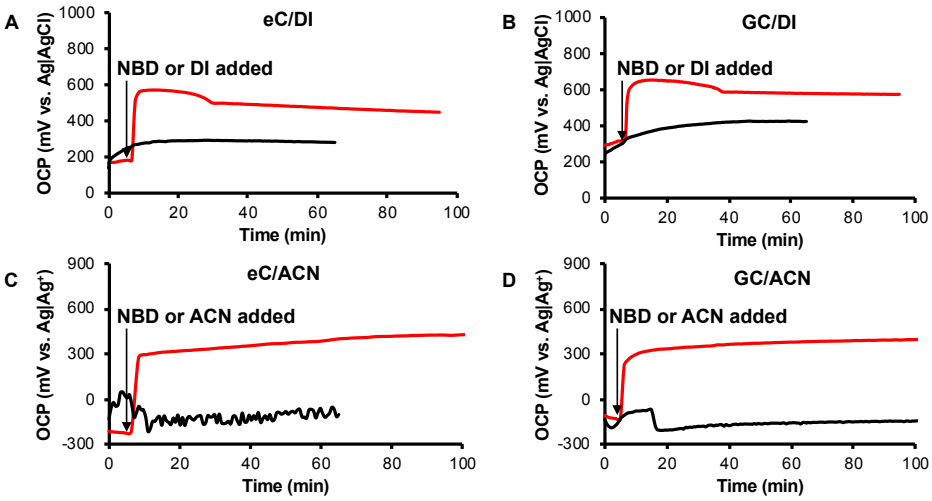

Figure 3-12. Left panel: OCP of eC electrodes vs immersion time in DI (A) and ACN (C). Right panel: OCP of GC electrodes vs immersion time in DI (B) and ACN (D). After 5 min (arrow), a small volume of (<1 mL) NBD was added to the solution to give a final concentration of 1 mM. Control experiments are depicted in black where the same volumes of the solvents (blank) were added to the solution.

The increase and decay of OCPs can be associated with the accumulation of positive charge on the electrode surface and the discharge of that accumulation. We thus assign the charging process to electron transfer from eC to NBD cations and/or to the attachment of cationic species and the discharge to an oxidation process whose details were not investigated here. The discharge process was attributed to the oxidation of adventitious solution impurities at gold[35] and GC,[50] and we assume similar mechanisms operate in this work. A discharge process was not observed in ACN during the time window in this study, and this could be due to the sustained charging and/or a slower discharge mechanism. Alternatively, the continued charging process in ACN might render the electrode substrate too positive to maintain film growth, thus resulting in a lower grafting yield. Lehr et al. reported that for spontaneous grafting of NBD to GC in acidic aqueous medium and ACN, slow film growth occurred in ACN for at least 13 h and increased the film density rather than thickness.[50] Seinberg et al. observed that diazonium-derived anthraquinone spontaneously grafted to GC at a faster rate in (neutral or acidic) aqueous media than in ACN; the same coverage was achieved after 30 min in DI and 24 h in ACN.[52] Thus, our OCPs results are consistent with the lower grafting yield/rate in ACN observed for both GC and eC in this work as well as with other researchers' findings.

The increase in OCP is consistent with the role of eC as an electron donor. While the OCP is low enough, electrons can be transferred from eC to the diazonium cations, and the NP film grows. As the OCP becomes too positive to favor NBD reduction, film growth slows to a stop, and the discharge process becomes dominant by oxidizing the electrode or solution impurities. Diazonium ions decompose in acidic water when a nucleophile such as an electron-donating π-electron system is present.[53] Here, eC (or GC) acts as a nucleophile, transferring electrons to reduce diazonium cations to phenyl radicals. Carbon is thought to supply electrons for spontaneous reduction processed by hole injection in its π system, as demonstrated by conductivity measurements.[54] This hole injection would lead to an increase in open circuit potential of carbon electrode until the reaction is self-limited.

OCP results, however, inadequately explain the different grafting yields obtained at GC and eC under the same deposition conditions since qualitatively similar behavior was obtained. Strano and co-workers proposed a two-step mechanism for the spontaneous attachment of 4-chlorobenzen diazonium salt at a single-walled carbon nanotube, with the first step involving the physical adsorption of aryldiazonium cations via formation of a charge-transfer complex and the second step involving nitrogen elimination and covalent bond formation.[55] This model has been suggested to be valid for disordered carbons as well.[28] Adsorption of quinones[7,56,57] and the electron-transfer kinetics of dopamine[58,59] (which requires adsorption sites as the first step) at carbon electrodes are thought to be promoted by surface roughness, graphitic content, and surface oxygenated functionalities. Therefore, in light of these studies, we speculate that the differences in roughness, graphitic content, and surface oxides between eC and GC might influence the first physisorption step and consequently the grafting yields.

The rms roughness of GC was reported to be 5.8 ± 1.3 nm,[7] higher than that of eC (0.72 ± 0.08 nm) by a factor of 8. Gold deposited on glass (roughness 5.1 nm) doubled nitrophenyl groups grafted to the surface in comparison with gold deposited on the smoother substrate silicon (roughness 2.9 nm).[38] GC is a graphitic material (100% sp^2 content), while eC has ~70% sp^2 hybridized carbons. Cullen et al. studied the spontaneous attachment of NBD from aqueous solutions onto amorphous carbon

materials that differ in sp^2 content and demonstrated that high graphitic sp^2 content is a strong predictor of high nitrophenyl grafting yields.[27] Freshly polished GC in alumina slurries typically has an O/C of 14% with phenols, carbonyls, and carboxylates among the various functional groups that are present;[60] the as-prepared eC has an O/C of ~6%. The phenol groups present at GC surface were proposed to undergo a coupling reaction with the diazonium cation and yield a hydrazine, which tentatively explains the presence of azo bonds directly on the surface. TOF-SIMS experiments with a close to monolayer of phenylene films electrografted to GC revealed the existence of a fragment that is in good agreement with this proposed scheme.[61] The carboxylates present at carbon black surfaces also were proposed to undergo a concerted dediazoniation of the diazonium cations and decarboxylation mechanism in the spontaneous reaction with NBD.[62] This mechanism also allows for the formation of an azo bond at the surface if the nitrogen departure does not occur.

Deconvolution of XPS C 1s spectra of unmodified and modified eC electrodes points to the involvement of surface carboxylates in the spontaneous grafting of aryldiazonium salts (Figure 3-13). The component at ~288 eV (C4), corresponding to the C=O linkages,[42] significantly decreased following modification with NBD and BBD, suggesting a significant loss of surface carboxylates (Table 3-3, two-tailed t-test at 95%). The disappearance of the COOH component in the C 1s spectrum also was observed after oxidized carbon black was functionalized with NBD.[62] Modification with CBD resulted in an increase in the component at ~288 eV, consistent with the attachment of CP groups to the surface. Thus, the spontaneous attachment of aryldiazonium salts to carbon electrodes is also available through a mechanism that involves surface phenolic and carboxylate groups, when oxygen functionalities are present, which occurs in concert with the heterogeneous electron transfer between eC surface and diazonium cations as discussed above. This mechanism partly would explain the lower grafting yields observed at eC as well as at the low surface oxides PPF substrate (O/C ~2–3%)[57] in comparison with GC.

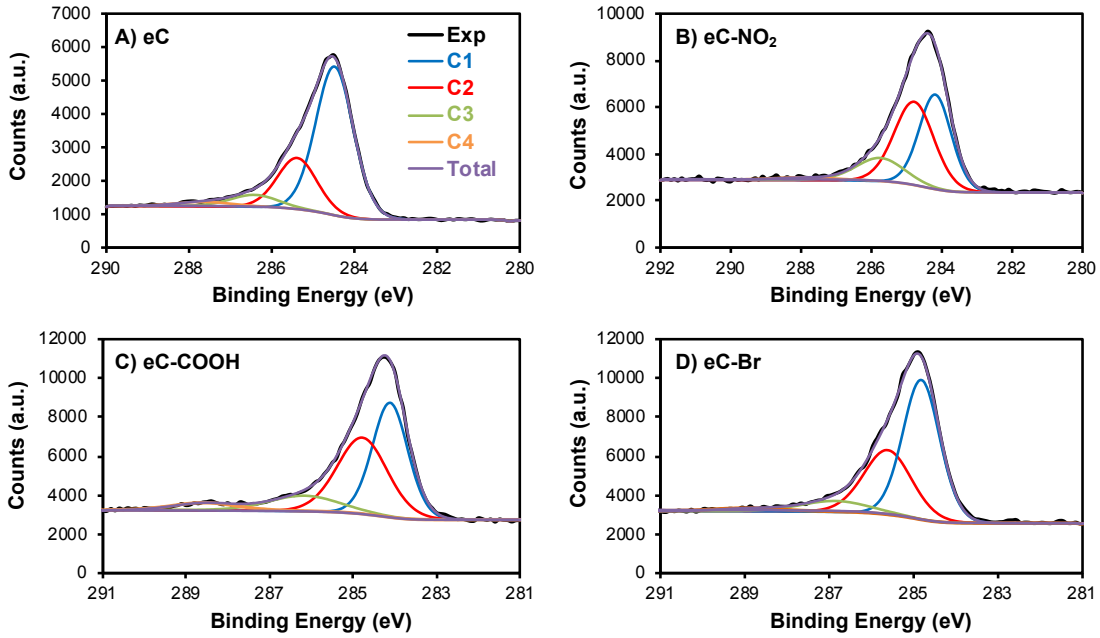

Figure 3-13. XPS C 1s core level spectra of bare (A) and modified eC electrodes obtained by immersion in 1 mM NBD (B), CBD (C), BBD (D) aqueous solutions for 30 min. The peaks at 284.3 eV (C1) and 285.3 eV (C2) are assigned to sp^2 and sp^3 hybrids, respectively.[63] The peaks at 286.5 eV (C3) and 288 eV (C4) are assigned to C–O and C=O bonds, respectively.

Table 3-3. Deconvolution of XPS C 1s spectra of unmodified and modified eC substrates

	eC	eC-NO_2	eC-COOH	eC-Br
sp^3/sp^2 (%)	38 ± 3	109 ± 2	93.9 ± 0.8	61 ± 6
C=O (%)	3.0 ± 0.6	2.01 ± 0.09	4.7 ± 0.5	1.89 ± 0.08

Deconvolution of XPS C 1s spectra of bare and modified eC also points to the conversion of sp^2 C to sp^3 C during the modification with aryldiazonium salts, that is observed similarly for the spontaneous functionalization of carbon nanotubes with diazonium compounds.[64,65] The extent of this conversion can be taken as a crude measure of grafting yields and is consistent with the AFM thickness results, with eC-NO_2 having the highest sp^3/sp^2 and eC-Br the lowest. The sp^2 to sp^3 conversion also signifies the covalent attachment of NP, CP, and BP groups to eC, consistent with the stability test discussed below. However, sp^2 to sp^3 ratios obtained by XPS are estimates which should be interpreted with caution and ideally cross-validated with Raman spectroscopy.

In summary, we believe that the spontaneous grafting to amorphous carbon electrodes occurs via at least two mechanisms: the well-known radical mechanism

and one that involves surface oxygenated functionalities (Figure 3-14). The reaction is self-limited, as increasing immersion time by 2-fold and NBD concentration by 10-fold does not lead to an increase in grafting yield, as discussed above. The reaction likely is limited by the availability of active edge sites and surface oxygenated functionalities. The initial monolayer is formed when the diazonium cation in solution accepts an electron from the eC substrate and eliminates nitrogen. When surface oxygenated functionalities are present, the initial layer also could be formed by a coupling reaction between surface phenol and carboxylate groups with diazonium cations, leading the formation of azo derivatives.[53,66] After the formation of the initial monolayer, the subsequent layer, if any, is formed by reducing diazonium cations in solution by electrons that tunnel through the attached phenyl layer or were conducted through the conjugated π-system[29,67,68] to a radical that attacks the para position of an already attached phenyl ring. Azo coupling also could occur within the multilayers.[49,69]

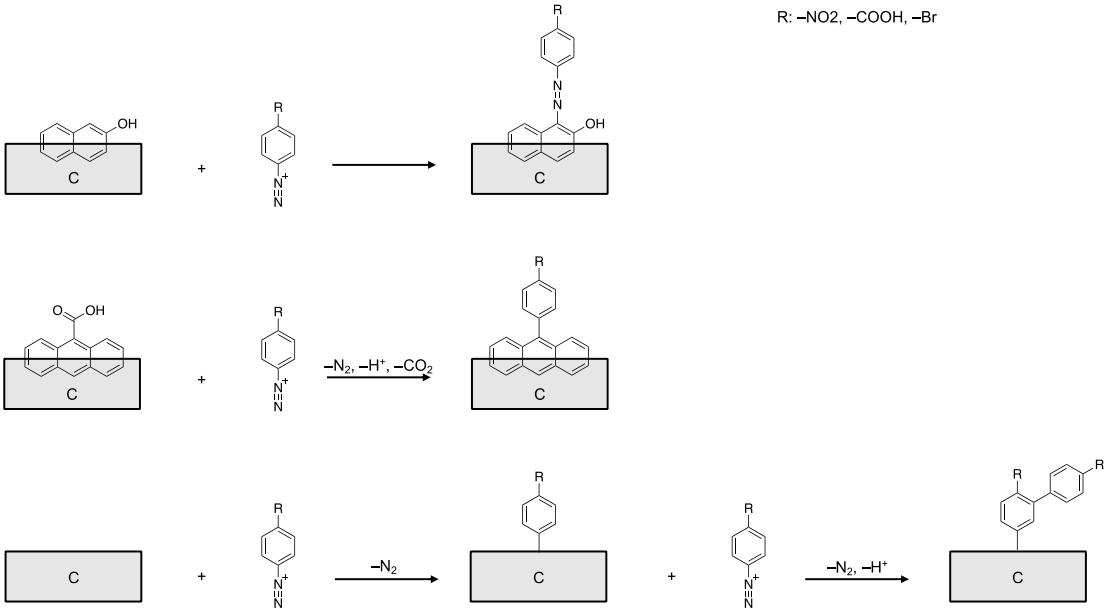

Figure 3-14. Proposed mechanisms of diazonium salts spontaneously grafted at eC/Au surface that involve oxygenated functionalities (top and middle) and the well-known radical mechanism (bottom).

Blocking properties of spontaneously grafted organic films. We examined the voltammetry of a $Fe(CN)_6^{3-}$ redox probe at bare and modified surfaces to give a measure of the blocking properties of the grafted layers. eC was modified, rinsed with

corresponding solvent, and dried before being transferred into an aqueous solution of $Fe(CN)_6^{3-}$. Figure 3-14A illustrates the response of $Fe(CN)_6^{3-/4-}$ at bare eC, spon/DI eC, spon/ACN eC, and echem eC. At pristine eC, the cyclic voltammogram of $Fe(CN)_6^{3-/4-}$ in 1 M KCl shows a reversible couple with ΔE_p = 98 mV (scan rate 0.2 V/s). Spon/ACN eC increased the ΔE_p to 556 mV, and the response is suppressed almost completely at spon/DI eC. The response of $Fe(CN)_6^{3-/4-}$ was blocked completely at the electrochemically modified electrode when a procedure that can produce thick NP films was used.[70] Suppression of the redox response of $Fe(CN)_6^{3-/4-}$ can be attributed to the hydrophobicity of the NP film as well as the change in electronic properties of eC during spontaneous grafting that consequently leads to a decreased electron transfer rate.

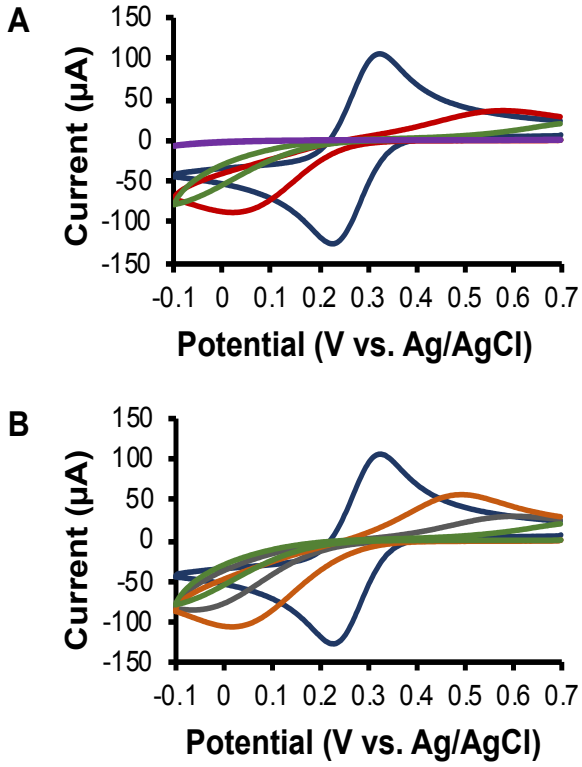

Figure 3-15. (A) Cyclic voltammograms of 1 mM $Fe(CN)_6^{3-}$ in 1 M KCl at bare eC (blue), eC modified by immersion in 1 mM NBD in DI for 30 min (green), eC modified by immersion in 10 mM NBD in ACN for 150 min (red), and eC modified by chronoamperometry in 10 mM NBD and 0.1 M $TBABF_4$ in ACN (-0.3 V for 5 min) (purple). (B) Cyclic voltammogram of 1 mM $Fe(CN)_6^{3-}$ in 1 M KCl at bare (blue) and modified eC electrodes obtained by immersion in 1 mM NBD (green), CBD (orange), BBD (grey) aqueous solutions for 30 min. Scan rate 0.2 V/s.

These results are indicative of a lower surface coverage or thinner film that was formed in ACN, even when a higher NBD concentration and a longer immersion time were used in this experiment. The NP film that spontaneously formed in aqueous solution is almost as nearly blocking as the thick electrochemically grafted film, consistent with the presence of a compact and homogenous layer.

In contrast, the NP films formed at GC under the same conditions have negligible effect on the electron-transfer rate of $Fe(CN)_6^{3-/4-}$ (Figure 3-15), even though they have higher surface coverage and potentially higher thickness, suggesting that non-uniform or defective films were formed at GC. It is likely that uniform and compact NP films formed at eC as suggested by CV of $Fe(CN)_6^{3-/4-}$ data, makes them more blocking to electron tunnelling, thereby stopping film growth at lower surface coverage and/or thickness in comparison with GC.

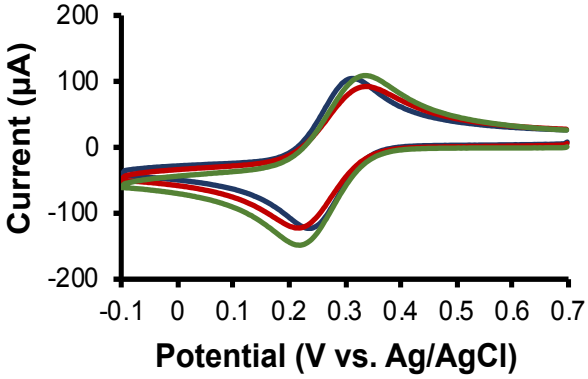

Figure 3-16. Cyclic voltammograms of 1 mM $Fe(CN)_6^{3-}$ in 1 M KCl at bare GC (blue), GC modified by immersion in 1 mM NBD in DI for 30 min (green), GC modified by immersion in 10 mM NBD in ACN for 150 min (red). Scan rate 0.2 V/s.

The blocking properties of CP and BP films used also were investigated and presented in Figure 3-14B. The NP film is the most blocking because of its relative thickness and hydrophobicity. The CP film is thicker than the BP and likely is to be deprotonated at neutral pH, as the pK_a of a multilayer CP film was estimated to be 2.8.[66] As such, the CP film will bear a negative charge, and the electrostatic interaction with the negatively charged $Fe(CN)_6^{3-}$ is expected to hinder the electron transfer process at eC-COOH. However, the hydrophobic effect may play a more important role here in suppressing the response of $Fe(CN)_6^{3-/4-}$ at eC-Br. In summary, spontaneous grafting of aryldiazonium salts from aqueous solutions does not hinder

the electron transfer processes completely as does electrochemical modification and could prove advantageous in the subsequent modification of the tethered layer with biomolecules, especially for CP films.

Stability of spontaneously grafted NP film. As a test of the strength of the C–C bond between the NP film and eC surface, we heated eC-NO_2 at 200 °C for 2 h, then conducted CV to confirm that the NP groups were still present on the electrode surface (Figure 3-16). The NP groups were still present after eC-NO_2 was left on the lab bench for 1 month. In both cases, we obtained cyclic voltammograms similar to that observed in Figure 3-2A. The stability of the NP film is indicative of covalent attachment of NP groups to eC electrode.

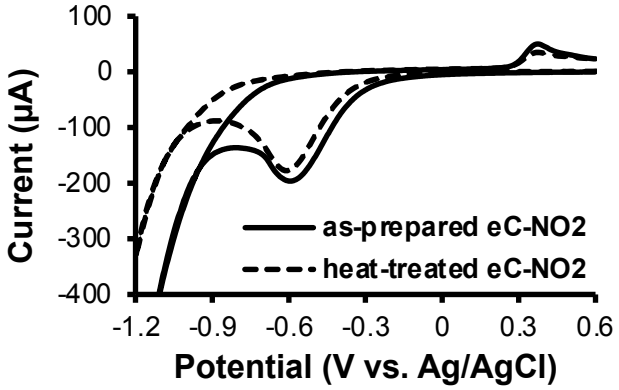

Figure 3-17. Cyclic voltammograms obtained in 0.1 M H_2SO_4 at 0.2 V/s on eC modified by immersion in 1 mM NBD aqueous solution for 30 min and similarly modified eC after heat treatment at 200 °C in a vacuum oven for 2 h.

3.4 Conclusion

Amorphous carbon substrates prepared by electron beam deposition or eC, show similar reactivity toward diazonium salts as those deposited by sputtering (aC). The nature of the surface, the deposition conditions, and the particular diazonium reagent used affect the grafting rates, yields, and the structure of the resulting organic films. eC gives lower surface coverage of NP groups than GC under the same deposition conditions. The spontaneous attachment has been found to be more efficient in aqueous solutions than in acetonitrile, and the structure of NP film grafted from aqueous solution is similar to that produced electrochemically. Homogenous and thin

organic layers were formed from the spontaneous grafting of all aryl diazonium salts used in this study, and the thicknesses of the resulting organic layers were found to correlate with the electron withdrawing abilities of the para-substituents. Derivatization of eC with aryl diazonium salts at OCP in aqueous medium offers a fast, simple method for functionalizing the surface, with minimal waste disposal issues. It could be a good alternative to SAM of thiols in the functionalization of SPR chips, where the multispots on the surface can be addressed by simple drop-casting. The good thermal stability of the C–C surface bond can accommodate the local temperature rise of molecular electronic devices during metal deposition and thus is important to successful fabrication of these devices.

References

(1) Jayasundara, D. R.; Cullen, R. J.; Colavita, P. E. In Situ and Real Time Characterization of Spontaneous Grafting of Aryldiazonium Salts at Carbon Surfaces. *Chem. Mater.* **2013**, *25* (7), 1144–1152. https://doi.org/10.1021/cm4007537.

(2) You, T.; Niwa, O.; Tomita, M.; Ichino, T.; Hirono, S. Electrochemical Oxidation of Alkylphenols on ECR-Sputtered Carbon Film Electrodes with Flat Sub-Nanometer Surfaces. *J. Electrochem. Soc.* **2002**, *149* (12), E479. https://doi.org/10.1149/1.1516222.

(3) Kamata, T.; Kato, D.; Ida, H.; Niwa, O. Structure and Electrochemical Characterization of Carbon Films Formed by Unbalanced Magnetron (UBM) Sputtering Method. *Diam. Relat. Mater.* **2014**, *49*, 25–32. https://doi.org/10.1016/j.diamond.2014.07.007.

(4) Jia, J.; Kato, D.; Kurita, R.; Sato, Y.; Maruyama, K.; Suzuki, K.; Hirono, S.; Ando, T.; Niwa, O. Structure and Electrochemical Properties of Carbon Films Prepared by a Electron Cyclotron Resonance Sputtering Method. *Anal. Chem.* **2007**, *79* (1), 98–105. https://doi.org/10.1021/ac0610558.

(5) Sekioka, N.; Kato, D.; Ueda, A.; Kamata, T.; Kurita, R.; Umemura, S.; Hirono, S.; Niwa, O. Controllable Electrode Activities of Nano-Carbon Films While Maintaining Surface Flatness by Electrochemical Pretreatment. *Carbon* **2008**, *46* (14), 1918–1926. https://doi.org/10.1016/j.carbon.2008.08.006.

(6) Kato, D.; Sekioka, N.; Ueda, A.; Kurita, R.; Hirono, S.; Suzuki, K.; Niwa, O. A Nanocarbon Film Electrode as a Platform for Exploring DNA Methylation. *J. Am. Chem. Soc.* **2008**, *130* (12), 3716–3717. https://doi.org/10.1021/ja710536p.

(7) Blackstock, J. J.; Rostami, A. A.; Nowak, A. M.; McCreery, R. L.; Freeman, M. R.; McDermott, M. T. Ultraflat Carbon Film Electrodes Prepared by Electron Beam Evaporation. *Anal. Chem.* **2004**, *76* (9), 2544–2552. https://doi.org/10.1021/ac035003j.

(8) Morteza Najarian, A.; Chen, R.; Balla, R. J.; Amemiya, S.; McCreery, R. L. Ultraflat, Pristine, and Robust Carbon Electrode for Fast Electron-Transfer Kinetics. *Anal. Chem.* **2017**, *89* (24), 13532–13540. https://doi.org/10.1021/acs.analchem.7b03903.

(9) Mattson, J. S.; Smith, C. A. Optically Transparent Carbon Film Electrodes for Infrared Spectroelectrochemistry. *Anal. Chem.* **1975**, *47* (7), 1122–1125. https://doi.org/10.1021/ac60357a070.

(10) DeAngelis, T. P.; Hurst, R. W.; Yacynych, A. M.; Mark, H. B.; Heineman, W. R.; Mattson, J. S. Carbon and Mercury-Carbon Optically Transparent Electrodes. *Anal. Chem.* **1977**, *49* (9), 1395–1398. https://doi.org/10.1021/ac50017a026.

(11) Lockett, M. R.; Weibel, S. C.; Phillips, M. F.; Shortreed, M. R.; Sun, B.; Corn, R. M.; Hamers, R. J.; Cerrina, F.; Smith, L. M. Carbon-on-Metal Films for Surface Plasmon Resonance Detection of DNA Arrays. *J. Am. Chem. Soc.* **2008**, *130* (27), 8611–8613. https://doi.org/10.1021/ja802454c.

(12) Lockett, M. R.; Smith, L. M. Fabrication and Characterization of DNA Arrays Prepared on Carbon-on-Metal Substrates. *Anal. Chem.* **2009**, *81* (15), 6429–6437. https://doi.org/10.1021/ac900807q.

(13) Yan, H.; Bergren, A. J.; McCreery, R. L. All-Carbon Molecular Tunnel Junctions. *J. Am. Chem. Soc.* **2011**, *133* (47), 19168–19177. https://doi.org/10.1021/ja206619a.

(14) Morteza Najarian, A.; Szeto, B.; Tefashe, U. M.; McCreery, R. L. Robust All-Carbon Molecular Junctions on Flexible or Semi-Transparent Substrates Using "Process-Friendly" Fabrication. *ACS Nano* **2016**, *10* (9), 8918–8928. https://doi.org/10.1021/acsnano.6b04900.

(15) Bélanger, D.; Pinson, J. Electrografting: A Powerful Method for Surface Modification. *Chem. Soc. Rev.* **2011**, *40* (7), 3995. https://doi.org/10.1039/c0cs00149j.

(16) Pinson, J.; Podvorica, F. Attachment of Organic Layers to Conductive or Semiconductive Surfaces by Reduction of Diazonium Salts. *Chem. Soc. Rev.* **2005**, *34* (5), 429. https://doi.org/10.1039/b406228k.

(17) Mahouche-Chergui, S.; Gam-Derouich, S.; Mangeney, C.; Chehimi, M. M. Aryl Diazonium Salts: A New Class of Coupling Agents for Bonding Polymers, Biomacromolecules and Nanoparticles to Surfaces. *Chem. Soc. Rev.* **2011**, *40* (7), 4143. https://doi.org/10.1039/c0cs00179a.

(18) Gooding, J. J. Advances in Interfacial Design for Electrochemical Biosensors and Sensors: Aryl Diazonium Salts for Modifying Carbon and Metal Electrodes. *Electroanalysis* **2008**, *20* (6), 573–582. https://doi.org/10.1002/elan.200704124.

(19) Paloma Yáñez-Sedeño; Susana Campuzano; José Pingarrón. Integrated Affinity Biosensing Platforms on Screen-Printed Electrodes Electrografted with Diazonium Salts. *Sensors* **2018**, *18* (3), 675. https://doi.org/10.3390/s18020675.

(20) Ghosh, D.; Pradhan, S.; Chen, W.; Chen, S. Titanium Nanoparticles Stabilized by Ti−C Covalent Bonds. *Chem. Mater.* **2008**, *20* (4), 1248–1250. https://doi.org/10.1021/cm703423k.

(21) Ghosh, D.; Chen, S. Solid-State Electronic Conductivity of Ruthenium Nanoparticles Passivated by Metal–Carbon Covalent Bonds. *Chem. Phys. Lett.* **2008**, *465* (1–3), 115–119. https://doi.org/10.1016/j.cplett.2008.09.066.

(22) Griffete, N.; Herbst, F.; Pinson, J.; Ammar, S.; Mangeney, C. Preparation of Water-Soluble Magnetic Nanocrystals Using Aryl Diazonium Salt Chemistry. *J. Am. Chem. Soc.* **2011**, *133* (6), 1646–1649. https://doi.org/10.1021/ja108928b.

(23) Laurentius, L.; Stoyanov, S. R.; Gusarov, S.; Kovalenko, A.; Du, R.; Lopinski, G. P.; McDermott, M. T. Diazonium-Derived Aryl Films on Gold Nanoparticles: Evidence for a Carbon–Gold Covalent Bond. *ACS Nano* **2011**, *5* (5), 4219–4227. https://doi.org/10.1021/nn201110r.

(24) Mirkhalaf, F.; Paprotny, J.; Schiffrin, D. J. Synthesis of Metal Nanoparticles Stabilized by Metal−Carbon Bonds. *J. Am. Chem. Soc.* **2006**, *128* (23), 7400–7401. https://doi.org/10.1021/ja058687g.

(25) Assresahegn, B. D.; Brousse, T.; Bélanger, D. Advances on the Use of Diazonium Chemistry for Functionalization of Materials Used in Energy Storage Systems. *Carbon* **2015**, *92*, 362–381. https://doi.org/10.1016/j.carbon.2015.05.030.

(26) Murphy, D. M.; Cullen, R. J.; Jayasundara, D. R.; Scanlan, E. M.; Colavita, P. E. Study of the Spontaneous Attachment of Polycyclic Aryldiazonium Salts onto Amorphous Carbon Substrates. *RSC Adv.* **2012**, *2* (16), 6527. https://doi.org/10.1039/c2ra20292a.

(27) Cullen, R. J.; Jayasundara, D. R.; Soldi, L.; Cheng, J. J.; Dufaure, G.; Colavita, P. E. Spontaneous Grafting of Nitrophenyl Groups on Amorphous Carbon Thin Films: A Structure–Reactivity Investigation. *Chem. Mater.* **2012**, *24* (6), 1031–1040. https://doi.org/10.1021/cm2030262.

(28) Murphy, D. M.; Cullen, R. J.; Jayasundara, D. R.; Doyle, R. L.; Lyons, M. E. G.; Colavita, P. E. Heterogeneous Charge Transfer at the Amorphous Carbon/Solution Interface: Effect on the Spontaneous Attachment of Aryldiazonium Salts. *J. Phys. Chem. C* **2013**, *117* (44), 22768–22777. https://doi.org/10.1021/jp406686e.

(29) Solak, A. O.; Eichorst, L. R.; Clark, W. J.; McCreery, R. L. Modified Carbon Surfaces as "Organic Electrodes" That Exhibit Conductance Switching. *Anal. Chem.* **2003**, *75* (2), 296–305. https://doi.org/10.1021/ac026107h.

(30) Patai, S. *The Chemistry of Diazonium and Diazo Groups, Part I*; John Wiley & Sons, Chichester, 1978.

(31) Anariba, F.; DuVall, S. H.; McCreery, R. L. Mono- and Multilayer Formation by Diazonium Reduction on Carbon Surfaces Monitored with Atomic Force Microscopy "Scratching." *Anal. Chem.* **2003**, *75* (15), 3837–3844. https://doi.org/10.1021/ac034026v.

(32) Kariuki, J. K.; McDermott, M. T. Formation of Multilayers on Glassy Carbon Electrodes via the Reduction of Diazonium Salts. *Langmuir* **2001**, *17* (19), 5947–5951. https://doi.org/10.1021/la010415d.

(33) Yu, S. S. C.; Tan, E. S. Q.; Jane, R. T.; Downard, A. J. An Electrochemical and XPS Study of Reduction of Nitrophenyl Films Covalently Grafted to Planar

Carbon Surfaces. *Langmuir* **2007**, *23* (22), 11074–11082. https://doi.org/10.1021/la701655w.

(34) Delamar, M.; Désarmot, G.; Fagebaume, O.; Hitmi, R.; Pinsonc, J.; Savéant, J.-M. Modification of Carbon Fiber Surfaces by Electrochemical Reduction of Aryl Diazonium Salts: Application to Carbon Epoxy Composites. *Carbon* **1997**, *35* (6), 801–807. https://doi.org/10.1016/S0008-6223(97)00010-9.

(35) Lehr, J.; Williamson, B. E.; Flavel, B. S.; Downard, A. J. Reaction of Gold Substrates with Diazonium Salts in Acidic Solution at Open-Circuit Potential. *Langmuir* **2009**, *25* (23), 13503–13509. https://doi.org/10.1021/la902002n.

(36) Lehr, J.; Garrett, D. J.; Paulik, M. G.; Flavel, B. S.; Brooksby, P. A.; Williamson, B. E.; Downard, A. J. Patterning of Metal, Carbon, and Semiconductor Substrates with Thin Organic Films by Microcontact Printing with Aryldiazonium Salt Inks. *Anal. Chem.* **2010**, *82* (16), 7027–7034. https://doi.org/10.1021/ac101785c.

(37) Liu, Y.-C.; McCreery, R. L. Reactions of Organic Monolayers on Carbon Surfaces Observed with Unenhanced Raman Spectroscopy. *J. Am. Chem. Soc.* **1995**, *117* (45), 11254–11259. https://doi.org/10.1021/ja00150a024.

(38) Mesnage, A.; Lefèvre, X.; Jégou, P.; Deniau, G.; Palacin, S. Spontaneous Grafting of Diazonium Salts: Chemical Mechanism on Metallic Surfaces. *Langmuir* **2012**, *28* (32), 11767–11778. https://doi.org/10.1021/la3011103.

(39) Adenier, A.; Cabet-Deliry, E.; Chaussé, A.; Griveau, S.; Mercier, F.; Pinson, J.; Vautrin-Ul, C. Grafting of Nitrophenyl Groups on Carbon and Metallic Surfaces without Electrochemical Induction. *Chem. Mater.* **2005**, *17* (3), 491–501. https://doi.org/10.1021/cm0490625.

(40) Garrett, D. J.; Lehr, J.; Miskelly, G. M.; Downard, A. J. Microcontact Printing Using the Spontaneous Reduction of Aryldiazonium Salts. *J. Am. Chem. Soc.* **2007**, *129* (50), 15456–15457. https://doi.org/10.1021/ja0775321.

(41) Chamoulaud, G.; Bélanger, D. Spontaneous Derivatization of a Copper Electrode with in Situ Generated Diazonium Cations in Aprotic and Aqueous Media. *J. Phys. Chem. C* **2007**, *111* (20), 7501–7507. https://doi.org/10.1021/jp0704012.

(42) Allongue, P.; Delamar, M.; Desbat, B.; Fagebaume, O.; Hitmi, R.; Pinson, J.; Savéant, J.-M. Covalent Modification of Carbon Surfaces by Aryl Radicals Generated from the Electrochemical Reduction of Diazonium Salts. *J. Am. Chem. Soc.* **1997**, *119* (1), 201–207. https://doi.org/10.1021/ja963354s.

(43) Shewchuk, D. M.; McDermott, M. T. Comparison of Diazonium Salt Derived and Thiol Derived Nitrobenzene Layers on Gold. *Langmuir* **2009**, *25* (8), 4556–4563. https://doi.org/10.1021/la8040083.

(44) Finn, Patricia.; Jolly, W. L. Nitrogen Ls Binding Energies of Some Azide, Dinitrogen, and Nitride Complexes of Transition Metals. *Inorg. Chem.* **1972**, *11* (6), 1434–1435. https://doi.org/10.1021/ic50112a056.

(45) Hetemi, D.; Noël, V.; Pinson, J. Grafting of Diazonium Salts on Surfaces: Application to Biosensors. *Biosensors* **2020**, *10* (1), 4. https://doi.org/10.3390/bios10010004.

(46) Combellas, C.; Delamar, M.; Kanoufi, F.; Pinson, J.; Podvorica, F. I. Spontaneous Grafting of Iron Surfaces by Reduction of Aryldiazonium Salts in

Acidic or Neutral Aqueous Solution. Application to the Protection of Iron against Corrosion. *Chem. Mater.* **2005**, *17* (15), 3968–3975. https://doi.org/10.1021/cm050339q.

(47) Koehler, F. M.; Jacobsen, A.; Ensslin, K.; Stampfer, C.; Stark, W. J. Selective Chemical Modification of Graphene Surfaces: Distinction Between Single- and Bilayer Graphene. *Small* **2010**, *6* (10), 1125–1130. https://doi.org/10.1002/smll.200902370.

(48) Podvorica, F. I.; Kanoufi, F.; Pinson, J.; Combellas, C. Spontaneous Grafting of Diazoates on Metals. *Electrochimica Acta* **2009**, *54* (8), 2164–2170. https://doi.org/10.1016/j.electacta.2008.10.017.

(49) Hurley, B. L.; McCreery, R. L. Covalent Bonding of Organic Molecules to Cu and Al Alloy 2024 T3 Surfaces via Diazonium Ion Reduction. *J. Electrochem. Soc.* **2004**, *151* (5), B252. https://doi.org/10.1149/1.1687428.

(50) Lehr, J.; Williamson, B. E.; Downard, A. J. Spontaneous Grafting of Nitrophenyl Groups to Planar Glassy Carbon Substrates: Evidence for Two Mechanisms. *J. Phys. Chem. C* **2011**, *115* (14), 6629–6634. https://doi.org/10.1021/jp111838r.

(51) Le Floch, F.; Simonato, J.-P.; Bidan, G. Electrochemical Signature of the Grafting of Diazonium Salts: A Probing Parameter for Monitoring the Electro-Addressed Functionalization of Devices. *Electrochimica Acta* **2009**, *54* (11), 3078–3085. https://doi.org/10.1016/j.electacta.2008.11.063.

(52) Seinberg, J.-M.; Kullapere, M.; Mäeorg, U.; Maschion, F. C.; Maia, G.; Schiffrin, D. J.; Tammeveski, K. Spontaneous Modification of Glassy Carbon Surface with Anthraquinone from the Solutions of Its Diazonium Derivative: An Oxygen Reduction Study. *J. Electroanal. Chem.* **2008**, *624* (1–2), 151–160. https://doi.org/10.1016/j.jelechem.2008.09.002.

(53) Zollinger, H. Reactivity and Stability of Arenediazonium Ions. *Acc. Chem. Res.* **1973**, *6* (10), 335–341. https://doi.org/10.1021/ar50070a002.

(54) Choi, H. C.; Shim, M.; Bangsaruntip, S.; Dai, H. Spontaneous Reduction of Metal Ions on the Sidewalls of Carbon Nanotubes. *J. Am. Chem. Soc.* **2002**, *124* (31), 9058–9059. https://doi.org/10.1021/ja026824t.

(55) Usrey, M. L.; Lippmann, E. S.; Strano, M. S. Evidence for a Two-Step Mechanism in Electronically Selective Single-Walled Carbon Nanotube Reactions. *J. Am. Chem. Soc.* **2005**, *127* (46), 16129–16135. https://doi.org/10.1021/ja0537530.

(56) Xu, J.; Chen, Q.; Swain, G. M. Anthraquinonedisulfonate Electrochemistry: A Comparison of Glassy Carbon, Hydrogenated Glassy Carbon, Highly Oriented Pyrolytic Graphite, and Diamond Electrodes. *Anal. Chem.* **1998**, *70* (15), 3146–3154. https://doi.org/10.1021/ac9800661.

(57) Ranganathan, S.; McCreery, R. L. Electroanalytical Performance of Carbon Films with Near-Atomic Flatness. *Anal. Chem.* **2001**, *73* (5), 893–900. https://doi.org/10.1021/ac0007534.

(58) Granger, M. C.; Witek, M.; Xu, J.; Wang, J.; Hupert, M.; Hanks, A.; Koppang, M. D.; Butler, J. E.; Lucazeau, G.; Mermoux, M.; Strojek, J. W.; Swain, G. M. Standard Electrochemical Behavior of High-Quality, Boron-Doped

Polycrystalline Diamond Thin-Film Electrodes. *Anal. Chem.* **2000**, *72* (16), 3793–3804. https://doi.org/10.1021/ac0000675.

(59) DuVall, S. H.; McCreery, R. L. Self-Catalysis by Catechols and Quinones during Heterogeneous Electron Transfer at Carbon Electrodes. *J. Am. Chem. Soc.* **2000**, *122* (28), 6759–6764. https://doi.org/10.1021/ja000227u.

(60) Chen, P.; McCreery, R. L. Control of Electron Transfer Kinetics at Glassy Carbon Electrodes by Specific Surface Modification. *Anal. Chem.* **1996**, *68* (22), 3958–3965. https://doi.org/10.1021/ac960492r.

(61) Doppelt, P.; Hallais, G.; Pinson, J.; Podvorica, F.; Verneyre, S. Surface Modification of Conducting Substrates. Existence of Azo Bonds in the Structure of Organic Layers Obtained from Diazonium Salts. *Chem. Mater.* **2007**, *19* (18), 4570–4575. https://doi.org/10.1021/cm0700551.

(62) Toupin, M.; Bélanger, D. Spontaneous Functionalization of Carbon Black by Reaction with 4-Nitrophenyldiazonium Cations. *Langmuir* **2008**, *24* (5), 1910–1917. https://doi.org/10.1021/la702556n.

(63) Díaz, J.; Paolicelli, G.; Ferrer, S.; Comin, F. Separation of the Sp 3 and Sp 2 Components in the C1 *s* Photoemission Spectra of Amorphous Carbon Films. *Phys. Rev. B* **1996**, *54* (11), 8064–8069. https://doi.org/10.1103/PhysRevB.54.8064.

(64) Bahr, J. L.; Tour, J. M. Highly Functionalized Carbon Nanotubes Using in Situ Generated Diazonium Compounds. *Chem. Mater.* **2001**, *13* (11), 3823–3824. https://doi.org/10.1021/cm0109903.

(65) Strano, M. S. Electronic Structure Control of Single-Walled Carbon Nanotube Functionalization. *Science* **2003**, *301* (5639), 1519–1522. https://doi.org/10.1126/science.1087691.

(66) Saby, C.; Ortiz, B.; Champagne, G. Y.; Bélanger, D. Electrochemical Modification of Glassy Carbon Electrode Using Aromatic Diazonium Salts. 1. Blocking Effect of 4-Nitrophenyl and 4-Carboxyphenyl Groups. *Langmuir* **1997**, *13* (25), 6805–6813. https://doi.org/10.1021/la961033o.

(67) Mirkin, C. A.; Ratner, M. A. Molecular Electronics. *Mol. Electron.* 36.

(68) Lee, H. J.; Cui, S.-Y.; Park, S.-M. Electrochemistry of Conductive Polymers: XXV. Electrochemical Preparation and Characterization of Poly(p-Phenylenes) from Biphenyl and p-Terphenyl. *J. Electrochem. Soc.* **2001**, *148* (10), D139. https://doi.org/10.1149/1.1401080.

(69) Menanteau, T.; Levillain, E.; Downard, A. J.; Breton, T. Evidence of Monolayer Formation via Diazonium Grafting with a Radical Scavenger: Electrochemical, AFM and XPS Monitoring. *Phys. Chem. Chem. Phys.* **2015**, *17* (19), 13137–13142. https://doi.org/10.1039/C5CP01401H.

(70) Adenier, A.; Barré, N.; Cabet-Deliry, E.; Chaussé, A.; Griveau, S.; Mercier, F.; Pinson, J.; Vautrin-Ul, C. Study of the Spontaneous Formation of Organic Layers on Carbon and Metal Surfaces from Diazonium Salts. *Surf Sci* **2006**, *600* (21), 4801–4812. https://doi.org/10.1016/j.susc.2006.07.061.

Chapter 4. Protein Adsorption at Amorphous Carbon Surfaces by Surface Plasmon Resonance Imaging

4.1 Introduction

Surface plasmon resonance (SPR) has been used routinely in the study of biomolecular interactions because it offers highly sensitive, in situ, real time, and label-free detection.[1] The sensing layer commonly consists of a thin metal film, which is capable of supporting surface plasmons in the near infrared and visible regions of the spectrum.[2,3] Surface plasmons are sensitive to changes in the refractive index of the sensing medium brought about by the binding of analyte molecules to their ligands immobilized on the SPR chip.[4] Gold thin films are used preferably as SPR substrates because they have stable optical and chemical properties.[4,5] Self-assembled thiolate monolayers on gold have been studied and characterized thoroughly and are, by far, the most widely used surface chemistry for SPR.[6,7] However, gold-thiol interactions are subject to oxidation and photodecomposition, which limits applications such as on-surface combinatorial chemistry and photolithography.[8] Silver films as SPR substrates have sharper angular resonance and thus increased sensitivity in the visible region compared with gold.[4] However, silver films are not commonly used like gold because they are oxidized easily in aqueous solutions; the oxidized surface complicates the ability to control the interfacial chemistry of biosensing.

Lamellar structures consisting of a thin protecting film deposited on top of the surface plasmon active metals have been proposed to circumvent the limitations discussed above. Lockett et al.[5,9] deposited a thin layer of amorphous carbon (7.5 nm) on gold and silver substrates to fabricate DNA arrays. The presence of a carbon overlayer allows for a robust surface modification based on covalent carbon–carbon bonds to be used. However, the sensitivity of carbon-on-metal substrates is 42% lower than that on gold because amorphous carbon layers absorb light in the visible range. Touahir et al.[10] reported the use of amorphous carbonated silicon as an optically transparent coating film in the visible range. A 5 nm thick layer of the

silicon–carbon alloy can enhance the sensitivity of the substrate significantly, but the reduced thickness of the coating resulted in a nonhomogeneous layer, as pinholes and intermixing between the amorphous alloy and the metal have been observed. More recently, graphene has been demonstrated theoretically and experimentally as an attractive coating on silver and gold because of the enhanced sensitivity resulting from increased adsorption of biomolecules to the high surface-to-volume graphene compared with gold.[1,4] The current major limitation of the graphene-based SPR chips, however, is its lack of specificity as π-π stacking interactions are not specific; any organic molecules or biomolecules bearing aromatic structures can adsorb strongly to graphene.[1,4]

Chapter 2 describes electron-beam evaporated carbon-on-gold films (eC/Au) for use as a disposable electrode material.[11] All layers can be deposited without breaking vacuum and have shown good adhesion to the substrate. The resulting films are very smooth and exhibit good electroanalytical performance, notably abnormally low quinone adsorption. eC is amorphous and hydrophilic, and possesses significant sp^3 content (~30%) and considerable O/C ratio (~6%), thus resembling sputtered amorphous carbon.[12] However, eC is not as well-studied as other carbon films.[13] To date, eC has been examined only for fabricating transparent carbon electrodes,[14,15] disposable electrode materials,[11,16] and molecular electronic devices.[17,18]

In this chapter, we explored various thicknesses of electron-beam evaporated carbon films deposited on gold as SPR substrates. Carbon films were deposited thinner, without pinholes or defects, resulting in minimal sensitivity loss compared with previous reports by Lockett et al, in which the carbon film thickness is 7.5 nm.[5,9] Then, eC/Au films are applied to study the nonspecific adsorption of proteins at the carbon surface. Nonspecific protein adsorption on surfaces is a universal phenomenon and the first event that happens when the surfaces come into contact with biological fluids. It often dictates subsequent events, such as activation of platelets and leucocytes, and blood coagulation.[19] Non-specific protein adsorption can impair performance of such devices as medical implants, drug delivery carriers, electrochemical sensors and biosensors in contact with biological fluids.[20,21] Since surface plasmons are sensitive to any binding occurring within a few hundreds of

nanometers at the sensor–solution interface,[22] nonspecific adsorption of proteins is the major roadblock in translating SPR sensing technologies to clinical applications.[23] Therefore, control over the nonspecific adsorption of proteins to surfaces is crucial in predicting and optimizing the performance of devices in biological applications. The results presented here also should be of interest to researchers in the field of biomaterials because the physicochemical properties of eC, as previously noted, resemble sputtered amorphous carbon which has emerged as a suitable coating for biomedical implants.[24–26]

4.2 Experimental

4.2.1 Chemicals and Materials

P-type, (100) oriented silicon wafers (University Wafers), SF-10 glass (Schott Glass), concentrated sulfuric acid (95%–98%, Caledon), hydrogen peroxide (Aldrich, 30% w/w), 2-propanol (certified ACS, Fisher), acetonitrile (ACN, for HPLC, gradient grade, ≥99.9%, Aldrich), acetone (ACS reagent, ≥99.5%, Aldrich), anhydrous ethyl alcohol (Commercial Alcohols), potassium chloride (ACS reagent, 99.0–100.5%, Aldrich), potassium ferricyanide (certified reagent, Caledon), hexaammineruthenium(III) chloride (98%, Aldrich), SDS (Bio-Rad Japan, electrophoresis purity reagent), bovine serum albumin (BSA, Aldrich, >= 98%, pH 7), fibrinogen from bovine plasma (Fib, Aldrich, Type I-S , 65–85% protein), ChromPure Rabbit IgG (whole molecule, Jackson ImmunoResearch), and phosphate buffered saline (PBS, Aldrich, 10× concentrate, BioReagent) were used as received. Solutions were prepared fresh daily with deionized (DI) water purified and deionized by a Barnstead E-Pure system (18.2 MΩ cm, ThermoFisher). Solutions used in electrochemistry experiments were purged with nitrogen gas for 10 min before use.

4.2.2 Substrate Preparation

Chromium (2 nm), gold (42 nm), and carbon (1–10 nm) layers deposited onto Si substrates were prepared, as detailed in Chapter 2. SPR substrates were chromium (2 nm), gold (42 nm), and carbon (1–10 nm) layers deposited onto SF-10 glass cut into

1.8 × 1.8 cm^2 chips. Prior to deposition, glass chips were cleaned with hot piranha solution (1:3 v/v H_2O_2 : conc. H_2SO_4), followed by thorough rinsing with DI and dried with nitrogen gas. [Warning: Piranha solution presents an explosion danger and should be handled with extreme care; it is a strong oxidant and reacts violently with many organic materials. All work should be performed under a fume hood. Wear personal safety equipment.] Substrates were prepared fresh daily and stored in a desiccator under vacuum at room temperature, until use.

4.2.3 Surface Characterization

Surface plasmon resonance imaging (SPRi) was obtained using a SPR Imager (GWC Technologies). The SPR imager has been described in detail elsewhere.[9] Protein and buffer solutions were introduced to the substrate surface via peristaltic flow through a fluid cell. Langmuir isotherms were obtained by fitting the experimental data using the one site ligand binding model included in SigmaPlot (Systat Software, Inc., San Jose, CA).

Infrared reflection-absorption spectroscopy (IRRAS) spectra were collected on a Nicolet 8700 Fourier transform infrared (FTIR) spectrometer (Thermo Fisher Scientific) equipped with a mercury cadmium telluride (MCT) detector, a specular reflectance accessory (80 Spec, Pike Technologies). 1024 spectra were collected at 80° incidence and 4 cm^{-1} resolution using a bare gold slide as background.

Contact angle measurements were performed with a 4 μL droplet volume using a Ráme-Hart goniometer (model 590) equipped with DROPimage advanced software. The reported values are the averages of two measurements on each sample (N = 3). The contact angle of water at eC_2/Au is 41º ± 3º.

Atomic Force Microscopy (AFM) images were collected with a Dimension Edge Atomic Force Microscope (Bruker) using commercial Si tips with a resonant frequency of 300 kHz and a force constant of 40 N/m (Tap300, Ted Pella, Inc.). The scan rate was 1–2 Hz, and the scanning density was 512 lines/frame. The thicknesses of the organic layers were determined by "AFM scratching," as previously described by Anariba et. al.[27] The applied force was determined empirically so that it is sufficient to remove the organic layers without damaging the surface. A set point

voltage of 0.5 V was used for all experiments. AFM images were processed with NanoScope Analysis v1.40. The images, with the exclusion of the 'scratched' regions, were flattened with a first-order polynomial before analysis. Then, a line-scan profile was drawn across the scratched region to determine the thickness of the organic layer.

Cyclic voltammetry (CV) was performed with a three-electrode cell and a bipotentiostat (model AFCBP1, Pine Instruments). Home-made Ag|AgCl|KCl (3.5 M) was used as a reference electrode, and a Pt mesh was used as a counter electrode. eC/Au or Au served as working electrodes, the geometrical area of which were defined by a Viton O-ring. Chronoamperometry in 1 mM $Fe(CN)_6^{3-}$ in 1 M KCl yielded an electrode area of 0.319 ± 0.005 cm^2 (N = 3). CV experiments were conducted in nitrogen-blanketed solutions at room temperature (22 ± 1 °C). Heterogenous electron-transfer rate constants were calculated for simple one electron redox system using the method of Nicholson as reported previously.[11]

4.3 Results and Discussion

A 10 nm eC overlayer on Au results in a significant decrease in sensitivity and an increase in the angle of resonance due to broadening of the SPR curves and decreased photo-plasmon coupling (Figure 4-1), which can be ascribed to the complex dielectric function of amorphous carbon.[28,29] The decreased slope of the scanning angle curve induced by eC coating leads to sensitivity loss in SPRi measurements (Figure 1-2). This was demonstrated in studies by Lockett et al.,[5,9] in which a 7.5 nm thick sputtered carbon layer induced up to 42% loss of sensitivity relative to a bare gold film. In that work, 7.5 nm is the minimum thickness to support the fabrication of DNA arrays consistently; carbon films thinner than 7.5 nm often delaminated during array synthesis, making the substrates unusable.

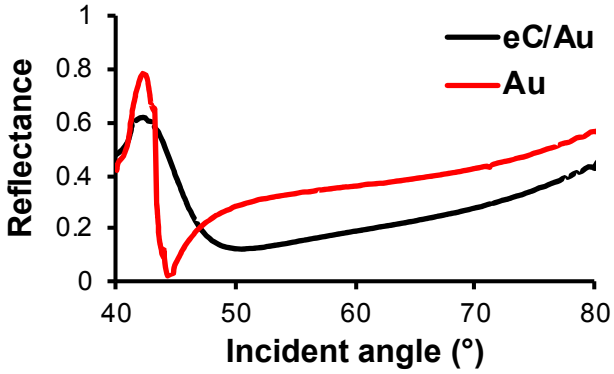

Figure 4-1. Scanning angle reflectivity curves of Au_{42} and eC_{10}/Au_{42} electron-beam evaporated onto BK7 glass substrates. Data were collected using a custom-built scanning angle SPR instrument with a 632.8 nm HeNe laser.

Fixed angle SPRi measurements were conducted for substrates with varying eC thicknesses (1–10 nm) to determine the effect of eC overlayer on the sensitivity of eC/Au substrates. The sensitivity of Au and eC/Au substrates was investigated experimentally by measuring the change in reflectivity ($\Delta\%R$) after the substrate is exposed to a series of water/ethanol solutions. Figures 4-2A and B show the typical continuous SPRi sensorgrams obtained at Au and eC_2/Au substrates (subscript indicates thickness in nm) after water/ethanol solutions (0–1% w/v ethanol solutions corresponding to a refractive index change of 3.0×10^{-4})[5] are injected into the cell. The staircase responses were used to generate a calibration plot, as shown in Figure 4-2C, which indicates that Δ%R varies linearly with refractive index, and the slopes of the curves can be taken as a measure of sensitivity. As can be seen from Figure 4-2, changes in reflectivity resulting from changes in the medium refractive index are larger at Au than at eC_2/Au. Comparing the slopes of the two calibration curves, $(2.9 \pm 0.4) \times 10^3$ for Au and $(2.6 \pm 0.2) \times 10^3$ for eC_2/Au, a 2 nm thick eC coating resulted in 10% loss of sensitivity relative to a bare gold film. This loss is minimal compared with the previously reported 42% loss determined by a similar method.[5,9]

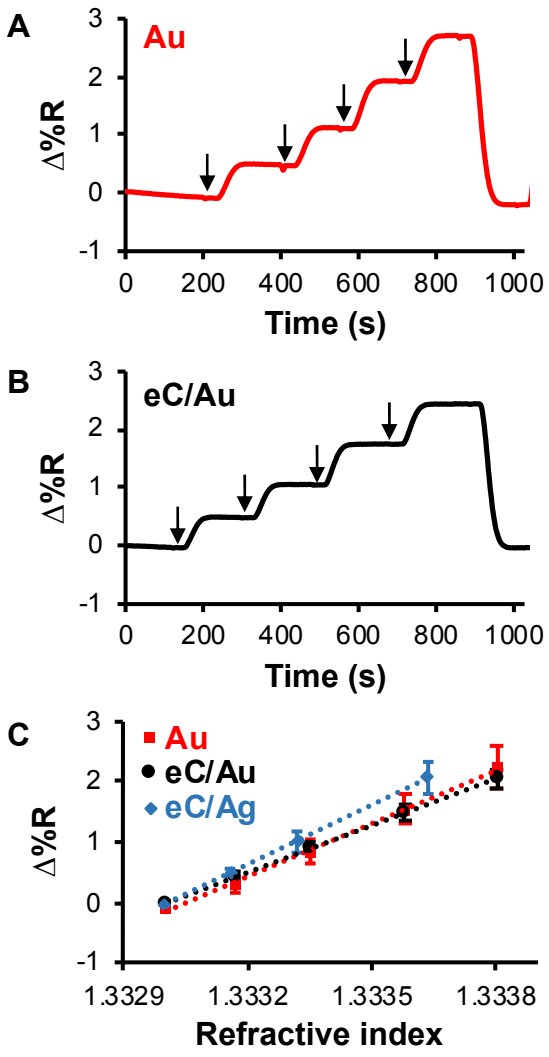

Figure 4-2. Sensitivity test at Au (red) and eC_2/Au (black) substrates. Representative continuous SPRi sensorgrams obtained at Au (A) and eC_2/Au (B) surfaces after water/ethanol solutions of different refractive indices are injected into the cell (indicated by black arrows). (C) Calibration plot of measured Δ%R vs refractive index of water/ethanol solutions. The slopes yielding the sensitivity calculated for Au, eC_2/Au, and eC_2/Ag are $(2.9 \pm 0.4) \times 10^3$, $(2.6 \pm 0.2) \times 10^3$, and $(3.3 \pm 0.4) \times 10^3$, respectively. Error bars are ±1 standard deviation.

The slopes of the calibration plots for 4 nm and 10 nm thick eC overlayers also were determined and presented in Table 4-1. Increasing eC thickness results in increasing sensitivity loss compared with the bare Au substrate. A carbon overlayer thus presents a trade-off between the sensitivity and stability of the substrate. Carbon layers prepared by electron-beam evaporation without breaking vacuum have shown good adhesion to the substrate, as we did not observe delamination of the eC layer from the substrate.[11] However, films that are too thin might form incomplete layers,

thereby exposing the underlying Au film. It is necessary to determine the minimum thickness of eC to minimize sensitivity loss while having adequate coverage.

Table 4-1. Sensitivity of various substrates determined by calibration of at least 3 replicate substrates with a series of water/ethanol solutions

Substrates	Slopes ($\times 10^3$, $\Delta\%R$/refractive index unit)
Au	2.9 ± 0.4
eC_2/Au	2.6 ± 0.2
eC_4/Au	2.4 ± 0.2
eC_{10}/Au	1.9 ± 0.1
eC_2/Ag	3.3 ± 0.4

In Chapter 2, we study the electrochemical performance of $Si/Cr_2/Au_{42}/eC_{10}$ electrodes (subscripts indicate thicknesses in nm) and probed the presence of pinholes, or incomplete coverage of 10 nm thick eC film, by stripping of underpotentially deposited (UPD) lead.[11] Briefly, a monolayer of lead adatoms can be deposited on Au surfaces at potentials slightly more positive than for bulk deposition of lead.[30–35] Subsequently, this lead monolayer can be stripped oxidatively from the gold surface, giving a sharp oxidative stripping wave at –0.2 V in a linear sweep voltammogram. We found that 10 nm thick eC can cover the Au layer completely. We thus used this method to probe the coverage of various eC layer thicknesses, and the results are reported in Figure 4-3. A sharp oxidative stripping wave at –0.2 V can be observed for the gold film (0 nm eC), which is characteristic of lead stripping from Au(111) crystal plane.[30] This wave is absent for other eC/Au substrates, indicating that no lead was deposited on these surfaces and that the Au layer was covered completely by eC. Additionally, 2 and 4 nm thick eC layers give almost identical voltammograms with smaller background current than 1 nm eC. While 1 nm eC films do not show any lead deposition and stripping, we interpret the larger background current as indicative of a defective film that does not cover the Au under layer completely. Figure 4-3 shows that 2 and 4 nm eC films are uniform and defect free. McCreery and co-workers have fabricated molecule/eC/Au junctions and reported that devices made from 1 nm eC thickness displayed characteristics similar to those without eC, while eC thicknesses between 2 and 30 nm show statistically indistinguishable nonlinear J–V responses.[17] This indicates that an eC thickness as

low as 2 nm can prevent Au from penetrating into the molecular layer effectively. Thus, in light of these findings, 2 nm thick eC was chosen for subsequent SPR experiments to minimize sensitivity loss while completely covering the underlying Au layer. The minimal sensitivity loss reported here makes carbon-on-gold films more useful as a SPR substrate.

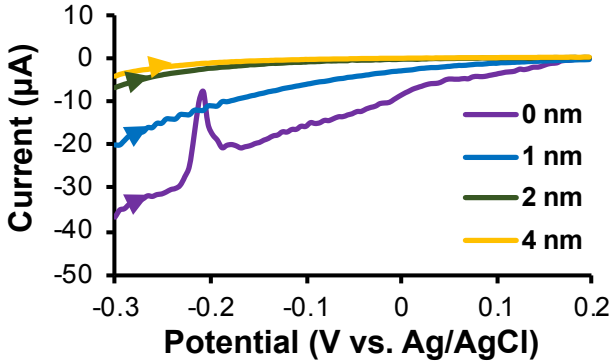

Figure 4-3. Overlay of linear sweep voltammograms of lead UPD stripping from Glass/Cr/Au/eC electrodes with various eC thicknesses ranging from 0 to 4 nm. The thicknesses of the Cr and Au layers were 2 and 42 nm, respectively (ν = 20 mV/s).

Silver has been shown to have higher sensitivity than gold as a plasmonic material since it has higher reflectivity and lower absorption in the visible and near-infrared regions.[9] However, silver is more readily oxidized than gold. The oxidized surface complicates the ability to control the interfacial chemistry for biosensing.[4] Thus, a thin carbon film acting as a protective overlayer and altering the surface chemistry of the silver substrate would be advantageous. Carbon-on-silver substrates have been reported to be ~12% more sensitive than carbon-on-gold counterparts, but this sensitivity increase is not enough to compete with bare gold films.[9] Thus, we prepared carbon-on-silver substrates by electron-beam evaporation and determined their sensitivity with a series of water/ethanol solutions, as detailed above. The silver layer thickness was chosen to be 41 nm, as this is the optimum thickness when a carbon overlayer is present.[9] We found that eC_2/Ag substrates have a sensitivity of $(3.3 \pm 0.4) \times 10^3$ (Figure 4-2C), which provides a 14% and 27% increase from those of bare Au and eC_2/Au films, respectively; the sensitivity of the eC/Ag is likely higher than reported here. Our measurements were made using 830 nm light, which is optimal for the resonance at 42 nm Au films. Measurements under conditions optimal

for the Ag resonance are expected to result in higher sensitivity. This result is promising for promoting the use of carbon-on-silver substrates in SPR sensing.

It is important to note that the carbon layer in our work can be made significantly thinner than previously reported by Lockett et al.[5,9] Defect-free, well-adhered 2 nm thick eC films are possible due to the deposition process used here. In our work, the glass substrates were cleaned thoroughly with piranha solution before loading into the vacuum chamber, and all layers were deposited by electron-beam evaporation without breaking vacuum. In previous work, glass substrates were cleaned with DI, and layers of Cr and Au were deposited with a metal evaporator before amorphous carbon films were applied to the surface by DC magnetron sputtering. We speculate that our deposition process results in enhanced adhesion of the carbon layer to the substrate, thereby enhancing the stability of the substrate.

Protein adsorption at eC/Au and Au surfaces was monitored in real time and quantified by SPR imaging (SPRi). In our previous study, we found that eC/Au exhibits abnormally low quinone adsorption and slow air passivation compared to other carbonaceous materials.[11] Here, we investigate whether eC/Au also shows low activity towards plasma proteins since low non-specific protein adsorption can benefit eC/Au as a SPR substrate over Au in the analysis of clinical samples.[23] We choose BSA and Fib as two model plasma proteins. Albumin is routinely used in many studies on biocompatibility of surfaces, as it is the most abundant plasma protein in humans and other mammals (40 mg/mL in blood plasma).[36] Fib has a high molecular weight and high surface affinity, which usually displaces preadsorbed proteins, as described by the Vroman effect.[37] Albumin adsorption on surfaces inhibits thrombus formation,[38] while Fib participates in blood coagulation, facilitates adhesion and aggregation of platelets, and is important in the processes of both haemostasis and thrombosis.[39]

Au and eC/Au were exposed to BSA and Fib solutions and monitored in real time by SPRi. The protein concentration was chosen to be 7 μM to facilitate comparison with another study on protein adsorption at amorphous carbon surfaces by localized SPR sensing.[12] All substrates were calibrated using at least three water/ethanol solutions prior to protein exposure. After calibration, PBS was injected,

followed by the protein solution and a final rinsing step with PBS to remove unadsorbed protein. Figure 4-4 demonstrates the full experiment including the calibration step.

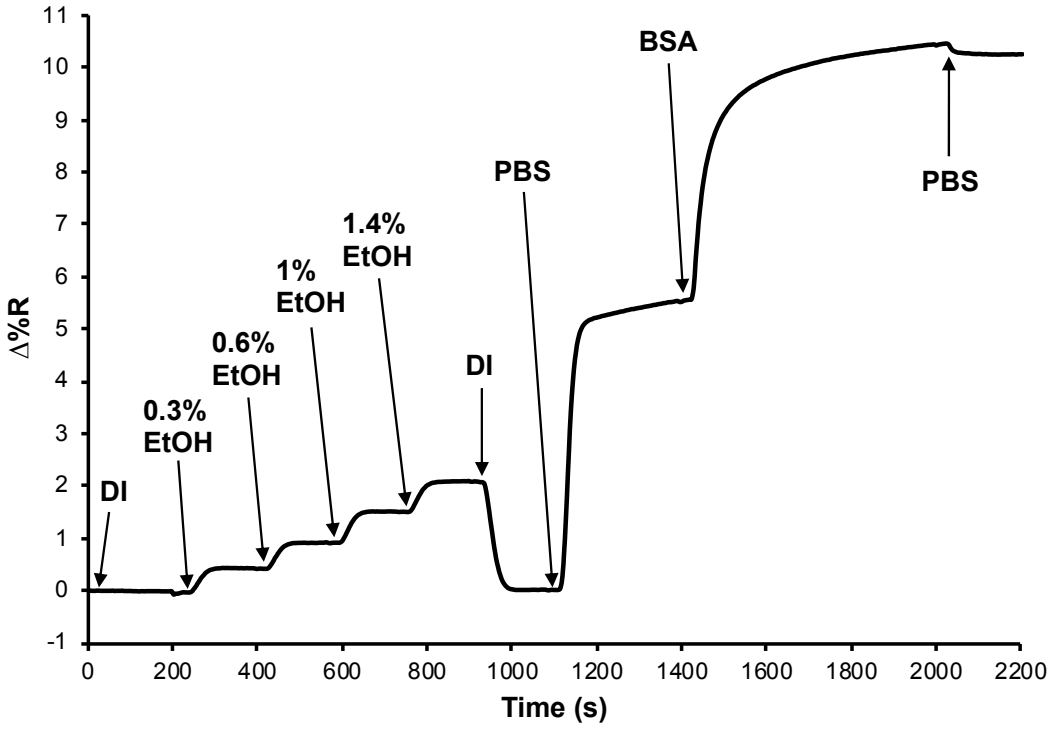

Figure 4-4. BSA adsorption experiment measured at an eC/Au substrate.

Figure 4-5A shows typical sensorgrams obtained at Au and eC/Au substrates after the injection of PBS and BSA solutions. For comparison, the sensitivity differences between eC/Au and Au are compensated by normalizing the SPRi signal of each substrate by the sensitivity determined from the calibration with water/ethanol solutions. The normalized $\Delta\%R$ vs time was calculated as $\Delta\%R_{max}/m$, where m is the slope obtained from the calibration of the corresponding substrate, and the results are reported in Table 4-2. BSA adsorbs at both Au and eC/Au to the same extent. The BSA adsorbed at eC/Au surface could not be displaced by PBS or SDS (1% w/w in PBS).

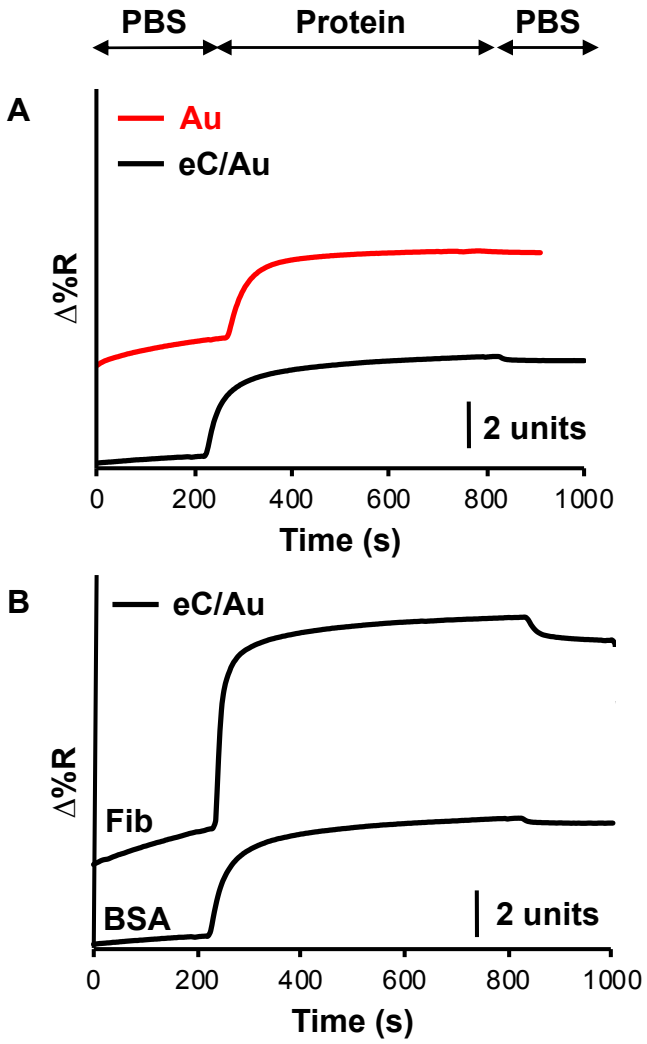

Figure 4-5. (A) Representative sensorgrams measured at Au (red) and eC/Au (black) substrates for in situ BSA adsorption. (B) Representative sensorgrams measured at eC/Au substrates for in situ 7 μM BSA and 7 μM Fib adsorption. The arrows indicate when proteins and PBS solutions were injected into the flow cell.

Table 4-2. Summary of results from SPRi and AFM measurements

Surface	Protein	Normalized Δ%*R* ($\times 10^{-3}$)	RMS Roughness (nm)	AFM Thickness (nm)	K_D (M)
Au	BSA	3.9 ± 0.1	–	–	–
	Fib	7.1 ± 0.8	–	–	–
eC/Au	BSA	3.9 ± 0.1	0.7 ± 0.1	1.1 ± 0.1	33×10^{-8}
	Fib	5.7 ± 0.4	0.8–2.5	2–3*	2.5×10^{-8}

*This excludes tall protrusions.

BSA often is used as a blocking layer against protein adsorption for sensing in complex media. A layer of BSA is pre-adsorbed to the sensor surface before exposure to the analyte solution. Subsequent flow of Fib solution over the pre-adsorbed BSA surface resulted in an increase in Δ%*R* (Figure 4-6); the overall Δ%*R* shift is (4.7 ± 0.3) × 10^{-3} (normalized for sensitivity), which lies between the adsorption values of each individual protein (Table 4-2). This suggests that the larger Fib molecule either displaces BSA or adsorbs on top the BSA layer. It is likely that a mixed layer of BSA and Fib resulted rather than multilayer adsorption, in accordance with the Vroman effect.[37,40] Adsorption of plasma proteins follows a competitive process, where initially adsorbed low-molecular weight protein (BSA) is displaced by a high-molecular weight protein (Fib) since it is more thermodynamically favorable; when the high-molecular weight protein adsorbs to the surface first, it is not displaced by the low-molecular weight protein.[37,40] The presence of a mixed protein layer can be verified by monitoring the Δ%*R* shift after introducing an antibody specific to either of the proteins to the mixed protein layer.[40]

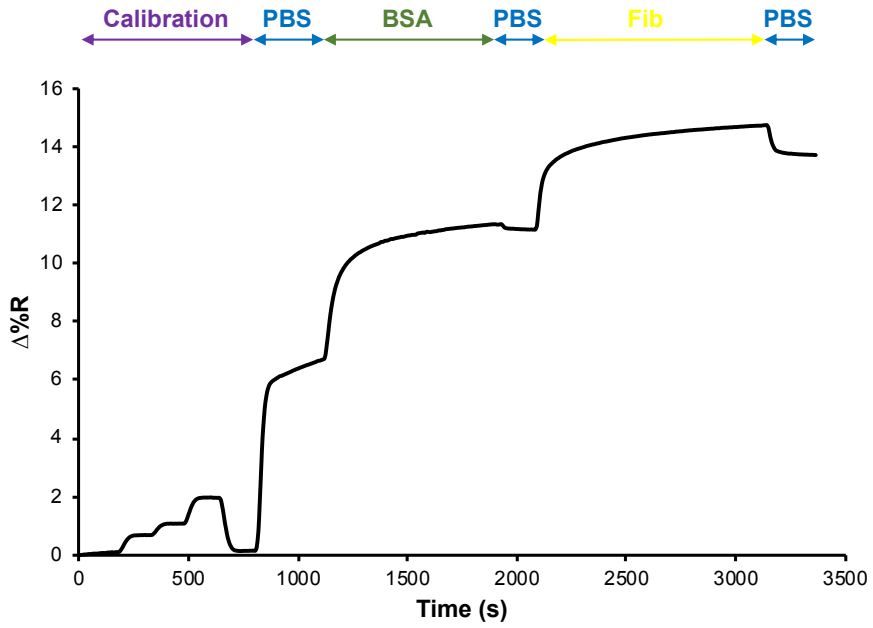

Figure 4-6. An SPR adsorption profile of a two-part adsorption experiment at an eC/Au substrate. Initially BSA is adsorbed to eC/Au followed by flowing Fib over the surface, producing an observed increase in Δ%R.

Adsorption of Fib was also compared at Au and eC/Au surfaces and the results are reported in Table 4-2. The $\Delta\%R$ shift at Au is higher than at eC/Au, indicating that Fib adsorbed more at the Au surface. Figure 4-5B shows sensorgrams of Fib and BSA adsorption at eC/Au surface; a sharper step and higher intensity can be seen in the sensorgram of Fib, indicating that Fib adsorbs faster and more than BSA at eC/Au surface. Pre-adsorbed Fib was not displaced by PBS or BSA, as flowing these solutions over the surface did not result in significant $\Delta\%R$ shift. From the normalized $\Delta\%R$ vs time calculated in Table 4-2, Fib adsorbs 50% more than BSA at eC/Au, which was observed similarly by Zen et al. at sputtered amorphous carbon surfaces.[12] The difference in adsorption between BSA and Fib is likely a result of kinetic control because the molar concentration of the proteins is identical.[12] A mass transport-controlled process would favor BSA, as it is a smaller protein with a higher diffusion coefficient than Fib (6×10^{-7} vs 2×10^{-7} cm^2 s^{-1}).[41]

Figure 4-7 presents adsorption isotherms of BSA and Fib at eC/Au. The isotherms of BSA and Fib reach plateaus at relatively low protein concentration (0.5 mg/mL), suggesting the saturation of binding sites at eC/Au above this concentration. The surface coverage of Fib is 50% higher than that of BSA for the same bulk concentration. The Langmuir model is used widely to model protein adsorption because it is simple and compatible with experimental data.[42] The hyperbolic Langmuir model as given by the following equation:

$$\text{normalized } \Delta\%R = \frac{\text{normalized}\Delta\%R_{\max}[\text{protein}]}{K_D + [\text{protein}]}$$

where normalized $\Delta\%R_{max}$ is the normalized $\Delta\%R$ at saturation and K_D is the dissociation constant of the interaction between protein molecules and eC/Au, yields reasonable fits to both BSA and Fib isotherms (dashed lines, Figure 4-7). K_D values of BSA and Fib are listed in Table 4-2. The K_D of Fib is one order of magnitude lower than that of BSA, suggesting that Fib interacts more strongly with eC/Au than BSA. The K_D of BSA is comparable with the value obtained for BSA adsorbing at graphene (1.5×10^{-8} M),[43] and lower than BSA adsorbing at carbon nanotubes (1.0×10^{-6} M).[42]

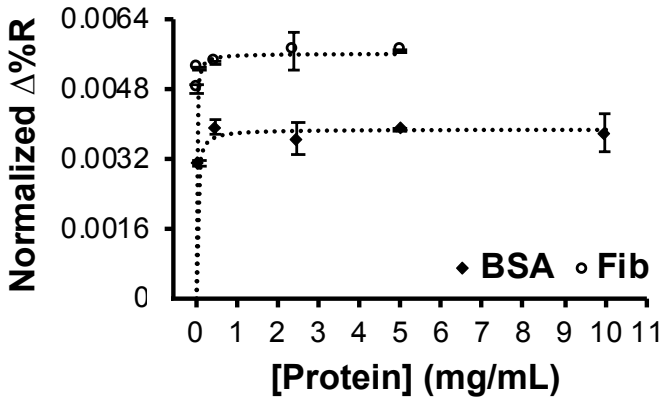

Figure 4-7. Adsorption isotherms of BSA (diamond) and Fib (circle) at eC/Au.

The adsorbed protein layers at eC/Au also was characterized via ex-situ IRRAS and AFM experiments. Figure 4-8 shows IRRAS spectra in the region 1300–1900 cm^{-1} of eC/Au surfaces after incubation in BSA and Fib solutions, followed by rinsing with PBS buffer. The two bands at 1664 and 1535 cm^{-1} were assigned to amide I and amide II nodes of amide groups in polypeptides, respectively.[44] The strong amide bands indicate that both BSA and Fib adsorbed irreversibly at eC/Au, and the higher intensity of Fib amide bands is consistent with a thicker adsorbed layer of Fib than BSA, in agreement with SPRi results.

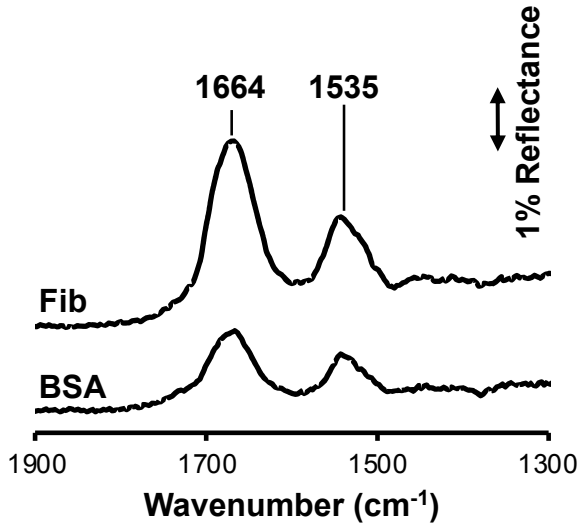

Figure 4-8. IRRAS spectra of eC/Au substrates showing the regions of amide I and II bands after 1 h incubation with 7 μM BSA (bottom) and 7 μM Fib (top) solutions.

The morphology of adsorbed protein layers at eC/Au was characterized by AFM. The root-mean-square (rms) roughness of bare eC/Au (Figure 4-9A) is 0.39 ± 0.05 nm. The formation of protein layers roughens eC/Au surfaces, leading to an increase in the root-mean-square (rms) roughness of eC/Au surfaces after protein adsorption (Table 4-2). AFM images in Figure 4-9B and C show eC/Au surfaces after incubation with BSA and Fib. BSA typically forms smooth layers, whereas Fib can form 5–40 nm thick agglomerates (data not shown).

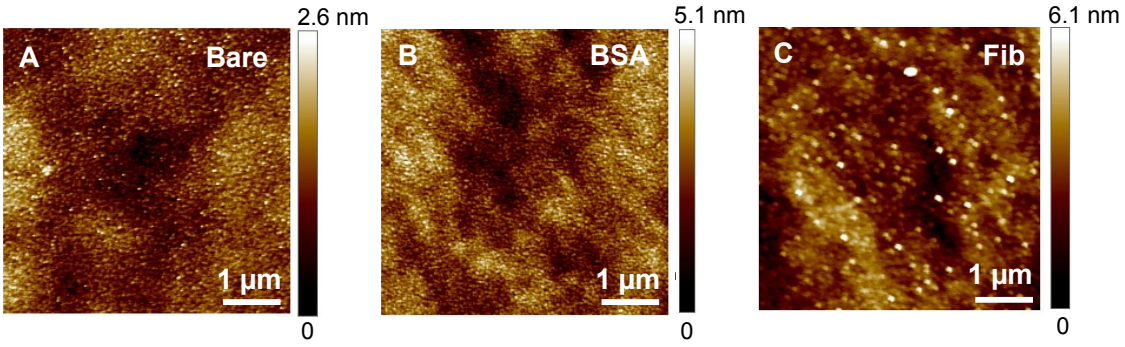

Figure 4-9. AFM images of bare eC/Au (A) and eC/Au surfaces after 1 h incubation with 7 µM BSA (B) and 7 µM Fib (C) solutions.

The thicknesses of the adsorbed protein layers were determined by AFM scratching and reported in Table 4-2. Briefly, the surface was scratched with an AFM tip in contact mode to remove a small section of the protein film; without changing the tip, the ploughed area was imaged in tapping mode, and the layer thickness was determined by cross-section analysis. Figure 4-10 shows a topographic image of eC/Au after incubation with BSA for 1 h, followed by scratching, and the corresponding cross-sectional depth profile of the top image. The high topographical features on the side of the scratch are debris that has built up during the scratch. AFM results indicate that Fib yields thicker layers than BSA at eC/Au surface, in good agreement with SPRi and IRRAS experiments.

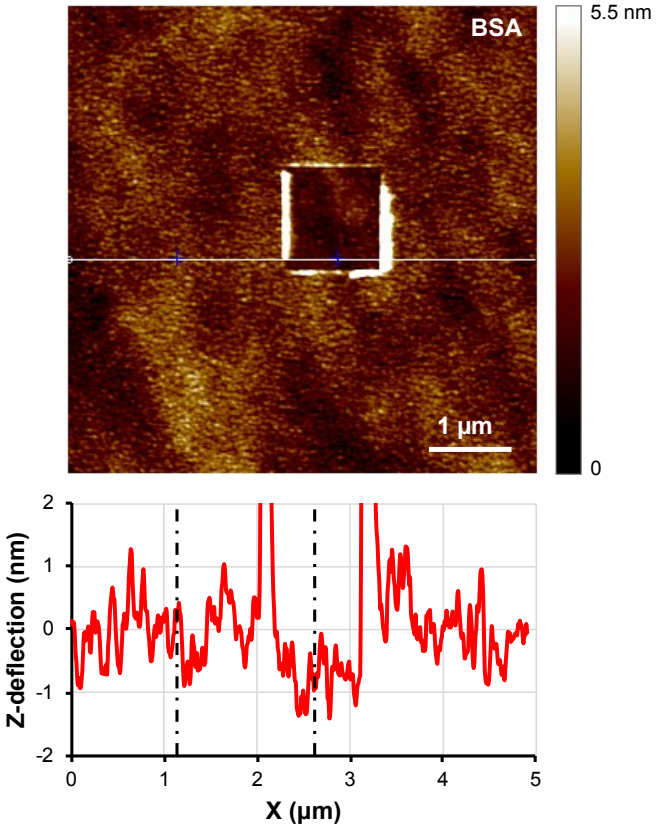

Figure 4-10. AFM of eC after incubation in BSA solution for 1 h after the scratching process (top) and the corresponding height profile across the step (bottom).

In summary, BSA adsorbs similarly at Au and eC/Au surfaces, but Fib adsorbs more at Au. Adsorption of protein at surfaces is thought to depend on both the properties of the protein and the physico-chemical properties of the surface. Surface properties, e.g., wettability, chemical composition, charge, heterogeneity, topography, and roughness, are believed to contribute greatly to adhesion, composition, and conformation of the adsorbed protein layer.[19] Both clean eC/Au and Au surfaces are hydrophilic, with water contact angles of ~40º after ~10 min air exposure after deposition.[45] The surface of Au can be contaminated quickly and become hydrophobic upon air exposure (water contact angle increases from 40º to 50º–60º after 90 min),[45] while the passivation of eC/Au is much slower (water contact angle increases from 44º to 51º after 1 day).[11] Additionally, the topography of eC/Au (rms roughness 0.39 nm) is smoother than that of Au (rms roughness 0.89 nm).[11] The difference in roughness is too small to have any significant effect on the contact angle values but likely could make a difference in Fib adsorption. We believe that the

quicker passivation with air exposure and the rougher surface of Au likely contribute to increased Fib adsorption. Diamond-like carbon having smooth topography has been shown to interact strongly with human albumin and inhibit the adsorption and retention of mid- and high-molecular weight proteins.[19]

Fib adsorbs to a greater extent than BSA from solutions of the same molar concentration, regardless of the surface examined, which can be attributed to the molecular dimensions of the proteins and their conformation at the surface/solution interface.[36] BSA has a molecular weight of 66.7 kDa and a globular structure with dimensions $4 \times 4 \times 7$ nm^3, while Fib has a molecular weight of 340 kDa and a rod-like structure with dimensions $5 \times 5 \times 47$ nm^3.[46] Thus, BSA, with a smaller molecular weight and dimensions, yields a thinner adsorbed layer than Fib. From the normalized Δ%R shifts reported in Table 4-2, a BSA/Fib ratio of 0.7 can be calculated for eC/Au, which is higher than the value of 0.5 for Au under the same experimental conditions. The BSA/Fib ratio at eC/Au is very similar to that obtained at sputtered amorphous carbon surfaces studied by localized SPR,[12] which is probably due to similar physico-chemical properties such, as sp^2 content, O/C ratio, and wettability of these surfaces. Haemocompatibility of diamond-like carbon is known to be associated with the high albumin/fibrinogen ratio,[47] as it is known that albumin reduces while Fib enhances the adhesion and activation of platelets.[48] Intermediate equilibrium contact angle values of 40º–50º have been shown to be favorable for the blood compatibility of the carbon coatings in regard to plasma protein adsorption and platelet activation.[19] Thus, electron-beam evaporated carbon potentially can act as an attractive coating for biomedical applications.

In Chapter 2, we have evaluated the analytical performance of eC/Au as a disposable electrode material, and we have shown that eC/Au exhibits comparable heterogeneous electron transfer rates for benchmark redox systems with glassy carbon electrodes.[11] Protein interactions at electrodes have long been of interest to researchers in the development of biosensors,[49–51] switchable membranes,[52–54] and biomedical implants.[55–57] Adsorption of proteins onto electrode surfaces is known to disturb electrochemical analysis of clinical samples.[58,59] Its influence on the voltametric behavior should, therefore, be examined carefully to permit reliable

electrochemical analysis of biological fluids.[60] Thus, we investigate the effects of protein adsorption on electron-transfer rates of eC/Au electrodes because of its potential use as a disposable electrode material. The eC thickness is 10 nm to facilitate comparisons with our previous electrochemical experiments. We also conduct the experiments with Au electrodes for comparison purposes. eC/Au exhibits similar electron transfer rates for $Ru(NH_3)_6^{3+}$ and $Fe(CN)_6^{3-}$ as Au electrodes (Table 4-3) but with smaller background currents (Figure 4-11 and 12). Exposure of eC/Au or Au electrodes to BSA or IgG solutions dramatically changes the electrochemical response of $Fe(CN)_6^{3-}$ at both Au and eC/Au electrodes (Figure 4-11), namely a decrease in peak current and broadened peak separation, and, consequently, a decrease in electron-transfer rates. The rate and extent of electron transfer blocking for both adsorbed BSA and IgG appear to be the same at both Au and eC/Au electrodes. This has been observed similarly by Moulton et al.[61,62] at a gold electrode, and Guo et al.[60] at platinum, gold, and glassy carbon electrodes. Adsorbed protein layers have negligible impacts on the electron transfer rate of $Ru(NH_3)_6^{3+}$ (Figure 4-12) for both Au and eC/Au electrodes. $Ru(NH_3)_6^{3+/2+}$ has been classified as an outer-sphere redox system, i.e., insensitive to the surface chemistry or adsorbed monolayers at the electrode.[63] Therefore, the presence of a protein layer has no effect on the electron transfer between the electrode and $Ru(NH_3)_6^{3+/2+}$ redox system. In contrast, the electron transfer rate of $Fe(CN)_6^{3-/4-}$ depends on the electrode surface condition;[64] thus, it is hindered by the presence of the protein layers. In short, protein adsorption at Au and eC/Au electrodes might seriously hinder electron-transfer rates of redox systems that require direct interaction with the electrode surface.

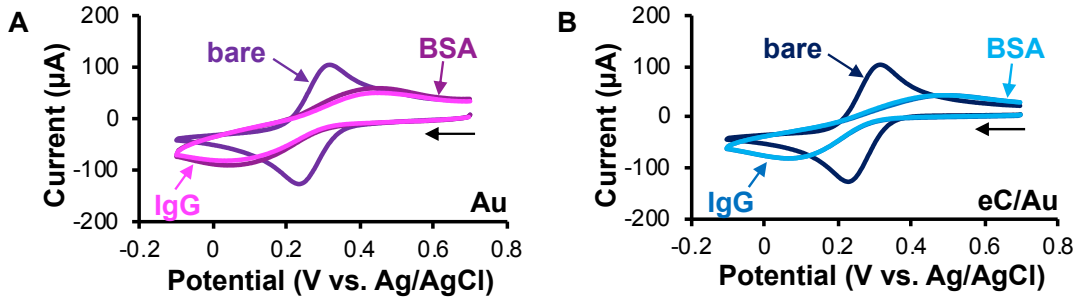

Figure 4-11. Cyclic voltammograms of 1 mM $Fe(CN)_6^{3-}$ in 1 M KCl aqueous solution at (A) Au and BSA-Au and IgG-Au electrodes and (B) eC/Au and BSA-eC/Au and IgG-eC/Au electrodes. The black arrows indicate the direction of the scan. Scan rate = 200 mV/s. The electrodes were immersed in 10 mg/mL BSA and 0.5 mg/mL IgG solutions prepared in PBS buffer for 30 min.

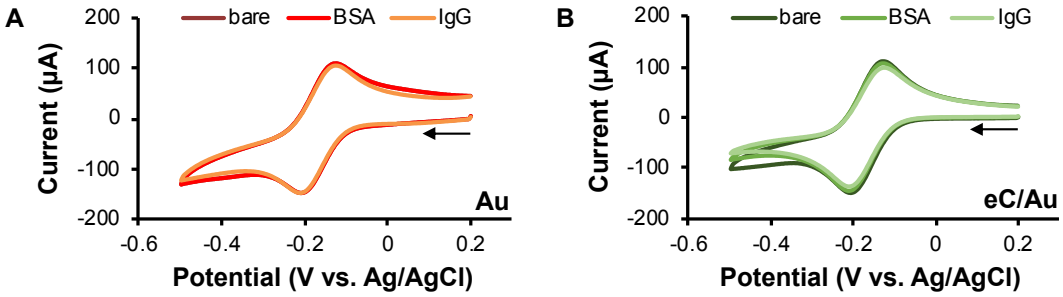

Figure 4-12. Cyclic voltammograms of 1 mM $Ru(NH_3)_6^{3+}$ in 1 M KCl aqueous solution at (A) Au and BSA-Au and IgG-Au electrodes and (B) eC/Au and BSA-eC/Au and IgG-eC/Au electrodes. The black arrows indicate the direction of the scan. Scan rate = 200 mV/s. The electrodes were immersed in 10 mg/mL BSA and 0.5 mg/mL IgG solutions prepared in PBS buffer for 30 min.

Table 4-3. Electron transfer rates of Au and eC/Au electrodes

	k^0 (cm/s)	
Electrode	$Fe(CN)_6^{3-/4}$ (1 M KCl)	$Ru(NH_3)_6^{3+/2+}$ (1 M KCl)
Au	1.3×10^{-2} (3.1%)	1.2×10^{-2} (7.8%)
eC/Au	8.8×10^{-3} (4.9%)	1.3×10^{-2} (7.3%)
BSA-Au	-	1.1×10^{-2} (1.2%)
BSA-eC/Au	-	1.2×10^{-2} (1.0%)
IgG-Au	-	1.2×10^{-2} (0.025%)
IgG-eC/Au	-	1.0×10^{-2} (0.36%)

Values in parentheses are the relative standard deviation of the mean for 3 different electrodes.

4.4 Conclusion

In this chapter, we explored the feasibility of carbon-on-metal films prepared by electron-beam evaporation as SPR substrates. All layers were deposited without breaking vacuum and show good adhesion to the substrate. A 2 nm thick layer of amorphous carbon deposited on an SPR-active gold or silver film offers a smooth, defect-free coating, which can significantly enhance the sensitivity of the substrate for SPR sensing. The eC/Au substrates were then applied to study the adsorption of plasma proteins in situ by SPRi. SPRi results show that BSA and Fib adsorb irreversibly at eC/Au, the extent of which is similar to that observed at Au and sputtered amorphous carbon surfaces. The low activity of eC/Au towards quinone molecules does not translate to protein molecules. However, this should not come as a surprise since carbon surfaces are known to have strong interactions with proteins, even for the relatively chemically inert low temperature isotropic carbon.[65] The readily adsorption of plasma proteins at eC/Au surfaces can hamper their performance as SPR substrates and electrode materials, pointing to the need for protein resistance modifications if eC/Au substrates are to be used in measurements of clinical samples.

References

(1) Patil, P. O.; Pandey, G. R.; Patil, A. G.; Borse, V. B.; Deshmukh, P. K.; Patil, D. R.; Tade, R. S.; Nangare, S. N.; Khan, Z. G.; Patil, A. M.; More, M. P.; Veerapandian, M.; Bari, S. B. Graphene-Based Nanocomposites for Sensitivity Enhancement of Surface Plasmon Resonance Sensor for Biological and Chemical Sensing: A Review. *Biosens. Bioelectron.* **2019**, *139*, 111324. https://doi.org/10.1016/j.bios.2019.111324.

(2) Mitsushio, M.; Miyashita, K.; Higo, M. Sensor Properties and Surface Characterization of the Metal-Deposited SPR Optical Fiber Sensors with Au, Ag, Cu, and Al. *Sens. Actuators Phys.* **2006**, *125* (2), 296–303. https://doi.org/10.1016/j.sna.2005.08.019.

(3) Ordal, M. A.; Long, L. L.; Bell, R. J.; Bell, S. E.; Bell, R. R.; Alexander, R. W.; Ward, C. A. Optical Properties of the Metals Al, Co, Cu, Au, Fe, Pb, Ni, Pd, Pt, Ag, Ti, and W in the Infrared and Far Infrared. *Appl. Opt.* **1983**, *22* (7), 1099. https://doi.org/10.1364/AO.22.001099.

(4) Szunerits, S.; Maalouli, N.; Wijaya, E.; Vilcot, J.-P.; Boukherroub, R. Recent Advances in the Development of Graphene-Based Surface Plasmon Resonance

(SPR) Interfaces. *Anal. Bioanal. Chem.* **2013**, *405* (5), 1435–1443. https://doi.org/10.1007/s00216-012-6624-0.

(5) Lockett, M. R.; Weibel, S. C.; Phillips, M. F.; Shortreed, M. R.; Sun, B.; Corn, R. M.; Hamers, R. J.; Cerrina, F.; Smith, L. M. Carbon-on-Metal Films for Surface Plasmon Resonance Detection of DNA Arrays. *J. Am. Chem. Soc.* **2008**, *130* (27), 8611–8613. https://doi.org/10.1021/ja802454c.

(6) Love, J. C.; Estroff, L. A.; Kriebel, J. K.; Nuzzo, R. G.; Whitesides, G. M. Self-Assembled Monolayers of Thiolates on Metals as a Form of Nanotechnology. *Chem. Rev.* **2005**, *105* (4), 1103–1170. https://doi.org/10.1021/cr0300789.

(7) Vericat, C.; Vela, M. E.; Benitez, G.; Carro, P.; Salvarezza, R. C. Self-Assembled Monolayers of Thiols and Dithiols on Gold: New Challenges for a Well-Known System. *Chem. Soc. Rev.* **2010**, *39* (5), 1805. https://doi.org/10.1039/b907301a.

(8) Ulman, A. *An Introduction to Ultrathin Organic Films: From Langmuir-Blodgett to Self-Assembly*; Academic Press: Boston, MA, 1991.

(9) Lockett, M. R.; Smith, L. M. Fabrication and Characterization of DNA Arrays Prepared on Carbon-on-Metal Substrates. *Anal. Chem.* **2009**, *81* (15), 6429–6437. https://doi.org/10.1021/ac900807q.

(10) Touahir, L.; Niedziółka-Jönsson, J.; Galopin, E.; Boukherroub, R.; Gouget-Laemmel, A. C.; Solomon, I.; Petukhov, M.; Chazalviel, J.-N.; Ozanam, F.; Szunerits, S. Surface Plasmon Resonance on Gold and Silver Films Coated with Thin Layers of Amorphous Silicon−Carbon Alloys. *Langmuir* **2010**, *26* (8), 6058–6065. https://doi.org/10.1021/la903896m.

(11) Nguyen, T. P.; McCreery, R. L.; McDermott, M. T. Evaluation of the Electroanalytical Performance of Carbon-on-Gold Films Prepared by Electron-Beam Evaporation. *The Analyst* **2020**, *145* (14), 5041–5052. https://doi.org/10.1039/D0AN00409J.

(12) Zen, F.; Karanikolas, V. D.; Behan, J. A.; Andersson, J.; Ciapetti, G.; Bradley, A. L.; Colavita, P. E. Nanoplasmonic Sensing at the Carbon-Bio Interface: Study of Protein Adsorption at Graphitic and Hydrogenated Carbon Surfaces. *Langmuir* **2017**, *33* (17), 4198–4206. https://doi.org/10.1021/acs.langmuir.7b00612.

(13) Morteza Najarian, A.; Chen, R.; Balla, R. J.; Amemiya, S.; McCreery, R. L. Ultraflat, Pristine, and Robust Carbon Electrode for Fast Electron-Transfer Kinetics. *Anal. Chem.* **2017**, *89* (24), 13532–13540. https://doi.org/10.1021/acs.analchem.7b03903.

(14) Mattson, J. S.; Smith, C. A. Optically Transparent Carbon Film Electrodes for Infrared Spectroelectrochemistry. *Anal. Chem.* **1975**, *47* (7), 1122–1125. https://doi.org/10.1021/ac60357a070.

(15) DeAngelis, T. P.; Hurst, R. W.; Yacynych, A. M.; Mark, H. B.; Heineman, W. R.; Mattson, J. S. Carbon and Mercury-Carbon Optically Transparent Electrodes. *Anal. Chem.* **1977**, *49* (9), 1395–1398. https://doi.org/10.1021/ac50017a026.

(16) Blackstock, J. J.; Rostami, A. A.; Nowak, A. M.; McCreery, R. L.; Freeman, M. R.; McDermott, M. T. Ultraflat Carbon Film Electrodes Prepared by

Electron Beam Evaporation. *Anal. Chem.* **2004**, *76* (9), 2544–2552. https://doi.org/10.1021/ac035003j.

(17) Yan, H.; Bergren, A. J.; McCreery, R. L. All-Carbon Molecular Tunnel Junctions. *J. Am. Chem. Soc.* **2011**, *133* (47), 19168–19177. https://doi.org/10.1021/ja206619a.

(18) Morteza Najarian, A.; Szeto, B.; Tefashe, U. M.; McCreery, R. L. Robust All-Carbon Molecular Junctions on Flexible or Semi-Transparent Substrates Using "Process-Friendly" Fabrication. *ACS Nano* **2016**, *10* (9), 8918–8928. https://doi.org/10.1021/acsnano.6b04900.

(19) Fedel, M.; Motta, A.; Maniglio, D.; Migliaresi, C. Carbon Coatings for Cardiovascular Applications: Physico-Chemical Properties and Blood Compatibility. *J. Biomater. Appl.* **2010**, *25* (1), 57–74. https://doi.org/10.1177/0885328209342000.

(20) Downard, A. J.; Jackson, S. L.; Tan, E. S. Q. Fluorescence Microscopy Study of Protein Adsorption at Modified Glassy Carbon Surfaces. *Aust. J. Chem.* **2005**, *58* (4), 275. https://doi.org/10.1071/CH04259.

(21) Hedayati, M.; Neufeld, M. J.; Reynolds, M. M.; Kipper, M. J. The Quest for Blood-Compatible Materials: Recent Advances and Future Technologies. *Mater. Sci. Eng. R Rep.* **2019**, *138*, 118–152. https://doi.org/10.1016/j.mser.2019.06.002.

(22) Homola, J. Surface Plasmon Resonance Sensors for Detection of Chemical and Biological Species. *Chem. Rev.* **2008**, *108* (2), 462–493. https://doi.org/10.1021/cr068107d.

(23) Masson, J.-F. Surface Plasmon Resonance Clinical Biosensors for Medical Diagnostics. *ACS Sens.* **2017**, *2* (1), 16–30. https://doi.org/10.1021/acssensors.6b00763.

(24) Roy, R. K.; Lee, K.-R. Biomedical Applications of Diamond-like Carbon Coatings: A Review. *J. Biomed. Mater. Res. B Appl. Biomater.* **2007**, *83B* (1), 72–84. https://doi.org/10.1002/jbm.b.30768.

(25) Stüber, M.; Niederberger, L.; Danneil, F.; Leiste, H.; Ulrich, S.; Welle, A.; Marin, M.; Fischer, H. Surface Topography, Surface Energy and Wettability of Magnetron-Sputtered Amorphous Carbon (a-C) Films and Their Relevance for Platelet Adhesion. *Adv. Eng. Mater.* **2007**, *9* (12), 1114–1122. https://doi.org/10.1002/adem.200700224.

(26) Sydow-Plum, G.; Tabrizian, M. Review of Stent Coating Strategies: Clinical Insights. *Mater. Sci. Technol.* **2008**, *24* (9), 1127–1143. https://doi.org/10.1179/174328408X341816.

(27) Anariba, F.; DuVall, S. H.; McCreery, R. L. Mono- and Multilayer Formation by Diazonium Reduction on Carbon Surfaces Monitored with Atomic Force Microscopy "Scratching." *Anal. Chem.* **2003**, *75* (15), 3837–3844. https://doi.org/10.1021/ac034026v.

(28) Robertson, J. Amorphous Carbon. *Adv. Phys.* **1986**, *35* (4), 317–374. https://doi.org/10.1080/00018738600101911.

(29) Sun, B.; Colavita, P. E.; Kim, H.; Lockett, M.; Marcus, M. S.; Smith, L. M.; Hamers, R. J. Covalent Photochemical Functionalization of Amorphous

Carbon Thin Films for Integrated Real-Time Biosensing. *Langmuir* **2006**, *22* (23), 9598–9605. https://doi.org/10.1021/la061749b.

(30) Finot, M. O.; Braybrook, G. D.; McDermott, M. T. Characterization of Electrochemically Deposited Gold Nanocrystals on Glassycarbon Electrodes. *J. Electroanal. Chem.* **1999**, *466* (2), 234–241. https://doi.org/10.1016/S0022-0728(99)00154-0.

(31) Adzic, R.; Yeager, E.; Cahan, B. D. Optical and Electrochemical Studies of Underpotential Deposition of Lead on Gold Evaporated and Single-Crystal Electrodes. *J. Electrochem. Soc.* **1974**, *121* (4), 474. https://doi.org/10.1149/1.2401841.

(32) Engelsmann, K. Underpotential Deposition of Lead on Polycrystalline and Single-Crystal Gold Surfaces Part II. Kinetics. *J. Electroanal. Chem.* **1980**, *114*, 11–24. https://doi.org/10.1016/0368-1874(80)80360-1.

(33) Engelsmann, K.; Lorenz, W. J.; Schmidt, E. Underpotential Deposition of Lead on Polycrystalline and Single-Crystal Gold Surfaces. Part I. Thermodynamics. *J. Electroanal. Chem.* **1980**, *114* (1), 1–10. https://doi.org/10.1016/S0022-0728(80)80431-1.

(34) Hamelin, A. Underpotential Deposition of Lead on Single Crystal Faces of Gold. Part I. The Influence of Crystallographic Orientation of the Substrate. *J. Electroanal. Chem.* **1984**, *165* (1–2), 167–180. https://doi.org/10.1016/S0022-0728(84)80095-9.

(35) Hamelin, A.; Lipkowski, J. Underpotential Deposition of Lead on Gold Single Crystal Faces. Part II. General Discussion. *J. Electroanal. Chem.* **1984**, *171* (1–2), 317–330. https://doi.org/10.1016/0022-0728(84)80123-0.

(36) Green, R. J.; Davies, J.; Roberts, C. J.; Tendler, S. J. B. Surface Plasmon Resonance for Real Time in Situ Analvsis of Protein Adsorption to Polymer I&faces. **1997**, *18* (5), 9.

(37) Vroman, L.; Adams, A. L. Findings with the Recording Ellipsometer Suggesting Rapid Exchange of Specific Plasma Proteins at Liquid/Solid Interfaces. *Surf. Sci.* **1969**, *16*, 438–446. https://doi.org/10.1016/0039-6028(69)90037-5.

(38) Sugio, S.; Kashima, A.; Mochizuki, S.; Noda, M.; Kobayashi, K. Crystal Structure of Human Serum Albumin at 2.5 Å Resolution. *Protein Eng. Des. Sel.* **1999**, *12* (6), 439–446. https://doi.org/10.1093/protein/12.6.439.

(39) Cacciafesta, P.; Humphris, A. D. L.; Jandt, K. D.; Miles, M. J. Human Plasma Fibrinogen Adsorption on Ultraflat Titanium Oxide Surfaces Studied with Atomic Force Microscopy. *Langmuir* **2000**, *16* (21), 8167–8175. https://doi.org/10.1021/la000362k.

(40) Green, R. J.; Davies, M. C.; Roberts, C. J.; Tendler, S. J. B. Competitive Protein Adsorption as Observed by Surface Plasmon Resonance. *Biomaterials* **1999**, *20* (4), 385–391. https://doi.org/10.1016/S0142-9612(98)00201-4.

(41) Andrade, D. Plasma Protein Adsorption: The Big Twelvea. 15.

(42) Enayatpour, B.; Rajabi, M.; Yari, M.; Reza Mirkhan, S. M.; Najafi, F.; Moradi, O.; Bharti, A. K.; Agarwal, S.; Gupta, V. K. Adsorption/Desorption Study of Proteins onto Multi-Walled Carbon Nanotubes and Amino Multi-Walled

Carbon Nanotubes Surfaces as Adsorbents. *J. Mol. Liq.* **2017**, *231*, 566–571. https://doi.org/10.1016/j.molliq.2017.02.013.

(43) Ohno, Y.; Maehashi, K.; Yamashiro, Y.; Matsumoto, K. Electrolyte-Gated Graphene Field-Effect Transistors for Detecting PH and Protein Adsorption. *Nano Lett.* **2009**, *9* (9), 3318–3322. https://doi.org/10.1021/nl901596m.

(44) Socrates, G. *Infrared and Raman Characteristic Group Frequencies: Table and Charts*; John Wiley & Sons, 2001.

(45) Smith, T. The Hydrophilic Nature of a Clean Gold Surface. *J. Colloid Interface Sci.* **1980**, *75* (1), 51–55. https://doi.org/10.1016/0021-9797(80)90348-3.

(46) Kim, J.; Somorjai, G. A. Molecular Packing of Lysozyme, Fibrinogen, and Bovine Serum Albumin on Hydrophilic and Hydrophobic Surfaces Studied by Infrared−Visible Sum Frequency Generation and Fluorescence Microscopy. *J. Am. Chem. Soc.* **2003**, *125* (10), 3150–3158. https://doi.org/10.1021/ja028987n.

(47) Fedel, M.; Motta, A.; Maniglio, D.; Migliaresi, C. Surface Properties and Blood Compatibility of Commercially Available Diamond-like Carbon Coatings for Cardiovascular Devices. *J. Biomed. Mater. Res. B Appl. Biomater.* **2008**, *90B* (1), 338–349. https://doi.org/10.1002/jbm.b.31291.

(48) Choi, H. W.; Dauskardt, R. H.; Lee, S.-C.; Lee, K.-R.; Oh, K. H. Characteristic of Silver Doped DLC Films on Surface Properties and Protein Adsorption. *Diam. Relat. Mater.* **2008**, *17* (3), 252–257. https://doi.org/10.1016/j.diamond.2007.12.034.

(49) Moulin, A. M. Microcantilever-Based Biosensors. **2000**, 9.

(50) van Noort, D.; Mandenius, C.-F. Porous Gold Surfaces for Biosensor Applications. *Biosens. Bioelectron.* **2000**, *15* (3–4), 203–209. https://doi.org/10.1016/S0956-5663(00)00061-0.

(51) Wu, Z.; Guan, L.; Shen, G.; Yu, R. Renewable Urea Sensor Based on a Self-Assembled Polyelectrolyte Layer. *The Analyst* **2002**, *127* (3), 391–395. https://doi.org/10.1039/b110050e.

(52) Yang, X.; Too, C. O.; Sparrow, L.; Ramshaw, J.; Wallace, G. G. Polypyrrole–Heparin System for the Separation of Thrombin. *React. Funct. Polym.* **2002**, *53* (1), 53–62. https://doi.org/10.1016/S1381-5148(02)00145-1.

(53) Zhou, D.; Too, C. O.; Wallace, G. G. Synthesis and Characterisation of Polypyrrole/Heparin Composites. *React. Funct. Polym.* **1999**, *39* (1), 19–26. https://doi.org/10.1016/S1381-5148(97)00149-1.

(54) Zhou, D.; Too, C. O.; Wallace, G. G.; Hodges, A. M.; Mau, A. W. H. Protein Transport and Separation Using Polypyrrole Coated, Platinised Polyvinylidene Fluoride Membranes. *React. Funct. Polym.* **2000**, *45* (3), 217–226. https://doi.org/10.1016/S1381-5148(00)00034-1.

(55) Contu, F.; Elsener, B.; Böhni, H. Characterization of Implant Materials in Fetal Bovine Serum and Sodium Sulfate by Electrochemical Impedance Spectroscopy. I. Mechanically Polished Samples: Implant Materials and EIS. I. *J. Biomed. Mater. Res.* **2002**, *62* (3), 412–421. https://doi.org/10.1002/jbm.10329.

(56) Jones, M. I.; McColl, I. R.; Grant, D. M.; Parker, K. G.; Parker, T. L. Protein Adsorption and Platelet Attachment and Activation, on TiN, TiC, and DLC

Coatings on Titanium for Cardiovascular Applications. *J. Biomed. Mater. Res.* **2000**, *52* (2), 413–421. https://doi.org/10.1002/1097-4636(200011)52:2<413::AID-JBM23>3.0.CO;2-U.

(57) Anderson, J. M.; Ziats, N. P.; Azeez, A.; Brunstedt, M. R.; Stack, S.; Bonfield, T. L. Protein Adsorption and Macrophage Activation on Polydimethylsiloxane and Silicone Rubber. *J. Biomater. Sci. Polym. Ed.* **1996**, *7* (2), 159–169. https://doi.org/10.1163/156856295X00670.

(58) Harrison, D. J. Effect of Blood on K+ion Sensitive Membrane Electrode Performance and Bulk Resistance. *J. Electroanal. Chem. Interfacial Electrochem.* **1990**, *278* (1–2), 193–204. https://doi.org/10.1016/0022-0728(90)85133-P.

(59) Downard, A. J.; Roddick, A. D. Protein Adsorption at Glassy Carbon Electrodes: The Effect of Covalently Bound Surface Groups. *Electroanalysis* **1995**, *7* (4), 376–378. https://doi.org/10.1002/elan.1140070414.

(60) Guo, B.; Anzai, J.; Osa, T. Adsorption Behavior of Serum Albumin on Electrode Surfaces and the Effects of Electrode Potential. **1996**, *44* (4), 800–803.

(61) Moulton, S. E.; Barisci, J. N.; Bath, A.; Stella, R.; Wallace, G. G. Studies of Double Layer Capacitance and Electron Transfer at a Gold Electrode Exposed to Protein Solutions. *Electrochimica Acta* **2004**, *49* (24), 4223–4230. https://doi.org/10.1016/j.electacta.2004.03.034.

(62) Moulton, S. E.; Barisci, J. N.; Bath, A.; Stella, R.; Wallace, G. G. Investigation of Protein Adsorption and Electrochemical Behavior at a Gold Electrode. *J. Colloid Interface Sci.* **2003**, *261* (2), 312–319. https://doi.org/10.1016/S0021-9797(03)00073-0.

(63) McCreery, R. L. Advanced Carbon Electrode Materials for Molecular Electrochemistry. *Chem. Rev.* **2008**, *108* (7), 2646–2687. https://doi.org/10.1021/cr068076m.

(64) Chen, P.; McCreery, R. L. Control of Electron Transfer Kinetics at Glassy Carbon Electrodes by Specific Surface Modification. *Anal. Chem.* **1996**, *68* (22), 3958–3965. https://doi.org/10.1021/ac960492r.

(65) Feng, L.; Andrade, J. D. Protein Adsorption on Low Temperature Isotropic Carbon: V. How Is It Related to Its Blood Compatibility? *J. Biomater. Sci. Polym. Ed.* **1996**, *7* (5), 439–452. https://doi.org/10.1163/156856295X00445.

Chapter 5. Immobilization of Biomolecules on SPR Carbon-on-Gold Chips by Spontaneous Grafting of Aryl Diazonium Salts

5.1 Introduction

Surface plasmon resonance (SPR) spectroscopy is a powerful and widely used analytical technique to study biomolecular interactions and biosensing.[1,2] It offers sensitive, real time measurement of binding events, without the need for labelling the target biomolecules.[3] The advance of SPR imaging (SPRi) in the 1980s has opened the door for multiplex detection, that is, monitoring simultaneously multiple events in an array format.[4] This is promising to reduce time and cost in high-throughput studies of enzyme kinetics, pharmaceutical screening, and biomolecule interactions (e.g., DNA/protein, protein/protein).[5–10]

In SPR-based biosensors, either the biorecognition element or the target molecule is immobilized on the solid surface, and the other one is in the solution.[3] As such, sensor performance, i.e., sensitivity, specificity, and robustness, depends on reproducible coverage and orientation of the immobilized species.[11,12] Common types of biorecognition elements that have been used in SPR affinity biosensors include antibodies, peptides, and aptamers.[3,13] Antibodies are used the most often, as they can be designed to have high affinity and specificity against a target molecule.[3] Hence, the following discussion is dedicated to the immobilization of antibodies. Chapter 4 introduced our work on eC/Au films for SPR applications. As already noted, Au films are the predominant substrates for SPR, and the previous work described below on antibody immobilization is primarily on Au surfaces.

The immobilization of antibodies to the surface can be done via physical adsorption, covalent attachment, and affinity capture.[3] The chosen surface attachment should provide a sufficient number of the antibodies on the sensing surface, retain their biological activity, and minimize non-specific binding.[3] Physical adsorption is straightforward and simple: the surface is placed in contact with the protein solution to promote adsorption, mainly based on the electrostatic interaction between the protein and the sensor surface.[13] While preserving the biological activity of the

biomolecule,[14,15] physical adsorption might result in poor reproducibility and low sensitivity due to leaching of the adsorbed proteins.[13]

Covalent attachment represents an attractive alternative to physical adsorption, as it potentially enhances the stability of the protein–surface attachment.[13] Here, the protein is coupled to an activated surface functionalized with moieties with binding capacity. Since a thin layer of gold (~50 nm) typically is used as an SPR substrate, self-assembled monolayers (SAMs) of alkanethiolates have been used widely to functionalize gold surfaces. Usually, a mixture of SAMs, long-chained (n = 12 and higher) alkanethiolates containing the desired end group and short-chained alkanethiolates containing an oligo(ethylene glycol) group for nonfouling background, have been developed.[16,17] Because proteins contain many functional groups (e.g., thiol, amino), covalent attachment can result in random orientation of the immobilized proteins as well as restrict their conformational flexibility, thereby impairing their function.[3]

Affinity capture represents yet another approach for antibody immobilization, which results in specific orientation of the antibody through selective binding. This is achieved by a high affinity or selective interaction between a surface bound species and an antibody.[3] The most common example of this approach is based on avidin–biotin chemistry: a biotinylated antibody can be attached to an avidin (or streptavidin) modified surface.[3] Alternatively, an unmodified antibody can bind to a protein A (or protein G) modified surface.[3] Protein A is a 42 kDa cell wall protein of the bacteria *Staphylococcus aureus* and interacts preferentially to the F_c region of the antibody, directing the binding sites F_{ab} away from the surface. The orientation of protein A dictates the orientation of the antibody and thus needs to be controlled.[18]

Although SAMs of alkanethiolates are almost exclusively used to immobilize biomolecules on SPR chips, the Au–S bonds are prone to oxidation and thus unstable.[19] The rate of oxidation depends on the alkyl chain length (shorter-chain length SAMs oxidize much faster than long-chain ones)[20,21] and the chemical nature of the terminal functional group.[22] The oxidized SAM is bound less strongly to the gold surface,[23] desorbing from the surface, thereby impairing the performance of the final device. The drawbacks of using Au and SAMs in SPR spectroscopy point to the

need for alternative surface chemistries. Electroreduction of aryl diazonium chemistry has been investigated as an alternative surface chemistry to SAMs due to the enhanced stability of the covalent Au–C bonds.[24]

Immobilization of proteins on SPR Au chip surfaces by electrochemical grafting of aryl diazonium salts has been demonstrated by several groups. In one approach, an aniline derivative is conjugated to the antibody, followed by diazotation of the aniline–antibody conjugation and subsequent electrodeposition on the surface.[25] The harsh conditions employed for diazotation (20 mM HCl and 20 mM $NaNO_2$ at ice cold temperature) might not be compatible with all proteins and can impact protein integrity.[26] Alternatively, the gold surface was modified first by electroreduction of aryl diazonium bearing a carboxylic function, followed by a carbodiimide activation and subsequent protein immobilization.[27–29] Notably, diazonium-modified gold chips showed a higher specific signal and a lower non-specific signal in comparison with thiol-modified surfaces.[28] To date, there has been no report on the use of spontaneous grafting of aryl diazonium salts for protein immobilization on SPR substrates.

In this chapter, we explored the use of spontaneous grafting of diazonium salts to immobilize proteins on eC/Au SPR chip surfaces. Thick multilayers produced on Au by the electroreduction approach have been shown to modify surface plasmon waves drastically, and even passivate them completely;[29] this could decrease the sensitivity of the SPR substrate. Previous work in our group also showed that controlling the thickness of electrochemically grafted aryl diazonium-derived films to monolayers resulted in the highest concentration of antibody immobilized.[27] The spontaneous approach, as has been shown in Chapter 3, produced monolayers and thus could increase the sensitivity of SPRi detection. Spontaneous grafting is not as fast as electroreduction but still within a reasonable timeframe (0.5 h) compared to SAMs (~24 h). In addition, it is simple to carry out and negates the use of electrochemical instrumentation, while still allowing for patterning of multispot SPRi chips by a robotic or handheld microspotter. In Chapter 4, eC/Au films were investigated as SPR substrates, and a thickness of 2 nm eC demonstrated minimal surface plasmon loss. Therefore, 2 nm eC on Au films continue to be used in this

chapter to explore the aryl diazonium surface chemistry for SPR sensing. This study may open the pathway for the combination of spontaneously adsorbed diazonium layers and eC/Au films to be a viable alternative to thiolate SAMs on Au for SPR sensing.

5.2 Experimental

5.2.1 Chemicals and Materials

P-type, (100) oriented silicon wafers (University Wafers), SF-10 glass (Schott Glass), concentrated sulfuric acid (95% to 98%, Caledon), hydrogen peroxide (Aldrich, 30% w/w), glycine (99%, Caledon) adjusted to pH 2.3 with hydrochloric acid (concentrated, Caledon), N-hydroxysuccinimide (NHS, 98%, Aldrich), 1-ethyl-3-(3-dimethylaminopropyl) carbodiimide hydrochloride (EDC, >98%, Aldrich), 4-aminobenzoic acid (Aldrich), tetrafluoroboric acid (48% wt in H_2O, Aldrich), sodium nitrite (Aldrich), 4-aminophenylacetic acid (Aldrich) polyoxyethylene-sorbitan monolaureate (Tween 20, Aldrich), tridecafluoro-1,1,2,2-tetrahydrooctyl)trichlorosilane (Gelest, Inc), recombinant protein A from Staphylococcus aureus (Aldrich, aqueous solution, ≥95% , HPLC), bovine serum albumin (BSA, Aldrich, ≥98%, pH 7), fibrinogen from bovine plasma (Fib, Aldrich, Type I-S , 65-85% protein), ChromPure Rabbit IgG (whole molecule, Jackson ImmunoResearch), ChromPure Goat Anti-Rabbit IgG (whole molecule, Jackson ImmunoResearch), and phosphate buffered saline (PBS, Aldrich, 10x concentrate, BioReagent) were used as received. 4-carboxybenzene diazonium tetrafluoroborate salt (CBD) and 4-carboxymethylbenzene diazonium tetrafluoroborate salt (CMBD) were synthesized and recrystallized before use, as detailed elsewhere.[30] Solutions were prepared fresh daily with deionized (DI) water, purified and deionized by a Barnstead E-Pure system (18.2 MΩ·cm, ThermoFisher).

5.2.2 Substrate Preparation

The SPR substrates were chromium (2 nm), gold (42 nm), and carbon (2 nm) layers deposited onto SF-10 glass cut into 1.8 × 1.8 cm^2 chips by electron-beam evaporation, as detailed in Chapter 2. The substrates consist of nine spots, each with a diameter of 1 mm. For AFM and FR-IRRAS measurements, chromium (2 nm), gold (42 nm), and carbon (2 nm) layers were deposited on silicon wafers. Prior to deposition, glass and silicon pieces were cleaned with hot piranha solution (1:3 v/v H_2O_2 : conc. H_2SO_4), followed by thorough rinsing with DI water and dried with nitrogen gas. [Warning: Piranha solution presents an explosion danger and should be handled with extreme care; it is a strong oxidant and reacts violently with many organic materials. All work should be performed under a fume hood. Wear personal safety equipment.] Substrates were prepared fresh daily and stored in a desiccator under vacuum at room temperature, until use.

5.2.3 Surface Modification

Diazonium salt deposition. SPRi chips were immersed in 1 mM aqueous solutions of CBD and CMBD for 30 min, then rinsed thoroughly with DI water, and dried with nitrogen gas.

Protein A immobilization. For covalent attachment, following surface modification with diazonium salts, the SPRi chips were exposed to a vapor of neat tridecafluoro-1,1,2,2-tetrahydrooctyl)trichlorosilane under reduced pressure overnight (~18 h), rendering the glass surface hydrophobic and permitting the localization of aqueous solution drops on the spots. Then, the chips were immersed in an activating solution composed of 0.1 M EDC and 0.1 M NHS for 90 min. A 2.5 µL drop of 7 µM protein A[11] was deposited manually on four spots of the chips with a micropipette and incubated for 30 min at 37 ºC. Then, the chips were immersed in PBSTA (1% BSA and 0.1% Tween 20 in PBS) for 20 min at 37 ºC to block the non-specific binding sites of the surface.[28] The chips were rinsed thoroughly with DI water and dried with nitrogen gas after each step.

For physical adsorption, a 2.5 µL drop of 7 µM protein A[11] was deposited manually on four spots of the chips with a micropipette and incubated for 30 min at

37 ºC. The substrates were subject to the same steps to create a hydrophobic background prior to protein A immobilization and block non-specific adsorption as described above.

5.2.4 Surface Characterization

Infrared reflection-absorption spectroscopy (IRRAS). IRRAS spectra were collected on a Nicolet 8700 Fourier transform infrared (FTIR) spectrometer (Thermo Fisher Scientific), equipped with a mercury cadmium telluride (MCT) detector, a specular reflectance accessory (80 Spec, Pike Technologies). 1024 spectra were collected at 80° incidence and 4 cm^{-1} resolution using a bare gold slide as background.

X-ray Photoelectron Spectroscopy (XPS). XPS experiments were performed at room temperature at nanoFAB using a Kratos Axis (Ultra) spectrometer with monochromatized Al K_α (1486.71 eV). The spectrometer was calibrated by Au $4f_{7/2}$ binding energy (84.0 eV) with reference to the Fermi level. The analysis chamber pressure is lower than 5×10^{-10} Torr. CASA XPS was used for atomic ratio calculations and component analysis. Note: Adventitious carbon was likely present and thus complicated the interpretation of C 1s spectra.

Contact Angle. Contact angle measurements were performed with a 4 μL droplet volume using a Ráme-Hart goniometer (model 590), equipped with DROPimage advanced software. The reported values are the averages of two measurements on each sample (N = 3).

Atomic Force Microscopy (AFM). AFM images were collected with a Dimension Edge Atomic Force Microscope (Bruker) using commercial Si tips with a resonant frequency of 300 kHz and a force constant of 40 N/m (Tap300, Ted Pella, Inc.). The scan rate was 1–2 Hz, and the scanning density was 512 lines/frame. The thicknesses of the organic layers were determined by "AFM scratching", as previously described by Anariba et. al.[31] The applied force was determined empirically so that it is sufficient to remove the organic layers without damaging the surface. A set point voltage of 0.5 V was used for all experiments. AFM images were processed with NanoScope Analysis v1.40. The images, with the exclusion of the 'scratched' regions, were flattened with a first-order polynomial before analysis.

Then, a line-scan profile was drawn across the scratched region to determine the thickness of the organic layer.

Surface plasmon resonance imaging (SPRi). Experiments were carried out using a SPR Imager (GWC Technologies) and V++ software. The SPR imager has been described in detail elsewhere.[32] Antibody and buffer solutions were introduced to the substrate surface via peristaltic flow through a fluid cell. After an equilibration step with PBS, rabbit IgG solution (10 µg/mL[28] in PBS) was introduced into the flow cell, followed by a regeneration step by injecting 0.2 M glycine, pH 2.3. Figure 5-1 is a schematic representation of the experimental procedure described here.

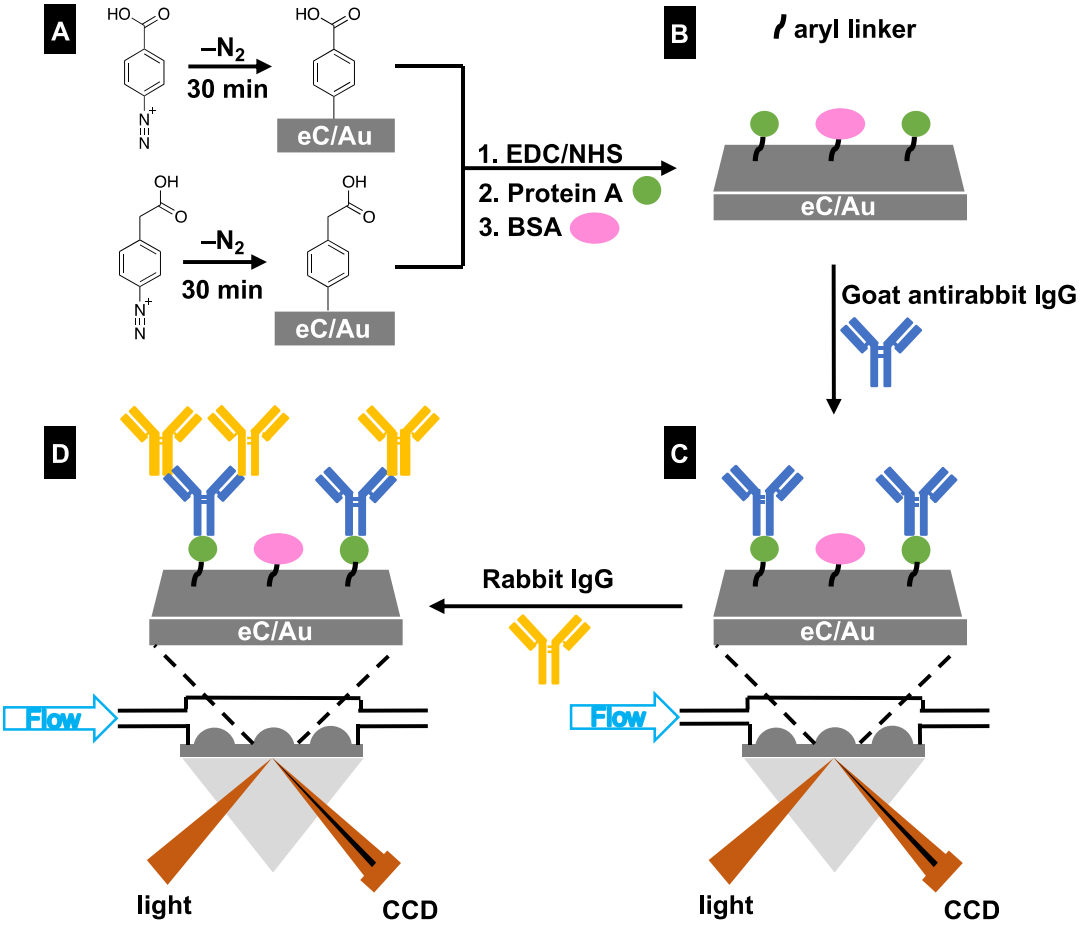

Figure 5-1. Schematic representation of the experimental procedure. (A) Surface modification with aryl diazonium salt. (B) Protein A immobilization onto the diazonium layer. SPRi measurement setup for the capture of goat anti-rabbit IgG, shown in (C) and subsequently rabbit IgG, shown in (D).

5.3 Results and Discussion

In Chapter 4, we have reported that 2 nm thick eC coating resulted in a minimal 10% loss of sensitivity relative to a bare gold film in SPRi measurements. Hence, we chose to proceed with a 2 nm thickness of eC layer in this chapter. The gold layer was 42 nm to support SPR. The goal of this chapter is to explore biofunctionalization of SPRi chips, based on pre-modification with aryl diazonium salts. Figure 5-1 presents a two-step procedure, in which spontaneous grafting of an aryl diazonium salt bearing a carboxylic functional group was introduced to the surface, followed by a carbodiimide activation of the modified surface. Covalent immobilization of a biomolecule using two diazonium salts bearing carboxylic functional groups was compared with the physical adsorption approach. Protein A is used as a model target to compare and optimize the immobilization strategy in terms of preservation of immobilized protein activity and regeneration of chip surface.

Diazonium deposition by spontaneous grafting. The eC/Au substrates were modified with diazonium salts bearing carboxy functional groups (4-carboxybenzene diazonium tetrafluoroborate/CBD and 4-carboxymethylbenzene diazonium tetrafluoroborate/CMBD) by immersion in the aqueous solutions thereof. Both CBD[27,29,33] and CMBD[28,33–35] are used in the electrografting of surfaces, but CMBD has been suggested to be less prone to protein fouling[33] and more reactive in the immobilization of enzymes than CBD.[35]

It has been shown that the aryl diazonium cation is dediazonized spontaneously via electron transfer from the surface in either aqueous or organic solutions.[36] Several parameters have been found to affect the spontaneous attachment, including immersion time, diazonium salt concentration, and solvents, as well as the nature of the substrate and the diazonium compound.[36] A detailed investigation of the spontaneous grafting on eC/Au is presented in Chapter 3. Based on this, a concentration of 1 mM in aqueous solution and a deposition time of 30 min were chosen as the deposition conditions here. The modified substrates were characterized by water contact angle, FT-IRRAS, XPS, and AFM to confirm the presence of the diazonium-derived layers on eC/Au substrates. A summary of the characterization results is presented in Table 5-1.

Table 5-1. Summary of Characterization Results on eC/Au and eC/Au Modified with CBD and CMBD Salts

Surface	Water contact angle	XPS C 288.5 eV (%)	AFM rms roughness (nm)	BSA-SPR $\Delta\%R$ ($\times 10^{-3}$)	Fib-SPR $\Delta\%R$ ($\times 10^{-3}$)
eC/Au	41° ± 3°	5.8	0.39 ± 0.05	3.9 ± 0.1	5.7 ± 0.4
eC/Au-CBD	22° ± 4°	8.9 ± 0.2	0.57 ± 0.03	3.9 ± 0.2	6.7 ± 0.3
eC/Au-CMBD	44° ± 2°	7.4 ± 0.4	0.56 ± 0.05	4.5 ± 0.1	6.7 ± 0.3

Water contact angle measurements. Figure 5-3 shows the water contact angles on unmodified and aryl diazonium-modified eC/Au substrates. Grafting with CBD resulted in a more hydrophilic surface, while CMBD slightly increased the water contact angle compared to unmodified substrates. The additional methylene group in CMBD renders the molecule more hydrophobic than CBD and likely contributes to the hydrophobicity of the modified surface. The water contact angle data are reported in Table 5-1.

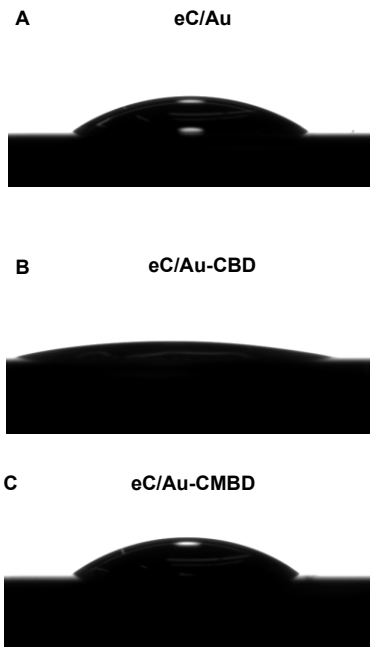

Figure 5-2. Water contact angle measurements on eC/Au and eC/Au modified with 4-carboxybenzene diazonium (CBD) and 4-carboxymethylbenzene diazonium (CMBD) salts.

Fourier transform infrared reflection absorption spectroscopy (FT-IRRAS). FT-IRRAS also was used to verify the surface attachment of CBD and

CMBD. Figure 5-4 presents FT-IRRAS spectra of unmodified (A) and aryl diazonium-modified eC/Au substrates (B). No band around 2300 cm^{-1}, which corresponds to the diazo stretch, was observed (not shown in the spectra), indicating the loss of dinitrogen during the spontaneous grafting reaction. The dominant bands centred at around 1716 cm^{-1} and 1608 cm^{-1} in Figure 5-4B are assigned to –C=O from carboxylic acid and –C=C or –C–H from the aromatic ring, respectively.[27] The IRRAS bands from CBD- and CMBD-derived substrates are comparable in terms of intensity, width and position, but CBD appears to result in a slightly higher yield. These bands are absent on an unmodified eC/Au substrate, indicating that they are the result of surface derivatization. The vibrations observed from the carboxylic acid and the aromatic ring indicate the successful surface modification with the two aryl diazonium salts by simple immersion.

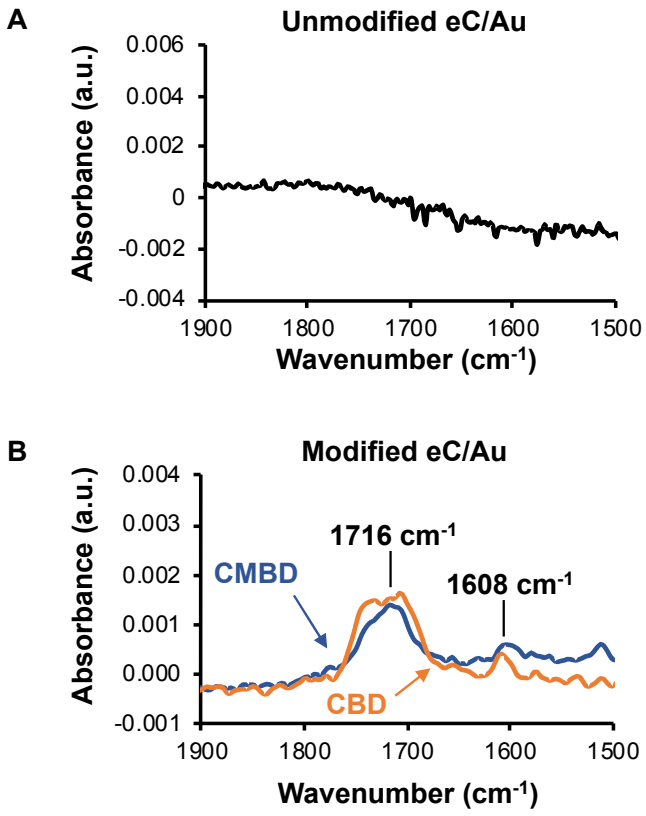

Figure 5-3. FT-IRRAS spectra of unmodified eC/Au (A) and eC/Au modified with 4-carboxybenzene diazonium (CBD) and 4-carboxymethylbenzene diazonium (CMBD) salts (B).

X-ray Photoelectron Spectroscopy (XPS). The aryl diazonium modified eC/Au substrates also were characterized by XPS. Survey spectra of modified substrates show an increased level of oxygen in comparison with the unmodified substrate, as expected for the introduction of carboxylic groups onto the surfaces. The O/C ratio of the unmodified eC/Au is 12%, and the O/C ratios of CBD-eC/Au and CMBD-eC/Au are 17% and 14%, respectively. Figure 5-5 shows high resolution spectra of C1s peaks of unmodified and modified eC/Au substrates, which were fitted with four components. The peaks at 284 eV (C1) and 285 eV (C2) are assigned to sp^2 and sp^3 hybrids, and the peaks at 286.5 eV (C3) and 288.5 eV (C4) are assigned to C–O and C=O bonds, respectively.[37,38] The component at 288.5 eV can be attributed to an oxidized carbon consistent with a –C=O bond of the carboxylic acid groups.[38] Quantification of this component (Table 5-1) indicates a significant increase after modification with aryl diazonium salts, and the yield of CBD is slightly higher than CMBD, which is in agreement with FT-IRRAS results.

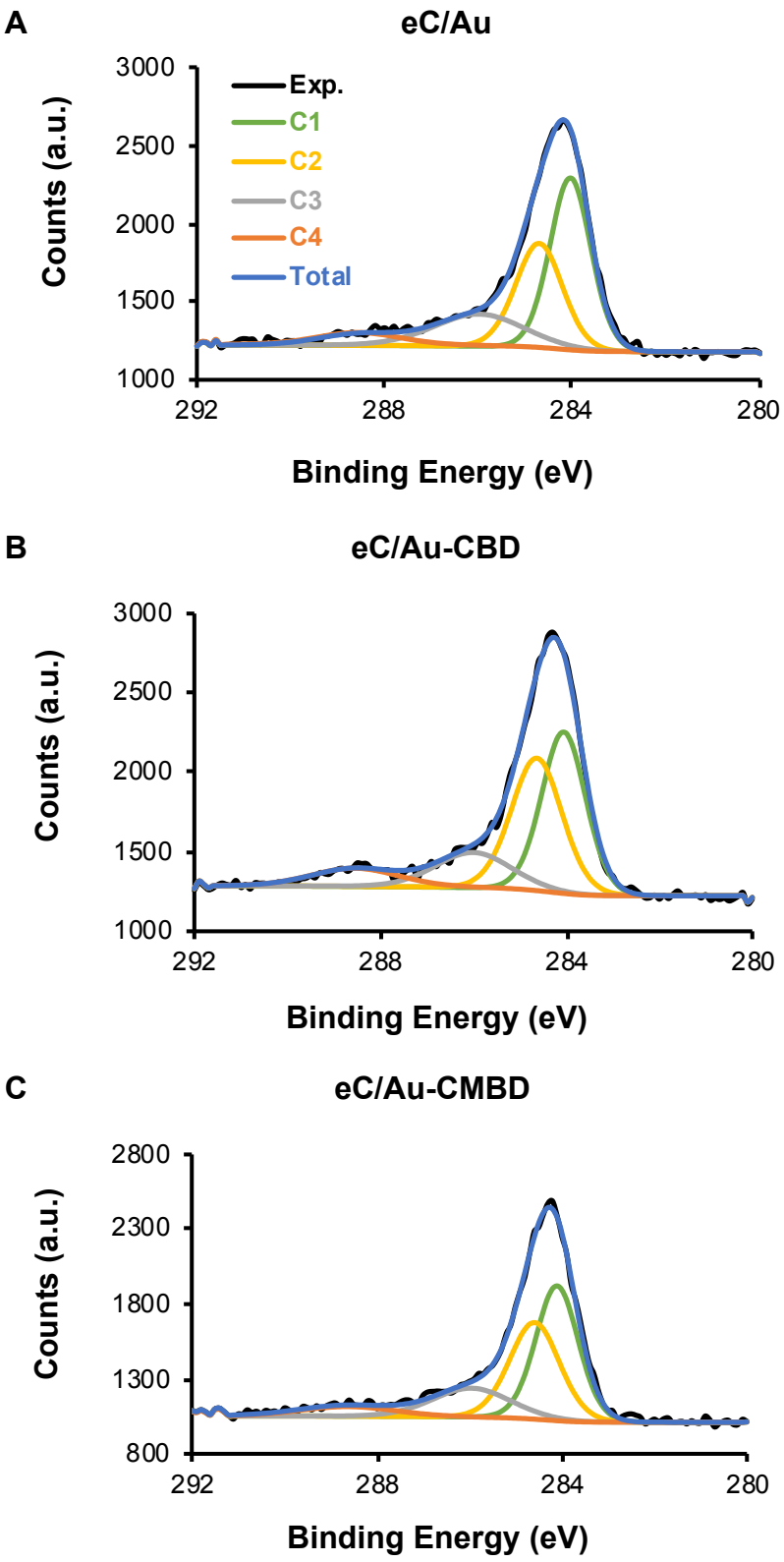

Figure 5-4. XPS C1 high resolution spectra of unmodified eC/Au (A), eC/Au modified with 4-carboxybenzene diazonium (CBD) salt (B), and 4-carboxymethylbenzene diazonium salt (CMBD) (C).

Atomic Force Microscopy (AFM). Evidence of successful modification also can be seen from Figure 5-6, which shows the AFM images of unmodified and modified eC/Au surfaces. Formation of aryl layers roughen the surface by ~1.5 fold for both CBD and CMBD (Table 5-1). The thickness of the grafted layer was determined by "AFM scratching" (described in detailed in Chapter 3) and was ~1 nm for CBD and ~ 0.9 nm for CMBD, suggesting that monolayers were formed. The height of a benzoic acid monolayer oriented perpendicular to the surface is ~0.7 nm,[27] so a thickness of ~1.0 nm corresponds to ~1.4 aryl layers that were grafted on the surface.

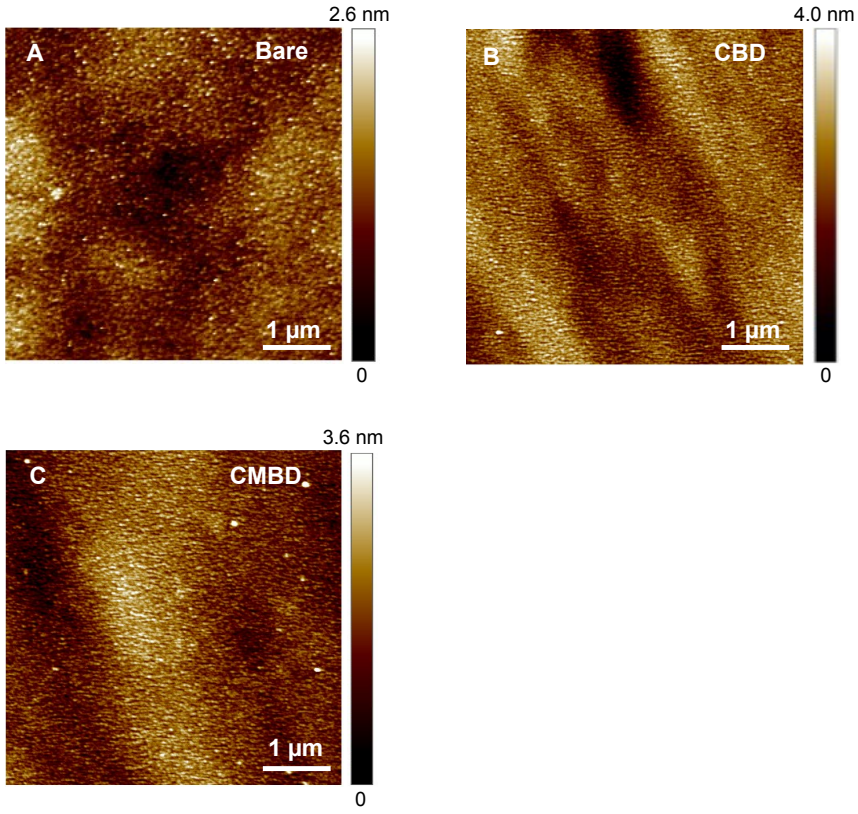

Figure 5-5. AFM images of eC/Au and eC/Au modified with 4-carboxybenzene diazonium (CBD) and 4-carboxymethylbenzene diazonium (CMBD) salts.

The wettability, FT-IRRAS, XPS, and AFM characterization results all point to the formation of carboxylic group-bearing aryl monolayers by simple immersion of eC/Au substrates in aqueous solutions of the salts. The results presented here are generally consistent with the results obtained in Chapter 3, when the modification

was done on 10 nm eC/42 nm Au substrates. Notably, CBD resulted in a slightly higher yield compared to CMBD. In Chapter 3, we reported that there is a correlation between the reduction potentials of the diazonium salts with the yield of the spontaneous grafting reaction, the more positive potential, the higher the yield. The reduction potentials of CBD and CMBD are –0.2 V[27] and –0.4 V[34] (vs Ag/Ag^+, in 0.1 M $TBABF_4$/ACN, on Au electrodes, scan rate 10 mV/s), respectively. CBD is easier to be reduced than CMBD, thus forming thicker aryl film.

Nonspecific adsorption of proteins on CBD- and CMBD-derived surfaces. CMBD electrografted on Au SPRi chips has been reported to exhibit lower non-specific adsorption of rabbit IgG than the SAM of thiotic acid.[28] In a study of protein adsorption by electrochemical methods, CMBD electrografted to glassy carbon reduced the amount of adsorbed BSA relative to the bare surface, while CBD showed similar extent of BSA adsorption as the unmodified electrode.[33] Therefore, we are interested in investigating the non-specific protein adsorption at eC/Au substrates spontaneously grafted with CBD and CMBD. BSA and Fib were chosen as two model plasma proteins.

The eC/Au substrates were modified with CBD and CMBD, then exposed to 7 μM BSA and Fib solutions and monitored in real time by SPRi. Using the procedure established in Chapter 4, all substrates were calibrated with four water/ethanol solutions prior to protein exposure. After the calibration step, PBS was injected, followed by protein solution and a final rinsing step with PBS to remove unadsorbed protein. A representative sensorgram of the BSA adsorption measurement at an CBD-eC/Au is shown in Figure 5-7. The Δ%R reported in Table 5-1 were normalized with the sensitivity of the surface determined from the calibration step with ethanol/water solutions, accounting for any differences in alignment across sensors and sensitivity to changes in bulk refractive index that result from the modification with the diazonium salts. The sensitivity of CBD-eC/Au is $(3.0 \pm 0.3) \times 10^3$ (n = 6), and the sensitivity of CMBD-eC/Au is $(2.8 \pm 0.2) \times 10^3$ (n = 7), slightly higher than the unmodified substrates $(2.6 \pm 0.2) \times 10^3$, indicating that modifying eC/Au with the two diazonium salts resulted in a similar sensitivity of the surfaces to bulk refractive index changes.

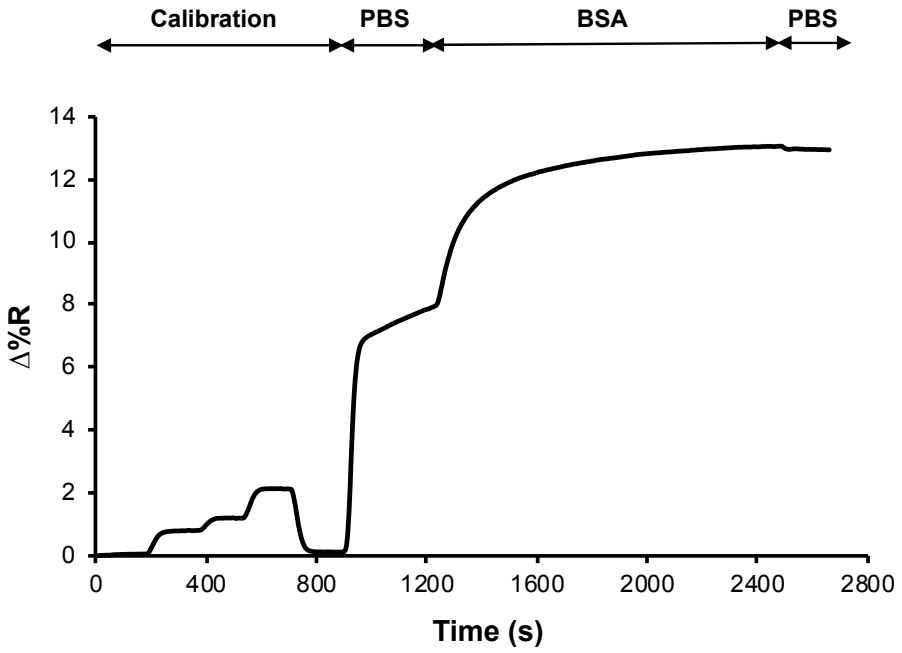

Figure 5-6. BSA adsorption experiment measured at an CBD-eC/Au substrate.

From Table 5-1, BSA adsorbed similarly at unmodified eC/Au and CBD-eC/Au and adsorbed more at CMBD-eC/Au. Fib adsorbed more at modified surfaces than unmodified ones. CMBD-eC/Au surfaces increased non-specific adsorption of BSA compared to CBD-eC/Au and did not exhibit the non-fouling property, as previously reported. It is somewhat surprising that surfaces terminated with carboxylic acid groups appear to promote protein adsorption relative to the bare surface. CMBD-eC/Au shows similar wettability as the unmodified surface, so wettability can be ruled out as a contributing factor. Several studies[39–42] on protein adsorption on Au modified with SAMs have reported that, despite their hydrophilicity and negative charge, COOH-terminated SAMs exhibit comparable protein adsorption to CH_3-terminated SAMs, a hydrophobic surface that is associated with high protein adsorption.[39,43] We speculate that the interactions between the proteins and the diazonium modified surface are likely electrostatic. At pH 7.4, both the carboxylic groups and the proteins should be negatively charged.[33,39,40] However, it is important to note that although the proteins carry a net negative charge, they still can adsorb to negatively charged surfaces through the positively charged domains residing on the

protein surface.[39] The proteins also could adsorb to negatively charged surfaces through an electrostatic bridge constructed by cationic counter ions.[40]

Protein A immobilization and antibody capture. Next, we determined whether these carboxylic acid functions bearing aryl layers are viable for subsequent immobilization of biomolecules to SPRi chip surfaces. The CBD and CMBD-modified eC/Au substrates are used to immobilize protein A covalently through carbodiimide chemistry and compared with the physical adsorption approach. Protein A interacts preferentially to the F_c region of the antibody, directing the binding sites F_{ab} away from the surface. This renders the antibody in a favorable orientation to interact with the antigen. In order to control the orientation of the antibody, the orientation of protein A itself needs to be controlled.[18]

The effectiveness of the immobilization of protein A onto the surface was quantified by monitoring the SPRi signal after the introduction of rabbit IgG solution. The aryl layers bearing carboxylic functional groups were activated, and protein A and BSA are immobilized as specific and control spots, respectively. Figure 5-8A shows a representative difference image of an eC/Au-CBD chip surface, in which the four brighter spots had been spotted with protein A. Physical and covalent approaches of protein A were compared. Representative sensorgrams are shown in Figure 5-8B, C, and D. For all surfaces under study, injection of rabbit IgG, which is one of the preferential targets of protein A,[28] over the chip surface significantly increased the Δ%R of protein A spots, as protein A captures rabbit IgG to the surface. The control spots (BSA spots) remained relatively insensitive to the IgG injection.

Regeneration ability of the surfaces also was studied and presented in Figure 5-8, which was carried out by injecting target rabbit IgG and regenerating the surface using 0.2 M glycine at pH 2.3. Due to the instrument's time limit, only two regeneration cycles were performed. The Δ%R for both the physical and covalent approaches remained stable and reproducible. The protein A-rabbit IgG interaction appears to be fully reversible, with a total recovery, as evidenced by the SPRi baseline signal at each regeneration cycle.

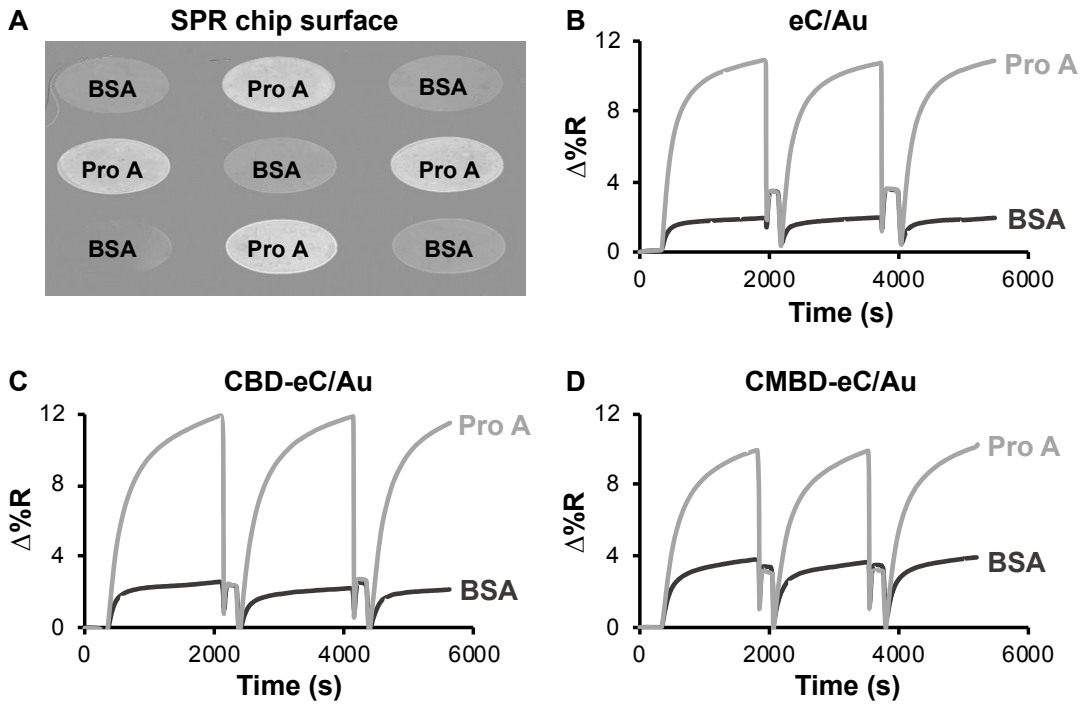

Figure 5-7. A) Representative different image of CBD-modified eC/Au chip. Sensorgrams at eC/Au surface (B), CBD-modified eC/Au (C), and CMBD-modified eC/Au, bearing spotted protein A and BSA. Injected rabbit IgG concentration 10 µg/mL. The injection is followed by a regeneration step with 0.2 M glycine, pH 2.3.

Immobilizing protein A by a CBD-derived surface is as effective as the physical approach, while CMBD-modified eC/Au resulted in a slightly lower IgG amount that was captured, which can be attributed to the lower yield of CMBD, as discussed above. This experiment was repeated on Au substrates, and we observed a similar trend. The SPRi results on Au and eC/Au substrates are reported in Figure 5-9 and Table 5-2. The lower SPR specific signals of eC/Au substrates compared to Au counterparts are consistent with the 10% sensitivity loss induced by the 2 nm eC layer reported in Chapter 4. The eC/Au substrates give more reproducible signals, as evidenced from the smaller standard deviations reported in Table 5-2.

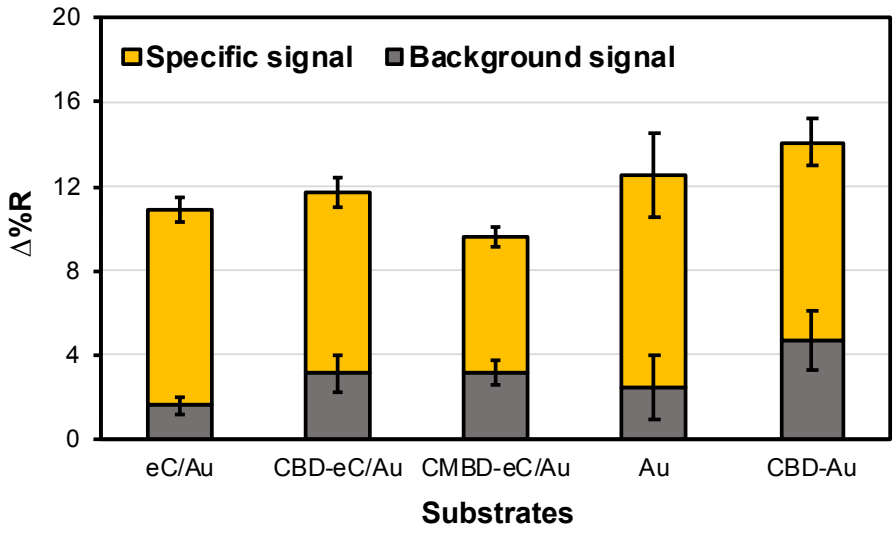

Figure 5-8. Δ%R of various SPRi substrates calculated from the sensorgrams in Figure 5-8. Error bars represent the standard deviation of the mean of at least two replicate substrates.

Table 5-2. SPRi Specific Δ%*R* Results

Surface	eC/Au	eC/Au-CBD	eC/Au-CMBD	Au	Au-CBD
Δ%*R* rIgG	9.3 ± 0.6	8.5 ± 0.7	6.5 ± 0.5	10 ± 2	9 ± 1

It is interesting to note that the background signal from the control BSA spots of diazonium modified substrates are higher than the unmodified substrates, which holds true for both Au and eC/Au substrates. This is consistent with the non-specific adsorption of BSA and Fib studied on eC/Au, CBD- and CMBD-modified eC/Au surfaces, as discussed above. Marquette et al.[28] suggested that CMBD electrografted to Au SPR substrates might act as a better antifouling coating than thiotic acid SAM. Similarly, Downard et al.[33] reported that an electrochemically modified glassy carbon electrode with CMBD is less prone to protein fouling than polished GC and that hydrophilic groups distanced from the surface by sufficiently long linkages could reduce protein adsorption. However, we did not observe the same antifouling effect in our study; this could be because the aryl layers resulting from spontaneous grafting are too thin, and the carboxylic groups are too close to the surface, so they did not reduce protein adsorption.

Biosensing demonstration. Protein A immobilization strategies were compared further in a proof-of-concept SPR immunoassay. The activity of the

immobilized antibody was determined by monitoring both the signal change for antibody capture and that due to antigen capture using SPRi. Using the same protocols described above, four spots of the eC/Au substrate were spotted with CBD and, subsequently, with EDC/NHS and protein A by manual pipetting (covalent attachment); another four spots were spotted with protein A (physical adsorption), and one unmodified spot served as a control (BSA), all on the same SPRi chip (Figure 5-10A). Goat anti-rabbit IgG at a concentration of 1300 nM was introduced to the surface; this concentration was shown to saturate the protein A layer.[27] Then, the antibody-modified surface was exposed to different concentrations of rabbit IgG solutions (from 5 to 1300 nM).

Similar amounts of goat anti-rabbit IgG were captured by protein A immobilized by either method, as evident from the representative sensorgram shown in Figure 5-10B. However, the covalent attachment is more efficient at capturing antigen from solution, resulting in higher signal for the immunoassay. The binding ratio, which is the ratio of signal changes for antibody capture and antigen capture, is commonly used as a measure of the activity of the antibody layer.[44–46] A higher ratio means more F_{ab} fragments are accessible for binding.[44] A ratio of ~2 was calculated for both attachment chemistries, which is in line with previously reported value.[27] The immobilized protein A preserves its affinity towards the antibody for both covalent and physical approaches.

The antigen binding curves are presented in Figure 5-10C, in which the antigen response has been corrected for non-specific binding and bulk refractive index change using the BSA control spot. The dashed lines in the plot were the fit obtained from least squares analysis with four parameter logistical model (equation 1) with the fitting parameters presented in Table 5-3. Equation 1 is often used to analyse antigen binding curves for immunoassays.[47]

$$\Delta\%R = \Delta\%R_{\min} + \frac{\Delta\%R_{\max} - \Delta\%R_{\min}}{1 + \left(\frac{[A]}{K_{\mathrm{d}}}\right)^{b}} \quad (1)$$

where $\Delta\%R_{\min}$ and $\Delta\%R_{\max}$ are asymptotic values obtained from the regression analysis, $[A]$ is the concentration of antibody in solution, K_D is the dissociation

constant, and *b* is the Hill coefficient that represents the slope of the curve at the inflection point. A Hill coefficient of -2 is expected for binding of a 2-site antibody.[48]

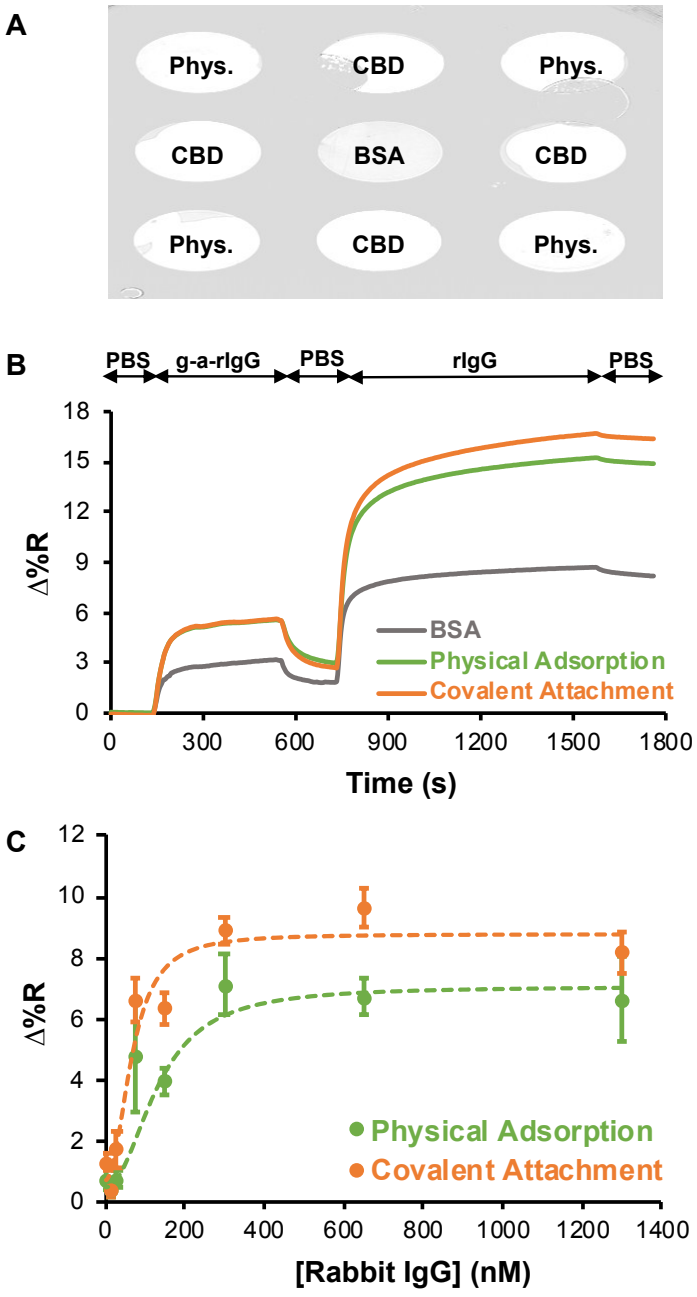

Figure 5-9. (A) Representative difference image of eC/Au SPR chip after injection of 1300 nM goat anti-rabbit IgG (g-a-rIgG), followed by 75 nM rabbit IgG (rIgG). (B) Representative sensorgram of eC/Au chip after injection of 1300 nM goat anti-rabbit IgG, followed by 1300 nM rabbit IgG. (C) Rabbit IgG binding curves obtained using different protein A immobilization chemistries. Error bars represent the standard deviation of the mean for replicate spots on a single chip.

Table 5-3. Curve Fitting Parameters for Antigen Binding Curves Obtained on Antibody Modified Surfaces

Antibody Attachment	R^2	K_{ADS} (M^{-1})	$\Delta\%R_{min}$	$\Delta\%R_{max}$	b
Physical Adsorption	0.98	8×10^6	0.5	7	-2
Covalent Attachment	0.96	1×10^7	0.7	9	-2

The strength of antigen binding ($K_{ADS} = 1/K_D$) to the antibody surfaces was found to be similar for both attachment chemistries (Table 5-3), and also in good agreement with those previously reported for surface-based measurements of binding affinity.[7,27] The results presented here indicate that covalent attachment using spontaneous adsorption of diazonium salts retains biological activities of the biomolecules and allows for sensitive detection. The selective patterning of closely spaced microspots also was demonstrated with spontaneous grafting of diazonium salts. This should open the door to selective patterning of the SPRi chips with diverse functional chemical groups and biomolecules of interest, similar to what has been achieved with electroaddressable deposition of aryl diazonium salts and diazonium-biomolecule conjugates on electrodes by Brozik and co-workers.[49–51]

5.4 Conclusion

Good SPR specific signal, regeneration potentialities, preserved biological activity of immobilized protein A, and favorable orientation of captured antibody together suggest that spontaneous grafting of aryl diazonium salts is a potential candidate for facile immobilization of biomolecules on SPRi substrates. The thick multilayers produced from electrografting of diazonium salts might decrease sensitivity in SPR measurements, and close to monolayers were found to be ideal for immunoassay performance.[27,29,34] Spontaneous grafting of diazonium salts is a simple strategy to produce monolayers. It also allows for selective patterning of the sensing surface and bulk manufacture of devices. Based on the good demonstration results presented here and the inherent stability of the covalent aryl-surface bonds, spontaneous adsorption of diazonium salts is a potential complement to the prevalent Au-SAM approach in the development of sensitive, stable SPR biosensors.

References

(1) Homola, J. Present and Future of Surface Plasmon Resonance Biosensors. *Anal. Bioanal. Chem.* **2003**, *377* (3), 528–539. https://doi.org/10.1007/s00216-003-2101-0.

(2) Rich, R. L.; Myszka, D. G. Survey of the 1999 Surface Plasmon Resonance Biosensor Literature. *J Mol Recognit* **2000**, 20.

(3) Homola, J. Surface Plasmon Resonance Sensors for Detection of Chemical and Biological Species. *Chem. Rev.* **2008**, *108* (2), 462–493. https://doi.org/10.1021/cr068107d.

(4) Rothenhiiusler, B.; Knollt, W. Surface-Plasmon Microscopy. **1988**, *332*, 615–617.

(5) Jordan, C. E.; Frutos, A. G.; Thiel, A. J.; Corn, R. M. Surface Plasmon Resonance Imaging Measurements of DNA Hybridization Adsorption and Streptavidin/DNA Multilayer Formation at Chemically Modified Gold Surfaces. *Anal. Chem.* **1997**, *69* (24), 4939–4947. https://doi.org/10.1021/ac9709763.

(6) Smith, E. A.; Thomas, W. D.; Kiessling, L. L.; Corn, R. M. Surface Plasmon Resonance Imaging Studies of Protein-Carbohydrate Interactions. *J. Am. Chem. Soc.* **2003**, *125* (20), 6140–6148. https://doi.org/10.1021/ja034165u.

(7) Kanda, V.; Kariuki, J. K.; Harrison, D. J.; McDermott, M. T. Label-Free Reading of Microarray-Based Immunoassays with Surface Plasmon Resonance Imaging. *Anal. Chem.* **2004**, *76* (24), 7257–7262. https://doi.org/10.1021/ac049318q.

(8) Shumaker-Parry, J. S.; Zareie, M. H.; Aebersold, R.; Campbell, C. T. Microspotting Streptavidin and Double-Stranded DNA Arrays on Gold for High-Throughput Studies of Protein−DNA Interactions by Surface Plasmon Resonance Microscopy. *Anal. Chem.* **2004**, *76* (4), 918–929. https://doi.org/10.1021/ac034964v.

(9) Lyon, L. A.; Musick, M. D.; Smith, P. C.; Reiss, B. D.; Peña, D. J.; Natan, M. J. Surface Plasmon Resonance of Colloidal Au-Modified Gold Films. *Sens. Actuators B Chem.* **1999**, *54* (1–2), 118–124. https://doi.org/10.1016/S0925-4005(98)00329-3.

(10) Wilkop, T.; Wang, Z.; Cheng, Q. Analysis of μ-Contact Printed Protein Patterns by SPR Imaging with a LED Light Source. *Langmuir* **2004**, *20* (25), 11141–11148. https://doi.org/10.1021/la048177k.

(11) Johnsson, B.; Löfås, S.; Lindquist, G. Immobilization of Proteins to a Carboxymethyldextran-Modified Gold Surface for Biospecific Interaction Analysis in Surface Plasmon Resonance Sensors. *Anal. Biochem.* **1991**, *198* (2), 268–277. https://doi.org/10.1016/0003-2697(91)90424-R.

(12) Hetemi, D.; Noël, V.; Pinson, J. Grafting of Diazonium Salts on Surfaces: Application to Biosensors. *Biosensors* **2020**, *10* (1), 4. https://doi.org/10.3390/bios10010004.

(13) Paloma Yáñez-Sedeño; Susana Campuzano; José Pingarrón. Integrated Affinity Biosensing Platforms on Screen-Printed Electrodes Electrografted

with Diazonium Salts. *Sensors* **2018**, *18* (3), 675. https://doi.org/10.3390/s18020675.

(14) Schreiber, A.; Feldbrügge, R.; Key, G.; Glatz, J. F. C.; Spener, F. An Immunosensor Based on Disposable Electrodes for Rapid Estimation of Fatty Acid-Binding Protein, an Early Marker of Myocardial Infarction. *Biosens. Bioelectron.* **1997**, *12* (11), 1131–1137. https://doi.org/10.1016/S0956-5663(97)00003-1.

(15) Hayat, A.; Barthelmebs, L.; Sassolas, A.; Marty, J.-L. An Electrochemical Immunosensor Based on Covalent Immobilization of Okadaic Acid onto Screen Printed Carbon Electrode via Diazotization-Coupling Reaction. *Talanta* **2011**, *85* (1), 513–518. https://doi.org/10.1016/j.talanta.2011.04.034.

(16) Jung, L. S.; Nelson, K. E.; Stayton, P. S.; Campbell, C. T. Binding and Dissociation Kinetics of Wild-Type and Mutant Streptavidins on Mixed Biotin-Containing Alkylthiolate Monolayers. *Langmuir* **2000**, *16* (24), 9421–9432. https://doi.org/10.1021/la000144r.

(17) Nelson, K. E.; Gamble, L.; Jung, L. S.; Boeckl, M. S.; Naeemi, E.; Golledge, S. L.; Sasaki, T.; Castner, D. G.; Campbell, C. T.; Stayton, P. S. Surface Characterization of Mixed Self-Assembled Monolayers Designed for Streptavidin Immobilization. *Langmuir* **2001**, *17* (9), 2807–2816. https://doi.org/10.1021/la001111e.

(18) Johnson, C. P.; Jensen, I. E.; Prakasam, A.; Vijayendran, R.; Leckband, D. Engineered Protein A for the Orientational Control of Immobilized Proteins. *Bioconjug. Chem.* **2003**, *14* (5), 974–978. https://doi.org/10.1021/bc034063t.

(19) Gooding, J. J.; Ciampi, S. The Molecular Level Modification of Surfaces: From Self-Assembled Monolayers to Complex Molecular Assemblies. *Chem. Soc. Rev.* **2011**, *40* (5), 2704. https://doi.org/10.1039/c0cs00139b.

(20) Hutt, D. A.; Leggett, G. J. Influence of Adsorbate Ordering on Rates of UV Photooxidation of Self-Assembled Monolayers. *J. Phys. Chem.* **1996**, *100* (16), 6657–6662. https://doi.org/10.1021/jp952734h.

(21) Cooper, E.; Leggett, G. J. Static Secondary Ion Mass Spectrometry Studies of Self-Assembled Monolayers: Influence of Adsorbate Chain Length and Terminal Functional Group on Rates of Photooxidation of Alkanethiols on Gold. *Langmuir* **1998**, *14* (17), 4795–4801. https://doi.org/10.1021/la9802567.

(22) Wong, S.-S.; Porter, M. D. Origin of the Multiple Voltammetric Desorption Waves of Long-Chain Alkanethiolate Monolayers Chemisorbed on Annealed Gold Electrodes. *J. Electroanal. Chem.* **2000**, *485* (2), 135–143. https://doi.org/10.1016/S0022-0728(00)00106-6.

(23) English, R. D.; Van Stipdonk, M. J.; Sabapathy, R. C.; Crooks, R. M.; Schweikert, E. A. Characterization of Photooxidized Self-Assembled Monolayers and Bilayers by Spontaneous Desorption Mass Spectrometry. *Anal. Chem.* **2000**, *72* (24), 5973–5980. https://doi.org/10.1021/ac0008892.

(24) Shewchuk, D. M.; McDermott, M. T. Comparison of Diazonium Salt Derived and Thiol Derived Nitrobenzene Layers on Gold. *Langmuir* **2009**, *25* (8), 4556–4563. https://doi.org/10.1021/la8040083.

(25) Corgier, B. P.; Bellon, S.; Anger-Leroy, M.; Blum, L. J.; Marquette, C. A. Protein−Diazonium Adduct Direct Electrografting onto SPRi-Biochip. *Langmuir* **2009**, *25* (16), 9619–9623. https://doi.org/10.1021/la900762s.

(26) Gooding, J. J. Advances in Interfacial Design for Electrochemical Biosensors and Sensors: Aryl Diazonium Salts for Modifying Carbon and Metal Electrodes. *Electroanalysis* **2008**, *20* (6), 573–582. https://doi.org/10.1002/elan.200704124.

(27) Grant, C. F. Development and Characterization of Interfacial Chemistry for Biomolecule Immobilization in Surface Plasmon Resonance Imaging Studies. PhD Thesis, University of Alberta, Edmonton, Alberta, 2009.

(28) Mandon, C. A.; Blum, L. J.; Marquette, C. A. Aryl Diazonium for Biomolecules Immobilization onto SPRi Chips. *ChemPhysChem* **2009**, *10* (18), 3273–3277. https://doi.org/10.1002/cphc.200900599.

(29) Fioresi, F.; Rouleau, A.; Maximova, K.; Vieillard, J.; Boireau, W.; Caille, C. E.; Soulignac, C.; Zeggari, R.; Clamens, T.; Lesouhaitier, O.; Mofaddel, N.; Derf, F. L. Electrografting of Diazonium Salt for SPR Application. *Mater. Today Proc.* **2019**, *6*, 340–344. https://doi.org/10.1016/j.matpr.2018.10.428.

(30) Solak, A. O.; Eichorst, L. R.; Clark, W. J.; McCreery, R. L. Modified Carbon Surfaces as "Organic Electrodes" That Exhibit Conductance Switching. *Anal. Chem.* **2003**, *75* (2), 296–305. https://doi.org/10.1021/ac026107h.

(31) Anariba, F.; DuVall, S. H.; McCreery, R. L. Mono- and Multilayer Formation by Diazonium Reduction on Carbon Surfaces Monitored with Atomic Force Microscopy "Scratching." *Anal. Chem.* **2003**, *75* (15), 3837–3844. https://doi.org/10.1021/ac034026v.

(32) Lockett, M. R.; Smith, L. M. Fabrication and Characterization of DNA Arrays Prepared on Carbon-on-Metal Substrates. *Anal. Chem.* **2009**, *81* (15), 6429–6437. https://doi.org/10.1021/ac900807q.

(33) Downard, A. J.; Roddick, A. D. Protein Adsorption at Glassy Carbon Electrodes: The Effect of Covalently Bound Surface Groups. *Electroanalysis* **1995**, *7* (4), 376–378. https://doi.org/10.1002/elan.1140070414.

(34) Toman, J. T. Electrografted Thick Diazonium Derived Films for Biosensing Applications. MSc thesis, University of Alberta, Edmonton, Alberta, 2013.

(35) Bourdillon, C.; Delamar, M.; Demaille, C.; Hitmi, R.; Moiroux, J.; Pinson, J. Immobilization of Glucose Oxidase on a Carbon Surface Derivatized by Electrochemical Reduction of Diazonium Salts. *J. Electroanal. Chem.* **1992**, *336* (1–2), 113–123. https://doi.org/10.1016/0022-0728(92)80266-7.

(36) Barrière, F.; Downard, A. J. Covalent Modification of Graphitic Carbon Substrates by Non-Electrochemical Methods. *J. Solid State Electrochem.* **2008**, *12* (10), 1231–1244. https://doi.org/10.1007/s10008-008-0526-2.

(37) Díaz, J.; Paolicelli, G.; Ferrer, S.; Comin, F. Separation of the Sp 3 and Sp 2 Components in the C1 *s* Photoemission Spectra of Amorphous Carbon Films. *Phys. Rev. B* **1996**, *54* (11), 8064–8069. https://doi.org/10.1103/PhysRevB.54.8064.

(38) Allongue, P.; Delamar, M.; Desbat, B.; Fagebaume, O.; Hitmi, R.; Pinson, J.; Savéant, J.-M. Covalent Modification of Carbon Surfaces by Aryl Radicals

Generated from the Electrochemical Reduction of Diazonium Salts. *J. Am. Chem. Soc.* **1997**, *119* (1), 201–207. https://doi.org/10.1021/ja963354s.

(39) Silin, V.; Weetall, H.; Vanderah, D. SPR Studies of the Non-Specific Adsorption Kinetics of Human IgG and BSA on Gold Surfaces Modified by Self-Assembled Monolayers (SAMs). *J. Colloid Interface Sci.* **1997**, *185*, 94–103.

(40) Martins, M. C. L.; Fonseca, C.; Barbosa, M. A.; Ratner, B. D. Albumin Adsorption on Alkanethiols Self-Assembled Monolayers on Gold Electrodes Studied by Chronopotentiometry. *Biomaterials* **2003**, *24* (21), 3697–3706. https://doi.org/10.1016/S0142-9612(03)00244-8.

(41) Tidwell, C. D.; Ertel, S. I.; Ratner, B. D.; Tarasevich, B. J.; Atre, S.; Allara, D. L. Endothelial Cell Growth and Protein Adsorption on Terminally Functionalized, Self-Assembled Monolayers of Alkanethiolates on Gold. *Langmuir* **1997**, *13* (13), 3404–3413. https://doi.org/10.1021/la9604341.

(42) Lopez, G. P.; Albers, M. W.; Schrieber, S. L.; Carroll, R.; Peralta, E.; Whitesides, G. M. Convenient Methods for Patterning the Adhesion of Mammalian Cells to Surfaces Using Self-Assembled Monolayers of Alkanethiolates on Gold. **1993**, *115*, 5877–5878.

(43) Sigal, G. B.; Mrksich, M.; Whitesides, G. M. Effect of Surface Wettability on the Adsorption of Proteins and Detergents. *J. Am. Chem. Soc.* **1998**, *120*, 3464–3473.

(44) Chen, S.; Liu, L.; Zhou, J.; Jiang, S. Controlling Antibody Orientation on Charged Self-Assembled Monolayers. *Langmuir* **2003**, *19* (7), 2859–2864. https://doi.org/10.1021/la026498v.

(45) Buijs, J.; White, D. D.; Norde, W. The Effect of Adsorption on the Antigen Binding by IgG and Its F(Ab′)2 Fragments. *Colloids Surf. B Biointerfaces* **1997**, *8*, 239–249. https://doi.org/10.1016/S0927-7765(96)01327-6.

(46) Caruso, F.; Rodda, E.; Furlong, D. N. Orientational Aspects of Antibody Immobilization and Immunological Activity on Quartz Crystal Microbalance Electrodes. *J. Colloid Interface Sci.* **1996**, *178* (1), 104–115. https://doi.org/10.1006/jcis.1996.0098.

(47) Rodbard, D.; Hutt, D. M. *Radioimmunoassay and Related Procedures in Medicine*; IAEA: Vienna, 1974; Vol. 1.

(48) Danson, R. E. a. M. J. *Enzyme Assays: A Practical Approach*, 2nd ed.; New York, 1993.

(49) Harper, J. C.; Polsky, R.; Wheeler, D. R.; Dirk, S. M.; Brozik, S. M. Selective Immobilization of DNA and Antibody Probes on Electrode Arrays: Simultaneous Electrochemical Detection of DNA and Protein on a Single Platform. *Langmuir* **2007**, *23* (16), 8285–8287. https://doi.org/10.1021/la701775g.

(50) Polsky, R.; Harper, J. C.; Wheeler, D. R.; Brozik, S. M. Multifunctional Electrode Arrays: Towards a Universal Detection Platform. *Electroanalysis* **2008**, *20* (6), 671–679. https://doi.org/10.1002/elan.200704129.

(51) Polsky, R.; Harper, J. C.; Wheeler, D. R.; Dirk, S. M.; Arango, D. C.; Brozik, S. M. Electrically Addressable Diazonium-Functionalized Antibodies for

Multianalyte Electrochemical Sensor Applications. *Biosens. Bioelectron.* **2008**, *23* (6), 757–764. https://doi.org/10.1016/j.bios.2007.08.013.

Chapter 6. Conclusions and Future Directions

6.1 Conclusions

SPR-based biosensing is among the most advanced label-free, real-time sensing technologies. Thin gold substrates and alkanethiol self-assembled monolayers are used widely in SPR-based biosensors, but they are limited in terms of sensitivity and long-term stability. The motivation behind the work in this thesis was to explore novel lamellar structures and surface functionalization strategies to improve the performance of SPR-based biosensors. This thesis demonstrates that a combination of carbon-on-metal films and spontaneously grafted diazonium layers can be a potential alternative to Au-thiolate SAMs for SPR sensing.

Chapter 2 reports thorough characterization of carbon-on-gold films prepared by electron-beam evaporation. Carbon deposited on gold films yield a very flat surface (0.72 nm root-mean-square roughness), with roughly 40% sp^3-hybridized amorphous carbon and O/C ratio of about 6%. These films also exhibit comparable electron-transfer kinetics of common redox systems in comparison with glassy carbon electrodes. Interestingly, carbon-on-gold films show insignificant adsorption of quinones, which is uncommonly observed with carbon materials. These results are helpful in guiding and understanding subsequent surface modification of these films, particularly by electrografting. In addition, with reproducible fast electron kinetics, low background current, negligible adsorption, and patternable flat surface, carbon-on-gold films are an attractive candidate for the development of electrochemical and electrochemical-SPR biosensors.

Chapter 3 explores the fundamentals of modifying carbon-on-gold films by spontaneous grafting of aryldiazonium salts. Deposition conditions, including immersion time, solvent, aryldiazonium salt concentration, and para-substituent, were optimized for eC/Au substrates. The spontaneously grafted aryl layers have similar structure to those electrochemically grafted. Homogenous, compact, and close to monolayers were formed by the spontaneous grafting strategy, and the thicknesses of the resulting layers were found to correlate with the electron withdrawing abilities of the para-substituents. Spontaneous grafting of aryl diazonium salts offers a fast,

simple method for functionalization of carbon-based materials. A detail examination of this surface chemistry sets the stage for its application in interfacial design for carbon-based SPR, electrochemical biosensors, and more.

Chapter 4 shows that carbon-on-metal films are viable as SPR substrates. We were able to deposit defect-free, well-adhered, and very thin eC coatings on gold and silver substrates, leading to minimal sensitivity loss for eC/Au films and enhanced sensitivity for eC/Ag films relative to gold counterparts. Non-specific adsorption of proteins on carbon-on-gold films also were investigated to prepare for applications of these substrates in complex biological fluid samples. The results show that common plasma proteins adsorb irreversibly at eC/Au, similar to that observed at Au and sputtered amorphous carbon surfaces. The low reactivity of eC/Au towards quinones in Chapter 2 did not translate to proteins here. This chapter paves the way for future studies on the development of carbon-based bioassays as well as novel non-fouling surface chemistry to minimize non-specific adsorption of proteins in real samples.

Chapter 5 develops a proof-of-concept SPR-based immunoassay utilizing carbon-on-gold films as substrates and spontaneous grafting of aryldiazonium salts to immobilize biomolecules. The grafted aryl layers were characterized, and close to monolayers of carboxy-bearing layers were obtained. The performance of the aryl layers to immobilize protein A covalently and the subsequent antibody capture was compared with physically adsorbed protein A. Covalent attachment using the spontaneous grafting strategy exhibits good SPR specific signal, regeneration potentialities, preserved biological activity of immobilized protein A, and favorable orientation of captured antibody. The ability to selectively pattern closely spaced microspots on the SPRi substrate also was demonstrated. This chapter shows the feasibility of spontaneous grafting of aryl diazonium salts for facile, spatially controlled immobilization of biomolecules on SPRi substrates. Based on the good demonstration results presented in this chapter and the inherent stability of the covalent aryl–surface bonds, spontaneous adsorption of diazonium salts can be a potential complement to the prevalent Au-SAM chemistry in the development of sensitive, stable SPR biosensors.

6.2 Future Directions

6.2.1 Carbon-on-Silver Films as SPR Substrates

The race towards higher sensitivity of SPR materials is continuing. In Chapter 4, we have shown that carbon films were deposited significantly thinner, defect-free, and well-adhered, resulting in minimal sensitivity loss of eC/Au substrates in comparison with previous reports. Carbon-on-silver films exhibit enhanced sensitivity relative to bare Au substrates. This result is promising for promoting the use of eC/Ag substrates in SPR sensing, as eC coating can protect the easily oxidizable silver while allowing for the use of various functionalization strategies to overcome the unstable metal–thiol bond. It is worth noting that the sensitivity of eC/Ag substrates is likely higher than reported here, as our SPRi instrumentation is not optimal for the resonance of Ag films. Further optimization of eC and Ag thicknesses and measurement conditions for eC/Au substrates are expected to result in even higher sensitivity. The work presented in this thesis on eC/Au films can serve as a guide for a thorough characterization and optimization of eC/Au films as SPR substrates.

6.2.2 Mix Layers with Spontaneous Grafting of Aryldiazonium Salts

The formation of mixed SAMs layers enables control over the density of surface attached biorecognition element[1] and provides multi-function surface layers (for example, immobilizing biorecognition elements and minimizing non-specific binding at the same time[2,3]). Formation of mixed layers of aryl diazonium salts via electrografting was reported first by Dequaire and co-workers in 2003[4] and still is a nascent field.[5] Knowledge and control over the resulting surface composition are limited, and applications of the mixed layers have not been reported extensively.[6] The level of sophistication that has been reached with mixed layers of thiolate SAMs has not been attained with aryldiazonium electrochemistry.[5,7] Formation of a mixed layer of aryl diazonium salts via spontaneous grafting remains completely unexplored. Surface functionalization with spontaneous adsorption of diazonium salts is an obvious topic for continuing investigation, especially layers with an anti-fouling property. Chapters 4 and 5 show that non-specific adsorption of proteins can be quite

significant in SPR measurements using eC/Au substrates. Carbon-on-metal films as SPR substrates are only at the proof-of-principle stage. Demonstrations of these substrates in complex biological fluids might be possible in the future with mixed layers capable of performing multiple functions, i.e., a mixture of bio-recognition immobilizing and antifouling components.

6.2.3 Carbon-on-Metal Films as a Versatile Analytical Platform

An interesting aspect of SPR is the possibility to couple it with complementary analytical techniques, making SPR more useful, with an unprecedented power of analysis. Combining SPR with other techniques has become more popular over the last decade and has been reviewed in some detail.[8] The hyphenation approaches include measurements of different physical phenomena using the same instrument and sequential measurements of the same sample using different instruments. The first approach can achieve a higher sensitivity and/or resolution.[8] For example, combining SPR and surface-enhanced Raman spectroscopy (SERS) leads to a 10^6 signal enhancement for single molecule detection.[9] The second approach can speed up and complement bioanalysis procedures.[8] An example is SPR hyphenated with mass spectrometry, enabling the rapid study of both the function and the structure of the molecules.[10] Electrochemical SPR instrumentation is already commercially available (Biosensing Instrument, Inc). These hyphenation approaches have been reported mostly on gold SPR substrates.

In this thesis, I have demonstrated the promising analytical performance of eC/Au as both electrode materials and SPR substrates. Preliminary results suggest eC/Au also can act as SERS substrates by exploiting plasmonic coupling with metal nanoparticles. In one experiment, Dr. Casey Rusin and I electrodeposited Au nanoparticles from a solution of $HAuCl_4$ onto polished GC, Si/Au (42 nm), and Si/Au (42 nm)/eC (10 nm) electrodes by chronoamperometry. Then, the electrodes were immersed in a solution of 4-mercaptobenzonitrile (MBN), a common Raman probe overnight. Figure 6-1 contains SERS spectra of MBN on these modified electrodes. The Au electrode shows no spectral features, and the GC electrode shows the characteristic D and G bands of disordered carbon materials.[11] Only eC/Au electrodes

show Raman bands that are characteristic of MBN. The band assignments for MBN are presented in Table 6-1.[12–14]

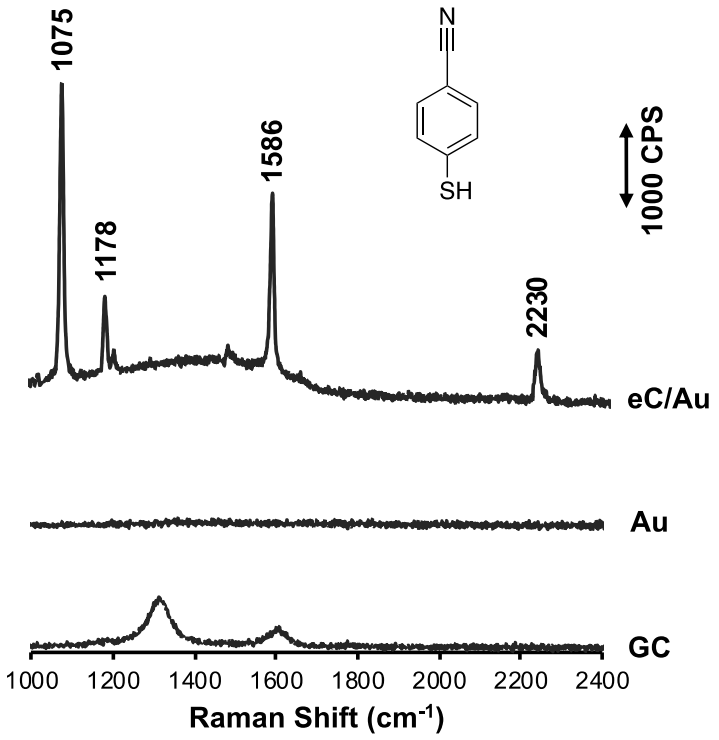

Figure 6-1. SERS spectra of MBN on eC/Au, Au, and GC substrates decorated with electrodeposited gold nanoparticles. The spectra were collected with Dr. Casey Rusin using a Renishaw inVia Raman Microscope. The setting was 785 nm laser, 0.1% power, and 10 s.

Table 6-1. Major Band Assignments Listed for the SERS spectrum of MBN

Band position (cm^{-1})	Band assignment[12–14]
1075	C–S and C–C stretch
1178	C–H bend and C–C stretch
1585	C–C stretch
2230	C≡N stretch

In another experiment, I modified Si/Au (42 nm)/eC (10 nm) substrates with chemically synthesized silver nanoparticles. First, eC/Au substrates were grafted spontaneously with 4-carboxybenzene diazonium salt. Then, using a procedure recently published by our group,[15] the substrates were immersed in a solution of $AgNO_3$, followed by mixing with ascorbic acid solution under heating and stirring conditions to synthesize silver nanoparticles. The 4-carboxyphenyl layers likely can help with preconcentrating of Ag^+ ions on the surface. A SERS spectrum (Figure 6-2)

was collected after the substrates were immersed in a MBN solution overnight. Again, four characteristic Raman bands of MBN were observed (Table 6-1).

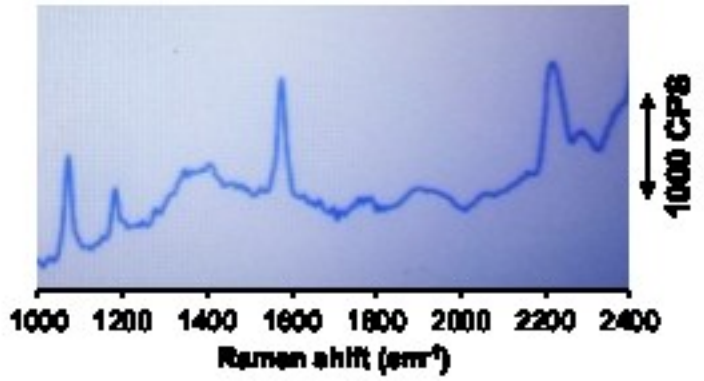

Figure 6-2. SERS spectrum of MBN on eC/Au substrates modified with chemically synthesized silver nanoparticles. The spectrum was collected with a B&W Tek TacticID handheld Raman device with 785 nm laser (spot size 100 μm). The handheld device was standardized using a polystyrene standard before data collection.

These preliminary results suggest that carbon-on-metal films can be useful in fundamental studies of plasmonic coupling effects between nanoparticles and substrates supporting propagating surface plasmons due to the tuneable thicknesses of the deposited layers. This will permit different combinations of metal nanoparticles and SPR supporting layers to be investigated, while different eC thicknesses can act as spacing layers. Additionally, nanoparticles are useful labels/signal amplifiers in electrochemistry and SPR. Combining carbon-on-metal substrates with nanoparticles (and surface chemistry) can allow for myriad nanostructures to be constructed and the use of SPR, electrochemistry, and SERS techniques in any combination or sequence. This will open new opportunities for the developments of new sensing interfaces with analysis power never seen before.

References

(1) Gooding, J. J.; Mearns, F.; Yang, W.; Liu, J. Self-Assembled Monolayers into the 21st Century: Recent Advances and Applications. Electroanalysis **2003**, 15 (2), 81–96. https://doi.org/10.1002/elan.200390017.

(2) Jung, L. S.; Nelson, K. E.; Stayton, P. S.; Campbell, C. T. Binding and Dissociation Kinetics of Wild-Type and Mutant Streptavidins on Mixed Biotin-

Containing Alkylthiolate Monolayers. Langmuir **2000**, 16 (24), 9421–9432. https://doi.org/10.1021/la000144r.

(3) Nelson, K. E.; Gamble, L.; Jung, L. S.; Boeckl, M. S.; Naeemi, E.; Golledge, S. L.; Sasaki, T.; Castner, D. G.; Campbell, C. T.; Stayton, P. S. Surface Characterization of Mixed Self-Assembled Monolayers Designed for Streptavidin Immobilization. Langmuir **2001**, 17 (9), 2807–2816. https://doi.org/10.1021/la001111e.

(4) Ruffien, A.; Dequaire, M.; Brossier, P. Covalent Immobilization of Oligonucleotides on P-Aminophenyl-Modified Carbon Screen-Printed Electrodes for Viral DNA Sensing. Chem. Commun. **2003**, No. 7, 912–913. https://doi.org/10.1039/b300439b.

(5) Jiang, C.; Moraes Silva, S.; Fan, S.; Wu, Y.; Alam, M. T.; Liu, G.; Justin Gooding, J. Aryldiazonium Salt Derived Mixed Organic Layers: From Surface Chemistry to Their Applications. J. Electroanal. Chem. **2017**, 785, 265–278. https://doi.org/10.1016/j.jelechem.2016.11.043.

(6) Gooding, J. J. Advances in Interfacial Design for Electrochemical Biosensors and Sensors: Aryl Diazonium Salts for Modifying Carbon and Metal Electrodes. Electroanalysis **2008**, 20 (6), 573–582. https://doi.org/10.1002/elan.200704124.

(7) Gooding, J. J.; Ciampi, S. The Molecular Level Modification of Surfaces: From Self-Assembled Monolayers to Complex Molecular Assemblies. Chem. Soc. Rev. **2011**, 40 (5), 2704. https://doi.org/10.1039/c0cs00139b.

(8) Abbas, A.; Linman, M. J.; Cheng, Q. New Trends in Instrumental Design for Surface Plasmon Resonance-Based Biosensors. Biosens. Bioelectron. **2011**, 26 (5), 1815–1824. https://doi.org/10.1016/j.bios.2010.09.030.

(9) Nie, S.; Emory, S. R. Probing Single Molecules and Single Nanoparticles by Surface-Enhanced Raman Scattering. **1997**, 275 (5303), 1102–1106.

(10) Nelson, R. W.; Krone, J. R.; Jansson, O. Surface Plasmon Resonance Biomolecular Interaction Analysis Mass Spectrometry. 2. Fiber Optic-Based Analysis. Anal. Chem. **1997**, 69 (21), 4369–4374. https://doi.org/10.1021/ac9705374.

(11) Wang, Y.; Alsmeyer, D. C.; McCreery, R. L. Raman Spectroscopy of Carbon Materials: Structural Basis of Observed Spectra. Chem. Mater. **1990**, 2 (5), 557–563. https://doi.org/10.1021/cm00011a018.

(12) Gkogkou, D.; Schreiber, B.; Shaykhutdinov, T.; Ly, H. K.; Kuhlmann, U.; Gernert, U.; Facsko, S.; Hildebrandt, P.; Esser, N.; Hinrichs, K.; Weidinger, I. M.; Oates, T. W. H. Polarization- and Wavelength-Dependent Surface-Enhanced Raman Spectroscopy Using Optically Anisotropic Rippled Substrates for Sensing. ACS Sens. **2016**, 1 (3), 318–323. https://doi.org/10.1021/acssensors.5b00176.

(13) Holze, R. Competition of Anchoring Groups in Adsorption on Gold Electrodes—a Comparative Spectroelectrochemical Study of 4-Mercaptobenzonitrile and Aromatic Nitriles. J. Solid State Electrochem. **2013**, 17 (7), 1869–1879. https://doi.org/10.1007/s10008-013-2076-5.

(14) Villarreal, E.; Li, G. G.; Zhang, Q.; Fu, X.; Wang, H. Nanoscale Surface Curvature Effects on Ligand–Nanoparticle Interactions: A Plasmon-Enhanced

Spectroscopic Study of Thiolated Ligand Adsorption, Desorption, and Exchange on Gold Nanoparticles. Nano Lett. **2017**, 17 (7), 4443–4452. https://doi.org/10.1021/acs.nanolett.7b01593.

(15) Rusin, C. J.; El Bakkari, M.; Du, R.; Boluk, Y.; McDermott, M. T. Plasmonic Cellulose Nanofibers as Water-Dispersible Surface-Enhanced Raman Scattering Substrates. ACS Appl. Nano Mater. **2020**, 3 (7), 6584–6597. https://doi.org/10.1021/acsanm.0c01045.

Bibliography (alphabetical by first author)

Abbas, A., Linman, M. J., & Cheng, Q. (2011). New trends in instrumental design for surface plasmon resonance-based biosensors. *Biosens. Bioelectron.*, *26*(5), 1815–1824. https://doi.org/10.1016/j.bios.2010.09.030

Adenier, A., Barré, N., Cabet-Deliry, E., Chaussé, A., Griveau, S., Mercier, F., Pinson, J., & Vautrin-Ul, C. (2006). Study of the spontaneous formation of organic layers on carbon and metal surfaces from diazonium salts. *Surface Science*, *600*(21), 4801–4812. https://doi.org/10.1016/j.susc.2006.07.061

Adenier, A., Cabet-Deliry, E., Chaussé, A., Griveau, S., Mercier, F., Pinson, J., & Vautrin-Ul, C. (2005). Grafting of Nitrophenyl Groups on Carbon and Metallic Surfaces without Electrochemical Induction. *Chemistry of Materials*, *17*(3), 491–501. https://doi.org/10.1021/cm0490625

Adzic, R., Yeager, E., & Cahan, B. D. (1974). Optical and Electrochemical Studies of Underpotential Deposition of Lead on Gold Evaporated and Single-Crystal Electrodes. *Journal of The Electrochemical Society*, *121*(4), 474. https://doi.org/10.1149/1.2401841

Allongue, P., Delamar, M., Desbat, B., Fagebaume, O., Hitmi, R., Pinson, J., & Savéant, J.-M. (1997). Covalent Modification of Carbon Surfaces by Aryl Radicals Generated from the Electrochemical Reduction of Diazonium Salts. *Journal of the American Chemical Society*, *119*(1), 201–207. https://doi.org/10.1021/ja963354s

Anariba, F., DuVall, S. H., & McCreery, R. L. (2003). Mono- and Multilayer Formation by Diazonium Reduction on Carbon Surfaces Monitored with Atomic Force Microscopy "Scratching." *Analytical Chemistry*, *75*(15), 3837–3844. https://doi.org/10.1021/ac034026v

Anderson, J. L., & Winograd, N. (1996). Film Electrodes. In P. T. Kissinger & W. R. Heineman (Eds.), *Laboratory Techniques in Electroanalytical Chemistry* (2nd ed., pp. 333–366). Marcel Dekker.

Anderson, J. M., Ziats, N. P., Azeez, A., Brunstedt, M. R., Stack, S., & Bonfield, T. L. (1996). Protein adsorption and macrophage activation on polydimethylsiloxane and silicone rubber. *Journal of Biomaterials Science, Polymer Edition*, *7*(2), 159–169. https://doi.org/10.1163/156856295X00670

Andrade, D. (n.d.). *Plasma Protein Adsorption: The Big Twelvea*. 15.

Assresahegn, B. D., Brousse, T., & Bélanger, D. (2015). Advances on the use of diazonium chemistry for functionalization of materials used in energy storage systems. *Carbon*, *92*, 362–381. https://doi.org/10.1016/j.carbon.2015.05.030

Azzaroni, O., Vela, M. E., Fonticelli, M., Benítez, G., Carro, P., Blum, B., & Salvarezza, R. C. (2003). Electrodesorption Potentials of Self-Assembled Alkanethiolate Monolayers on Copper Electrodes. An Experimental and Theoretical Study. *The Journal of Physical Chemistry B*, *107*(48), 13446–13454. https://doi.org/10.1021/jp036319y

Bahr, J. L., & Tour, J. M. (2001). Highly Functionalized Carbon Nanotubes Using in Situ Generated Diazonium Compounds. *Chemistry of Materials*, *13*(11), 3823–3824. https://doi.org/10.1021/cm0109903

Bain, C. D., Troughton, E. B., Tao, Y. T., Evall, J., Whitesides, G. M., & Nuzzo, R. G. (1989). Formation of monolayer films by the spontaneous assembly of organic thiols from solution onto gold. *Journal of the American Chemical Society*, *111*(1), 321–335. https://doi.org/10.1021/ja00183a049

Barrière, F., & Downard, A. J. (2008). Covalent modification of graphitic carbon substrates by non-electrochemical methods. *Journal of Solid State Electrochemistry*, *12*(10), 1231–1244. https://doi.org/10.1007/s10008-008-0526-2

Bélanger, D., & Pinson, J. (2011). Electrografting: A powerful method for surface modification. *Chemical Society Reviews*, *40*(7), 3995. https://doi.org/10.1039/c0cs00149j

Benlahsen, M., Cachet, H., Charvet, S., Debiemme-Chouvy, C., Deslouis, C., Lagrini, A., & Vivier, V. (2005). Improvement and characterization of the electrochemical reactivity of amorphous carbon nitride electrodes. *Electrochemistry Communications*, *7*(5), 496–499. https://doi.org/10.1016/j.elecom.2005.03.003

Bertilsson, L., & Liedberg, B. (1993). Infrared study of thiol monolayer assemblies on gold: Preparation, characterization, and functionalization of mixed monolayers. *Langmuir*, *9*(1), 141–149. https://doi.org/10.1021/la00025a032

Besold, J., Thielsch, R., Matz, N., Frenzel, C., Born, R., & Möbius, A. (1997). Surface and bulk properties of electron beam evaporated carbon films. *Thin Solid Films*, *293*(1–2), 96–102. https://doi.org/10.1016/S0040-6090(96)09000-1

Bhatia, P., & Gupta, B. D. (2012). Fabrication and characterization of a surface plasmon resonance based fiber optic urea sensor for biomedical applications. *Sensors and Actuators B: Chemical*, *161*(1), 434–438. https://doi.org/10.1016/j.snb.2011.10.056

Blackstock, J. J., Rostami, A. A., Nowak, A. M., McCreery, R. L., Freeman, M. R., & McDermott, M. T. (2004). Ultraflat Carbon Film Electrodes Prepared by Electron Beam Evaporation. *Analytical Chemistry*, *76*(9), 2544–2552. https://doi.org/10.1021/ac035003j

Boozer, C., Kim, G., Cong, S., Guan, H., & Londergan, T. (2006). Looking towards label-free biomolecular interaction analysis in a high-throughput format: A review of new surface plasmon resonance technologies. *Current Opinion in Biotechnology*, *17*(4), 400–405. https://doi.org/10.1016/j.copbio.2006.06.012

Bourdillon, C., Delamar, M., Demaille, C., Hitmi, R., Moiroux, J., & Pinson, J. (1992). Immobilization of glucose oxidase on a carbon surface derivatized by electrochemical reduction of diazonium salts. *Journal of Electroanalytical Chemistry*, *336*(1–2), 113–123. https://doi.org/10.1016/0022-0728(92)80266-7

Brooksby, P. A., & Downard, A. J. (2004). Electrochemical and Atomic Force Microscopy Study of Carbon Surface Modification via Diazonium Reduction in Aqueous and Acetonitrile Solutions. *Langmuir*, *20*(12), 5038–5045. https://doi.org/10.1021/la049616i

Brown, A. P., & Anson, F. C. (1977). Cyclic and Differential Pulse Voltammetric Behavior of Reactants Confined to the Electrode Surface. *Analytical Chemistry*, *49*(11), 1589–1595. https://doi.org/10.1021/ac50019a033

Brown, A. P., Koval, C., & Anson, F. C. (1976). Illustrative Electrochemical Behavior of Reactants Irreversibly Adsorbed on Graphite Electrode Surfaces. *Journal of Electroanalytical Chemistry*, *72*, 379–387.

Buijs, J., White, D. D., & Norde, W. (1997). The effect of adsorption on the antigen binding by IgG and its F(ab′)2 fragments. *Colloids and Surfaces B: Biointerfaces*, *8*, 239–249. https://doi.org/10.1016/S0927-7765(96)01327-6

Cacciafesta, P., Humphris, A. D. L., Jandt, K. D., & Miles, M. J. (2000). Human Plasma Fibrinogen Adsorption on Ultraflat Titanium Oxide Surfaces Studied with Atomic Force Microscopy. *Langmuir*, *16*(21), 8167–8175. https://doi.org/10.1021/la000362k

Caruso, F., Rodda, E., & Furlong, D. N. (1996). Orientational Aspects of Antibody Immobilization and Immunological Activity on Quartz Crystal Microbalance Electrodes. *Journal of Colloid and Interface Science*, *178*(1), 104–115. https://doi.org/10.1006/jcis.1996.0098

Ceccato, M., Bousquet, A., Hinge, M., Pedersen, S. U., & Daasbjerg, K. (2011). Using a Mediating Effect in the Electroreduction of Aryldiazonium Salts To Prepare Conducting Organic Films of High Thickness. *Chemistry of Materials*, *23*(6), 1551–1557. https://doi.org/10.1021/cm1033244

Chamoulaud, G., & Bélanger, D. (2007). Spontaneous Derivatization of a Copper Electrode with in Situ Generated Diazonium Cations in Aprotic and Aqueous Media. *The Journal of Physical Chemistry C*, *111*(20), 7501–7507. https://doi.org/10.1021/jp0704012

Chen, J. S., Lau, S. P., Tay, B. K., Chen, G. Y., Sun, Z., Tan, Y. Y., Tan, G., & Chai, J. W. (2001). Surface energy of amorphous carbon films containing iron. *Journal of Applied Physics*, *89*(12), 7814–7819. https://doi.org/10.1063/1.1375808

Chen, P., & McCreery, R. L. (1996). Control of Electron Transfer Kinetics at Glassy Carbon Electrodes by Specific Surface Modification. *Analytical Chemistry*, *68*(22), 3958–3965. https://doi.org/10.1021/ac960492r

Chen, Q., & Swain, G. M. (1998). Structural characterization, electrochemical reactivity, and response stability of hydrogenated glassy carbon electrodes. *Langmuir*, *14*(24), 7017–7026. https://doi.org/10.1021/la980907z

Chen, R., Balla, R. J., Li, Z., Liu, H., & Amemiya, S. (2016). Origin of asymmetry of paired nanogap voltammograms based on scanning electrochemical microscopy: Contamination not adsorption. *Analytical Chemistry*, *88*(16), 8323–8331. https://doi.org/10.1021/acs.analchem.6b02273

Chen, R., Hu, K., Yu, Y., Mirkin, M. V., & Amemiya, S. (2016). Focused-Ion-Beam-Milled Carbon Nanoelectrodes for Scanning Electrochemical Microscopy. *Journal of The Electrochemical Society*, *163*(4), H3032–H3037. https://doi.org/10.1149/2.0071604jes

Chen, R., Najarian, A. M., Kurapati, N., Balla, R. J., Oleinick, A., Svir, I., Amatore, C., McCreery, R. L., & Amemiya, S. (2018). Self-Inhibitory Electron Transfer of the Co(III)/Co(II)-Complex Redox Couple at Pristine Carbon Electrode

[Research-article]. *Analytical Chemistry*, *90*(18), 11115–11123. https://doi.org/10.1021/acs.analchem.8b03023

Chen, R., Nioradze, N., Santhosh, P., Li, Z., Surwade, S. P., Shenoy, G. J., Parobek, D. G., Kim, M. A., Liu, H., & Amemiya, S. (2015). Ultrafast Electron Transfer Kinetics of Graphene Grown by Chemical Vapor Deposition. *Angewandte Chemie - International Edition*, *54*(50), 15134–15137. https://doi.org/10.1002/anie.201507005

Chen, S., Liu, L., Zhou, J., & Jiang, S. (2003). Controlling Antibody Orientation on Charged Self-Assembled Monolayers. *Langmuir*, *19*(7), 2859–2864. https://doi.org/10.1021/la026498v

Choi, H. C., Shim, M., Bangsaruntip, S., & Dai, H. (2002). Spontaneous Reduction of Metal Ions on the Sidewalls of Carbon Nanotubes. *Journal of the American Chemical Society*, *124*(31), 9058–9059. https://doi.org/10.1021/ja026824t

Choi, H. W., Dauskardt, R. H., Lee, S.-C., Lee, K.-R., & Oh, K. H. (2008). Characteristic of silver doped DLC films on surface properties and protein adsorption. *Diamond and Related Materials*, *17*(3), 252–257. https://doi.org/10.1016/j.diamond.2007.12.034

Choi, S. H., Kim, Y. L., & Byun, K. M. (2011). Graphene-on-silver substrates for sensitive surface plasmon resonance imaging biosensors. *Optics Express*, *19*(2), 458. https://doi.org/10.1364/OE.19.000458

Chrétien, J.-M., Ghanem, M. A., Bartlett, P. N., & Kilburn, J. D. (2008). Covalent Tethering of Organic Functionality to the Surface of Glassy Carbon Electrodes by Using Electrochemical and Solid-Phase Synthesis Methodologies. *Chemistry - A European Journal*, *14*(8), 2548–2556. https://doi.org/10.1002/chem.200701559

Combellas, C., Delamar, M., Kanoufi, F., Pinson, J., & Podvorica, F. I. (2005). Spontaneous Grafting of Iron Surfaces by Reduction of Aryldiazonium Salts in Acidic or Neutral Aqueous Solution. Application to the Protection of Iron against Corrosion. *Chemistry of Materials*, *17*(15), 3968–3975. https://doi.org/10.1021/cm050339q

Combellas, C., Kanoufi, F., Pinson, J., & Podvorica, F. I. (2008). Sterically Hindered Diazonium Salts for the Grafting of a Monolayer on Metals. *Journal of the American Chemical Society*, *130*(27), 8576–8577. https://doi.org/10.1021/ja8018912

Contu, F., Elsener, B., & Böhni, H. (2002). Characterization of implant materials in fetal bovine serum and sodium sulfate by electrochemical impedance spectroscopy. I. Mechanically polished samples: Implant Materials and EIS. I. *Journal of Biomedical Materials Research*, *62*(3), 412–421. https://doi.org/10.1002/jbm.10329

Cooper, E., & Leggett, G. J. (1998). Static Secondary Ion Mass Spectrometry Studies of Self-Assembled Monolayers: Influence of Adsorbate Chain Length and Terminal Functional Group on Rates of Photooxidation of Alkanethiols on Gold. *Langmuir*, *14*(17), 4795–4801. https://doi.org/10.1021/la9802567

Corgier, B. P., Bellon, S., Anger-Leroy, M., Blum, L. J., & Marquette, C. A. (2009). Protein−Diazonium Adduct Direct Electrografting onto SPRi-Biochip. *Langmuir*, *25*(16), 9619–9623. https://doi.org/10.1021/la900762s

Cortés, E., Rubert, A. A., Benitez, G., Carro, P., Vela, M. E., & Salvarezza, R. C. (2009). Enhanced Stability of Thiolate Self-Assembled Monolayers (SAMs) on Nanostructured Gold Substrates. *Langmuir*, *25*(10), 5661–5666. https://doi.org/10.1021/la804251a

Couture, M., Zhao, S. S., & Masson, J.-F. (2013). Modern surface plasmon resonance for bioanalytics and biophysics. *Physical Chemistry Chemical Physics*, *15*(27), 11190. https://doi.org/10.1039/c3cp50281c

Cullen, R. J., Jayasundara, D. R., Soldi, L., Cheng, J. J., Dufaure, G., & Colavita, P. E. (2012). Spontaneous Grafting of Nitrophenyl Groups on Amorphous Carbon Thin Films: A Structure–Reactivity Investigation. *Chemistry of Materials*, *24*(6), 1031–1040. https://doi.org/10.1021/cm2030262

D'Amours, M., & Bélanger, D. (2003). Stability of Substituted Phenyl Groups Electrochemically Grafted at Carbon Electrode Surface. *The Journal of Physical Chemistry B*, *107*(20), 4811–4817. https://doi.org/10.1021/jp027223r

Danson, R. E. a. M. J. (1993). *Enzyme Assays: A Practical Approach* (2nd ed.).

de la Llave, E., Ricci, A., Calvo, E. J., & Scherlis, D. A. (2008). Binding between Carbon and the Au(111) Surface and What Makes It Different from the S−Au(111) Bond. *The Journal of Physical Chemistry C*, *112*(45), 17611–17617. https://doi.org/10.1021/jp8036395

de Villeneuve, C. H., Pinson, J., Bernard, M. C., & Allongue, P. (1997). Electrochemical Formation of Close-Packed Phenyl Layers on Si(111). *The Journal of Physical Chemistry B*, *101*(14), 2415–2420. https://doi.org/10.1021/jp962581d

DeAngelis, T. P., Hurst, R. W., Yacynych, A. M., Mark, H. B., Heineman, W. R., & Mattson, J. S. (1977). Carbon and Mercury–Carbon Optically Transparent Electrodes. *Analytical Chemistry*, *49*(9), 1395–1398. https://doi.org/10.1021/ac50017a026

Delamar, M., Désarmot, G., Fagebaume, O., Hitmi, R., Pinsonc, J., & Savéant, J.-M. (1997). Modification of carbon fiber surfaces by electrochemical reduction of aryl diazonium salts: Application to carbon epoxy composites. *Carbon*, *35*(6), 801–807. https://doi.org/10.1016/S0008-6223(97)00010-9

Delamar, M., Hitmi, R., Pinson, J., & Saveant, J. M. (1992). Covalent modification of carbon surfaces by grafting of functionalized aryl radicals produced from electrochemical reduction of diazonium salts. *Journal of the American Chemical Society*, *114*(14), 5883–5884. https://doi.org/10.1021/ja00040a074

Díaz, J., Paolicelli, G., Ferrer, S., & Comin, F. (1996). Separation of the sp 3 and sp 2 components in the C1 *s* photoemission spectra of amorphous carbon films. *Physical Review B*, *54*(11), 8064–8069. https://doi.org/10.1103/PhysRevB.54.8064

Doppelt, P., Hallais, G., Pinson, J., Podvorica, F., & Verneyre, S. (2007). Surface Modification of Conducting Substrates. Existence of Azo Bonds in the Structure of Organic Layers Obtained from Diazonium Salts. *Chemistry of Materials*, *19*(18), 4570–4575. https://doi.org/10.1021/cm0700551

Downard, A. J. (2000a). Electrochemically Assisted Covalent Modification of Carbon Electrodes. *Electroanalysis*, *12*(14), 1085–1096. https://doi.org/10.1002/1521-4109(200010)12:14<1085::AID-ELAN1085>3.0.CO;2-A

Downard, A. J. (2000b). Potential-Dependence of Self-Limited Films Formed by Reduction of Aryldiazonium Salts at Glassy Carbon Electrodes. *Langmuir*, *16*(24), 9680–9682. https://doi.org/10.1021/la000866i

Downard, A. J., Jackson, S. L., & Tan, E. S. Q. (2005). Fluorescence Microscopy Study of Protein Adsorption at Modified Glassy Carbon Surfaces. *Australian Journal of Chemistry*, *58*(4), 275. https://doi.org/10.1071/CH04259

Downard, A. J., & Prince, M. J. (2001). Barrier Properties of Organic Monolayers on Glassy Carbon Electrodes. *Langmuir*, *17*(18), 5581–5586. https://doi.org/10.1021/la010499q

Downard, A. J., & Roddick, A. D. (1995). Protein adsorption at glassy carbon electrodes: The effect of covalently bound surface groups. *Electroanalysis*, *7*(4), 376–378. https://doi.org/10.1002/elan.1140070414

Dubois, L. H., & Nuzzo, R. G. (1992). Synthesis, Structure, and Properties of Model Organic Surfaces. *Annual Review of Physical Chemistry*, *43*(1), 437–463. https://doi.org/10.1146/annurev.pc.43.100192.002253

Dumitrescu, I., Dudin, P. V., Edgeworth, J. P., Macpherson, J. V., & Unwin, P. R. (2010). Electron transfer kinetics at single-walled carbon nanotube electrodes using scanning electrochemical microscopy. *Journal of Physical Chemistry C*, *114*(6), 2633–2639. https://doi.org/10.1021/jp908830d

DuVall, S. H., & McCreery, R. L. (2000). Self-catalysis by Catechols and Quinones during Heterogeneous Electron Transfer at Carbon Electrodes. *Journal of the American Chemical Society*, *122*(28), 6759–6764. https://doi.org/10.1021/ja000227u

El-Sayed, I. H., Huang, X., & El-Sayed, M. A. (2005). Surface Plasmon Resonance Scattering and Absorption of anti-EGFR Antibody Conjugated Gold Nanoparticles in Cancer Diagnostics: Applications in Oral Cancer. *Nano Letters*, *5*(5), 829–834. https://doi.org/10.1021/nl050074e

Enayatpour, B., Rajabi, M., Yari, M., Reza Mirkhan, S. M., Najafi, F., Moradi, O., Bharti, A. K., Agarwal, S., & Gupta, V. K. (2017). Adsorption/desorption study of proteins onto multi-walled carbon nanotubes and amino multi-walled carbon nanotubes surfaces as adsorbents. *Journal of Molecular Liquids*, *231*, 566–571. https://doi.org/10.1016/j.molliq.2017.02.013

Engelsmann, K. (1980). Underpotential deposition of lead on polycrystalline and single-crystal gold surfaces Part II. Kinetics. *Journal of Electroanalytical Chemistry*, *114*, 11–24. https://doi.org/10.1016/0368-1874(80)80360-1

Engelsmann, K., Lorenz, W. J., & Schmidt, E. (1980). Underpotential deposition of lead on polycrystalline and single-crystal gold surfaces. Part I. Thermodynamics. *Journal of Electroanalytical Chemistry*, *114*(1), 1–10. https://doi.org/10.1016/S0022-0728(80)80431-1

English, R. D., Van Stipdonk, M. J., Sabapathy, R. C., Crooks, R. M., & Schweikert, E. A. (2000). Characterization of Photooxidized Self-Assembled Monolayers and Bilayers by Spontaneous Desorption Mass Spectrometry. *Analytical Chemistry*, *72*(24), 5973–5980. https://doi.org/10.1021/ac0008892

Eriksson, A., Norekrans, A. S., & Carlsson, J. O. (1992). Surface structural and electrochemical investigations of pyrolytic carbon film electrodes prepared by chemical vapour deposition using ethene as carbon source. *Journal of*

Electroanalytical Chemistry, *324*(1–2), 291–305. https://doi.org/10.1016/0022-0728(92)80052-6

Everett, W. Russell., Welch, T. L., Reed, Laura., & Fritsch-Faules, Ingrid. (1995). Potential-Dependent Stability of Self-Assembled Organothiols on Gold Electrodes in Methylene Chloride. *Analytical Chemistry*, *67*(2), 292–298. https://doi.org/10.1021/ac00098a010

Fanjul-Bolado, P., Hernández-Santos, D., Lamas-Ardisana, P. J., Martín-Pernía, A., & Costa-García, A. (2008). Electrochemical characterization of screen-printed and conventional carbon paste electrodes. *Electrochimica Acta*, *53*(10), 3635–3642. https://doi.org/10.1016/j.electacta.2007.12.044

Fano, U. (1941). The Theory of Anomalous Diffraction Gratings and of Quasi-Stationary Waves on Metallic Surfaces (Sommerfeld's Waves). *Journal of the Optical Society of America*, *31*(3), 213. https://doi.org/10.1364/JOSA.31.000213

Fedel, M., Motta, A., Maniglio, D., & Migliaresi, C. (2008). Surface properties and blood compatibility of commercially available diamond-like carbon coatings for cardiovascular devices. *Journal of Biomedical Materials Research Part B: Applied Biomaterials*, *90B*(1), 338–349. https://doi.org/10.1002/jbm.b.31291

Fedel, M., Motta, A., Maniglio, D., & Migliaresi, C. (2010). Carbon Coatings for Cardiovascular Applications: Physico-Chemical Properties and Blood Compatibility. *Journal of Biomaterials Applications*, *25*(1), 57–74. https://doi.org/10.1177/0885328209342000

Feng, L., & Andrade, J. D. (1996). Protein adsorption on low temperature isotropic carbon: V. How is it related to its blood compatibility? *Journal of Biomaterials Science, Polymer Edition*, *7*(5), 439–452. https://doi.org/10.1163/156856295X00445

Ferrari, A. C., & Robertson, J. (2000). Interpretation of Raman spectra of disordered and amorphous carbon. *Physical Review B*, *61*(20), 14095–14107. https://doi.org/10.1103/PhysRevB.61.14095

Finklea, H. O., Avery, S., Lynch, M., & Furtsch, T. (1987). Blocking oriented monolayers of alkyl mercaptans on gold electrodes. *Langmuir*, *3*(3), 409–413. https://doi.org/10.1021/la00075a024

Finn, Patricia., & Jolly, W. L. (1972). Nitrogen ls binding energies of some azide, dinitrogen, and nitride complexes of transition metals. *Inorganic Chemistry*, *11*(6), 1434–1435. https://doi.org/10.1021/ic50112a056

Finot, M. O., Braybrook, G. D., & McDermott, M. T. (1999). Characterization of electrochemically deposited gold nanocrystals on glassycarbon electrodes. *Journal of Electroanalytical Chemistry*, *466*(2), 234–241. https://doi.org/10.1016/S0022-0728(99)00154-0

Fioresi, F., Rouleau, A., Maximova, K., Vieillard, J., Boireau, W., Caille, C. E., Soulignac, C., Zeggari, R., Clamens, T., Lesouhaitier, O., Mofaddel, N., & Derf, F. L. (2019). Electrografting of diazonium salt for SPR application. *Materials Today: Proceedings*, *6*, 340–344. https://doi.org/10.1016/j.matpr.2018.10.428

Franzen, S. (2008). Surface Plasmon Polaritons and Screened Plasma Absorption in Indium Tin Oxide Compared to Silver and Gold. *The Journal of Physical Chemistry C*, *112*(15), 6027–6032. https://doi.org/10.1021/jp7097813

Frasconi, M., Tortolini, C., Botrè, F., & Mazzei, F. (2010). Multifunctional Au Nanoparticle Dendrimer-Based Surface Plasmon Resonance Biosensor and Its Application for Improved Insulin Detection. *Analytical Chemistry*, *82*(17), 7335–7342. https://doi.org/10.1021/ac101319k

Frutos, A. G., & Corn, R. M. (1998). SPR of Ultrathin Organic Films. *Analytical Chemistry*, *70*(13), 449A-455A. https://doi.org/10.1021/ac981909r

Gam-Derouich, S., Gosecka, M., Lepinay, S., Turmine, M., Carbonnier, B., Basinska, T., Slomkowski, S., Millot, M.-C., Othmane, A., Ben Hassen-Chehimi, D., & Chehimi, M. M. (2011). Highly Hydrophilic Surfaces from Polyglycidol Grafts with Dual Antifouling and Specific Protein Recognition Properties. *Langmuir*, *27*(15), 9285–9294. https://doi.org/10.1021/la200290k

Garg, N., Carrasquillo-Molina, E., & Lee, T. R. (2002). Self-Assembled Monolayers Composed of Aromatic Thiols on Gold: Structural Characterization and Thermal Stability in Solution. *Langmuir*, *18*(7), 2717–2726. https://doi.org/10.1021/la0115278

Garrett, D. J., Lehr, J., Miskelly, G. M., & Downard, A. J. (2007). Microcontact Printing Using the Spontaneous Reduction of Aryldiazonium Salts. *Journal of the American Chemical Society*, *129*(50), 15456–15457. https://doi.org/10.1021/ja0775321

Gerischer, H. (1985). An interpretation of the double layer capacity of graphite electrodes in relation to the density of states at the Fermi level. *The Journal of Physical Chemistry*, *89*(20), 4249–4251. https://doi.org/10.1021/j100266a020

Gerischer, H., McIntyre, R., Scherson, D., & Storck, W. (1987). Density of the electronic states of graphite: Derivation from differential capacitance measurements. *The Journal of Physical Chemistry*, *91*(7), 1930–1935. https://doi.org/10.1021/j100291a049

Ghosh, D., & Chen, S. (2008). Solid-state electronic conductivity of ruthenium nanoparticles passivated by metal–carbon covalent bonds. *Chemical Physics Letters*, *465*(1–3), 115–119. https://doi.org/10.1016/j.cplett.2008.09.066

Ghosh, D., Pradhan, S., Chen, W., & Chen, S. (2008). Titanium Nanoparticles Stabilized by Ti−C Covalent Bonds. *Chemistry of Materials*, *20*(4), 1248–1250. https://doi.org/10.1021/cm703423k

Gifford, L. K., Sendroiu, I. E., Corn, R. M., & Lupták, A. (2010). Attomole Detection of Mesophilic DNA Polymerase Products by Nanoparticle-Enhanced Surface Plasmon Resonance Imaging on Glassified Gold Surfaces. *Journal of the American Chemical Society*, *132*(27), 9265–9267. https://doi.org/10.1021/ja103043p

Gkogkou, D., Schreiber, B., Shaykhutdinov, T., Ly, H. K., Kuhlmann, U., Gernert, U., Facsko, S., Hildebrandt, P., Esser, N., Hinrichs, K., Weidinger, I. M., & Oates, T. W. H. (2016). Polarization- and Wavelength-Dependent Surface-Enhanced Raman Spectroscopy Using Optically Anisotropic Rippled Substrates for Sensing. *ACS Sensors*, *1*(3), 318–323. https://doi.org/10.1021/acssensors.5b00176

Golub, E., Pelossof, G., Freeman, R., Zhang, H., & Willner, I. (2009). Electrochemical, Photoelectrochemical, and Surface Plasmon Resonance Detection of Cocaine Using Supramolecular Aptamer Complexes and Metallic or Semiconductor Nanoparticles. *Analytical Chemistry*, *81*(22), 9291–9298. https://doi.org/10.1021/ac901551q

Gooding, J. J. (2008). Advances in Interfacial Design for Electrochemical Biosensors and Sensors: Aryl Diazonium Salts for Modifying Carbon and Metal Electrodes. *Electroanalysis*, *20*(6), 573–582. https://doi.org/10.1002/elan.200704124

Gooding, J. J., & Ciampi, S. (2011). The molecular level modification of surfaces: From self-assembled monolayers to complex molecular assemblies. *Chemical Society Reviews*, *40*(5), 2704. https://doi.org/10.1039/c0cs00139b

Gooding, J. J., Mearns, F., Yang, W., & Liu, J. (2003). Self-Assembled Monolayers into the 21st Century: Recent Advances and Applications. *Electroanalysis*, *15*(2), 81–96. https://doi.org/10.1002/elan.200390017

Granger, M. C., Witek, M., Xu, J., Wang, J., Hupert, M., Hanks, A., Koppang, M. D., Butler, J. E., Lucazeau, G., Mermoux, M., Strojek, J. W., & Swain, G. M. (2000). Standard electrochemical behavior of high-quality, boron-doped polycrystalline diamond thin-film electrodes. *Analytical Chemistry*, *72*(16), 3793–3804. https://doi.org/10.1021/ac0000675

Grant, C. F. (2009). *Development and Characterization of Interfacial Chemistry for Biomolecule Immobilization in Surface Plasmon Resonance Imaging Studies* [PhD Thesis]. University of Alberta.

Green, R. J., Davies, J., Roberts, C. J., & Tendler, S. J. B. (1997). *Surface plasmon resonance for real time in situ analvsis of Protein adsorption to polymer i&faces*. *18*(5), 9.

Green, R. J., Davies, M. C., Roberts, C. J., & Tendler, S. J. B. (1999). Competitive protein adsorption as observed by surface plasmon resonance. *Biomaterials*, *20*(4), 385–391. https://doi.org/10.1016/S0142-9612(98)00201-4

Griffete, N., Herbst, F., Pinson, J., Ammar, S., & Mangeney, C. (2011). Preparation of Water-Soluble Magnetic Nanocrystals Using Aryl Diazonium Salt Chemistry. *Journal of the American Chemical Society*, *133*(6), 1646–1649. https://doi.org/10.1021/ja108928b

Güell, A. G., Ebejer, N., Snowden, M. E., McKelvey, K., Macpherson, J. V., & Unwin, P. R. (2012). Quantitative nanoscale visualization of heterogeneous electron transfer rates in 2D carbon nanotube networks. *Proceedings of the National Academy of Sciences of the United States of America*, *109*(29), 11487–11492. https://doi.org/10.1073/pnas.1203671109

Guo, B., Anzai, J., & Osa, T. (1996). *Adsorption Behavior of Serum Albumin on Electrode Surfaces and the Effects of Electrode Potential*. *44*(4), 800–803.

Hamelin, A. (1984). Underpotential deposition of lead on single crystal faces of gold. Part I. The influence of crystallographic orientation of the substrate. *Journal of Electroanalytical Chemistry*, *165*(1–2), 167–180. https://doi.org/10.1016/S0022-0728(84)80095-9

Hamelin, A., & Lipkowski, J. (1984). Underpotential deposition of lead on gold single crystal faces. Part II. General discussion. *Journal of Electroanalytical*

Chemistry, *171*(1–2), 317–330. https://doi.org/10.1016/0022-0728(84)80123-0

Harper, J. C., Polsky, R., Wheeler, D. R., Dirk, S. M., & Brozik, S. M. (2007). Selective Immobilization of DNA and Antibody Probes on Electrode Arrays: Simultaneous Electrochemical Detection of DNA and Protein on a Single Platform. *Langmuir*, *23*(16), 8285–8287. https://doi.org/10.1021/la701775g

Harris, A. L., Rothberg, L., Dubois, L. H., Levinos, N. J., & Dhar, L. (1990). Molecular vibrational energy relaxation at a metal surface: Methyl thiolate on Ag(111). *Physical Review Letters*, *64*(17), 2086–2089. https://doi.org/10.1103/PhysRevLett.64.2086

Harrison, D. J. (1990). Effect of blood on K+ion sensitive membrane electrode performance and bulk resistance. *Journal of Electroanalytical Chemistry and Interfacial Electrochemistry*, *278*(1–2), 193–204. https://doi.org/10.1016/0022-0728(90)85133-P

Hayat, A., Barthelmebs, L., Sassolas, A., & Marty, J.-L. (2011). An electrochemical immunosensor based on covalent immobilization of okadaic acid onto screen printed carbon electrode via diazotization-coupling reaction. *Talanta*, *85*(1), 513–518. https://doi.org/10.1016/j.talanta.2011.04.034

Hedayati, M., Neufeld, M. J., Reynolds, M. M., & Kipper, M. J. (2019). The quest for blood-compatible materials: Recent advances and future technologies. *Materials Science and Engineering: R: Reports*, *138*, 118–152. https://doi.org/10.1016/j.mser.2019.06.002

Hetemi, D., Noël, V., & Pinson, J. (2020). Grafting of Diazonium Salts on Surfaces: Application to Biosensors. *Biosensors*, *10*(1), 4. https://doi.org/10.3390/bios10010004

Hirono, S., Umemura, S., Tomita, M., & Kaneko, R. (2002). Superhard conductive carbon nanocrystallite films. *Applied Physics Letters*, *80*(3), 425–427. https://doi.org/10.1063/1.1435402

Holze, R. (2013). Competition of anchoring groups in adsorption on gold electrodes—A comparative spectroelectrochemical study of 4-mercaptobenzonitrile and aromatic nitriles. *Journal of Solid State Electrochemistry*, *17*(7), 1869–1879. https://doi.org/10.1007/s10008-013-2076-5

Homola, J. (2003). Present and future of surface plasmon resonance biosensors. *Analytical and Bioanalytical Chemistry*, *377*(3), 528–539. https://doi.org/10.1007/s00216-003-2101-0

Homola, J. (2006). *Surface Plasmon Resonance Based Sensors*. Springer: Berlin, Germany.

Homola, J. (2008). Surface Plasmon Resonance Sensors for Detection of Chemical and Biological Species. *Chemical Reviews*, *108*(2), 462–493. https://doi.org/10.1021/cr068107d

Homola, J., Yee, S. S., & Gauglitz, G. (1999). Surface plasmon resonance sensors: Review. *Sensors and Actuators B: Chemical*, *54*(1–2), 3–15. https://doi.org/10.1016/S0925-4005(98)00321-9

Hurley, B. L., & McCreery, R. L. (2004). Covalent Bonding of Organic Molecules to Cu and Al Alloy 2024 T3 Surfaces via Diazonium Ion Reduction. *Journal of The Electrochemical Society*, *151*(5), B252. https://doi.org/10.1149/1.1687428

Hutt, D. A., & Leggett, G. J. (1996). Influence of Adsorbate Ordering on Rates of UV Photooxidation of Self-Assembled Monolayers. *The Journal of Physical Chemistry*, *100*(16), 6657–6662. https://doi.org/10.1021/jp952734h

Jayasundara, D. R., Cullen, R. J., & Colavita, P. E. (2013). In Situ and Real Time Characterization of Spontaneous Grafting of Aryldiazonium Salts at Carbon Surfaces. *Chemistry of Materials*, *25*(7), 1144–1152. https://doi.org/10.1021/cm4007537

Jeong, J.-A., & Kim, H.-K. (2009). Low resistance and highly transparent ITO–Ag–ITO multilayer electrode using surface plasmon resonance of Ag layer for bulk-heterojunction organic solar cells. *Solar Energy Materials and Solar Cells*, *93*(10), 1801–1809. https://doi.org/10.1016/j.solmat.2009.06.014

Jia, J., Kato, D., Kurita, R., Sato, Y., Maruyama, K., Suzuki, K., Hirono, S., Ando, T., & Niwa, O. (2007). Structure and electrochemical properties of carbon films prepared by a electron cyclotron resonance sputtering method. *Analytical Chemistry*, *79*(1), 98–105. https://doi.org/10.1021/ac0610558

Jiang, C., Alam, M. T., Parker, S. G., Darwish, N., & Gooding, J. J. (2016). Strategies To Achieve Control over the Surface Ratio of Two Different Components on Modified Electrodes Using Aryldiazonium Salts. *Langmuir*, *32*(10), 2509–2517. https://doi.org/10.1021/acs.langmuir.5b04550

Jiang, C., Moraes Silva, S., Fan, S., Wu, Y., Alam, M. T., Liu, G., & Justin Gooding, J. (2017). Aryldiazonium salt derived mixed organic layers: From surface chemistry to their applications. *Journal of Electroanalytical Chemistry*, *785*, 265–278. https://doi.org/10.1016/j.jelechem.2016.11.043

Johnson, C. P., Jensen, I. E., Prakasam, A., Vijayendran, R., & Leckband, D. (2003). Engineered Protein A for the Orientational Control of Immobilized Proteins. *Bioconjugate Chemistry*, *14*(5), 974–978. https://doi.org/10.1021/bc034063t

Johnsson, B., Löfås, S., & Lindquist, G. (1991). Immobilization of proteins to a carboxymethyldextran-modified gold surface for biospecific interaction analysis in surface plasmon resonance sensors. *Analytical Biochemistry*, *198*(2), 268–277. https://doi.org/10.1016/0003-2697(91)90424-R

Jones, M. I., McColl, I. R., Grant, D. M., Parker, K. G., & Parker, T. L. (2000). Protein adsorption and platelet attachment and activation, on TiN, TiC, and DLC coatings on titanium for cardiovascular applications. *Journal of Biomedical Materials Research*, *52*(2), 413–421. https://doi.org/10.1002/1097-4636(200011)52:2<413::AID-JBM23>3.0.CO;2-U

Jordan, C. E., Frutos, A. G., Thiel, A. J., & Corn, R. M. (1997). Surface Plasmon Resonance Imaging Measurements of DNA Hybridization Adsorption and Streptavidin/DNA Multilayer Formation at Chemically Modified Gold Surfaces. *Analytical Chemistry*, *69*(24), 4939–4947. https://doi.org/10.1021/ac9709763

Jung, L. S., Nelson, K. E., Stayton, P. S., & Campbell, C. T. (2000). Binding and Dissociation Kinetics of Wild-Type and Mutant Streptavidins on Mixed

Biotin-Containing Alkylthiolate Monolayers. *Langmuir*, *16*(24), 9421–9432. https://doi.org/10.1021/la000144r

Kamata, T., Kato, D., Ida, H., & Niwa, O. (2014). Structure and electrochemical characterization of carbon films formed by unbalanced magnetron (UBM) sputtering method. *Diamond and Related Materials*, *49*, 25–32. https://doi.org/10.1016/j.diamond.2014.07.007

Kambhampati, D. K., Jakob, T. A. M., Robertson, J. W., Cai, M., Pemberton, J. E., & Knoll, W. (2001). Novel Silicon Dioxide Sol−Gel Films for Potential Sensor Applications: A Surface Plasmon Resonance Study. *Langmuir*, *17*(4), 1169–1175. https://doi.org/10.1021/la001250w

Kanda, V., Kariuki, J. K., Harrison, D. J., & McDermott, M. T. (2004). Label-Free Reading of Microarray-Based Immunoassays with Surface Plasmon Resonance Imaging. *Analytical Chemistry*, *76*(24), 7257–7262. https://doi.org/10.1021/ac049318q

Kariuki, J. K., & McDermott, M. T. (2001). Formation of Multilayers on Glassy Carbon Electrodes via the Reduction of Diazonium Salts. *Langmuir*, *17*(19), 5947–5951. https://doi.org/10.1021/la010415d

Kato, D., Sekioka, N., Ueda, A., Kurita, R., Hirono, S., Suzuki, K., & Niwa, O. (2008). A nanocarbon film electrode as a platform for exploring DNA methylation. *Journal of the American Chemical Society*, *130*(12), 3716–3717. https://doi.org/10.1021/ja710536p

Kim, J., Choi, H., Nahm, C., & Park, B. (2012). Surface-plasmon resonance for photoluminescence and solar-cell applications. *Electronic Materials Letters*, *8*(4), 351–364. https://doi.org/10.1007/s13391-012-2117-8

Kim, J., & Somorjai, G. A. (2003). Molecular Packing of Lysozyme, Fibrinogen, and Bovine Serum Albumin on Hydrophilic and Hydrophobic Surfaces Studied by Infrared−Visible Sum Frequency Generation and Fluorescence Microscopy. *Journal of the American Chemical Society*, *125*(10), 3150–3158. https://doi.org/10.1021/ja028987n

Koehler, F. M., Jacobsen, A., Ensslin, K., Stampfer, C., & Stark, W. J. (2010). Selective Chemical Modification of Graphene Surfaces: Distinction Between Single- and Bilayer Graphene. *Small*, *6*(10), 1125–1130. https://doi.org/10.1002/smll.200902370

Kozbial, A., Li, Z., Sun, J., Gong, X., Zhou, F., Wang, Y., Xu, H., Liu, H., & Li, L. (2014). Understanding the intrinsic water wettability of graphite. *Carbon*, *74*, 218–225. https://doi.org/10.1016/j.carbon.2014.03.025

Kreno, L. E., Hupp, J. T., & Van Duyne, R. P. (2010). Metal−Organic Framework Thin Film for Enhanced Localized Surface Plasmon Resonance Gas Sensing. *Analytical Chemistry*, *82*(19), 8042–8046. https://doi.org/10.1021/ac102127p

Kretschmann, E., & Raether, H. (1968). Radiative Decay of Non Radiative Surface Plasmons Excited by Light. *Zeitschrift Fur Naturforschung Part A-Astrophysik Physik Und Physikalische Chemie*, *23*, 2135–2136.

Kuo, T. C., & McCreery, R. L. (1999). Surface chemistry and electron-transfer kinetics of hydrogen-modified glassy carbon electrodes. *Analytical Chemistry*, *71*(8), 1553–1560. https://doi.org/10.1021/ac9807666

Kwok, S. C. H., Wang, J., & Chu, P. K. (2005). Surface energy, wettability, and blood compatibility phosphorus doped diamond-like carbon films. *Diamond and Related Materials*, *14*(1), 78–85. https://doi.org/10.1016/j.diamond.2004.07.019

Laurentius, L., Stoyanov, S. R., Gusarov, S., Kovalenko, A., Du, R., Lopinski, G. P., & McDermott, M. T. (2011). Diazonium-Derived Aryl Films on Gold Nanoparticles: Evidence for a Carbon–Gold Covalent Bond. *ACS Nano*, *5*(5), 4219–4227. https://doi.org/10.1021/nn201110r

Le Floch, F., Simonato, J.-P., & Bidan, G. (2009). Electrochemical signature of the grafting of diazonium salts: A probing parameter for monitoring the electro-addressed functionalization of devices. *Electrochimica Acta*, *54*(11), 3078–3085. https://doi.org/10.1016/j.electacta.2008.11.063

Lee, H. J., Cui, S.-Y., & Park, S.-M. (2001). Electrochemistry of Conductive Polymers: XXV. Electrochemical Preparation and Characterization of Poly(p-phenylenes) from Biphenyl and p-Terphenyl. *Journal of The Electrochemical Society*, *148*(10), D139. https://doi.org/10.1149/1.1401080

Lehr, J., Garrett, D. J., Paulik, M. G., Flavel, B. S., Brooksby, P. A., Williamson, B. E., & Downard, A. J. (2010). Patterning of Metal, Carbon, and Semiconductor Substrates with Thin Organic Films by Microcontact Printing with Aryldiazonium Salt Inks. *Analytical Chemistry*, *82*(16), 7027–7034. https://doi.org/10.1021/ac101785c

Lehr, J., Williamson, B. E., & Downard, A. J. (2011). Spontaneous Grafting of Nitrophenyl Groups to Planar Glassy Carbon Substrates: Evidence for Two Mechanisms. *The Journal of Physical Chemistry C*, *115*(14), 6629–6634. https://doi.org/10.1021/jp111838r

Lehr, J., Williamson, B. E., Flavel, B. S., & Downard, A. J. (2009). Reaction of Gold Substrates with Diazonium Salts in Acidic Solution at Open-Circuit Potential. *Langmuir*, *25*(23), 13503–13509. https://doi.org/10.1021/la902002n

Li, Y., Liu, X., & Lin, Z. (2012). Recent developments and applications of surface plasmon resonance biosensors for the detection of mycotoxins in foodstuffs. *Food Chemistry*, *132*(3), 1549–1554. https://doi.org/10.1016/j.foodchem.2011.10.109

Li, Z., Wang, Y., Kozbial, A., Shenoy, G., Zhou, F., McGinley, R., Ireland, P., Morganstein, B., Kunkel, A., Surwade, S. P., Li, L., & Liu, H. (2013). Effect of airborne contaminants on the wettability of supported graphene and graphite. *Nature Materials*, *12*(10), 925–931. https://doi.org/10.1038/nmat3709

Liedberg, B., Nylander, C., & Lunström, I. (1983). Surface plasmon resonance for gas detection and biosensing. *Sensors and Actuators*, *4*, 299–304. https://doi.org/10.1016/0250-6874(83)85036-7

Liu, H., Wang, B., Leong, E. S. P., Yang, P., Zong, Y., Si, G., Teng, J., & Maier, S. A. (2010). Enhanced Surface Plasmon Resonance on a Smooth Silver Film with a Seed Growth Layer. *ACS Nano*, *4*(6), 3139–3146. https://doi.org/10.1021/nn100466p

Liu, Y.-C., & McCreery, R. L. (1995). Reactions of Organic Monolayers on Carbon Surfaces Observed with Unenhanced Raman Spectroscopy. *Journal of the*

American Chemical Society, *117*(45), 11254–11259. https://doi.org/10.1021/ja00150a024

Lockert, M. R., Weibel, S. C., Phillips, M. F., Shortreed, M. R., Sun, B., Corn, R. M., Hamers, R. J., Cerrina, F., & Smith, L. M. (2008). Carbon-on-metal films for surface plasmon resonance detection of DNA arrays. *Journal of the American Chemical Society*, *130*(27), 8611–8613. https://doi.org/10.1021/ja802454c

Lockett, M. R., & Smith, L. M. (2009). Fabrication and characterization of DNA arrays prepared on carbon-on-metal substrates. *Analytical Chemistry*, *81*(15), 6429–6437. https://doi.org/10.1021/ac900807q

Lockett, M. R., Weibel, S. C., Phillips, M. F., Shortreed, M. R., Sun, B., Corn, R. M., Hamers, R. J., Cerrina, F., & Smith, L. M. (2008). Carbon-on-Metal Films for Surface Plasmon Resonance Detection of DNA Arrays. *Journal of the American Chemical Society*, *130*(27), 8611–8613. https://doi.org/10.1021/ja802454c

Lopez, G. P., Albers, M. W., Schrieber, S. L., Carroll, R., Peralta, E., & Whitesides, G. M. (1993). *Convenient Methods for Patterning the Adhesion of Mammalian Cells to Surfaces Using Self-Assembled Monolayers of Alkanethiolates on Gold*. *115*, 5877–5878.

Losic, D., Gooding, J. J., Shapter, J. G., Hibbert, D. B., & Short, K. (2001). The Influence of the Underlying Gold Substrate on Glucose Oxidase Electrodes Fabricated Using Self-Assembled Monolayers. *Electroanalysis*, *13*(17), 1385–1393. https://doi.org/10.1002/1521-4109(200111)13:17<1385::AID-ELAN1385>3.0.CO;2-L

Losic, D., Shapter, J. G., & Gooding, J. J. (2001). Influence of Surface Topography on Alkanethiol SAMs Assembled from Solution and by Microcontact Printing. *Langmuir*, *17*(11), 3307–3316. https://doi.org/10.1021/la001462t

Louault, C., D'Amours, M., & Bélanger, D. (2008). The Electrochemical Grafting of a Mixture of Substituted Phenyl Groups at a Glassy Carbon Electrode Surface. *ChemPhysChem*, *9*(8), 1164–1170. https://doi.org/10.1002/cphc.200800016

Love, J. C., Estroff, L. A., Kriebel, J. K., Nuzzo, R. G., & Whitesides, G. M. (2005). Self-Assembled Monolayers of Thiolates on Metals as a Form of Nanotechnology. *Chemical Reviews*, *105*(4), 1103–1170. https://doi.org/10.1021/cr0300789

Love, J. C., Wolfe, D. B., Haasch, R., Chabinyc, M. L., Paul, K. E., Whitesides, G. M., & Nuzzo, R. G. (n.d.). *Formation and Structure of Self-Assembled Monolayers of Alkanethiolates on Palladium*. 13.

Lu, X., Zheng, H., Li, X.-Q., Yuan, X.-X., Li, H., Deng, L.-G., Zhang, H., Wang, W.-Z., Yang, G.-S., Meng, M., Xi, R.-M., & Aboul-Enein, H. Y. (2012). Detection of ractopamine residues in pork by surface plasmon resonance-based biosensor inhibition immunoassay. *Food Chemistry*, *130*(4), 1061–1065. https://doi.org/10.1016/j.foodchem.2011.07.133

Luong, J. H. T., Male, K. B., & Glennon, J. D. (2009). Boron-doped diamond electrode: Synthesis, characterization, functionalization and analytical applications. *Analyst*, *134*(10), 1965–1979. https://doi.org/10.1039/b910206j

Lyon, L. A., Musick, M. D., Smith, P. C., Reiss, B. D., Peña, D. J., & Natan, M. J. (1999). Surface plasmon resonance of colloidal Au-modified gold films.

Sensors and Actuators B: Chemical, *54*(1–2), 118–124. https://doi.org/10.1016/S0925-4005(98)00329-3

Mahouche-Chergui, S., Gam-Derouich, S., Mangeney, C., & Chehimi, M. M. (2011). Aryl diazonium salts: A new class of coupling agents for bonding polymers, biomacromolecules and nanoparticles to surfaces. *Chemical Society Reviews*, *40*(7), 4143. https://doi.org/10.1039/c0cs00179a

Mandon, C. A., Blum, L. J., & Marquette, C. A. (2009). Aryl Diazonium for Biomolecules Immobilization onto SPRi Chips. *ChemPhysChem*, *10*(18), 3273–3277. https://doi.org/10.1002/cphc.200900599

Manesse, M., Sanjines, R., Stambouli, V., Boukherroub, R., & Szunerits, S. (2008). Preparation and characterization of antimony-doped SnO2 thin films on gold and silver substrates for electrochemical and surface plasmon resonance studies. *Electrochemistry Communications*, *10*(7), 1041–1043. https://doi.org/10.1016/j.elecom.2008.04.036

Manesse, M., Stambouli, V., Boukherroub, R., & Szunerits, S. (2008). Electrochemical impedance spectroscopy and surface plasmon resonance studies of DNA hybridization on gold/SiOx interfaces. *The Analyst*, *133*(8), 1097. https://doi.org/10.1039/b804825h

Mani, R. C., Sunkara, M. K., Baldwin, R. P., Gullapalli, J., Chaney, J. A., Bhimarasetti, G., Cowley, J. M., Rao, A. M., & Rao, R. (2005). Nanocrystalline Graphite for Electrochemical Sensing. *Journal of The Electrochemical Society*, *152*(4), E154. https://doi.org/10.1149/1.1870772

Martins, M. C. L., Fonseca, C., Barbosa, M. A., & Ratner, B. D. (2003). Albumin adsorption on alkanethiols self-assembled monolayers on gold electrodes studied by chronopotentiometry. *Biomaterials*, *24*(21), 3697–3706. https://doi.org/10.1016/S0142-9612(03)00244-8

Masson, J.-F. (2017). Surface Plasmon Resonance Clinical Biosensors for Medical Diagnostics. *ACS Sensors*, *2*(1), 16–30. https://doi.org/10.1021/acssensors.6b00763

Mattia, D., Bau, H. H., & Gogotsi, Y. (2006). Wetting of CVD carbon films by polar and nonpolar liquids and implications for carbon nanopipes. *Langmuir*, *22*(4), 1789–1794. https://doi.org/10.1021/la0518288

Mattson, J. S., & Smith, C. A. (1975). Optically Transparent Carbon Film Electrodes for Infrared Spectroelectrochemistry. *Analytical Chemistry*, *47*(7), 1122–1125. https://doi.org/10.1021/ac60357a070

McCreery, R. L. (2008). Advanced carbon electrode materials for molecular electrochemistry. *Chemical Reviews*, *108*(7), 2646–2687. https://doi.org/10.1021/cr068076m

McCreery, R. L., Cline, K. K., McDermott, C. A., & McDermott, M. T. (1994). Control of reactivity at carbon electrode surfaces. *Colloids and Surfaces A: Physicochemical and Engineering Aspects*, *93*(C), 211–219. https://doi.org/10.1016/0927-7757(94)02899-0

McDermott, M. T., & McCreery, R. L. (1994). Scanning Tunneling Microscopy of Ordered Graphite and Glassy Carbon Surfaces: Electronic Control of Quinone Adsorption. *Langmuir*, *10*(11), 4307–4314. https://doi.org/10.1021/la00023a062

Mekhalif, Z., Riga, J., Pireaux, J.-J., & Delhalle, J. (1997). Self-Assembled Monolayers of *n* -Dodecanethiol on Electrochemically Modified Polycrystalline Nickel Surfaces. *Langmuir*, *13*(8), 2285–2290. https://doi.org/10.1021/la960528a

Menanteau, T., Levillain, E., Downard, A. J., & Breton, T. (2015). Evidence of monolayer formation via diazonium grafting with a radical scavenger: Electrochemical, AFM and XPS monitoring. *Physical Chemistry Chemical Physics*, *17*(19), 13137–13142. https://doi.org/10.1039/C5CP01401H

Menegazzo, N., Zou, Q., & Booksh, K. S. (2012). Characterization of electrografted 4-aminophenylalanine layers for low non-specific binding of proteins. *New Journal of Chemistry*, *36*(4), 963. https://doi.org/10.1039/c2nj20930f

Mesnage, A., Lefèvre, X., Jégou, P., Deniau, G., & Palacin, S. (2012). Spontaneous Grafting of Diazonium Salts: Chemical Mechanism on Metallic Surfaces. *Langmuir*, *28*(32), 11767–11778. https://doi.org/10.1021/la3011103

Mirkhalaf, F., Paprotny, J., & Schiffrin, D. J. (2006). Synthesis of Metal Nanoparticles Stabilized by Metal−Carbon Bonds. *Journal of the American Chemical Society*, *128*(23), 7400–7401. https://doi.org/10.1021/ja058687g

Mirkin, C. A., & Ratner, M. A. (n.d.). Molecular Electronics. *MOLECULAR ELECTRONICS*, 36.

Mitsushio, M., Miyashita, K., & Higo, M. (2006). Sensor properties and surface characterization of the metal-deposited SPR optical fiber sensors with Au, Ag, Cu, and Al. *Sensors and Actuators A: Physical*, *125*(2), 296–303. https://doi.org/10.1016/j.sna.2005.08.019

Mohamed, H. M. (2016). Screen-printed disposable electrodes: Pharmaceutical applications and recent developments. *TrAC - Trends in Analytical Chemistry*, *82*, 1–11. https://doi.org/10.1016/j.trac.2016.02.010

Morteza Najarian, A., Chen, R., Balla, R. J., Amemiya, S., & McCreery, R. L. (2017). Ultraflat, Pristine, and Robust Carbon Electrode for Fast Electron-Transfer Kinetics. *Analytical Chemistry*, *89*(24), 13532–13540. https://doi.org/10.1021/acs.analchem.7b03903

Morteza Najarian, A., Szeto, B., Tefashe, U. M., & McCreery, R. L. (2016). Robust All-Carbon Molecular Junctions on Flexible or Semi-Transparent Substrates Using "Process-Friendly" Fabrication. *ACS Nano*, *10*(9), 8918–8928. https://doi.org/10.1021/acsnano.6b04900

Moulin, A. M. (2000). *Microcantilever-based biosensors*. 9.

Moulton, S. E., Barisci, J. N., Bath, A., Stella, R., & Wallace, G. G. (2003). Investigation of protein adsorption and electrochemical behavior at a gold electrode. *Journal of Colloid and Interface Science*, *261*(2), 312–319. https://doi.org/10.1016/S0021-9797(03)00073-0

Moulton, S. E., Barisci, J. N., Bath, A., Stella, R., & Wallace, G. G. (2004). Studies of double layer capacitance and electron transfer at a gold electrode exposed to protein solutions. *Electrochimica Acta*, *49*(24), 4223–4230. https://doi.org/10.1016/j.electacta.2004.03.034

Murphy, D. M., Cullen, R. J., Jayasundara, D. R., Doyle, R. L., Lyons, M. E. G., & Colavita, P. E. (2013). Heterogeneous Charge Transfer at the Amorphous Carbon/Solution Interface: Effect on the Spontaneous Attachment of

Aryldiazonium Salts. *The Journal of Physical Chemistry C*, *117*(44), 22768–22777. https://doi.org/10.1021/jp406686e

Murphy, D. M., Cullen, R. J., Jayasundara, D. R., Scanlan, E. M., & Colavita, P. E. (2012). Study of the spontaneous attachment of polycyclic aryldiazonium salts onto amorphous carbon substrates. *RSC Advances*, *2*(16), 6527. https://doi.org/10.1039/c2ra20292a

Nelson, K. E., Gamble, L., Jung, L. S., Boeckl, M. S., Naeemi, E., Golledge, S. L., Sasaki, T., Castner, D. G., Campbell, C. T., & Stayton, P. S. (2001). Surface Characterization of Mixed Self-Assembled Monolayers Designed for Streptavidin Immobilization. *Langmuir*, *17*(9), 2807–2816. https://doi.org/10.1021/la001111e

Nelson, R. W., Krone, J. R., & Jansson, O. (1997). Surface Plasmon Resonance Biomolecular Interaction Analysis Mass Spectrometry. 2. Fiber Optic-Based Analysis. *Analytical Chemistry*, *69*(21), 4369–4374. https://doi.org/10.1021/ac9705374

Nguyen, T. P., McCreery, R. L., & McDermott, M. T. (2020). Evaluation of the electroanalytical performance of carbon-on-gold films prepared by electron-beam evaporation. *The Analyst*, *145*(14), 5041–5052. https://doi.org/10.1039/D0AN00409J

Nicholson, R. S. (1965). Theory and Application of Cyclic Voltammetry for Measurement of Electrode Reaction Kinetics. *Analytical Chemistry*, *37*(11), 1351–1355. https://doi.org/10.1021/ac60230a016

Nie, S., & Emory, S. R. (1997). *Probing Single Molecules and Single Nanoparticles by Surface-Enhanced Raman Scattering*. *275*(5303), 1102–1106.

Nioradze, N., Chen, R., Kurapati, N., Khvataeva-Domanov, A., Mabic, S., & Amemiya, S. (2015). Organic contamination of highly oriented pyrolytic graphite as studied by scanning electrochemical microscopy. *Analytical Chemistry*, *87*(9), 4836–4843. https://doi.org/10.1021/acs.analchem.5b00213

Niwa, Osamu., & Tabei, Hisao. (1994). Voltammetric measurements of reversible and quasi-reversible redox species using carbon film based interdigitated array microelectrodes. *Analytical Chemistry*, *66*(2), 285–289. https://doi.org/10.1021/ac00074a016

Nuzzo, R. G., & Allara, D. L. (1983). Adsorption of bifunctional organic disulfides on gold surfaces. *Journal of the American Chemical Society*, *105*(13), 4481–4483. https://doi.org/10.1021/ja00351a063

Ohno, Y., Maehashi, K., Yamashiro, Y., & Matsumoto, K. (2009). Electrolyte-Gated Graphene Field-Effect Transistors for Detecting pH and Protein Adsorption. *Nano Letters*, *9*(9), 3318–3322. https://doi.org/10.1021/nl901596m

Ordal, M. A., Long, L. L., Bell, R. J., Bell, S. E., Bell, R. R., Alexander, R. W., & Ward, C. A. (1983). Optical properties of the metals Al, Co, Cu, Au, Fe, Pb, Ni, Pd, Pt, Ag, Ti, and W in the infrared and far infrared. *Applied Optics*, *22*(7), 1099. https://doi.org/10.1364/AO.22.001099

O'Shannessy, D. J., Brigham-Burke, M., & Peck, K. (1992). Immobilization Chemistries Suitable for Use in the BlAcore Surface Plasmon Resonance Detector. *Analytical Biochemistry*, *205*, 132–136.

Otto, A. (1968). Excitation of nonradiative surface plasma waves in silver by the method of frustrated total reflection. *Zeitschrift Für Physik A Hadrons and Nuclei*, *216*(4), 398–410. https://doi.org/10.1007/BF01391532

Oznuluer, T., Pince, E., Polat, E. O., Balci, O., Salihoglu, O., & Kocabas, C. (2011). Synthesis of graphene on gold. *Applied Physics Letters*, *98*(18), 183101. https://doi.org/10.1063/1.3584006

Paloma Yáñez-Sedeño, Susana Campuzano, & José Pingarrón. (2018). Integrated Affinity Biosensing Platforms on Screen-Printed Electrodes Electrografted with Diazonium Salts. *Sensors*, *18*(3), 675. https://doi.org/10.3390/s18020675

Patai, S. (1978). *The Chemistry of Diazonium and Diazo Groups, Part I*. John Wiley & Sons, Chichester.

Patel, A. N., Collignon, M. G., OConnell, M. A., Hung, W. O. Y., McKelvey, K., MacPherson, J. V., & Unwin, P. R. (2012). A new view of electrochemistry at highly oriented pyrolytic graphite. *Journal of the American Chemical Society*, *134*(49), 20117–20130. https://doi.org/10.1021/ja308615h

Patil, P. O., Pandey, G. R., Patil, A. G., Borse, V. B., Deshmukh, P. K., Patil, D. R., Tade, R. S., Nangare, S. N., Khan, Z. G., Patil, A. M., More, M. P., Veerapandian, M., & Bari, S. B. (2019). Graphene-based nanocomposites for sensitivity enhancement of surface plasmon resonance sensor for biological and chemical sensing: A review. *Biosensors and Bioelectronics*, *139*, 111324. https://doi.org/10.1016/j.bios.2019.111324

Patten, H. V., Meadows, K. E., Hutton, L. A., Iacobini, J. G., Battistel, D., McKelvey, K., Colburn, A. W., Newton, M. E., MacPherson, J. V., & Unwin, P. R. (2012). Electrochemical mapping reveals direct correlation between heterogeneous electron-transfer kinetics and local density of states in diamond electrodes. *Angewandte Chemie - International Edition*, *51*(28), 7002–7006. https://doi.org/10.1002/anie.201203057

Phillips, K. S., Han, J.-H., Martinez, M., Wang, Z., Carter, D., & Cheng, Q. (2006). Nanoscale Glassification of Gold Substrates for Surface Plasmon Resonance Analysis of Protein Toxins with Supported Lipid Membranes. *Analytical Chemistry*, *78*(2), 596–603. https://doi.org/10.1021/ac051644y

Phillips, K. S., Wilkop, T., Wu, J.-J., Al-Kaysi, R. O., & Cheng, Q. (2006). Surface Plasmon Resonance Imaging Analysis of Protein-Receptor Binding in Supported Membrane Arrays on Gold Substrates with Calcinated Silicate Films. *Journal of the American Chemical Society*, *128*(30), 9590–9591. https://doi.org/10.1021/ja0628102

Pinson, J., & Podvorica, F. (2005). Attachment of organic layers to conductive or semiconductive surfaces by reduction of diazonium salts. *Chemical Society Reviews*, *34*(5), 429. https://doi.org/10.1039/b406228k

Pirlot, C., Delhalle, J., Pireaux, J. J., & Mekhalif, Z. (2001). Surface modification of polycrystalline iron surfaces by n-dodecanethiol: An XPS investigation. *Surface and Coatings Technology*, *138*(2–3), 166–172. https://doi.org/10.1016/S0257-8972(00)01130-0

Podvorica, F. I., Kanoufi, F., Pinson, J., & Combellas, C. (2009). Spontaneous grafting of diazoates on metals. *Electrochimica Acta*, *54*(8), 2164–2170. https://doi.org/10.1016/j.electacta.2008.10.017

Polsky, R., Harper, J. C., Dirk, S. M., Arango, D. C., Wheeler, D. R., & Brozik, S. M. (2007). Diazonium-Functionalized Horseradish Peroxidase Immobilized via Addressable Electrodeposition: Direct Electron Transfer and Electrochemical Detection. *Langmuir*, *23*(2), 364–366. https://doi.org/10.1021/la062916a

Polsky, R., Harper, J. C., Wheeler, D. R., & Brozik, S. M. (2008). Multifunctional Electrode Arrays: Towards a Universal Detection Platform. *Electroanalysis*, *20*(6), 671–679. https://doi.org/10.1002/elan.200704129

Polsky, R., Harper, J. C., Wheeler, D. R., Dirk, S. M., Arango, D. C., & Brozik, S. M. (2008). Electrically addressable diazonium-functionalized antibodies for multianalyte electrochemical sensor applications. *Biosensors and Bioelectronics*, *23*(6), 757–764. https://doi.org/10.1016/j.bios.2007.08.013

Porter, M. D., Bright, T. B., Allara, D. L., & Chidsey, C. E. D. (1987). Spontaneously organized molecular assemblies. 4. Structural characterization of n-alkyl thiol monolayers on gold by optical ellipsometry, infrared spectroscopy, and electrochemistry. *Journal of the American Chemical Society*, *109*(12), 3559–3568. https://doi.org/10.1021/ja00246a011

Qiao, L., Wang, D., Zuo, L., Ye, Y., Qian, J., Chen, H., & He, S. (2011). Localized surface plasmon resonance enhanced organic solar cell with gold nanospheres. *Applied Energy*, *88*(3), 848–852. https://doi.org/10.1016/j.apenergy.2010.09.021

Ranganathan, S., & McCreery, R. L. (2001). Electroanalytical performance of carbon films with near-atomic flatness. *Analytical Chemistry*, *73*(5), 893–900. https://doi.org/10.1021/ac0007534

Ranganathan, S., McCreery, R., Majji, S. M., & Madou, M. (2000). Photoresist-Derived Carbon for Microelectromechanical Systems and Electrochemical Applications. *Journal of The Electrochemical Society*, *147*(1), 277. https://doi.org/10.1149/1.1393188

Rich, R. L., & Myszka, D. G. (2000). Survey of the 1999 surface plasmon resonance biosensor literature. *J. Mol. Recognit.*, 20.

Riskin, M., Tel-Vered, R., Lioubashevski, O., & Willner, I. (2009). Ultrasensitive Surface Plasmon Resonance Detection of Trinitrotoluene by a Bis-aniline-Cross-Linked Au Nanoparticles Composite. *Journal of the American Chemical Society*, *131*(21), 7368–7378. https://doi.org/10.1021/ja9001212

Ritchie, R., Arakawa, E., Cowan, J., & Hamm, R. (1968). Surface-Plasmon Resonance Effect in Grating Diffraction. *Physical Review Letters*, *21*(22), 1530–1533. https://doi.org/10.1103/PhysRevLett.21.1530

Ritzefeld, M., & Sewald, N. (2012). Real-Time Analysis of Specific Protein-DNA Interactions with Surface Plasmon Resonance. *Journal of Amino Acids*, *2012*, 1–19. https://doi.org/10.1155/2012/816032

Robertson, J. (1986). Amorphous carbon. *Advances in Physics*, *35*(4), 317–374. https://doi.org/10.1080/00018738600101911

Rodbard, D., & Hutt, D. M. (1974). *Radioimmunoassay and related procedures in medicine* (Vol. 1). IAEA: Vienna.

Rothenhiiusler, B., & Knollt, W. (1988). *Surface-plasmon microscopy*. *332*, 615–617.

Roy, R. K., & Lee, K.-R. (2007). Biomedical applications of diamond-like carbon coatings: A review. *Journal of Biomedical Materials Research Part B: Applied Biomaterials*, *83B*(1), 72–84. https://doi.org/10.1002/jbm.b.30768

Ruffien, A., Dequaire, M., & Brossier, P. (2003). Covalent immobilization of oligonucleotides on p-aminophenyl-modified carbon screen-printed electrodes for viral DNA sensing. *Chemical Communications*, *7*, 912–913. https://doi.org/10.1039/b300439b

Rusin, C. J., El Bakkari, M., Du, R., Boluk, Y., & McDermott, M. T. (2020). Plasmonic Cellulose Nanofibers as Water-Dispersible Surface-Enhanced Raman Scattering Substrates. *ACS Applied Nano Materials*, *3*(7), 6584–6597. https://doi.org/10.1021/acsanm.0c01045

Saby, C., Ortiz, B., Champagne, G. Y., & Bélanger, D. (1997). Electrochemical Modification of Glassy Carbon Electrode Using Aromatic Diazonium Salts. 1. Blocking Effect of 4-Nitrophenyl and 4-Carboxyphenyl Groups. *Langmuir*, *13*(25), 6805–6813. https://doi.org/10.1021/la961033o

Sachan, P., & Mondal, P. C. (2020). Versatile electrochemical approaches towards the fabrication of molecular electronic devices. *The Analyst*, *145*(5), 1563–1582. https://doi.org/10.1039/C9AN01948K

Sadrolhosseini, A. R., Moksin, M. M., Yunus, W. M. M., Talib, Z. A., & Abdi, M. M. (2011). Surface plasmon resonance detection of copper corrosion in biodiesel using polypyrrole-chitosan layer sensor. *Optical Review*, *18*(4), 331–337. https://doi.org/10.1007/s10043-011-0064-5

Satriano, C., Edvardsson, M., Ohlsson, G., Wang, G., Svedhem, S., & Kasemo, B. (2010). Plasma Oxidized Polyhydroxymethylsiloxane—A New Smooth Surface for Supported Lipid Bilayer Formation. *Langmuir*, *26*(8), 5715–5725. https://doi.org/10.1021/la903826d

Satriano, C., Marletta, G., & Kasemo, B. (2008). Oxygen plasma-induced conversion of polysiloxane into hydrophilic and smooth SiO_x surfaces: Hydrophilic and smooth SiO_x surfaces by O_2 plasma of polysiloxane. *Surface and Interface Analysis*, *40*(3–4), 649–656. https://doi.org/10.1002/sia.2764

Schlesinger, R. (1997). Development of Thin Film Electrodes Based on Sputtered Amorphous Carbon. *Journal of The Electrochemical Society*, *144*(1), 6. https://doi.org/10.1149/1.1837358

Schreiber, A., Feldbrügge, R., Key, G., Glatz, J. F. C., & Spener, F. (1997). An immunosensor based on disposable electrodes for rapid estimation of fatty acid-binding protein, an early marker of myocardial infarction. *Biosensors and Bioelectronics*, *12*(11), 1131–1137. https://doi.org/10.1016/S0956-5663(97)00003-1

Schulz, H., Leonhardt, M., Scheibe, H. J., & Schultrich, B. (2005). Ultra hydrophobic wetting behaviour of amorphous carbon films. *Surface and Coatings Technology*, *200*(1-4 SPEC. ISS.), 1123–1126. https://doi.org/10.1016/j.surfcoat.2005.02.019

Seinberg, J.-M., Kullapere, M., Mäeorg, U., Maschion, F. C., Maia, G., Schiffrin, D. J., & Tammeveski, K. (2008). Spontaneous modification of glassy carbon surface with anthraquinone from the solutions of its diazonium derivative: An

oxygen reduction study. *Journal of Electroanalytical Chemistry*, *624*(1–2), 151–160. https://doi.org/10.1016/j.jelechem.2008.09.002

Sekioka, N., Kato, D., Ueda, A., Kamata, T., Kurita, R., Umemura, S., Hirono, S., & Niwa, O. (2008). Controllable electrode activities of nano-carbon films while maintaining surface flatness by electrochemical pretreatment. *Carbon*, *46*(14), 1918–1926. https://doi.org/10.1016/j.carbon.2008.08.006

Shewchuk, D. M., & McDermott, M. T. (2009). Comparison of Diazonium Salt Derived and Thiol Derived Nitrobenzene Layers on Gold. *Langmuir*, *25*(8), 4556–4563. https://doi.org/10.1021/la8040083

Shumaker-Parry, J. S., Zareie, M. H., Aebersold, R., & Campbell, C. T. (2004). Microspotting Streptavidin and Double-Stranded DNA Arrays on Gold for High-Throughput Studies of Protein−DNA Interactions by Surface Plasmon Resonance Microscopy. *Analytical Chemistry*, *76*(4), 918–929. https://doi.org/10.1021/ac034964v

Sigal, G. B., Mrksich, M., & Whitesides, G. M. (1998). *Effect of Surface Wettability on the Adsorption of Proteins and Detergents*. *120*, 3464–3473.

Silin, V., Weetall, H., & Vanderah, D. (1997). *SPR Studies of the Non-specific Adsorption Kinetics of Human IgG and BSA on Gold Surfaces Modified by Self-Assembled Monolayers (SAMs)*. *185*, 94–103.

Smith, E. A., Thomas, W. D., Kiessling, L. L., & Corn, R. M. (2003). Surface Plasmon Resonance Imaging Studies of Protein-Carbohydrate Interactions. *Journal of the American Chemical Society*, *125*(20), 6140–6148. https://doi.org/10.1021/ja034165u

Smith, T. (1980). The hydrophilic nature of a clean gold surface. *Journal of Colloid and Interface Science*, *75*(1), 51–55. https://doi.org/10.1016/0021-9797(80)90348-3

Socrates, G. (2001). *Infrared and Raman Characteristic Group Frequencies: Table and Charts*. John Wiley & Sons.

Solak, A. O., Eichorst, L. R., Clark, W. J., & McCreery, R. L. (2003). Modified Carbon Surfaces as "Organic Electrodes" That Exhibit Conductance Switching. *Analytical Chemistry*, *75*(2), 296–305. https://doi.org/10.1021/ac026107h

Strano, M. S. (2003). Electronic Structure Control of Single-Walled Carbon Nanotube Functionalization. *Science*, *301*(5639), 1519–1522. https://doi.org/10.1126/science.1087691

Stüber, M., Niederberger, L., Danneil, F., Leiste, H., Ulrich, S., Welle, A., Marin, M., & Fischer, H. (2007). Surface Topography, Surface Energy and Wettability of Magnetron-Sputtered Amorphous Carbon (a-C) Films and Their Relevance for Platelet Adhesion. *Advanced Engineering Materials*, *9*(12), 1114–1122. https://doi.org/10.1002/adem.200700224

Sugio, S., Kashima, A., Mochizuki, S., Noda, M., & Kobayashi, K. (1999). Crystal structure of human serum albumin at 2.5 Å resolution. *Protein Engineering, Design and Selection*, *12*(6), 439–446. https://doi.org/10.1093/protein/12.6.439

Sun, B., Colavita, P. E., Kim, H., Lockett, M., Marcus, M. S., Smith, L. M., & Hamers, R. J. (2006). Covalent Photochemical Functionalization of

Amorphous Carbon Thin Films for Integrated Real-Time Biosensing. *Langmuir*, *22*(23), 9598–9605. https://doi.org/10.1021/la061749b

Sydow-Plum, G., & Tabrizian, M. (2008). Review of stent coating strategies: Clinical insights. *Materials Science and Technology*, *24*(9), 1127–1143. https://doi.org/10.1179/174328408X341816

Szunerits, S., & Boukherroub, R. (2006). Electrochemical investigation of gold/silica thin film interfaces for electrochemical surface plasmon resonance studies. *Electrochemistry Communications*, *8*(3), 439–444. https://doi.org/10.1016/j.elecom.2006.01.006

Szunerits, S., Castel, X., & Boukherroub, R. (2008a). Preparation of Electrochemical and Surface Plasmon Resonance Active Interfaces: Deposition of Indium Tin Oxide on Silver Thin Films. *The Journal of Physical Chemistry C*, *112*(29), 10883–10888. https://doi.org/10.1021/jp8025682

Szunerits, S., Castel, X., & Boukherroub, R. (2008b). Surface Plasmon Resonance Investigation of Silver and Gold Films Coated with Thin Indium Tin Oxide Layers: Influence on Stability and Sensitivity. *The Journal of Physical Chemistry C*, *112*(40), 15813–15817. https://doi.org/10.1021/jp8049137

Szunerits, S., Maalouli, N., Wijaya, E., Vilcot, J.-P., & Boukherroub, R. (2013). Recent advances in the development of graphene-based surface plasmon resonance (SPR) interfaces. *Analytical and Bioanalytical Chemistry*, *405*(5), 1435–1443. https://doi.org/10.1007/s00216-012-6624-0

Taleat, Z., Khoshroo, A., & Mazloum-Ardakani, M. (2014). Screen-printed electrodes for biosensing: A review (2008-2013). *Microchimica Acta*, *181*(9–10), 865–891. https://doi.org/10.1007/s00604-014-1181-1

Tan, S. Y., Lazenby, R. A., Bano, K., Zhang, J., Bond, A. M., Macpherson, J. V., & Unwin, P. R. (2017). Comparison of fast electron transfer kinetics at platinum, gold, glassy carbon and diamond electrodes using Fourier-transformed AC voltammetry and scanning electrochemical microscopy. *Physical Chemistry Chemical Physics*, *19*(13), 8726–8734. https://doi.org/10.1039/c7cp00968b

Tidwell, C. D., Ertel, S. I., Ratner, B. D., Tarasevich, B. J., Atre, S., & Allara, D. L. (1997). Endothelial Cell Growth and Protein Adsorption on Terminally Functionalized, Self-Assembled Monolayers of Alkanethiolates on Gold. *Langmuir*, *13*(13), 3404–3413. https://doi.org/10.1021/la9604341

Toman, J. T. (2013). *Electrografted Thick Diazonium Derived Films for Biosensing Applications* [MSc thesis]. University of Alberta.

Touahir, L., Niedziółka-Jönsson, J., Galopin, E., Boukherroub, R., Gouget-Laemmel, A. C., Solomon, I., Petukhov, M., Chazalviel, J.-N., Ozanam, F., & Szunerits, S. (2010). Surface Plasmon Resonance on Gold and Silver Films Coated with Thin Layers of Amorphous Silicon−Carbon Alloys. *Langmuir*, *26*(8), 6058–6065. https://doi.org/10.1021/la903896m

Toupin, M., & Bélanger, D. (2008). Spontaneous Functionalization of Carbon Black by Reaction with 4-Nitrophenyldiazonium Cations. *Langmuir*, *24*(5), 1910–1917. https://doi.org/10.1021/la702556n

Ulman, A. (1991). *An Introduction to Ultrathin Organic Films: From Langmuir-Blodgett to Self-Assembly*. Academic Press: Boston, MA.

Ulman, A. (1996). Formation and Structure of Self-Assembled Monolayers. *Chemical Reviews*, *96*(4), 1533–1554. https://doi.org/10.1021/cr9502357

Usrey, M. L., Lippmann, E. S., & Strano, M. S. (2005). Evidence for a Two-Step Mechanism in Electronically Selective Single-Walled Carbon Nanotube Reactions. *Journal of the American Chemical Society*, *127*(46), 16129–16135. https://doi.org/10.1021/ja0537530

van Noort, D., & Mandenius, C.-F. (2000). Porous gold surfaces for biosensor applications. *Biosensors and Bioelectronics*, *15*(3–4), 203–209. https://doi.org/10.1016/S0956-5663(00)00061-0

Vericat, C., Vela, M. E., Benitez, G., Carro, P., & Salvarezza, R. C. (2010). Self-assembled monolayers of thiols and dithiols on gold: New challenges for a well-known system. *Chemical Society Reviews*, *39*(5), 1805. https://doi.org/10.1039/b907301a

Villarreal, E., Li, G. G., Zhang, Q., Fu, X., & Wang, H. (2017). Nanoscale Surface Curvature Effects on Ligand–Nanoparticle Interactions: A Plasmon-Enhanced Spectroscopic Study of Thiolated Ligand Adsorption, Desorption, and Exchange on Gold Nanoparticles. *Nano Letters*, *17*(7), 4443–4452. https://doi.org/10.1021/acs.nanolett.7b01593

Vroman, L., & Adams, A. L. (1969). Findings with the recording ellipsometer suggesting rapid exchange of specific plasma proteins at liquid/solid interfaces. *Surface Science*, *16*, 438–446. https://doi.org/10.1016/0039-6028(69)90037-5

Wang, J., Tian, B., Nascimento, V. B., & Angnes, L. (1998). Performance of screen-printed carbon electrodes fabricated from different carbon inks. *Electrochimica Acta*, *43*(23), 3459–3465. https://doi.org/10.1016/S0013-4686(98)00092-9

Wang, Y., Alsmeyer, D. C., & McCreery, R. L. (1990). Raman spectroscopy of carbon materials: Structural basis of observed spectra. *Chemistry of Materials*, *2*(5), 557–563. https://doi.org/10.1021/cm00011a018

Wijaya, E., Lenaerts, C., Maricot, S., Hastanin, J., Habraken, S., Vilcot, J.-P., Boukherroub, R., & Szunerits, S. (2011). Surface plasmon resonance-based biosensors: From the development of different SPR structures to novel surface functionalization strategies. *Current Opinion in Solid State and Materials Science*, *15*(5), 208–224. https://doi.org/10.1016/j.cossms.2011.05.001

Wilkop, T., Wang, Z., & Cheng, Q. (2004). Analysis of μ-Contact Printed Protein Patterns by SPR Imaging with a LED Light Source. *Langmuir*, *20*(25), 11141–11148. https://doi.org/10.1021/la048177k

Williams, J. A., & Gorman, C. B. (2007). Alkanethiol Reductive Desorption from Self-Assembled Monolayers on Gold, Platinum, and Palladium Substrates. *The Journal of Physical Chemistry C*, *111*(34), 12804–12810. https://doi.org/10.1021/jp072869a

Wong, S.-S., & Porter, M. D. (2000). Origin of the multiple voltammetric desorption waves of long-chain alkanethiolate monolayers chemisorbed on annealed gold electrodes. *Journal of Electroanalytical Chemistry*, *485*(2), 135–143. https://doi.org/10.1016/S0022-0728(00)00106-6

Wood, R. W. (1902). XLII. *On a remarkable case of uneven distribution of light in a diffraction grating spectrum*. *The London, Edinburgh, and Dublin Philosophical Magazine and Journal of Science*, *4*(21), 396–402. https://doi.org/10.1080/14786440209462857

Wu, L., Chu, H. S., Koh, W. S., & Li, E. P. (2010). Highly sensitive graphene biosensors based on surface plasmon resonance. *Optics Express*, *18*(14), 14395. https://doi.org/10.1364/OE.18.014395

Wu, Z., Guan, L., Shen, G., & Yu, R. (2002). Renewable urea sensor based on a self-assembled polyelectrolyte layer. *The Analyst*, *127*(3), 391–395. https://doi.org/10.1039/b110050e

Xu, J., Chen, Q., & Swain, G. M. (1998). Anthraquinonedisulfonate Electrochemistry: A Comparison of Glassy Carbon, Hydrogenated Glassy Carbon, Highly Oriented Pyrolytic Graphite, and Diamond Electrodes. *Analytical Chemistry*, *70*(15), 3146–3154. https://doi.org/10.1021/ac9800661

Xu, J., Granger, M. C., Chen, Q., Strojek, J. W., Lister, T. E., & Swain, G. M. (1997). Peer Reviewed: Boron-Doped Diamond Thin-Film Electrodes. *Analytical Chemistry*, *69*(19), 591A-597A. https://doi.org/10.1021/ac971791z

Yan, H., Bergren, A. J., & McCreery, R. L. (2011). All-Carbon Molecular Tunnel Junctions. *Journal of the American Chemical Society*, *133*(47), 19168–19177. https://doi.org/10.1021/ja206619a

Yang, G., Amro, N. A., Starkewolfe, Z. B., & Liu, G. (2004). Molecular-Level Approach to Inhibit Degradations of Alkanethiol Self-Assembled Monolayers in Aqueous Media. *Langmuir*, *20*(10), 3995–4003. https://doi.org/10.1021/la0499160

Yang, X., Too, C. O., Sparrow, L., Ramshaw, J., & Wallace, G. G. (2002). Polypyrrole–heparin system for the separation of thrombin. *Reactive and Functional Polymers*, *53*(1), 53–62. https://doi.org/10.1016/S1381-5148(02)00145-1

You, T., Niwa, O., Tomita, M., Ichino, T., & Hirono, S. (2002). Electrochemical Oxidation of Alkylphenols on ECR-Sputtered Carbon Film Electrodes with Flat Sub-nanometer Surfaces. *Journal of The Electrochemical Society*, *149*(12), E479. https://doi.org/10.1149/1.1516222

Yu, S. S. C., Tan, E. S. Q., Jane, R. T., & Downard, A. J. (2007). An Electrochemical and XPS Study of Reduction of Nitrophenyl Films Covalently Grafted to Planar Carbon Surfaces. *Langmuir*, *23*(22), 11074–11082. https://doi.org/10.1021/la701655w

Zayats, A. V., Smolyaninov, I. I., & Maradudin, A. A. (2005). Nano-optics of surface plasmon polaritons. *Physics Reports*, *408*(3–4), 131–314. https://doi.org/10.1016/j.physrep.2004.11.001

Zen, F., Karanikolas, V. D., Behan, J. A., Andersson, J., Ciapetti, G., Bradley, A. L., & Colavita, P. E. (2017). Nanoplasmonic Sensing at the Carbon-Bio Interface: Study of Protein Adsorption at Graphitic and Hydrogenated Carbon Surfaces. *Langmuir*, *33*(17), 4198–4206. https://doi.org/10.1021/acs.langmuir.7b00612

Zeng, A., Liu, E., Tan, S. N., Zhang, S., & Gao, J. (2002). Cyclic voltammetry studies of sputtered nitrogen doped diamond-like carbon film electrodes.

Electroanalysis, *14*(15–16), 1110–1115. https://doi.org/10.1002/1521-4109(200208)14:15/16<1110::AID-ELAN1110>3.0.CO;2-E

Zhou, D., Too, C. O., & Wallace, G. G. (1999). Synthesis and characterisation of polypyrrole/heparin composites. *Reactive and Functional Polymers*, *39*(1), 19–26. https://doi.org/10.1016/S1381-5148(97)00149-1

Zhou, D., Too, C. O., Wallace, G. G., Hodges, A. M., & Mau, A. W. H. (2000). Protein transport and separation using polypyrrole coated, platinised polyvinylidene fluoride membranes. *Reactive and Functional Polymers*, *45*(3), 217–226. https://doi.org/10.1016/S1381-5148(00)00034-1

Zhou, Y., Wang, B., Song, X., Li, E., Li, G., Zhao, S., & Yan, H. (2006). Control over the wettability of amorphous carbon films in a large range from hydrophilicity to super-hydrophobicity. *Applied Surface Science*, *253*(5), 2690–2694. https://doi.org/10.1016/j.apsusc.2006.05.118

Zollinger, H. (1973). Reactivity and stability of arenediazonium ions. *Accounts of Chemical Research*, *6*(10), 335–341. https://doi.org/10.1021/ar50070a002